# STUDY OF EXCITATION FUNCTIONS FOR ALPHA INDUCED REACTIONS IN SOME NUCLEI AT CYCLOTRON ENERGIES

## ABSTRACT

THESIS
FOR
Doctor of Philosophy
(PHYSICS)
1992



DEPARTMENT OF PHYSICS
ALIGARH MUSLIM UNIVERSITY
ALIGARH (INDIA)

MANOJ KUMAR BHARDWAJ

# ABSTRACT

In recent years, there has been an increasing interest to look into the nuclear interaction mechanisms via. pre-equilibrium emission of particles followed by the equilibrium decay. This has been used in explaining many types of the reactions. Hence, the better understanding of the pre-equilibriu emission mechanism is necessary and for this purpose more and more accurate experimental data are necessary. With this motivation, in the present work, the excitation functions for (α,n), (α,2n) reactions in $^{113}$In; (α,n), (α,2n), (α,3n), (α,4n), (α,pn), (α,2p) reactions in $^{115}$In; (α,n), (α,2n), (α,3n), (α,4n), (α,5n) reactions in $^{191}$Ir; (α,3n), (α,4n), (α,5n) reactions in $^{193}$Ir, (α,n), (α,2n), (α,4n), (α,p3n) reactions in $^{121}$Sb and (α,n), (α,3n), (α,4n) reactions in $^{123}$Sb have been measured. This thesi is ramified into five chapters.

In the chapter I, a general introduction regarding nuclear reactions, nuclear reaction theories, technique of measurements, nuclear model code and a brief idea of the results, are given.

After the development of isochronous cyclotron, the projectiles excited upto very high energies became available and a long tail in the excitation function was observed. In order to explain this, many semi-classical models have been proposed which are given in chapter II. The model calculations are done

by using ALICE/LIVERMORE-82 computer code. The details of this computer code are given in the chapter III.

The stacked foil activation technique was followed in the present experiment. The stack of the In, Ir, Sb were bombarded with 50 MeV, 55 MeV, 55 MeV energy of α-particle beam respectively, at Variable Energy Cyclotron Centre, Calcutta (India) for the suitable periods, keeping in view the thickness of the sample, the melting point of the element and half lives of the yields. The residual activities were recorded with the help of a 100 $cm^3$ Ge(Li) detector coupled with a pre-calibrated multichannel analyser and associated electronics. The efficiency and energy calibrations wer done using a standard $^{152}Eu$ gamma point source of known strength keeping it at target position. In the measurement of flux, the α-particles were counted from an integrated beam charge where the beam was totally stopped in an electrically insulated irradiation heads, serving as a kind of Faraday cup. The flux was checked by the $^{65}Cu(\alpha,2n)^{67}Ga$ monitor reaction also. Other experimental details are given in the chapter IV measured values of the results are also tabulated in this chapter.

The experimental values of the results are compared also with theoretically calculated values as well as the literature values (if available). The excitation functions calculated by the consideration of equilibrium and pre-equilibrium both (GDH model) and the equilibrium only (Weisskopf-Ewing model) do not match with each other. Beyond the peak of the excitation

function calculated from Weisskopf-Ewing model goes down very fast while, that calculated from GDH model has a long tail. Our experimentally measured results are close to the GDH model calculations which indicates that the long tails in the excitation functions cannot be accounted for by pure equilibrium reaction mechanism. In order to explain this tail, the concept of proper admixture of equilibrium and pre-equilibrium process is needed. Presently, the percentage of the pre-equilibrium fraction ($f_{PE}$) is also calculated and concluded that this fraction increases very fast with the energy of incident α-beam but at the higher energies the rate of increament of $f_{PE}$ decreases. The threshold of pre-equilibrium emission is higher for lower mass number. The value of $f_{PE}$ is higher for higher mass number at a given α-particle energy. The choice of four exciton state (2n+2p+0h) gives the best fit to our experimental data.


# STUDY OF EXCITATION FUNCTIONS FOR ALPHA INDUCED REACTIONS IN SOME NUCLEI AT CYCLOTRON ENERGIES

THESIS

FOR

Doctor of Philosophy

(PHYSICS)

1992

DEPARTMENT OF PHYSICS
ALIGARH MUSLIM UNIVERSITY
ALIGARH (INDIA)

MANOJ KUMAR BHARDWAJ

Dedicated

To My

Parents

Certified that the work presented in this thesis is the original work of Mr. Manoj Kumar Bhardwaj, done under my supervision.

4.8.92

( A.K. CHAUBEY )

READER
DEPARTMENT OF PHYSICS
ALIGARH MUSLIM UNIVERSITY
ALIGARH-202002.

# A C K N O W L E D G E M E N T S

I wish to express my humble gratitude to my able supervisor, Dr. A.K. Chaubey, who refined upon my little knowledge to read between the lines of tedious research work. I owe to Dr. A.K. Chaubey under whose creative direction and sound guidance I could cross the threshold of the work submitted hereby.

I am grateful to Prof. B.N. Khanna, Chairman, Department of Physics, Prof. Israr Ahmad, Ex-Chairman, Department of Physics for providing me the departmental facilities to carry out this work. I also wish to tender my indebtedness to Prof. Israr Ahmad, Coordinator DSA Physics, Prof. M.Z. Rahman Khan, Coordinator DSA Physics (on leave) for financial support from DSA grant.

I am very much thankful to the personnel of Variable Energy Cyclotron Centre, Calcutta and all my colleagues and well wishers, particularly Dr. M.A. Ansari, Dr. I.A. Rizvi, Mr. H. Singh and Mr. N. Peer Mohamed Sathik who directly or indirectly helped me in winding up the work.

( MANOJ KUMAR BHARDWAJ )

# A B S T R A C T

In recent years, there has been an increasing interest to look into the nuclear interaction mechanisms via. pre-equilibrium emission of particles followed by the equilibrium decay. This has been used in explaining many types of the reactions. Hence, the better understanding of the pre-equilibrium emission mechanism is necessary and for this purpose more and more accurate experimental data are necessary. With this motivation, in the present work, the excitation functions for (α,n), (α,2n) reactions in $^{113}$In; (α,n), (α,2n), (α,3n), (α,4n), (α,pn), (α,2p) reactions in $^{115}$In; (α,n), (α,2n), (α,3n), (α,4n), (α,5n) reactions in $^{191}$Ir; (α,3n), (α,4n), (α,5n) reactions in $^{193}$Ir, (α,n), (α,2n), (α,4n), (α,p3n) reactions in $^{121}$Sb and (α,n), (α,3n), (α,4n) reactions in $^{123}$Sb have been measured. This thesis is ramified into five chapters.

In the chapter I, a general introduction regarding nuclear reactions, nuclear reaction theories, technique of measurements, nuclear model code and a brief idea of the results, are given.

After the development of isochronous cyclotron, the projectiles excited upto very high energies became available and a long tail in the excitation function was observed. In order to explain this, many semi-classical models have been proposed which are given in chapter II. The model calculations are done

by using ALICE/LIVERMORE-82 computer code. The details of this computer code are given in the chapter III.

The stacked foil activation technique was followed in the present experiment. The stack of the In, Ir, Sb were bombarded with 50 MeV, 55 MeV, 55 MeV energy of α-particle beam respectively, at Variable Energy Cyclotron Centre, Calcutta (India) for the suitable periods, keeping in view the thickness of the sample, the melting point of the element and half lives of the yields. The residual activities were recorded with the help of a 100 $cm^3$ Ge(Li) detector coupled with a pre-calibrated multichannel analyser and associated electronics. The efficiency and energy calibrations were done using a standard $^{152}Eu$ gamma point source of known strength keeping it at target position. In the measurement of flux, the α-particles were counted from an integrated beam charge where the beam was totally stopped in an electrically insulated irradiation heads, serving as a kind of Faraday cup. The flux was checked by the $^{65}Cu(\alpha,2n)^{67}Ga$ monitor reaction also. Other experimental details are given in the chapter IV measured values of the results are also tabulated in this chapter.

The experimental values of the results are compared also with theoretically calculated values as well as the literature values (if available). The excitation functions calculated by the consideration of equilibrium and pre-equilibrium both (GDH model) and the equilibrium only (Weisskopf-Ewing model) do not matches with each other. Beyond the peak of the excitation

function calculated from Weisskopf-Ewing model goes down very fast while, that calculated from GDH model has a long tail. Our experimentally measured results are close to the GDH model calculations which indicates that the long tails in the excitation functions cannot be accounted for by pure equilibrium reaction mechanism. In order to explain this tail, the concept of proper admixture of equilibrium and pre-equilibrium process is needed. Presently, the percentage of the pre-equilibrium fraction ($f_{PE}$) is also calculated and concluded that this fraction increases very fast with the energy of incident α-beam but at the higher energies the rate of increament of $f_{PE}$ decreases. The threshold of pre-equilibrium emission is higher for lower mass number. The value of $f_{PE}$ is higher for higher mass number at a given α-particle energy. The choice of four exciton state (2n+2p+0h) gives the best fit to our experimental data.

# CONTENTS


| | | Page Nos. |
|---|---|---|
| CHAPTER-I | Introduction | 01 |
| | References | 11 |
| CHAPTER-II | Nuclear Reaction Theories | 15 |
| | 2.1 Compound Nucleus Theory | 16 |
| | 2.2 Statistical Theory | 18 |
| | 2.3 Intra Nuclear Cascade Model | 23 |
| | 2.4 Harp Miller-Berne (HMB) Model | 25 |
| | 2.5 Exciton Model | 28 |
| | 2.6 Hybrid and Geometry Dependent Hybrid Model | 34 |
| | References | 38 |
| CHAPTER-III | Computer Code | 41 |
| | 3.1 Different Calculations with code | 42 |
| | 3.2 Subroutine List in ALICE/LIVERMORE-82 | 44 |
| | 3.3 Formulation | 47 |
| | 3.4 Use of the Code | 53 |
| | References | 56 |
| CHAPTER-IV | 4.1 Techniques of Measurement | 58 |
| | 4.2 Sample Preparation | 60 |
| | 4.3 Calibration of Detector | 61 |
| | 4.4 Detector Efficiency | 61 |
| | 4.5 Irradiations | 63 |
| | 4.6 Counting of Produced Activity | 65 |
| | 4.7 Formulation | 68 |
| | 4.8 Experimental Results | 72 |
| | References | 163 |

CHAPTER-V Results and Discussion 165

5.1 Measured Results 166

5.2 Theoretical Predictions 185

5.3 Discussion of the Results 187

References 201

List of Publication and Research Papers 203

# CHAPTER-I

## INTRODUCTION

The study of nuclear reactions has been one of the most interesting topics since last several years. The nuclear reactions are understood in terms of three mechanisms, viz., the direct reactions, the compound nuclear reactions and the pre-compound or pre-equilibrium process. In direct reactions only a few nucleons are involved and the emitted particle comes out in a time of the order of the time taken by the projectile to go through the nucleus or $\sim 10^{-22}$ sec. while the compound nuclear reaction takes place at the end of very large number of internal collisions and therefore takes compratively a long time ($\sim 10^{-16}$ sec.). In between the direct reaction and the compound nucleus reactions intermediate processes are likely to occur. A series of complicated collisions inside the nucleus follows the initial interaction and there is certain probability for particle emission after each one of these collisions. The intermediate process may be attributed to the pre-equilibrium emission . Today the accelerator technology is very much developed, therefore a beam of high energy particle like proton, deuteron, and heavy ions is easily available with the help of accelerating machines, such as the Van-de-Graaff generator, the cockroft Walton accelerator, the

cyclotron, and the pelletron. Particle beams so obtained may be used for the bombardment with a variety of targets and this facility enables us to study experimentally various types of nuclear reactions and phenomena, produced in nuclides covering the periodic table.

The study of nuclear reactions provides knowledge about the nature of nuclear forces and nuclear structure such as shell effect [1,2] nuclear density [3] and the nuclear reaction mechanisms [1,2,4-8]. The study is also useful in the construction of nuclear level schemes. The only way to delve the secretes of nucleus is, to send in a probe particle and to study the outcome. In practice the target is bombarded with a beam of particles.

In the beginning only the direct and compound nucleus reactions were known. The compound nucleus mechanism is more appropriate at relatively lower energies, while the direct reaction mechanism is more probable at higher energies of excitation. According to the compound nucleus theory, the reaction takes place in two steps. First the formation of the compound nucleus and sharing of incident energy among all the nucleon and in second step the compound nucleus decays to the final products [10]. The mode of decay and formation of the compound nucleus are different to each other, except for the requirement of various conservation laws [11,12]. In direct reactions, the incoming particle goes directly into an empty particle orbit of the target nucleus. The excess energy of the

particle is emitted in the form of gamma radiations. After the development of isochronous cyclotron in 1960, the projectiles excited upto very high energies became available [13] and the experimental features of the nuclear reactions were studied by several investigators and they pointed out that some reactions took place in between of the time scale of the direct reaction and the compound nucleus reaction. They manifest themselves in high energy tails of the excitation function, non-Maxwellian hard components in the particle spectra and a gradually changing pattern of angular distributions, from forward peaking to fore- and -off symmetry. These new experimental features could neither be explained by compound nucleus model nor by direct reaction model [14-16]. The energy spectrum of a particle in high energy nuclear reaction is shown in fig. 1. In this figure the broad peak in the low energy region corresponds to evaporation from a compound nucleus, while the sharp peaks in the high energy region correspond to population of low lying states in the residual nucleus which can be attributed to the direct reactions. The smooth distribution in between these two extremes may be attributed to the pre-compound or pre-equilibrium decay [1,3,17].

The pre-equilibrium may be considered as a bridge between the two extremes [18-24]. A series of complicated collisions inside the nucleus follows the initial interaction and there stands a certain probability for particle emission after each one of these collisions. In these intermediate processes the selectivity of the direct reactions is lost. Also only a few

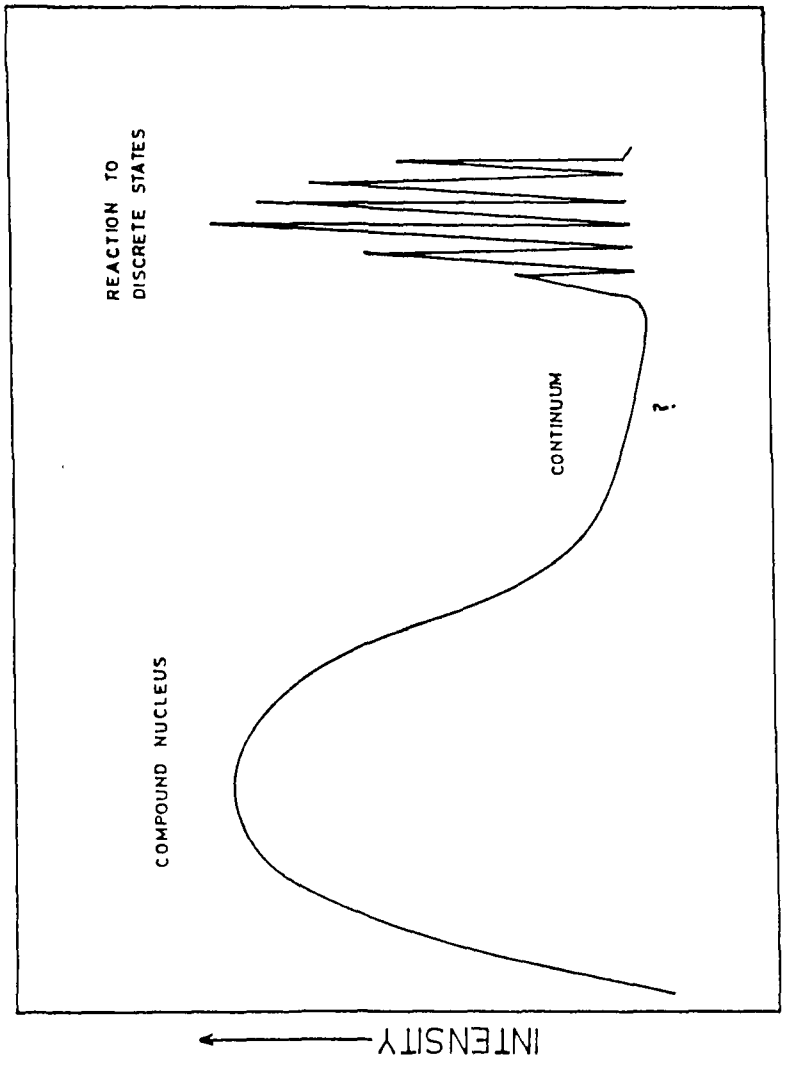


Fig. 1 Typical particle spectrum obtained in a high energy nuclear reaction.

degrees of freedom are involved i.e. the number of excited particles and holes which share the excitation energy of the intermediate system is small. The study of pre-equilibrium phenomena is useful in fusion reactor design [25], radiotherapy [26], space explorations [27] and astrophysics [28]. As the exact law governing the nucleon-nucleon interaction is unknown, so it is not possible to give a general mathematical description of a nuclear reaction. Which is a many-body nucleon-nucleon interaction. As an alternative, the model approach is used to explain the facts. These models are proposed on reasonable assumptions and guided by some experimental observations without really solving the dynamics of many body systems [29]. The most important models are (1) Intranuclear cascade model (2) Harp-Miller-Berne model (3) Exciton model (4) Hybrid model (5) Geometry dependent hybrid model.

The intranuclear cascade (INC) model gives a classical approach to precompound decay [30,31]. The trajectories of the nucleons are followed one at a time during the cascade until some arbitrary energy generally considerably above the average equilibrium value has been attained by the nucleon (Monte Carlo methods) [32]. The numerical simulation of the scattering process is based on experimental free nucleon-nucleon scattering cross-sections and angular distribution. Upto 1975, this was the only pre-equilibrium model capable to predict angular distributions of emitted particles.

The Harp, Miller and Berne (HBM) [33] model suggested in 1969 can predict both shape and absolute cross-section of spectra. This model is associated with a couple of differential equations to solve the problems by computer and can be applied to nuclear induced reaction at moderate excitation energy [13]. The total excitation energy of the nucleons is divided into bins. The number of single particle levels in each bin is calculated using a Fermi gas distribution and stored. The occupation of nucleons in each bin changes in time due to the intranuclear collisions. The evolution of this excited nuclear Fermi gas is followed through numerical computation of the relative occupation of each bin as a function of time by solving the set of coupled differential equations. The internal transition and the particle emission into the continuum are calculated statistically and the cross-section for each process is divided accordingly. The two-body transition rates are calculated using nucleon-nucleon scattering cross-sections and transition rates into the continuum are calculated by using inverse cross-sections and free particle phase space factors. In the contrast to the INC model. This model permits a quantum-statistical treatment, although in practice the transition rates are computed in a classical manner. However, it can not predict angular distributions. Another practical disadvantage of the Harp-Miller-Berne model is its computational complexity. To remove this problem of computational complexity, the exciton and hybrid models are developed by taking additional assumptions.

The exciton model is capable to explain the similarities of spectral components beyond the evaporation maxima from different targets [14]. This model was proposed by Griffin. In this model each state is characterized by the number of excited particles (p) plus holes (h) defined with respect to the Fermi energy of the targets and assume a statistical population of these states in the equilibration sequence. With increase of particle (p) and hole (h) number towards the equilibration value, the probability of emission of any particle decreases exponentially and hence the emission rate. Instead of tracing the evolution of the occupation of each energy bin as in the HMB model, one merely traces the temporal development of the exciton number $n_o$, which changes in time, as a result of intranuclear collisions. This assumption makes pre-equilibrium theory emenable to practical calculations.

The hybrid model proposed by Blann in 1971, is the combination of simplifying aspects of HMB model and Griffin model [34,35]. Excited particles population during equilibration are calculated assuming equally spaced single particle states, classified according to the number of particles and holes they contain as in Griffin exciton model. The intranuclear transition rates (Matrix element) are determined from free nucleon-nucleon scattering cross-section as in HMB model. A further formulation is made in which nuclear geometry effects are also considered and the modified model is named as geometry dependent hybrid model [13]. The detail of these models is given in the chapter II.

Bohr bombarded the gold foil with α-particle and observed the outcomes, to calculate the size of nucleus. This particle is still regarded as most useful probe for learning the shape of the nucleus. Due to the complex structure, it interacts with the matter in a complicated way. However, its attenuation in nuclear matter restricts the interaction to the low density surface region of the nucleus, particularly if the alpha particle bombarding energy is not too high. In the high energy nuclear reaction studies the α-particle is regarded as an important projectile. It helps in populating the high angular momentum states by imparting [4] the considerable angular momentum to the target nucleus and hence various types of the nuclear reactions can be studied.

A lot of work has been done on nuclear reactions covering almost whole periodic table [36-43]. The situation of reaction mechanism is not satisfactory over a wide range of periodic table and energy of projectiles. The experimental results observed by different group of workers are not in good agreement with the results calculated theoretically. In order to have a more accurate knowledge, it is necessary to measure the reaction cross-section.

In the present experiment the α-induced reactions in $^{113}In$, $^{115}In$; $^{121}Sb$, $^{123}Sb$, $^{191}Ir$, $^{193}Ir$ have been studied. For this purpose, the targets made of natural indium, antimony and iridium were bombarded separately, with the beam of α-particles of 50 MeV, 55 MeV, and 55 MeV respectively and the stack foil activation

technique was followed. This α-particles beam was obtained from Variable Energy Cyclotron Centre, Calcutta and the activities were counted by analyzing the gamma rays emitted from residual nuclei in the time lapse between the bombardment of the target foils and the counting of the gamma rays emitting from them. The characteristic gamma rays were detected by 100 $cm^3$ ORTEC Ge(Li) detector. The gamma ray spectra were taken with the help of pre-calibrated multichannel analyser and associated electronics. Other experimental details are given in chapter IV. The excitation function for $^{113}In(\alpha,n)^{116}Sb$, $^{113}In(\alpha,2n)^{115}Sb$, $^{115}In(\alpha,n)^{118}Sb$, $^{115}In(\alpha,2n)^{117}Sb$, $^{115}In(\alpha,3n)^{116}Sb$, $^{115}In(\alpha,pn)^{117}Sn$, $^{115}In(\alpha,2p)^{117}In$, $^{121}Sb(\alpha,n)^{124}I$, $^{121}Sb(\alpha,2n)^{123}I$, $^{121}Sb(\alpha,4n)^{122}I$, $^{121}Sb(\alpha,p3n)^{121}Te$ $^{123}Sb(\alpha,n)^{126}I$, $^{123}Sb(\alpha,3n)^{124}I$, $^{123}Sb(\alpha,4n)^{123}I$, $^{191}Ir(\alpha,n)^{194}Au$, $^{191}Ir(\alpha,2n)^{193}Au$, $^{191}Ir(\alpha,3n)^{192}Au$, $^{191}Ir(\alpha,4n)^{191}Au$, $^{191}Ir(\alpha,5n)^{190}Au$, $^{193}Ir(\alpha,3n)^{194}Au$, $^{193}Ir(\alpha,4n)^{193}Au$ and $^{193}Ir(\alpha,5n)^{192}Au$ have been measured. The pre-equilibrium fraction for these elements have also been estimated.

The excitation function of the aforesaid reactions have also been calculated theoretically. These calculations were done by using ALICE/LIVERMORE-82 [44] computer code. This code helps in calculations of pre-equilibrium, compound/statistical fission in the general framework of Weisskopf-Ewing evaporation model [45], the Bohr-Wheeler model [46,47] for fission and the hybrid and geometry dependent hybrid model [34,35] for pre-equilibrium decay. It is very much useful for the study of excitation functions of neutron, proton, deuteron and α-particle induced reactions. The

less necessity of the input parameters makes it more purposeful. There are very few options to the user. Other details of the code are given in the chapter III. A comparison between the excitation functions measured experimentally and calculated theoretically is also made and it is found that the experiment is in good agreement with the theory. The detailed discussion of the comparison is given in chapter V.

The excitation functions for the reactions in $^{113,115}In$ and $^{191,193}Ir$ have been reported for the first time to the best of our knowledge [48,49].

## REFERENCES

[1] M. Blann and G. Markel: Phys. Rev. B137 (1965) 367.

[2] W.W. Bowman and M. Blann: Nucl. Phys. A131 (1969) 513.

[3] A.R. Barnett and J.S. Liley: Phys. Rev. C9 (1974) 2010.

[4] T. Matsuo, J.M.Matuszek, Jr., N.D. Dudey and T.T. Sugihara: Phys. Rev. B139 (1965) 886.

[5] E.T.Chulick and J.B. Natowitz: Nucl. Phys. A173 (1971) 487.

[6] A. Djaloeis, P. Jahn, H.J. Probst and C. Mayer-Boricke: Nucl . Phys. A250 (1975) 149.

[7] C.L. Branquinho, S.M.A. Hoffmann, G.W.A. Newton, V.J. Robinson, H.Y. Wang and I.S. Grant: J. Inorg.Nucl. Chem. 41 (1979) 617.

[8] P. Misaelides and H. Munzel: J. Inorg.Nucl. Chem. 42 (1980) 937.

[9] G.W.A. Newton, V.J. Robinson and E.M. Shaw: J. Inorg.Nucl. Chem. 43 (1981) 1739.

[10] I.A. Rizvi: Ph.D. Thesis, A.M.U. (1988).

[11] J.M.Marrion and J.L.Fowler: Fast Neutron Physics, (Interscience Publishers, New York, 1963) Part II, 1525.

[12] R.R. Roy and B.P. Nigam: Nucl. Phys. (John Wiley and Sons Inc., New York, 1967) 200.

[13] Emilio Segre, J. Robb Groves, H. Pieere Mays: Ann. Rev. Nucl. Sci. 25 (1975) 124.

[14] V.A. Sidorov: Nucl. Phys. 35 (1965) 253.

[15] C. Holbrow, H. Barschall: Nucl. Phys. 42 (1963) 264.

[16] R. Wood, R. Brochers, H. Barschall: Nucl. Phys. 71 (1965) 529.

[17] J.M. Blatt and V.F. Weisskopf: Theoretical Nuclear Physics, John Wiley and Sons, 1952.

[18] M. Blann: Ann. Rev. Nucl. Sci. 25 (1975) 123.

[19] E. Gadioli and E. Gadioli Erba: Nuclear Theory for applications 1980, IAEA-SMR-68/1, Vienna (1981) p. 3.

[20] H. Feshbach, A.K. Kerman and S. Koonin: Ann. Phys. (N.Y) 125 (1980) 429.

[21] P.E. Hodgson: Heavy Ion Collisions-Proc. of Inter. Summer School, La-Rabida, Spain, 1982, p.220.

[22] H. Jahn: Nuclear Theory for applications- 1982, IAEA-SMR-93, Vienna (1984) 39.

[23] V.E. Bunakov: Nuclear Theory Applications-1978, IAEA-SMR-43, Vienna (1980) 255.

[24] H. Jahn: Nuclear Theory for Applications-1978, IAEA-SMR-43, Vienna (1980) 239.

[25] BNL Report BNL-NCS-50681, 1977 (unpublished).

[26] U. Klein, G. Buche, W. Kluge, H. Matthay and G. Mechtersheimer: Nucl. Phys. A329 (1979) 339.

[27] V.V.Verbinski and W.R. Burrus; Phys. Rev. 177 (1969) 1671.

[28] C.K. Garret and A.L. Twikervich: Phys. Rev. C8 (1973) 594.

[29] N. Austen: Direct Nuclear Reaction Theories (Willey Interscience, New York) (1965).

[30] H.W. Bertini, G.D. Harp and F.E. Bertrand: Phys. Rev. C10 (1974) 2472.

[31] K. Chen, G. Friedlander, G.D. Harp and J.M. Miller: Phys. Rev. 166 (1968) 949.

[32] H. Gruppelaar, P. Nagel and P.E. Hodgson: Revista del Nuo Cim. 9 No. 7.1 (1986).

[33] G.D. Harp, J.M. Miller and B.J. Berne: Phys. Rev. 165 (1968) 1166.

[34] M. Blann: Phys. Rev. Lett. 27 (1971) 337, 27 (1971) 700 (E), 27 (1971) 1550 (E).

[35] M. Blann: Phys. Rev. Lett. 28 (1972) 157.

[36] H.D. Bhardwaj and R. Prasad: Nucl. Instr. Method A242 (1985) 286.

[37] M. Ismil and A.S. Divatia Pramana J. Phys. 30(1988) 193.

[38] I.A. Rizvi, M.K. Bhardwaj, M. Afzal Ansari and A.K. Chaubey, Appl. Radiat. Isot. 41 (1990) 215.

[39] A.K. Chaubey, M.K. Bhardwaj, R.P. Gautam, R.K.Y. Singh, M. Afzal Ansari, I.A. Rizvi and H. Singh: Appl. Radiat. Isot. 41 (1990)401.

[40] I.A. Rizvi, M.K. Bhardwaj, M. Afzal Ansari and A.K. Chaubey, Can. J. Phys. 67 (1989) 1091.

[41] H.D. Bhardwaj, A.K. Gautam and R. Prasad: Pramana - J. Phys. 31 (1988) 109.

[42] I.A. Rizvi, M.K. Bhardwaj, M. Afzal Ansari and A.K. Chaubey: Can. J. Phys. 67 (1989) 870.

[43] I.A. Rizvi, M. Afzal Ansari, R.P. Gautam, R.K.Y. Singh and A.K. Chaubey: J. Phys. Soc. Jpn. 56 (1987), 3135.

[44] M. Blann and J. Bisplinghoff, ALICE/LIVERMORE-82 Lawrence Livermore National Laboratory Report UCID 19614 (1982).

[45] V.F. Weisskopf and D.H. Ewing: Phys. Rev. 57 (1940) 472.

[46] N. Bohr and J.A. Wheeler: Phys. Rev. 56 (1939) 426.

[47] R. Vandenbosch and J.R. Huizenga: Nuclear Fission (Academic Press, New York) (1973).

[48] M.K. Bhardwaj, I.A. Rizvi and A.K. Chaubey: IJMPE (Accepted for publication) 1992.

[49] M.K. Bhardwaj, I.A. Rizvi and A.K. Chaubey: Phys. Rev. C Vol. 45 No. 5, (1992) 2338.

# CHAPTER-II

## NUCLEAR REACTION THEORIES

Today the accelerator technology is very much developed, therefore easily a beam of light particles as well as the heavy ions can be obtained for the bombardment with a variety of targets. However, unlike the electro magnetic interactions, the exact law governing nucleon-nucleon interaction is unknown. Therefore, it is not possible to give a mathematical description of a nuclear reaction which is a many body nucleon-nucleon interaction. As an alternative, the model approach is used to explain the facts. These models are proposed on reasonable assumptions and guided by some experimental observations without really solving the dynamics of many body system [1].

Mostly, on the basis of time, the nuclear reactions are divided into two categories i.e., direct reactions and the compound nuclear reactions. The reactions which occur within the time ($\backsim 10^{-22}$ sec) taken by the projectile to cross the nuclear diameter are called direct reactions while the reactions which take place at the end of very large number of internal collisions and therefore takes comparatively a long time($\backsim 10^{-16}$ sec) are compound nucleus reactions.

In between of the direct and compound nucleus reactions, intermediate processes are likely to occur. These intermediate pro-

cesses are named as the pre-equilibrium decay. The nature of such type of the reactions is different from the compound nucleus reaction and the direct reactions and inexplicable by existing direct reaction or compound nucleus models [2-4]. To explain the experimental facts many semi-classical models have been proposed [5-12]. Apart from these semi-classical models of the nuclear reactions for the successful reproduction of the excitation function data, efforts are in progress to give full quantum mechanical picture [13-19] in the frame work of multistep theories proposed by Feshback et.al.[17] and others [16,18,19]. The semi-classical models which are mostly used to explain the pre-equilibrium decay processes are classified as:

1. Intranuclear Cascade Model
2. Harp-Miller-Berne (HMB) Model
3. Exciton Model
4. Hybrid Model
5. Geometry Dependent Hybrid Model

## 2.1 Compound Nucleus Theory

Bohr [20] in 1936,suggested that a nuclear reaction could be considered to take place in two steps. First, the formation of compound nucleus by the combination of the target nucleus and bombarding particle. Second, the disintegration of compound nucleus into the products of the reaction. The two stages are independent. The compound nucleus can disintegrate in various possible ways

which do not depend on the mode of production. The assumptions are consistant with the idea that the nucleus is made of a number of nucleons held together by short range forces. As the incident particle enters the target, it loses its energy which is shared by all the nucleons in the nucleus before the emission of any particle. The compound nucleus may exist in numerous excited virtual states or levels [21]. In order to calculate the cross-section of a nuclear reaction, the cross-section of two processes should be calculated.

Each excited state of the compound nucleus has a certain mean life-time $\tau$ . The nucleus exists in excited state for a certain average time before the decay with the emission of a particle or a gamma ray. The probability of decay of the compound nucleus is expressed in terms of the energy level width which is given as:

$$\Gamma = \frac{h}{2\pi\tau} = \frac{h\lambda}{2\pi} \qquad \text{.....(2.1)}$$

where $\lambda$ = decay constant.

This level width is regarded as the uncertainty $\Delta E$ in the energy of a state. The total width $\Gamma$ is the sum of the partial width for each mode of decay.

$$\Gamma = \Gamma_a + \Gamma_b + \Gamma_c + \text{..... etc.} \qquad \text{.....(2.2)}$$

The theoretical calculation of cross-section has been

carried out by Breit and Wigner (1936) for an isolated resonance. The result is simply quoted:

$$\sigma(a,b) \; \alpha \left(\frac{\lambda}{2\pi}\right)^2 \frac{\Gamma_a \Gamma_b}{(E-E')^2 + \left(\frac{\Gamma}{2}\right)^2} \qquad \ldots\ldots\ldots(2.3)$$

where

$E'$ = Energy of level of compound nucleus

$E$ = Energy with which compound nucleus is formed

$a$ = Incident particle, $b$ = Outgoing particle

$\lambda$ = de-Broglie wavelength of incident particle

$\sigma(a,b)$ = Reaction cross-section.

This formulation is valid only for the light nuclei where the excited states are widely spaced.

For heavy nuclei, the excited states are very close so that they form an effective energy continuum hence the cross-section is calculated by the processes of averaging over many levels, allowing for the 'overlapping' of neighbouring resonances.

## 2.2 Statistical Theory

The statistical theory is based mainly on the three assumptions. That are (i) The incident and the target nucleus forms a compound nucleus and available excitation energy is distributed among the several particles of the compound nucleus in a random manner, within the $\backsim 10^{-15}$ sec. after the formation

of compound nucleus, the excitation energy possibly concentrate on any one particle which can escape from the nucleus.
(ii) For sufficiently high excitation energy, the overlapping levels are excited and the number of excited levels is too large to be treated individually. This requires Fermi statistics.
(iii) The mode of decay of the compound nucleus is independent of the mode of formation and depends only on its energy (E), angular momentum (J) and parity $\pi$.

In order to calculate the average reaction cross-section ($\bar{\sigma}_{jk}$), the Weisskopf - Ewing statistical model [22] is used. According to this model

$$\bar{\sigma}_{jk} = \sigma_{comp}(j) \left(\frac{G_k}{G}\right) \qquad \ldots\ldots(2.4)$$

where $j$ = Incident particle

$k$ = Outgoing particle

$\sigma_{comp}(j)$ = Cross-section of the compound nucleus

$\frac{G_k}{G}$ = Branching ratio

With application of the assumption of statistical theory, the average total cross-section of the reaction I(j,k)L averaged over many resonance structures may be given as [20,23]

$$\bar{\sigma}_{jk} = \sum_{J,\pi} \sigma_{jk}^{J^{\pi}} \qquad \ldots\ldots(2.5)$$

and with application of the assumption of compound nucleus formation, we have

$$\bar{\sigma}_{jk} = [\sigma_{comp}{}^{J^\pi}(j)] \left[\frac{G_t{}^{J^\pi}}{\Sigma\, G_t{}^{J^\pi}}\right] \qquad \ldots\ldots(2.6)$$

The sum over $t$ runs over all reaction alternatives available to the compound nucleus. As equation (2.6) is now valid for each $J,\pi$ separately, the factorization of the cross-section as in equation (2.6) does not imply that the compound nucleus forgets its total angular momentum and parity [24].

The relation between compound-nucleus cross-section and the branching ratio can be found by the following reciprocity theorem:

$$\frac{\bar{\sigma}_{jk}{}^{J^\pi}}{\bar{\sigma}_{kj}{}^{J^\pi}} = \frac{K_k^2}{K_j^2} \qquad \ldots\ldots(2.7)$$

where $K_k$ and $K_j$ are the wave numbers for the relative motion of the pair $k$ and $j$.

From the equation (2.6) and (2.7), we have

$$G_j{}^{J^\pi} = K_j^2\, \sigma_{comp}{}^{J^\pi}(j) \qquad \ldots\ldots(2.8)$$

Each $\sigma_{comp}(j)$ is found from the optical model absorption cross-section $\sigma_j(abs)$ for the pair $j$. In terms of the complex phase shifts $\delta_{jl}$ of the optical model, we find

$$\sigma_j(\text{abs}) = \frac{\pi}{K_j^2} \sum_{\ell} (2J+1)\,(1 - |e^{2i\delta_{J\ell}}|^2) \qquad \ldots\ldots(2.9)$$

$$= \sum_{J,\pi} \frac{\pi}{K_j^2} \frac{(2J+1)}{(2J_j+1)\,(2J_I+1)} \sum_{I=J-S}^{J+S} \sum_{S=J_I-J_j}^{J_I+J_j} (1 - |e^{2i\delta_{J\ell}}|^2)$$

$$= \sum_{J,\pi} \sigma_{\text{comp}}^{J^\pi}(j) \qquad \ldots\ldots(2.10)$$

where $J_j$ = Spin of the incident particle $j$.

By comparing the equation (2. 8), (2. 9) and (2.10), we get

$$G_j\, J^\pi = \sum_{S,\ell} T_\ell(j) \qquad \ldots\ldots(2.11)$$

where $T_\ell(j) = 1 - |e^{2i\delta_{j\ell}}|^2$

By using the equations (2.6 ), (2.9 ) and (2.11), we find

$$\bar{\sigma}_{jk} = \frac{\pi}{K_j^2} \sum_{J,\pi} \frac{(2J+1)}{(2J_I+1)(2J_j+1)} \Big[\sum_{S,\ell} T_\ell(j)\Big] \Big[\frac{\sum_{S',\ell'} T_{\ell'}(k)}{\sum_{t,S'',\ell''} T_{\ell''}(t)}\Big] \qquad \ldots\ldots(2.12)$$

In this equation $S$ and $\ell$ refer to the incoming channel $j$ of the reaction, $S'$, $\ell'$ refer to the outgoing channel $k$ while $S''$, $\ell''$ are summand over all channels ( t ) to which compound

nucleus can decay. The above expression can also be written as

$$\bar{\sigma}_{jk}^{\mu\nu}(E_j^{\mu}) = \frac{\pi \lambda_j^{2}}{(2J_I^{\mu}+1)(2J_j+1)} \sum_{J,\pi} \frac{(2J+1)\, T_j^{\mu}(J^{\pi})\, T_k^{\nu}(J^{\pi})}{T_{tot}(J^{\pi})} \qquad \ldots\ldots(2.13)$$

where $\bar{\sigma}_{jk}^{\mu\nu}(E_j^{\mu}) = \bar{\sigma}_{jk}$ is the average cross-section for the reaction $I + j \longrightarrow L + K$ when I, L is in the $\mu$ and $\nu$ state respectively. $\mu, \nu$ are representing the bound state in target nucleus I and residual nucleus L respectively.

$T_j^{\mu}(J^{\pi}) = \sum_{S,\ell} T_{\ell}(j)$ is the total transmission function for forming the state $J^{\pi}$ in the compound nucleus by a combination of $I^{\mu}+j$, $T_k^{\nu}(J^{\pi}) = \sum_{S,\ell'} T_{\ell'}(k)$ is the transmission function for the decay of the $J^{\pi}$ into $L^{\nu} + K$, $T_{tot}(J^{\pi}) = \sum_{t,S'',\ell''} T_{\ell''}(t)$ is the total transmission function for the decay of the compound nuclear state with the spin J and parity $\pi$, which is

$$T_{tot}(J^{\pi}) = \sum_{i,\lambda} T_i^{\lambda}(J^{\pi})$$

where i denotes the particle in any combination of nucleus and particle to which compound nuclear state can decay and is any unbound or bound state, in the residual nucleus which is

energetically accessible from $I^{\mu} + j$ interacting with energy $E_j^{\mu}$.

This is the general expression to calculate the total cross-section of the reaction. This is obtained in the frame-work of Hauser-Feshbach statistical theory [21,24,25] of nuclear reaction but in any experiment , total cross-section is taken as the average over all energy states and is given as,

$$\bar{\sigma}_{j,k} = \sum_{\nu} \sigma_{j,k} = \frac{\pi \lambda_j^2}{(2J_I + 1)(2J_j + 1)} \sum_{J,\pi} (2J+1) \frac{T_j(J^{\pi}) \, T_k(J^{\pi})}{T_{tot}(J^{\pi})} \qquad \ldots\ldots(2.14)$$

where

$$T_j(J^{\pi}) = \sum_{\ell, s} T_j(J^{\pi}, \ell, s)$$

and $$T_k(J^{\pi}) = \sum_{\ell', s'} T_k(J^{\pi}, \ell', s')$$

As in practice, generally, the targets are found in its ground state, so $\mu$ is taken as zero.

## 2.3 Intranuclear Cascade Model

First of all this model was proposed by Serber [26] and modification was done by others [27-32] with the moto of explaining the various experimental nuclear reaction data. Diagramatically cascade model can be represented as shown in the fig. 2.1. Here,

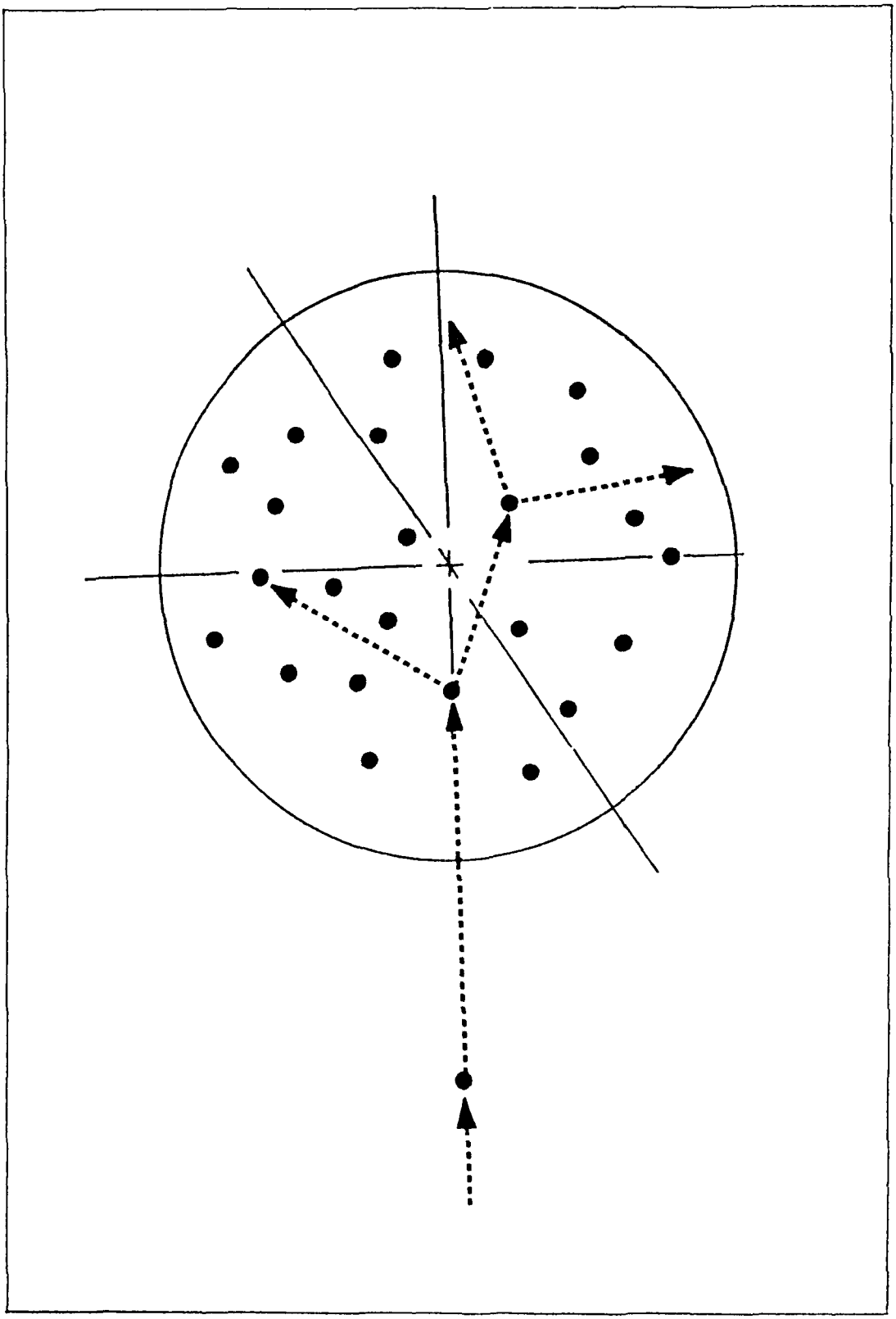

Fig. 2.1 Pictorial representation of the Intranuclear Cascade Model. The nature of the model in following classical trajectories following successive binary collisions is indicated.

it can be seen that the succession of two-body interactions is followed in three diamensional geometry. In the employed method of calculation the trejectories of the nucleons are followed one at a time during the cascade until some arbitrary energy generally considerably above the average equilibrium value has been attained by the nucleon. With the help of such an approach, the time evolution of the reaction can be generated but after few collisions the actual calculation becomes too much complicated. The cascade model is capable to predict angular distribution. No other model is capable to do so. In the medium energy range it does not predict them well.

## 2.4 Harp Miller-Berne (HMB) Model

The physical description of this model [11] is described in the fig.(2.2). Consider the initiation of the reaction at the time $\tau_o$ . Energy bins of width 1 MeV are defined, and the number of single particle level which are available in each bin are calculated using a Fermi gas distribution. The calculation can be made either beginning with some initial arbitrary population of excited particles and holes or with a nucleus in the ground state. In the calculation, the fractional occupation of each bin is taken as a function of time. The rate of allowed transitions of all the nucleons in the nucleus for a given incident nucleon is calculated as is the rate of emission of excited particles into the continuum. Both the internal and the particle

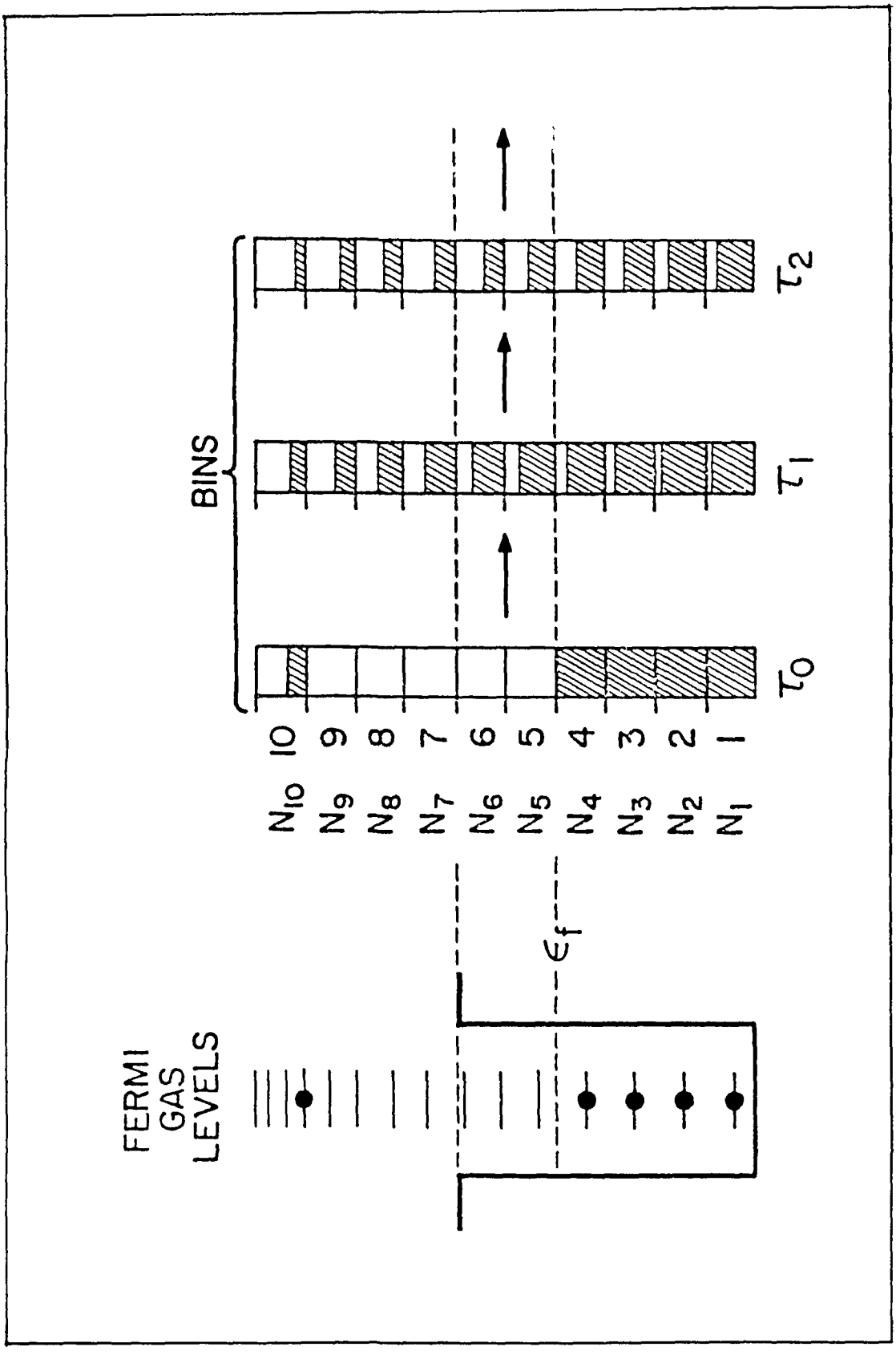


Fig. 2.2 Pictorial representation of the Harp-Millar-Berne Model. The shaded areas represent the occupied fraction of each bin, with occupations changing after each time interval.

emission into the continuum are calculated statistically and the cross-section is divided accordingly. Nucleon-Nucleon scattering cross-sections are used for calculating the two body transition rates with each energy partition being assigned equal-a-priori probability. The two body transmission rates are calculated using free particle phase space factor and inverse cross-sections.

After computing the relative probabilities of scattering into and out of each bin and, of emission from bins above the particle binding energies, population of all bins are changed accordingly, as shown in centre of the fig. 2.2. The calculation is repeated in units of time shorter than the N-N collision time. The equilibrium state in the model is realized by solution of a set of differential equations.

Later, Harp and Miller [6] considered the nucleus as composed of independent proton and neutron Fermi gases . The internal configuration of any nucleus at any instant is specified by the proton and neutron occupation numbers. There is another consideration also that the equilibrium of gases takes place through binary nucleon-nucleon collisions. Correspondingly, a new set of master equation is obtained, the solution of which gives the proton and neutron occupation numbers.

## 2.5 Exciton Model

This model was proposed by Griffin [5]. In this model, the problems of following the bin population in time, in Harp Miller and Berne model, are avoided by substituting the densities of states characterized by particle - hole number with a statistical assumption for the population of each of the intermediate states in the equilibration sequence. The physical illustration of the exciton model is given in the fig. 2.3. In this figure a nucleon is shown entering the nuclear potential in the left. This state is characterized by 1p Oh state. All the fermions are in their ground state. The first interaction may therefore lead to a 2p 1h (two particle and one hole) states, and it is assumed that all configurations of a given exciton state are equally probable. These successive two body interactions may further lead either to 3p 2h state, back to initial 1p Oh state or even to different 2p 1h state. The assumption of probability of the configuration proportional to the density of accessible final states has been taken. The number of particles and holes in the initial configuration are least. The level densities are rapidly increasing functions of increasing particle and hole (p-h) numbers, and the system goes predominantly in the direction of equilibrium as shown in the fig. 2.3 with the larger arrows in that direction. The each intermediate configuration is characterized by the specific particle hole number. Some fraction of these configurations will have atleast one particle with energy

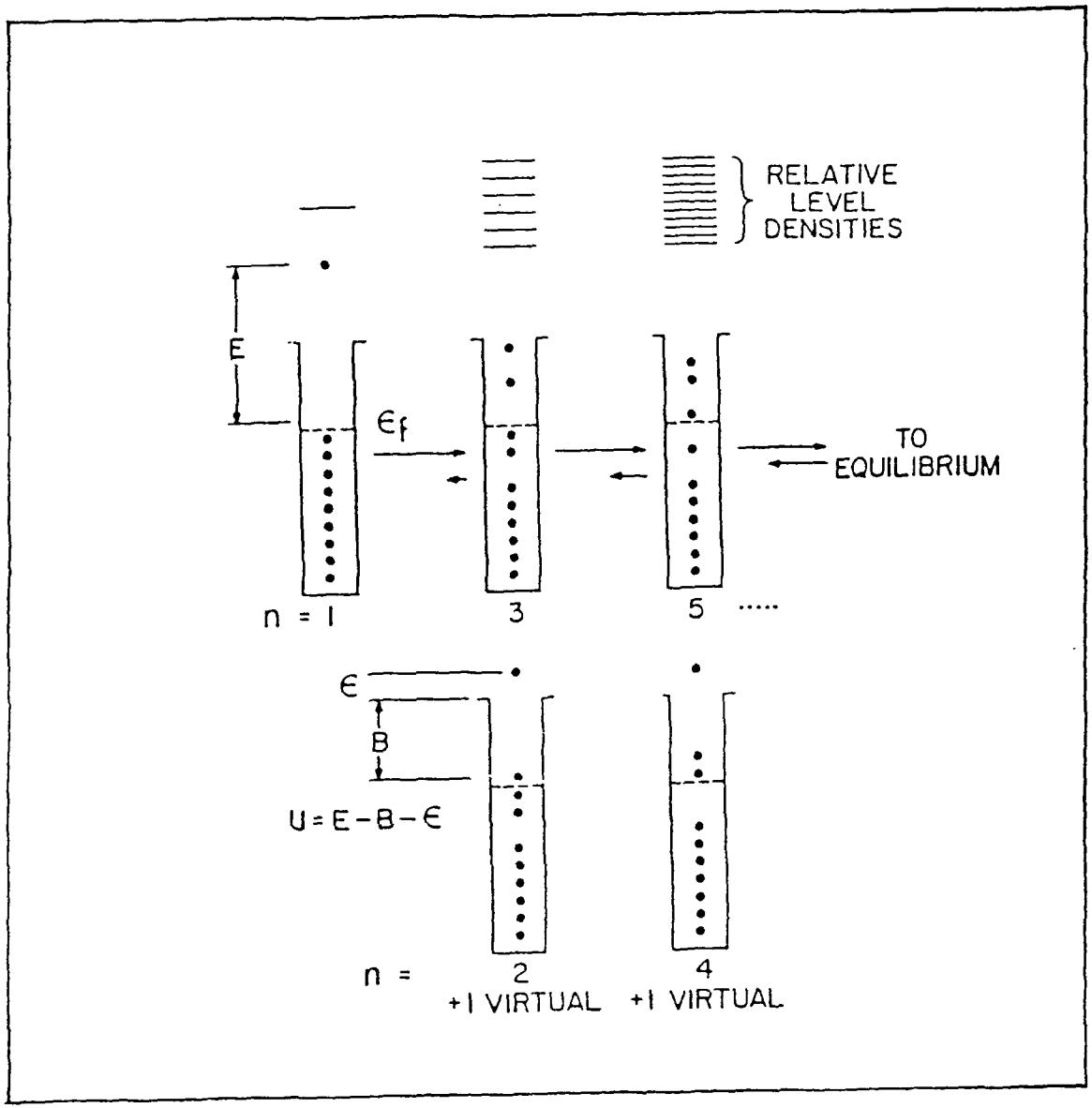


Fig. 2.3 Pictorial representation of the ideas inherent in the exciton model. Successive two-body interactions are indicated with some fraction of each exciton hierarchy having unbound particles.

higher than its binding energy. With the help of this fraction in a given exciton state, the relative probability of emission of a particle from a state of given exciton number can easily be calculated. By summing over the contribution from each state, the total spectrum emitted prior to equilibrium may be calculated on the relative basis.

It is to be noted that for the simplest states there is highest probability of having high kinetic energy particle emission,as the average excitation per particle must be highest. With increasing particle (p) and hole (h) number, the probability of emission of any particle decreases exponentially and hence the emission rate. The main assumption which has been taken in this model is that every configuration of each intermediate state occures with a equal prior probability during the equilibration process.

The role of level density in the exciton model is very important. Single particle densities are often used to calculate the exciton level densities, assuming the nucleus to be degenerated Fermi gas with equi distant levels [28]. The expression of William [33] for the particle-hole density in the uniform spacing model is given below

$$\rho_n(E) = \frac{g[gE - A(p,h)]^{n-1}}{p!\ h!\ (n-1)!} \qquad \text{.....(2.15)}$$

where $n = p+h$

and $A(p,h) = \frac{1}{4}(p^2+h^2) + \frac{1}{4}(p-h) - \frac{1}{2}h$

While the Ericson's expression [34] for calculating the single particle level density $\rho$ at excitation E is given as

$$\rho_n(E) = \frac{g\,(gE)^{n-1}}{p!\,h!\,(n-1)} \qquad \ldots\ldots(2.16)$$

With the assumption that for the n-exciton states, in which at least one particle is at an energy $\epsilon + B$ above the Fermi Energy, the fraction is given as

$$\rho_n(U,\epsilon)/\rho_n(E) = \rho_{p,h}(U,\epsilon)/\rho_{p,n}(E) \qquad \ldots\ldots(2.17)$$

where

U = Excitation energy of the residual nucleus

$\epsilon$ = Channel energy of the emitted particle

The probability of decay from n exciton state is expressed as

$$\rho_n(\epsilon)\,d\epsilon = (2s+1)\left[\frac{\rho_n(U,\epsilon)}{\rho_n(E)}\right] \Omega \cdot \frac{4\pi p^2 dp}{h^3} \cdot \frac{\sigma v}{\Omega}\,\tau_n \qquad \ldots\ldots(2.18)$$

Where $\tau_n$ denotes the life time of an n exciton state, the other factors being the particle spin degeneracy, the phase space and penetrability factors. The total decay probability can be obtained from equation (2.18) by substituting for level densities

from equation (2.15) and summing it from initial exciton number $n_o$ to equilibrium exciton number $\bar{n}$ in steps of $\Delta n = +2$

$$\rho(\epsilon)\, d\epsilon = \sum_{n=n_o}^{\bar{n}} \rho_n(\epsilon)\, d\epsilon$$

$$= \frac{(2s+1)\, m\epsilon\, \sigma}{\pi^2 \hbar^3\, gE} \sum_{\substack{n=n_o \\ \Delta n=+2}}^{\bar{n}} \left(\frac{U}{E}\right)^{n-2} p(n-1)\ \tau_n\, d\epsilon \qquad .....(2.19)$$

The value of the mean life time $\tau_n$ can be calculated on the relative basis [35] given as following

$$\lambda_{n,n'} = \frac{1}{\tau_n} = \frac{2\pi}{\hbar} |M|^2\ \rho_{n'}(E) \qquad .....(2.20)$$

where

$|M|$ = Matrix element for the residual two body interaction

$\rho_{n'}(E)$ = The density of accessible final state

$\lambda_{n,n'}$ = Transition rate from an initial exciton state (n) to a final state (n').

The expressions for the internal transition ratios given by the Willium [33] are following :

$$\lambda_+ = \frac{2\pi}{\hbar} |\bar{M}|^2\ \frac{g^3 U^2}{(n+1)} \qquad .....(2.21)$$

$$\lambda_- = \frac{2\pi}{\hbar} |\bar{M}|^2 \; g \; p \; h \; (n-2) \qquad .....(2.22)$$

$$\lambda_o = \frac{2\pi}{\hbar} |\bar{M}|^2 \; g^2 \; U \left[\frac{1}{4}(3n-2)\right] \qquad .....(2.23)$$

where

$\lambda_+$ = Relative internal transition ratio for $\Delta n = +2$

$\lambda_-$ = Relative internal transition ratio for $\Delta n = -2$

$\lambda_o$ = Relative internal transition ratio for $\Delta n = 0$

It may be seen from these results that $\lambda_{n+2} >> \lambda_{n-2}$ if $n << \bar{n}$. Assuming that $\lambda_{n+2} = \lambda_{n-2}$ at equilibrium $(n = \bar{n})$, it follows that

$$\bar{n} = \sqrt{2gE} \qquad .....(2.24)$$

The matrix element $|M|$ for residual two body interaction is not well known. In the expression,given by William, the average matrix element $|\bar{M}|$ is used. It is reasonable to assume the energy independent matrix elements [8] and energy dependent matrix elements at low and high excitation energies respectively. The expression for the energy dependence of matrix element given by the Kalbach-Cline [36] is as following:

$$|\bar{M}|^2 = F \; M. \; A^{-3} \; E^{-1} \qquad .....(2.25)$$

where A = Mass number

E = Excitation energy of the compound system

FM = An adjustable parameter ranging from 95-7000 $MeV^3$ [37]

Recently proposed expressions [38] for the residual two body matrix element are as following:

$$|\bar{M}|^2(n,E) = \frac{FM}{A^3 e}\left(\frac{e}{7\ MeV}\right)^{1/2}\left(\frac{e}{2\ MeV}\right)^{1/2} \quad e < 2\ MeV \qquad .....(2.26)$$

$$|\bar{M}|^2(n,E) = \frac{FM}{A^3 e}\left(\frac{e}{7\ MeV}\right)^{1/2} \quad 2\ MeV \leqslant e < 7\ MeV \qquad .....(2.27)$$

$$|\bar{M}|^2(n,E) = \frac{FM}{A^3 e} \quad 7\ MeV \leqslant e \leqslant 15\ MeV \qquad .....(2.28)$$

$$|\bar{M}|^2(n,E) = \frac{FM}{A^3 e}\left(\frac{15\ MeV}{e}\right)^{1/2} \quad 15\ MeV < e \qquad .....(2.29)$$

Where $e = \frac{E}{n}$ is called the average excitation energy per exciton.

## 2.6 Hybrid And Geometry Dependent Hybrid Model

In the hybrid model, the fraction of pre-equilibrium decay is predicted. This fraction of pre-equilibrium decay is considered as the function of excitation energy, target mass and charge, and

the type of projectile. This model was proposed by Blann [9] and is incorporated by the basic principles of the exciton model and those of the Harp-Miller and Berne (HMB) model. In this model the excited particle populations during equilibration are calculated using partial state densities according to the exciton model. The calculation of intranuclear transition rates of the excited particles are done from the calculation of mean free path of nucleons in nuclear matter as in the HMB model. The mean free paths are evaluated either from N-N scattering cross-section or from imaginary optical potential [39]. Finally, this mean free path is divided by particle velocity to obtain the nuclear transition rates. The expression to calculate the pre-equilibrium decay probability in the hybrid model is given as [7,40]

$$P_x(\epsilon)d\epsilon = \sum_{n=n_o}^{\bar{n}} \left[nP_x \frac{\rho_{p,h}(U,\epsilon)}{\rho_{p,h}(E)} g\, d\epsilon\right] \left[\frac{\lambda_c(\epsilon)}{\lambda_c(\epsilon) + \lambda_{n+2}(\epsilon)}\right] D_n$$

$$= \sum_{n=n_o}^{\bar{n}} n\, P_x(\epsilon)d\epsilon \qquad \text{.....(2.30)}$$

where

$n P_x$ = The number of particles of the type $x$

$\left[n P_x \frac{\rho_{p,h}(U,\epsilon)}{\rho_{p,h}(E)} g d\epsilon\right]$ = The number of particles of type $x$ emitted in the energy range $\epsilon$ to $\epsilon + d\epsilon$ and $U = E - B\nu$ ,

$$\left[\frac{\lambda_c(\epsilon)}{\lambda_c(\epsilon) + \lambda_{n+2}(\epsilon)}\right] = \text{The probability of the particles being emitted into the continuum}$$

$\lambda_c(\epsilon)$ = Rate of intranuclear transitions

Dn = Population surving particle emission from simpler states.

A further formulation [10] was made in which nuclear geometry effects were also considered and was named as the geometry dependent hybrid model. This model is based on the impact parameters for the partial waves initiating the reaction. It was assumed that the reaction initiated by each partial wave proceeds in the spherical shell-shaped region of thickness with radius defined by the initial impact parameter. In pre-equilibrium formulism, the diffused surface properties sampled by the higher parameters were crudely incorporated. In GDH model, the energy differential pre-equilibrium cross-section for particle emission is given as

$$\frac{d\sigma x(\epsilon)}{d\epsilon} = \pi \lambda^{2} \sum_{\ell=0}^{\infty} (2\ell+1)\, T_{\ell}\, P_x(1,\epsilon) \quad \ldots\ldots(2.31)$$

The pre-equilibrium decay probability is calculated as the function of nuclear level density. This nuclear level density is given by the Fermi density distribution as

$$d(R_1) = ds\,[\exp(R_\ell - C)/0.55\ \text{fm} + 1]^{-1} \qquad \ldots\ldots\ldots(2.32)$$

where $ds$ = saturation density of nuclear matter

$C$ = Charge radius

$R_\ell$ = Radius of $\ell$th partial wave

This charge radius can be given as [41,42]

$$C = 1.18\,A^{1/3}\left[1-\left(\frac{1}{1.18\,A^{1/3}}\right)^{2}\right] + \qquad \ldots\ldots\ldots(2.33)$$

and this $R\ell$ can be expressed as

$$R_\ell = \lambda(R + 1/2) \qquad \ldots\ldots\ldots(2.34)$$

The Fermi energy $\epsilon_F$ and single particle level density $(g_x)$ are dependent of nuclear matter density and this may be given as

$$\epsilon_F(R_\ell) = \epsilon_F\,[\,<d(R_\ell)>\,/\,ds]^{2/3}\ \text{MeV} \qquad \ldots\ldots\ldots(2.35)$$

and

$$g_x(R_\ell) = [\epsilon_F\,/\,\epsilon_F(R_\ell)]\,[A/28] \qquad \ldots\ldots\ldots(2.36)$$

where

$E_F$ = Fermi energy at the saturation of density

$x$ = type of particle

## REFERENCES


[1] N. Austen, Direct Nuclear Reaction Theories [Willey Interscience, New York] (1965).

[2] V.A. Sidorov: Nucl. Phys. 35 (1965) 253.

[3] C. Holbrow and H. Barschall: Nucl. Phys. 42 (1963) 264.

[4] R. Wood, R. Broschers and H. Barschall: Nucl. Phys. 71 (1965) 529.

[5] J.J. Griffin: Phys. Rev. Lett. 17 (1966) 478.

[6] G.D. Harp and J.M. Miller: Phys. Rev. C3 (1971) 1847.

[7] M. Blann: Ann. Rev. Nucl. Sci. 25 (1975) 123.

[8] E. Gadioli, E. Gadioli Erba and P.G. Sona: Nucl. Phys. A217 (1973) 589.

[9] M. Blann: Phys. Rev. Lett. 27 (1971) 337; 27 (1971) 700 (E); 27 (1971) 1550 (E).

[10] M. Blann: Phys. Rev. Lett. 28 (1972) 757.

[11] G.D. Harp, J.M. Miller and B.J. Berne: Phys. Rev. 165 (1968) 1166.

[12] C.K. Cline and M. Blann: Nucl. Phys. A172 (1971) 225.

[13] D. Agassi, H.A. Weidenmuller and G.Matnzouranis: Phys. Rev. 22 (1975) 145.

[14] T. Tamura, T. Udagawa, D.H. Feng and K.K. Kan : Phys. Lett. B68 (1977) 109.

[15] T. Tamura and T. Udagawa: Phys. Lett. B78 (1978) 189.

[16] P.E. Hodgson, Workshop on Applied Nuclear Theory and Nuclear model calculations for Nuclear Technology Applications, Report ICTP, SMR/204-5 (1988).

[17] H. Feshback, A. Kerman and S.E.Koonin: Ann. Phys. 125 (1980) 429.

[18] L. Avaladi, R. Bonetti and L. Colli-Milazzo: Phys. Lett. 94B (1980) 463.

[19] G.M. Field, R. Bonetti and P.E. Hodgson: J. Phys. G12 (1986) 93.

[20] N. Bohr: Nature 137 (1936) 344.

[21] P.E. Hodgson; Nuclear Reactions and Nuclear Structure, (Calarendon Press, Oxford, 1971) 284.

[22] V.F. Weisskopf and D.H. Ewing: Phys. Rev. 57 (1940) 472.

[23] M. Afzal Ansari; Ph.D. Thesis, Aligarh Muslim University, Aligarh (1982).

[24] E. Vogt: Advances in Nuclear Physics, (Plenum Press, New York, 1968) Vol. I, 261.

[25] W. Hauser and H. Feshbach: Phys. Rev. 87 (1952) 366.

[26] R. Serber: Phys. Rev. 72 (1947) 1114.

[27] H.W. Bertini: Phys. Rev. 131 (1963) 1801.

[28] K. Chen, G. Friedlander and J.M. Miller: Phys. Rev. 176 (1968) 1208.

[29] K. Chen, G. Friedlander, G.D. Harp and J.M. Miller: Phys. Rev. C4 (1974) 2234.

[30] H.W.Bertini:Phys. Rev. C5 (1972) 2118: C6 (1973) 1045.

[31] K. Cehn, Z. Fraenkel, G. Friedlander, J.P. Grover, J.M. Miller and Y. Shimamoto: Phys. Rev. 166 (1968) 949.

[32] H.W. Bertini, G.D. Harp and F.E. Bertrand: Phys. Rev. C10 (1974) 2472.

[33] F.C. Williams Jr: Nucl. Phys. A166 (1971) 231.

[34] T. Ericson: Adv. Phys. 9 (1960) 425.

[35] M. Blann: Phys. Rev. Lett 21 (1968) 1357.

[36] C. Kalbach-cline: Nucl. Phys. A210 (1973) 590.

[37] K.K. Gudima, S.G. Mashnik and V.D. Toneev: Nucl. Phys. A401 (1983) 329.

[38] C. Kalbach: Z. Phys. A287 (1978) 319.

[39] M. Blann: Nucl. Phys. A213 (1973) 570.

[40] M. Blann: Lecture given in 'Workshop on Applied Nuclear Theory and Nuclear Model Calculations for Nuclear Technology Applications' 15 Feb. - 18 March, 1988, ICTP, Trieste (Italy).

[41] M. Blann and H.K. Vonach: Phys. Rev. C28 (1983) 1475.

[42] I.A. Rizvi: Ph.D. Thesis, Aligarh Muslim University, Aligarh (1988).

# CHAPTER-III

## COMPUTER CODE

The computer can be defined as a device which automatically performs logical operations on the input information or data and outputs the answers according to the preplanned set/code of instructions stored within it. Obviously, it is the programmer who does all the thinking required to figure out how to solve different problems. A user can use the computer without knowing much about it. Different type of the codes are required for different types of the calculations. Presently, to calculate the excitation function of the nuclear reactions, ALICE/LIVERMORE-82 [1] computer code has been used. This is made for doing the calculations of pre-equilibrium, compound/statistical fission in the general framework of the Weisskopf-Ewing evaporation model [2], the Bohr-Wheeler model [3,4] for fission and the hybrid and geometry dependent hybrid models [5-7] for pre-equilibrium decay. This code is the revised version of the ALICE [8] and OVERLAID ALICE [9] codes. ALICE/LIVERMORE-82 computer code is used to calculate the excitation function of neutron, proton, deuteron and $\alpha$-particle induced reactions. This code is best in view of the less requirements of code space and running time. It requires least necessary input parameters of the target nuclei and leaves very few options to the user.

## 3.1 Different Calculations With Code

This code can successfully perform the calculations and combinations of the following types:

(1) In this code the calculations are based on standard Weisskopf Ewing Model [2]. The emitted particle in reactions may be either neutron ; neutron and deuteron; neutron, proton and alpha; or neutron, proton, alpha and deuteron. The reactions in which the compound nucleus are of the excitation energy upto 200 MeV can be studied. Residual nuclei of a grid 11 mass unit wide by 9 atomic numbers deep may be calculated as the code is presently dimensioned. In the output the particle spectra can be selected as in addition to individual product yields and fission cross-sections.

The evaporation cascade can be computed with 1 MeV bin width with the method described in literature [10].

In this code, the inverse reaction cross-section may either be read-in from cards, computed with a classical sharp cutoff model or by default are computed by a optical model subroutine.

(2) The upper limit to the enhancement of gamma-ray de-excitation due to answer momentum effects is obtained by the selection of an s-wave approximation [11,12]. In this option the calculation of (1) is performed for every partial wave in

the entrance channel and it is assumed that the rotational energy for each partial wave irrevocably committed to rotational motion and therefore unavailable for particle emission. The selection of rotational energy versus J may be done either as the rigid spherical rotor value or from the equilibrium deformed rotating liquid drop model of Cohen et al.[13]. The transmission coefficients for entrance channel partial waves have been provided by parabolic model [14] routine for alpha particle or by the optical model routine.

(3) Using angular momentum dependent ground state and saddle point energies, according to Bohr-Wheeler approach [3] the evaporation calculation can include fission competition. The saddle point energies come from the Cohen et al. rotating liquid drop calculations. The calculations are done for each partial wave; upper and lower limit on angular momentum may be selected. To modify the liquid drop fission barrier by some multiplicative factor as well as the ratio of ground state to saddle point level densities $(a_f/a_n)$ (default = 1). There is an option by which we can assume that nuclear emission reduces the daughter nucleus angular momentum from that of the parent nucleus. This option is not incorporated in the present calculation. It is better to use more rigorous codes if detail in angular momentum removal becomes more important. In this model there is a provision to do precompound calculations via the hybrid or geometry dependent hybrid model . If this option is selected in conjunction with fission, it is

assumed by the authors that the fast precompound process will proceed fission without any competition or increasing the excitation energies, the fission and evaporation widths also increase and hence this assumption may fail.

## 3.2 Subroutines List In ALICE/LIVERMORE-82

There are several subroutines in this code:

### 3.2.1 Lymass (Binden, Mass)

For the formation of the compound nucleus and the n, p, alpha and d binding energies the LYMASS subroutine calculates the Q-value for all nuclides of interest in the evaporation chain. By using the Myers-Swiatecki/Lysekil mass formula [15], the calculation is performed.

The option exists (mc > 10) of selecting experimental masses where known, using the mass formula only when experimental masses are not contained in the table (MASS). When the experimental masses option is selected [16], the Q-value and binding energies are both computed using experimental masses. The experimental nuclidic mass routines (BINDEN, MASS) are actually called up by the LYMASS routine.

#### 3.2.1.1 Pairing Options

The basic pairing options are four in number, available in the code through input variable (switch) MP, which may be MP = 0,1, 2 or 3.

We consider the option MP = 3.

The definitions of options are as follows:

MP = 0 By using a mass formula with the odd even pairing term equal to zero for all nuclides, all masses are calculated. On this procedure some reaction will tell that this amounts to odd-even effect on level densities.

MP = 1 As for MP = 3, but the pairing is taken as zero for even-even nuclides, $-\delta$ for odd-even and $-2\delta$ for odd-odd nuclides. This gives a backshifted level density/pairing treatment [17].

MP = 2 The user will supply pairing values for each nuclide in the A by Z array of interest (defined by input parameters NA, NZ). For an array NA + 2 by NZ + 2, pairing values must be supplied actually.

MP = 3 By using either experimental masses or Lysekil masses all masses are calculated with the pairing term $\delta = 11/\sqrt{A}$ taking as zero for odd-even nuclides. $+\delta$ for even-even nuclides and $-\delta$ for odd-odd nuclides. The thermodynamic energies are reduced by delta when effective excitations are computed for use in level densities.

### 3.2.1.2 Experimental Masses

For MC = 10, Lysekil masses are replaced by experimental masses.

### 3.2.2 Over (TLJ)

These are optical model subroutines used to calculate inverse reaction cross-sections for neutrons, protons, deuterons and alpha particles. They are used also to calculate reaction and partial reaction cross-sections when neutrons, protons or deuterons are projectiles. The major part of computational time is ordinarily spent in these routines when that are taken.

### 3.2.3 Sigi

This is a subroutine which uses classical sharp-outoff algorithms to compute inverse reaction cross-sections. The algorithms may be found elsewhere [18]. This subroutines requires less than 1% of the time of optical model routine OVER.

### 3.2.4 Parap

Other than for incident neutrons, protons or deuterons or unless read in as input, all reaction cross-sections and partial cross-sections are calculated using the parabolic model in routine PARAP.

### 3.2.5 Fisrot

In this subroutine by using the rotating liquid drop model of Cohen, Plasil and Swiatecki [13], angular momentum

dependent liquid drop fission barriers, saddle point and ground state energies are calculated.

### 3.2.6 Hybrid (MFP, NUCMFP)

This routine is used to calculate the precompound decay using the hybrid [5] and geometry dependent hybrid models [6]. The present code version selects most precompound parameters for user via built in default options.

The intranuclear transition rates are supplied by MFP subroutine, using nuclear optical model [19] and the same intranuclear transition rates are supplied by NUCMFP, using Pauli corrected nucleon-nucleon scattering cross-sections.

### 3.2.7 PLT/PLEXC

With the help of these subroutines we can plot excitation functions on the output device for printed output.

### 3.2.8 SHAFT

This subroutine comes in use when we want to get many of the print statements for cross-section and spectra.

## 3.3 Formulation

In alpha induced reactions there are several emitted particles depending upon the seperation energies and excitation energies of the compound nucleus. The cross-section for emitting

a particle at channel energy $\epsilon$ may be written as

$$(d\sigma/d\epsilon)_v = \pi \lambda\!\!\!^{-2} \sum_{I=0}^{\infty} (2I+1)\, T_l(2S_v+1) \times \sum_{I=0}^{\infty} T_v^{\ell}(\epsilon) \sum_{J=|I-l|}^{l+l} \sigma(E,J)/D \quad \ldots\ldots(3.1)$$

where

$\lambda\!\!\!^{-}$ = Reduced de-Brogli wavelength of the incident ion.

$T_L$ = Transmission coefficient for lth. partial wave.

$\rho(E,J)$ = Spin dependent level density for residual nucleus.

D = Integral of numerator over all particles and emission energies.

Let us suppose that $\rho(E,J)$ is replaced by $(E,I)$ then

$$(d\sigma/d\epsilon)_v = \pi \lambda\!\!\!^{-2} \sum_{I=0}^{\infty} (2I+1)\, T_I(2S_v+1) \times \sum_{I=0}^{\infty} (2I+1)\, T_v^{\ell}(\epsilon)\, \sigma(E,I)/D \quad \ldots\ldots(3.2)$$

$$\Sigma(2I+1)\, T_v^{\ell}(\epsilon) = 2\sigma v(\epsilon)\, m\epsilon/\pi\hbar^2 \quad \ldots\ldots(3.3)$$

$$(d\sigma/d\epsilon)_v = \Sigma_{I=0}^{o}\, \sigma I2(2Sv+1)\, \sigma v(\epsilon)\, m\epsilon\, \rho(E,I)/D' \quad \ldots\ldots(3.4)$$

This assumption is known as s-wave approximation. For further simplicity let us assume that the compound nucleus angular momentum reasonably represents the average residual nucleus angular momentum following particle evaporation. To reach the Weisskopf result, let us suppose that the nuclear moment of inertia is infinite. Then if

$$\rho(E,I) \propto (2I + 1)\,\rho(\epsilon - E_{ROT}(I)) \qquad \ldots\ldots\ldots (3.5)$$

with $E_{ROT}(I) = 0$ $\ldots\ldots\ldots (3.6)$

we get

$$(d\sigma/d\epsilon)_v = \sum_{I=0}^{o} \sigma_I(2S_v + 1)\,\sigma_v(\epsilon)m\epsilon\,\rho(\epsilon)/D' \qquad \ldots\ldots\ldots (3.7)$$

which is the expression of Weisskopf.

Consider the physical meaning of approximations in terms of contour diagrams of fig. 3.1. An infinite moment of inertia means that there is no level density cutoff at high spin; all population above the particle binding energy can emit another particle. Assigning a finite moment of inertia reduces the phase space for emission from nuclei at high angular momentum, as is shown by the hatched regior of fig. 3.1.

The expression for the particle emission and fission width, using saddle point and yrast energies based upon the

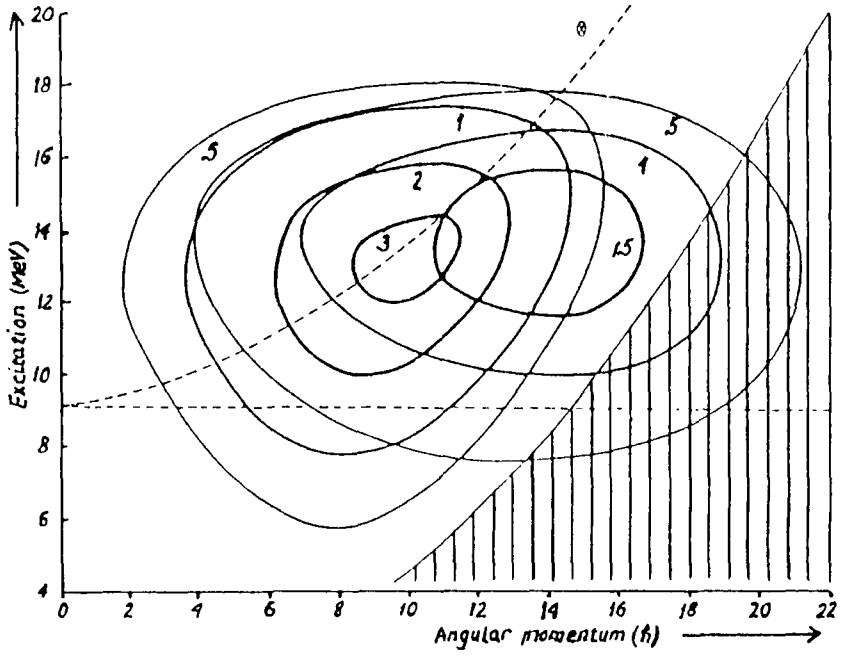


Fig. 3.1 E-J Contour diagram for compound nucleus particle evaporation.

RLDM are given as

$$T_v \alpha (2S_v+1) \sum_{I=0} \sum_{J=|I-1|}^{I+1} (2J+1) \int_0^{E-E_{min}(J)-B_v} \rho_v[ -E_{min}(J)-B_v - \epsilon JT_v(\epsilon )d\epsilon$$

$$T_f \alpha (2I+1) \int_0^{C-E_{sp}(I)} \rho_f[\epsilon -E_{sp}(I) - K]dk \qquad .....(3.8)$$

It will be helpful to comment on the logic of the computer codes used to evaluate eqn. (3.1) to (3.8). To calculate the Weisskopf or s-wave approximation, with codes ALICE, OVERLAIDALICE, ALICE/ LIVERMORE 82, the core of the code is to be divided into the chart of the nuclides as shown in the fig. 3.2. A compound nucleus is formed at some excitation energy and with some cross-section. Then the Weisskopf calculation is taken with 1 MeV grid size to do the evaporation of a neutron, proton, alpha or deuteron storing the residual nucleus population into the appropriate bin. If we select an s-wave calculation, a suitable distribution of CN excitation is used as a starting point. Then the control or logic moves over to the A-1 bin which is resulted by the emission of neutron from the compound nucleus. This bin can also be resulted with the emission of proton, deuteron, alpha particle. The residual nuclei obtained from the emission of aforesaid particles, are stored in the respective bins. In this code the cross-section is used in the highest energy bin of A-1 and then

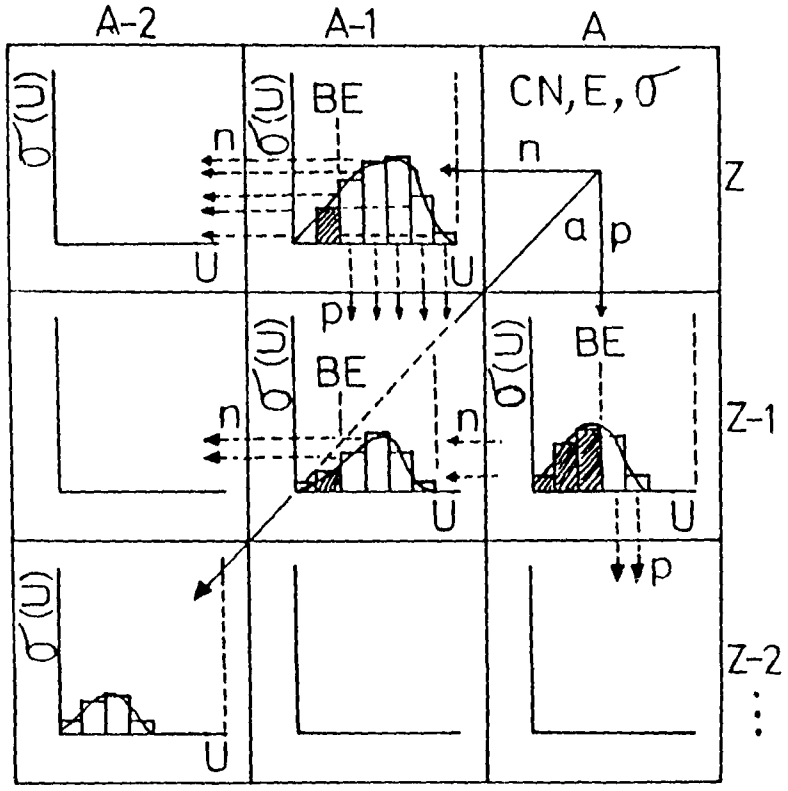


Fig. 3.2 Logic flow of the ALICE/ LIVERMORE-82 code.

this cross-section is redistributed in the same manner. After that the control comes down to the next residual excitation bin and the process continues upto the moment all the cross-section redistributed and assumed it up in the appropriate bins of the residual nuclides. This logic is repeated, going across the A as far as requested by an input parameter. After it the control comes down in Z to the nucleus A-1, Z-1 and this process is repeated till all calculations are not completed for each input parameter.

In this code, the competition can also be included by performing the calculation for each partial wave in the entrance channel, assuming s-wave approximation or some other arbitrary assumptions. It has not been included in the present calculations.

If one wants more rigorous calculations, he should use the spin dependent codes ALERT I and II but we have not corporated with this option in our present work.

## 3.4 Use Of The Code

In the present code a stored table of level densities pow (2000) is used, represented by the formula

$$f(U) = (U - \delta)^{-5/4} \exp\left(2\sqrt{a(U - \delta)}\right)$$

where the value of default option parameter is a = A/9. Here A is not the mass number of residual nuclei but that of the compound

nucleus. It is useful to replace the pow(IB) by $(IB/10)^{-5/4}$ $\exp(2\sqrt{a_{res} \cdot IB/10})$ where 'float of IB' is the residual excitation times ten; and $a_{res}$ represents the mass number of the residual nucleus divided by PLD value in the input parameter. With this we shall get a space saving and more accurate results but CPU time will increase. We can get some more exact results by using a 1 MeV bin size instead of 0.5 MeV. The interpolation of the cross-section has not been taken into account within a bin rather the summation is done near the integer bin. It is assumed that the particle binding energies are of the order of 5 MeV. It indicates binning uncertainity which is very less in comparison of others.

## TABLE 3.1

## DEFINITION OF SYMBOLS

| | |
|---|---|
| $T_f$, $T_v$ | Fission and particle emission widths. |
| I, J | Emitting and residual-nucleus angular momentum. |
| $S_v$, $B_y$ | Intrinsic spin and binding energy of particle v (with v = n, p, d or alpha). |
| $T_v^l(C)$ | Transmission coefficient for K.E. $\epsilon$ and orbital angular momentum l. |
| $\rho_f$, $\rho_v$ | Level densities at fission saddle point and for particle emission; $\rho \alpha U^{-5/4} \exp(2\sqrt{a(U-\delta)})$ |
| $a_f$, $a_v$ | Single particle level densities at fission saddle point and equilibirum deformation used in $a_f$ and $a_v$. |
| B(I) | Rotating liquid drop fission barrier at angular momentum I. |
| Bf | Scaling parameter to adjust the fission barriers. |
| $E_{min}(I)$ | Rotational energy for a nucleus at angular momentum I and equilibrium deformation from RLDM. |
| $E_{sp}(I)$ | Rotational energy of a nucleus with angular momentum I at the saddle point deformation from RLDM. |
| E | Excitation energy in the emitting nucleus. |

## REFERENCES


[1] M. Blann and J. Bisplinghaff: Lawrence Livermore National Laboratory, Computer Code ALICE/LIVERMORE-82, Report UCID-19614 (1982).

[2] V.F. Weisskopf and D.H. Ewing: Phys. Rev. 57 (1940) 472.

[3] N. Bohr and J.A. Wheeler: Phys. Rev. 56 (1939) 426.

[4] R. Vandenbosch and J.R. Huizenga: Nuclear Fission Academic Press, New York, (1973).

[5] M. Blann: Phys. Rev. Lett. 27 (1971) 337.

[6] M. Blann: Phys. Rev. Lett. 28 (1972) 757.

[7] M. Blann and H.K. Vonach: Phys. Rev. C28 (1983) 1475.

[8] M. Blann and F. Plasil: University of Rochester Report COO-3994-10 (1973).

[9] M. Blann: University of Rochester Report COO-3494-29 (1975).

[10] M. Blann: Nucl. Phys. 80 (1966) 223.

[11] T. Ericson: Adv. Phys. 9 (1960) 425.

[12] M. Blann and G. Markel: Phys. Rev. B137 (1965) 367.

[13] S. Cohen, F. Plasil and W.J. Swiatecki: Ann. Phys. 82 (1974) 557.

[14] T.D. Thomas: Phys. Rev. 116 (1959) 703.

[15] W.D. Myers and W.J. Swiatecki: Ark. Fys. 36 (1967) 343.

[16] J.H.E. Mattauch, W. Thiele and A.H. Wapstra: Nucl. Phys. 67 (1965) 1.

[17] J.R. Huizenga, H.K. Vonach, A.A. Katsanos, A.S. Gorski and C.J. Stephan: Phys. Rev. 182 (1969) 1149.

[18] M. Blann: Phys. Rev. C21 (1980) 1770.

[19] F.D. Becchetti and G.W. Greenlees: Phys. Rev. 182 (1969) 1190.

[20] K. Kikuchi and M. Kawai: 'Nuclear Matter and Nuclear reactions', North Holland Publishing Co. (1968).

# CHAPTER IV

# EXPERIMENTAL DETAILS

## 4.1 Techniques Of Measurement

The reaction cross-sections may be measured using any of the following two techniques:

1. In-beam or on-line technique
2. Off-beam or off-line technique

### 4.1.1 In-beam Technique

This is the technique in which the irradiation of the traget sample and the detection of radiations emitted from the product nuclei, is done simultaneously. To study the cross-section of a particular reaction, we analyse the prompt gamma ray spectra associated with the reaction. The decay scheme of the residual nuclei should be well known. Due to complex gamma ray spectra, sometimes gamma-gamma coincidences are also necessary for the proper identification of the gamma rays. The gamma ray detector should be well shielded so that background neutrons emitted in the reaction may not damage the detector.

### 4.1.2 Off-beam Technique

In this technique the target is irradiated first, after that the analysis of product nuclei is done. That is why this

technique is also named as activation technique. The beta or gamma activities associated with the product nucleus can be studied by using the appropriate detectors. It is very much advantageous technique because in this technique the reaction cross-section at several incident energies can be studied with a single irradiation by arranging the target foils in the form of a stack. On the other hand this technique is limited to those isotopes only, which are stable but their product nuclides are unstable and have convenient half lives because the detection of radiation coming from the product nuclei and the irradiation of the target nuclei are done separately so there is some lapse of time between these two processes, therefore, if the half life of the product nucleus is very short, then the activity due to this product nucleus will decay out. Moreover, the decay scheme of the product nuclei should be properly established. We have many advantages inherent in this technique due to high sensitivity with which this induced activity can be detected and individual characteristic modes of decay of each radio-isotope. Some of the particular advantages are; extremely high sensitivity; selectivity and possibility of non-destructive analysis. Cross-sections$\sim$1 $\mu$b have been measured [1] using activation technique. Presently, the off-line technique has been followed for the cross-section measurements.

## 4.2 Sample Preparation

Sample of the elements under study were made from spectroscopic iridium, indium and antimony by using the vacuum evaporation technique in the target division of Variable Energy Cyclotron Centre Calcutta, India. The powder of aforesaid elements were deposited onto the aluminium sheets. The target foils were square cuts of the side 1.5 cm and accurately weighed so that the thickness of each foil was accurately known. The thickness of target foils in different elements varies from $\mu g/cm^2$ to $mg/cm^2$. These target foils were fixed with the help of zepon in acetone onto the aluminium holders having a circular hole of diameter 1.2 cm in its centre. The zepon held the target foils to the target holders after the evaporation of acetone. These target foils with the holders were arranged in the form of a stack. In between the target foils the aluminium foils of different thickness were also inserted to act as degrader. The bombardment of the particular foil with the desired incident energy of alpha particle beam was done by selecting proper thickness of the degrader. For checking of the background activity produced in the target holder two blank target holders, one in the beginning and other at the end of stack were put at the time of irradiation.

## 4.3 Calibration Of Detector

For the proper identification of emitted gamma radiations, the detector should be accurately calibrated. In fact it is the calibration of the pulse height in terms of absolute gamma ray energy and this is very important [2,3]. For this purpose, some standard gamma ray sources having the gamma energies that are not different from those to be measured, are used. In our present experiment the lithium drifted Germanium detector [Ge(Li)] of active volume 100 cc coupled with multichannel analyser and other required electronics was used to follow the activity of irradiated sample. The energy calibration of this detector was done by using $^{152}Eu$ gamma standard source. To obtain the calibration curve, the calibration data was fitted to a straight line using a standard computer programme. Gamma rays of our interest present in the spectrum of activated smaple could be identified with the help of this energy calibration.

## 4.4 Detector Efficiency

The detector efficiency may be defined as the function of the detector geometry and the probability of an interaction in it. For the efficiency calibration many gamma rays are needed which can be obtained from different individual sources. But this method introduces some error due to non-reproducibility of geometry. These errors may be removed by the use of single source emitting many gamma rays. In the present measurements

$^{152}Eu$ gamma point standard source has been used for the determination of detector efficiency.

The expression to determine the intrinsic photopeak detection efficiency of a gamma point source is as given below:

$$\epsilon = \frac{C \exp(\lambda t)}{S_o \cdot \theta \cdot G} \qquad \text{.....(4.1)}$$

where

C = Count rate under the photopeak

$\lambda$ = Decay constant of source

t = Time interval between the date of manufacturing of source and the time of experiment

So = Strength of the source

$\theta$ = Absolute intensity of relevent gamma ray

G = Geometrical factor given as $G = \Omega/4\pi$ where $\Omega$ is the solid angle in steradians, subtended by the detector surface facing the source

The factor C can be determined by measuring the photopeak area for a fixed period for all the gamma peaks and can be determined from the dimension and source-detector distance. Mathematically this is given as below:

$$\Omega = 2\pi \left[1 - \frac{d}{\sqrt{d^2+R^2}}\right] \qquad \text{.....(4.2)}$$

where

d = The distance of source from detector surface

R = The radius of the detector crystal

To avoid the probable error in geometry factor, we have determined the relative detection efficiency by using the expression given below:

$$\epsilon \cdot G = \frac{C \exp(\lambda t)}{S_o \cdot \theta} \qquad \ldots\ldots\ldots(4.3)$$

In our present experiment, C is measured for 30 minutes for each photopeak. During this period of 30 minutes, the geometry of source was kept constant. The values of $T_{1/2}$ (To calculate $\lambda$ ) and $\theta$ are taken from reference No. [4] and the value of $S_o$ is taken from the data supplied by the manufacturer. The geometry dependent detection efficiency curves of 100 cc Ge(Li) detector for different source detector distances are shown in the figs. 4.1-4.3.

## 4.5 Irradiations

The target samples were irradiated with the diffused α-beam of diameter 8 mm by following the stacked foil activation technique which is generally used for the study of charged particle reaction cross-sections [5-10]. In this technique the stack is made by the proper arrangement of the target foils.

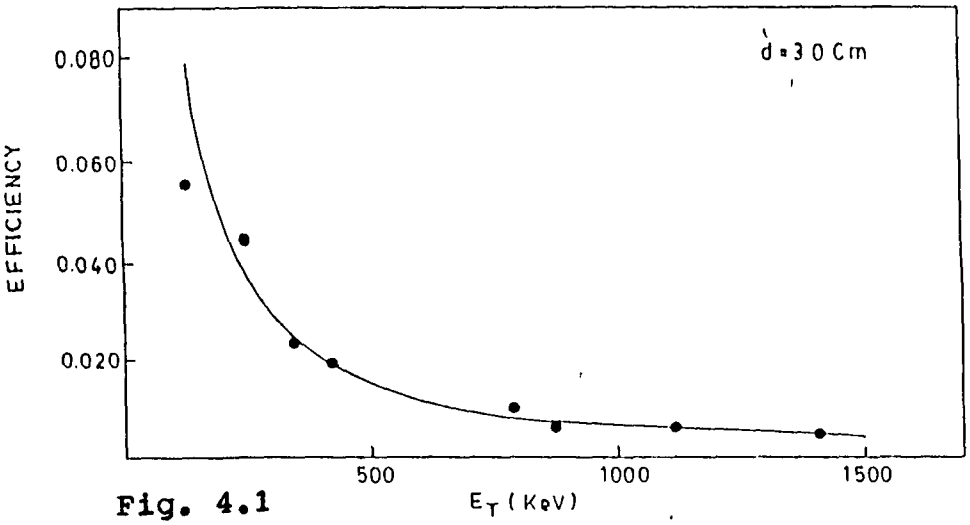


Fig. 4.1

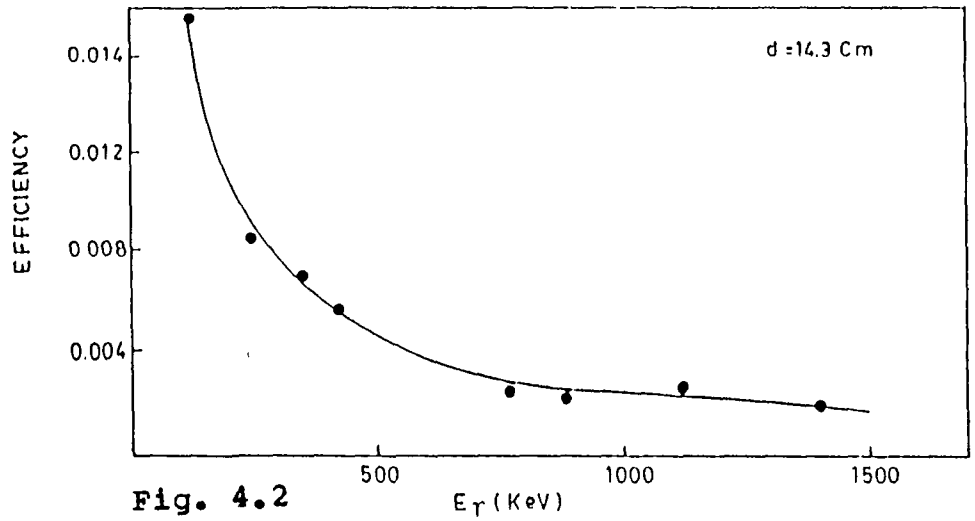


Fig. 4.2

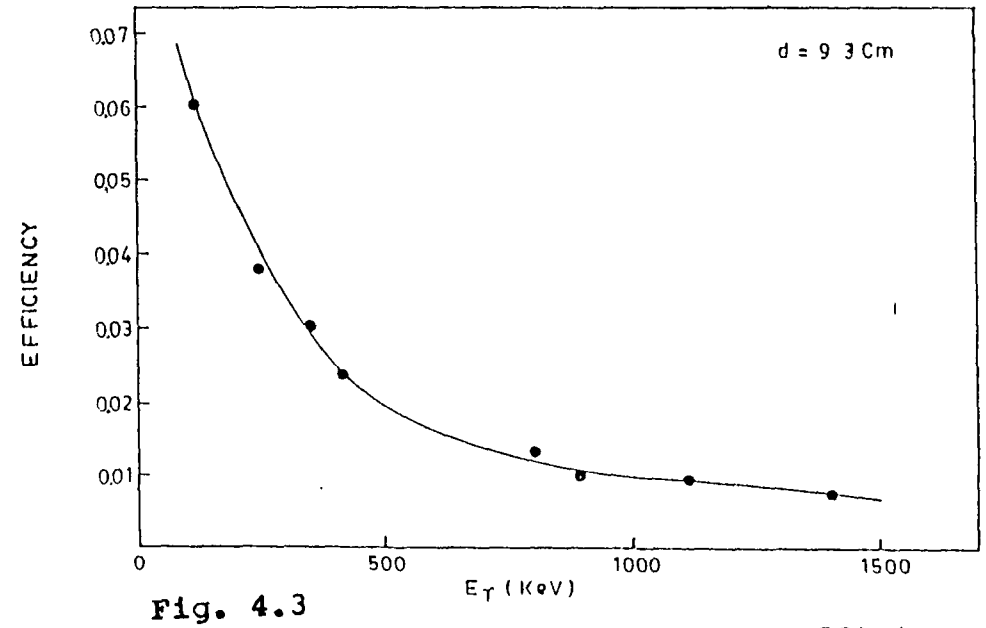


Fig. 4.3

Fig. 4.1, 4.2, 4.3 Geometry dependent efficiency curve for 100 $cm^3$ Ge(Li) detector at the source-detector surface distances d = 3.0 cm, 14.3 cm. 9.3 cm respectively.

In between the target foils, the degrader foils can also be inserted to hit the particular foil with the desired incident energy. Irradiation of the target stack was done at Variable Energy Cyclotron Centre, Calcutta (India). The maximum energy of the incident α-beam on the first foil of the stack varies from 50-55 MeV for different cases and period of the bombardment varies from 1.0 - 1.5 hrs. Since the beam current fluctuations during the irradiations were very small, the average incident flux was calculated by using the total charge collected in the Faraday Cup. The incident energy on the different foils in the stack was calculated by considering the foil thickness and relevent α-particle stopping power. The tables of Northcliffe and Schilling were adopted for these calculations [11]. The uncertainity of $\pm$ 0.5 MeV in the initial beam energy was also taken into the consideration.

The stacks were clamped in a water-cooled 'Faraday Cup', which was insulated from the rest of the system, in order to measure the beam current of the α-particles striking the target foils. A typical experimental set up for the stack irradiation is shown in the fig. 4.4.

## 4.6 Counting Of Produced Activity

After the irradiation, the stacks of the foils were detached from the 'Faraday Cup' and also the foils were detached from the aluminium holders and then one by one foils were brought

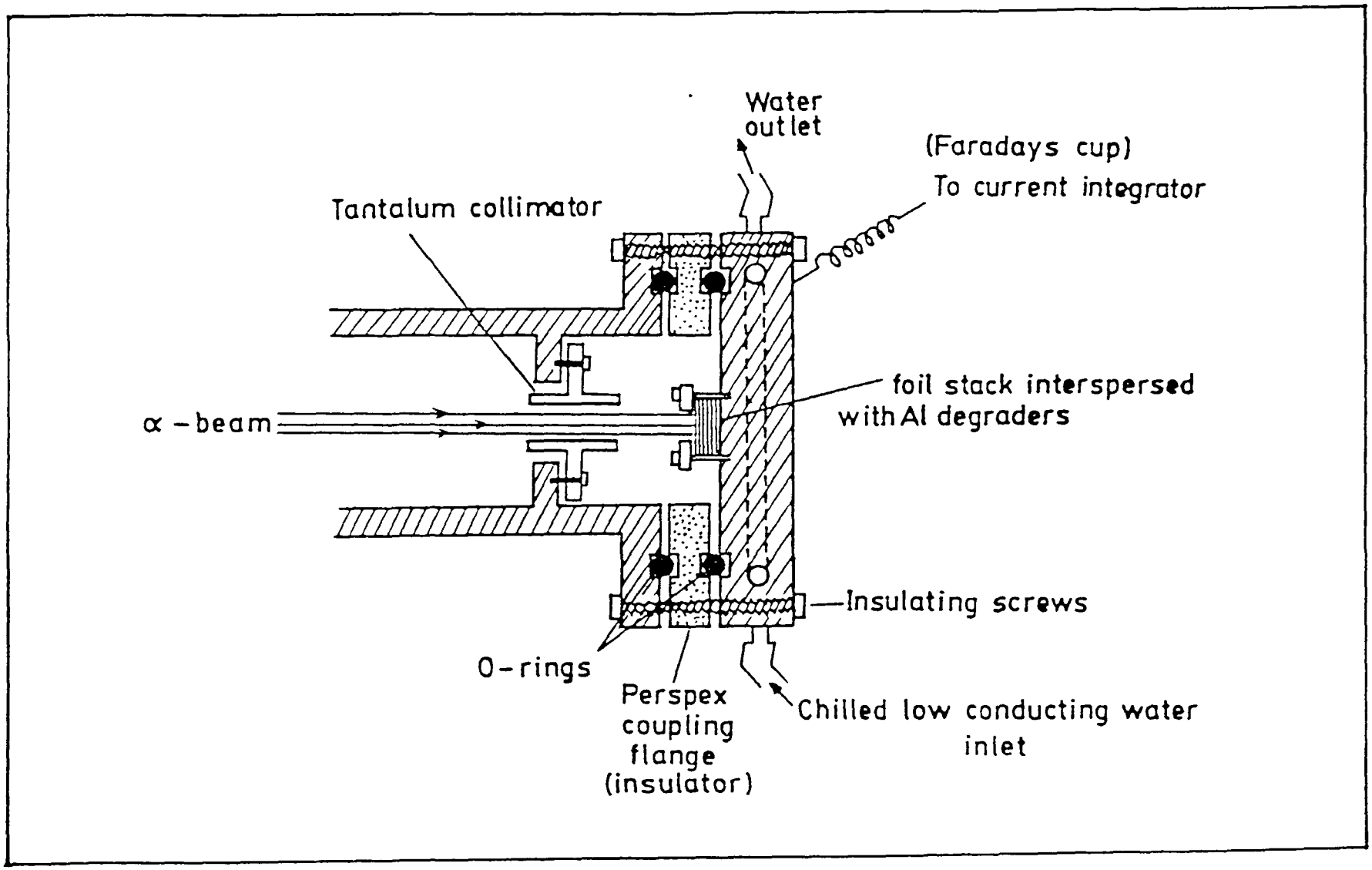


Fig. 4.4 A typical experimental set-up for the stack irradiation with alpha particle beam.

to the counting room to be mounted in the desired geometry for counting the gamma activities. The counting geometry was chosen in such a way so that the count rate is appreciable and at the same time the dead time of the detector is low. Use of Germenium detectors were preferred for detecting the characteristic gamma ray spectra because this type of the detectors have very good resolution and this property helps not only to seperate closely spaced peak but also, nicely detect the weak gamma rays of discrete energies when superimposed on a broad continuum. A 100 cc ORTEC Ge(Li) detector having a resolution of 1.8 KeV at 1.33 MeV was used for this purpose.

The pre-calibrated multichannel analyser was used to analyse the gamma ray spectra. If any gamma activity is present in the counting room, then it is sure that it will affect our desired spectra so before taking the spectra of induced activity, a background spectrum was taken in order to check the presence of any background gamma peak due to contamination of the detector surroundings. As our target foils were made by the deposition of target material on the backing of aluminium sheet so the gamma peak in aluminium, if any, will also come in our desired spectra,that's why this fact was also kept in mind in the analysis of gamma ray spectra. The recording time period were chosen in such a way so as to get the good counting statistics. The recording time was corrected for the dead time of analyser system.

The reaction products were identified by the characteristic gamma lines obtained from their decay. The counts under the photopeaks were calculated by subtracting the background counts from total counts.

## 4.7 Formulation

The expression for cross-section of a nuclear reaction may be written from the consideration of rate of formation of activity and its decay rate. If a target is irradiated by a projectile of flux $\phi$ then the rate of production ($R_p$) of any activity is given as [12,13]

$$R_p = \sigma \phi N_o \qquad \text{.....(4.4)}$$

where $\sigma$ is the activation cross-section and $N_o$ the number of target nuclei in the sample under investigation. The mathematical expression of $N_o$ is given as

$$No = m N f / A_o \qquad \text{.....(4.5)}$$

where m is the mass of the sample, N is the Avogadro's number, f is the abundance of the isotope in the target and $A_o$ is the atomic mass of the element in amu.

Let the target be irradiated with the incident beam for the time $t_1$ to produce a radioactive reaction product y.

The equation governing the growth of y-type activity during irradiation can be written as

$$(dy/dt) = \sigma \phi N_o - y\lambda \qquad .....(4.6)$$

where $\lambda$ represents the decay constant of y-type nuclei and y is the number of radioactive atoms present. The activity of y-type nuclei at the instant of stopping of irradiation is given by

$$W = y \cdot \lambda$$

$$= \sigma \phi N_o \left[1-\exp(-\lambda t_1)\right] \qquad .....(4.7)$$

where $t_1$ is the time of irradiation of the target.

The factor $[1 - \exp(-\lambda t_1)]$ is called as saturation factor.

If we measure the activity after a gap of time $t'$ from the stop of irradiation then it is given as

$$(dy/dt)_{t=t'} = W \exp(-\lambda t')$$

or $$(dy/dt)_{t=t'} = \sigma \phi N_o [1-\exp(-\lambda t_1)] \exp(-\lambda t')$$

or $$dy = \sigma \phi N_o [1-\exp(-\lambda t_1)] \exp(-\lambda t')\, dt' \qquad .....(4.8)$$

If the counting of gamma rays emitted from irradiated sample is

done for $t_3$ second after the $t_2$ second of stop of irradiation and, if $D_o$ be the actual number of disintegrations from the radioactive sample recorded in $t_3$ time, then

$$D_o = \int dy$$

or

$$D_o = \int_{t_1}^{t_2+t_3} \sigma \phi N_o [1-\exp(-\lambda t_1)] \exp(-\lambda t')dt'$$

or

$$D_o = \sigma \phi N_o [1-\exp(-\lambda t_1)] \int_{t_2}^{t_2+t_3} \exp(-\lambda t')dt'$$

or

$$D_o = \frac{\sigma \phi N_o [1-\exp(-\lambda t_1)] [1-\exp(-\lambda t_3)]}{\exp(\lambda t_2)} \quad .....(4.9)$$

If A is the number of counts under the particular photopeak as detected by detector, $\epsilon$ is the efficiency of the detector, G is the geometry factor, $\theta$ is the absolute intensity, K is the self absorption correction factor for the gamma ray under study which can be calculated as [14]

$$K = [1-\exp(-\mu d)]/\mu d$$

where $\mu$ = gamma ray absorption coefficient taken from reference [15]

$d$ = thickness of the target under investigation

Then, the actual number of disintegrations $D_o$ will be as follows:

$$D_O = (A/\epsilon \cdot G. \Theta. K) \qquad .....(4.10)$$

putting the value of $D_0$ in above equation, the expression for $\sigma$ can be written as:

$$\sigma = \frac{A \exp(\lambda t_2)}{\phi N_o \epsilon G.\Theta.K. [1-\exp(-\lambda t_1)] [1-\exp(-\lambda t_3)]} \qquad .....(4.11)$$

Thus, using above expression one can calculate the activation cross-section.

In the present measurements where more than two gamma rays are available at the same energy in any reaction, then the experimental cross-section value is taken as the weighted average of the individual cross-sections of these gamma rays. This was done in following way [16].

Let us suppose $X_1 \pm \Delta X_1$, $X_2 \pm \Delta X_2$, $X_3 \pm \Delta X_3$, $X_4 \pm \Delta X_4$ ..... are the different values of a quantity, then the weighted average of these values can be expressed as

$$\bar{X} = \frac{\Sigma W_i X_i}{\Sigma W_i} \qquad .....(4.12)$$

where the $W_i$ is given as

$$W_i = \frac{1}{(\Delta X_i)^2} \qquad .....(4.13)$$

and

$$\text{The external error} = \left[\frac{\Sigma W_i (\bar{X}-X_i)^2}{n(n-1)\Sigma W_i}\right]^{1/2} \qquad .....(4.14)$$

and

$$\text{The internal error} = [\Sigma W_i]^{-1/2} \qquad \ldots\ldots\ldots(4.15)$$

For this purpose, a computer programme has been made by using the equations (4.11) to (4.15)

## 4.8 Experimental Results

In present work the alpha induced reactions have been measured. The type of the reactions are written as $(\alpha, xn)$ reactions. Where $x = 1,2,3,\ldots\ldots$ .Natural iridium, indium and antimony have been used as the target samples. The natural iridium has two isotopes $^{191}Ir$ and $^{193}Ir$ with the abundance 37.3% and 62.7% respectively and the natural indium has the isotopes $^{113}In$, $^{115}In$ with the natural abundance 4.3%, 95.7% respectively; while the natural antimony has the isotopes the $^{121}Sb$ and $^{123}Sb$ with the natural abundance 57.3% and 42.7% respectively. The stacks of the target foils were irradiated with the alpha particle beam in the channel I of the Variable Energy Cyclotron Centre, Calcutta. After that various reactions were observed by taking the spectrum of characteristic gamma lines obtained from the decay of the residual nuclei.

In the present measurement various reactions were possible but we have studied only those which gave appreciable activity for meaningful excitation function. The possible reaction channels, residual nuclei, Q-value, half life of the residual

nuclei,energies and absolute intensity of gamma rays pertinent to the reaction channels are listed in the table 4.1 - 4.3. The decay data are according to reference 4. The excitation function of the reactions are calculated by following only those gamma rays which have the good appreciable absolute intensity, hence the weak gamma rays are excluded where the strong ones are available for the same emitting nuclide and also these are listed in the table 4.1 - 4.3. The detailed description of the measurements is given separately for each target and for each reaction. The cross-sections were calculated by using the equation 4.11. The errors quoted in the measured cross-section values are external only.

## 4.8(a) Errors In Measurement

The estimation of errors is necessary because no experiment can be done with 100% accuracy. In the present experiment, errors were minimised but even then there may be some variations which could not be avoided. The estimation of these errors is briefly discussed below:

1. The spectrometer should be well stabilized to minimize the error due any type of erratic behaviour of the equipments.

Table 4.1

Nuclear Spectroscopic Data for the Reaction in $^{113,115}In$.

| Reaction | Product nucleus | Half-life | Gamma Energy (MeV) | Gamma Intensity (%) | Q-value (MeV) |
|---|---|---|---|---|---|
| $^{113}In(\alpha,n)$ | $^{116g}Sb$ | 15.8 m | 0.932 | 24.80 | - 7.97 |
| | | | 1.293 | 85.00 | |
| | | | 2.225 | 14.20 | |
| | | | 2.843 | 1.00 | |
| $^{113}In(\alpha,n)$ | $^{116m}Sb$ | 1.005 h | 0.135 | 29.00 | - 7.97 |
| | | | 0.407 | 42.00 | |
| | | | 0.436 | 4.10 | |
| | | | 0.542 | 52.00 | |
| | | | 0.844 | 12.00 | |
| | | | 0.972 | 72.00 | |
| | | | 1.072 | 28.10 | |
| | | | 1.293 | 100.00 | |
| $^{113}In(\alpha,2n)$ | $^{115}Sb$ | .32.1 m | 0.489 | 1.30 | - 16.06 |
| | | | 0.497 | 98.00 | |
| | | | 0.986 | 0.35 | |
| | | | 1.236 | 0.58 | |

Contd.....

| | | | | | |
|---|---|---|---|---|---|
| $^{115}In(\alpha,n)$ | $^{118g}Sb$ | 3.6 m | 0.528 | 0.38 | - 7.24 |
| | | | 0.827 | 0.36 | |
| | | | 1.229 | 2.47 | |
| | | | 1.267 | 0.57 | |
| $^{115}In(\alpha,n)$ | $^{118m}Sb$ | 5.0 h | 0.253 | 99.00 | - 7.24 |
| | | | 1.050 | 97.00 | |
| | | | 1.091 | 3.50 | |
| | | | 1.229 | 99.90 | |
| $^{115}In(\alpha,2n)$ | $^{117}Sb$ | 2.8 h | 0.159 | 85.90 | - 14.62 |
| | | | 0.861 | 0.31 | |
| | | | 1.004 | 0.21 | |
| | | | 1.019 | 0.11 | |
| $^{115}In(\alpha,3n)$ | $^{116g}Sb$ | 15.8 m | 0.932 | 24.80 | - 24.31 |
| | | | 1.293 | 85.00 | |
| | | | 2.225 | 14.20 | |
| | | | 2.843 | 1.00 | |
| $^{115}In(\alpha,3n)$ | $^{116m}Sb$ | 1.00 h | 0.135 | 29.00 | - 24.31 |
| | | | 0.407 | 42.00 | |
| | | | 0.436 | 4.10 | |
| | | | 0.542 | 52.00 | |
| | | | 0.844 | 12.00 | |
| | | | 0.972 | 72.00 | |
| | | | 1.072 | 28.10 | |
| | | | 1.293 | 100.00 | |

Contd...

| | | | | | |
|---|---|---|---|---|---|
| $^{115}In(\alpha,4n)$ | $^{115}Sb$ | 32.1 m | 0.489 | 1.3 | - 32.40 |
| | | | 0.497 | 98.0 | |
| | | | 0.986 | 0.35 | |
| | | | 1.236 | 0.58 | |
| $^{115}In(\alpha,2p)$ | $^{117g}In$ | 43.8 m | 0.159 | 87.0 | - 12.75 |
| | | | 0.396 | 0.14 | |
| | | | 0.552 | 99.7 | |
| | $^{117m}In$ | 1.94 h | 0.159 | 15.9 | |
| | | | 0.315 | 19.1 | |
| $^{115}In(\alpha,pn)$ | $^{117m}Sn$ | 13.61 d | 0.156 | 2.11 | - 12.10 |
| | | | 0.159 | 86.4 | |

Table 4.2

Nuclear Spectroscopic Data for the Reaction in $^{191,193}Ir$.

| Reaction | Product Nucleus | Half-life | Gamma Energy (MeV) | Gamma Intensity (%) | Q-value |
|---|---|---|---|---|---|
| $^{191}Ir(\alpha,n)$ | $^{194m1}Au$ | 600 ms | 0.008 | 1.50 | -10.09 |
| | | | 0.009 | 32.00 | |
| | | | 0.011 | 34.00 | |
| | | | 0.013 | 7.20 | |
| | | | 0.045 | 5.30 | |
| $^{191}Ir(\alpha,n)$ | $^{194m2}Au$ | 420 ms | 0.128 | 25.00 | -10.09 |
| | | | 0.137 | 16.00 | |
| | | | 0.162 | 9.30 | |
| | | | 0.170 | 25.30 | |
| $^{191}Ir(\alpha,n)$ | $^{194g}Au$ | 1.646 d | 0.293 | 11.10 | -10.09 |
| | | | 0.328 | 63.00 | |
| | | | 0.364 | 1.47 | |
| | | | 0.482 | 1.17 | |
| | | | 0.528 | 1.70 | |
| | | | 0.622 | 1.48 | |
| | | | 0.645 | 2.29 | |
| | | | 1.175 | 2.12 | |
| | | | 1.468 | 6.70 | |

Contd.....

| | | | | | |
|---|---|---|---|---|---|
| $^{191}Ir(\alpha,2n)$ | $^{193m}Au$ | 3.9 s | 0.219 | 3.34 | -17.06 |
| | | | 0.258 | 66.00 | |
| $^{191}Ir(\alpha,2n)$ | $^{193g}Au$ | 17.65 h | 0.112 | 2.00 | -17.06 |
| | | | 0.173 | 2.90 | |
| | | | 0.186 | 10.10 | |
| | | | 0.255 | 6.70 | |
| | | | 0.268 | 3.90 | |
| | | | 0.439 | 1.91 | |
| $^{191}Ir(\alpha,3n)$ | $^{192m}Au$ | 167 m | 0.103 | not known | -25.71 |
| | | | 0.107 | -do- | |
| | | | 0.128 | -do- | |
| | | | 0.146 | -do- | |
| $^{191}Ir(\alpha,3n)$ | $^{192g}Au$ | 4.94 h | 0.295 | 22.70 | -25.71 |
| | | | 0.316 | 58.00 | |
| | | | 0.468 | 1.75 | |
| | | | 0.477 | 1.08 | |
| | | | 0.612 | 4.27 | |
| $^{191}Ir(\alpha,4n)$ | $^{191m}Au$ | 920 ms | 0.241 | 13.70 | -32.68 |
| | | | 0.252 | 60.00 | |
| $^{191}Ir(\alpha,4n)$ | $^{191g}Au$ | 3.18 h | 0.132 | 1.15 | -32.68 |
| | | | 0.166 | 3.12 | |
| | | | 0.194 | 2.58 | |
| | | | 0.277 | 6.80 | |
| | | | 0.586 | 16.00 | |
| | | | 0.674 | 6.40 | |

Contd....

| | | | | | |
|---|---|---|---|---|---|
| $^{191}Ir(\alpha,5n)$ | $^{190}Au$ | 42.8 m | 0.295 | 71.00 | -41.75 |
| | | | 0.301 | 25.10 | |
| | | | 0.319 | 5.50 | |
| | | | 0.441 | 4.30 | |
| | | | 0.597 | 10.10 | |
| $^{193}Ir(\alpha,3n)$ | $^{194m1}Au$ | 600 ms | 0.008 | 1.50 | -24.05 |
| | | | 0.009 | 32.00 | |
| | | | 0.011 | 34.00 | |
| | | | 0.013 | 7.20 | |
| | | | 0.045 | 5.30 | |
| $^{193}Ir(\alpha,3n)$ | $^{194m2}Au$ | 420 ms | 0.128 | 25.00 | -24.05 |
| | | | 0.137 | 16.00 | |
| | | | 0.162 | 9.30 | |
| | | | 0.170 | 25.30 | |
| $^{193}Ir(\alpha,3n)$ | $^{194g}Au$ | 1.646 d | 0.293 | 11.10 | -24.05 |
| | | | 0.328 | 63.00 | |
| | | | 0.364 | 1.47 | |
| | | | 0.482 | 1.17 | |
| | | | 0.528 | 1.70 | |
| | | | 0.622 | 1.48 | |
| | | | 0.645 | 2.29 | |
| | | | 1.175 | 2.12 | |
| | | | 1.468 | 6.70 | |

Contd.....

| | | | | | |
|---|---|---|---|---|---|
| $^{193}Ir(\alpha,4n)$ | $^{193m}Au$ | 3.9 s | 0.219 | 3.34 | -28.50 |
| | | | 0.258 | 66.00 | |
| $^{193}Ir(\alpha,4n)$ | $^{193g}Au$ | 17.65 h | 0.112 | 2.00 | -28.50 |
| | | | 0.173 | 2.90 | |
| | | | 0.186 | 10.10 | |
| | | | 0.255 | 6.70 | |
| | | | 0.268 | 3.90 | |
| | | | 0.439 | 1.91 | |
| $^{193}Ir(\alpha,5n)$ | $^{192m}Au$ | 167 ms | 0.103 | Not known | -39.68 |
| | | | 0.107 | -do- | |
| | | | 0.128 | -do- | |
| | | | 0.146 | -do- | |
| $^{193}Ir(\alpha,5n)$ | $^{192g}Au$ | 4.94 h | 0.295 | 22.70 | -39.68 |
| | | | 0.316 | 58.00 | |
| | | | 0.468 | 1.75 | |
| | | | 0.477 | 1.08 | |
| | | | 0.612 | 4.27 | |

Table 4.3

Nuclear Spectroscopic Data for the Reaction in $^{121,123}Sb$.

| Reaction | Product Nucleus | Half-life | Gamma Energy (MeV) | Gamma Intensity (%) | Q-value (MeV) |
|---|---|---|---|---|---|
| $^{121}Sb(\alpha,n)$ | $^{124}I$ | 4.18 d | 0.603 | 61.00 | - 7.88 |
| | | | 0.722 | 9.96 | |
| | | | 1.325 | 1.45 | |
| | | | 1.376 | 1.66 | |
| | | | 1.509 | 2.99 | |
| | | | 1.690 | 10.41 | |
| $^{121}Sb(\alpha,2n)$ | $^{123}I$ | 13.2 h | 0.159 | 83.30 | -15.35 |
| | | | 0.364 | 0.13 | |
| | | | 0.439 | 0.43 | |
| | | | 0.505 | 0.32 | |
| | | | 0.528 | 1.39 | |
| $^{121}Sb(\alpha,4n)$ | $^{121}I$ | 2.12 h | 0.212 | 84.00 | -33.23 |
| | | | 0.319 | 1.04 | |
| | | | 0.475 | 1.04 | |
| | | | 0.531 | 6.10 | |
| | | | 0.589 | 1.50 | |

Contd.....

| | | | | | |
|---|---|---|---|---|---|
| $^{123}Sb(\alpha,n)$ | $^{126}I$ | 13.02 d | 0.389 | 34.10 | - 6.95 |
| | | | 0.491 | 2.85 | |
| | | | 0.666 | 33.10 | |
| | | | 0.753 | 4.16 | |
| $^{123}Sb(\alpha,3n)$ | $^{124}I$ | 4.18 d | 0.603 | 61.00 | -23.64 |
| | | | 0.722 | 9.96 | |
| | | | 1.325 | 1.45 | |
| | | | 1.376 | 1.66 | |
| | | | 1.509 | 2.99 | |
| | | | 1.690 | 10.41 | |
| $^{123}Sb(\alpha,4n)$ | $^{123}I$ | 13.2 h | 0.159 | 83.30 | -31.15 |
| | | | 0.364 | 0.13 | |
| | | | 0.439 | 0.43 | |
| | | | 0.505 | 0.32 | |
| | | | 0.528 | 1.39 | |

2. The efficiency of the detector is one of the major source of creation of error. This error can be minimized by the determination of efficiency very carefully and obtaining the efficiency curve by using best polynomial fit.

3. Incomplete charge collection of the Faraday Cup in the current integrator reading may also introduce some errors. In the present measurement, there was no error due to this factor.

4. The error in the number of interacting nuclei of the target is also a factor to create the error in the result and this error is due to the error in the measurement of mass of the target sample. To minimize this error, the accuracy in cutting of the target to the standard size and use of micro balance are the important considerations. Maximum error estimated being less than 0.5% .

5. If the time interval between the moment of the start and stop of irradiation; stop of irradiation and start of counting is not noted down exactly, it may also create some errors. In our experiment there was no error due to this factor.

6. At the time of counting the activity, the non-reproducibility of identical geometries of the sample may also produce some errors. This error is minimized by fixing the sample in fixed geometries. Presently, this error is measured less than 0.5% .

7. The excitation function may have some errors due to error associated with the decay data of product nucleus obtained in the reaction. This error was minimized by using latest available data [4]. The uncertainities in the results due to this factor are not included in the uncertainities quoted in the experimental results.

8. One of the main sourse of the errors is the statical variation in the photopeak counts. This will be different for different gamma photopeaks. In the spectrum, some peaks were not in the standard form due to the presence of background, at those places the peaks were reformed to come in the Gaussian shape. The error due to this reformation has also been taken into the consideration.

9. Another very important factor of errors in the measurement is the fluctuation in the beam current. Beam current was kept most of the time nearly constant and if there was large fluctuation in beam current for appreciable time the data was rejected. Two or three copper foil were inserted in the stack under study to check the value of flux of alpha particle beam. Using standard $^{65}Cu(\alpha,2n)^{67}Ga$ reaction, the $\alpha$-flux was calculated at two or three energies. Mean value of this flux was found to be very close to the flux measured using Faraday cup.

10. The error in the measurement of incident energy of particle due to straggling is neglected.

### 4.8.1 Target Nucleus $^{113,115}In$

In the present work indium target was made by the deposition of indium metal on aluminium sheet of thickness 3.83 mg/$cm^2$ with the help of vacuum evaporation technique at target division of Variable Energy Cyclotron Centre, Calcutta. After the deposition, this foil was cut into ten square pieces of arm 1.5 cm and these pieces were weighed separately with microbalance. The thickness of these pieces of target foils was found to be 3.34 mg/$cm^2$. These pieces were glued to an aluminium frame having a circular hole of diameter 1.2 cm in its centre. Then these target foils were arranged into the form of a stack. In the target stack, three aluminium foils of thickness 20.387 mg/$cm^2$, ten aluminium foils of thickness 6.75 mg/$cm^2$ and two copper foils of thickness 10.68 mg/$cm^2$ were also sandwiched in between the target foils. The stack arrangement is shown in the fig. 4.5 This target stack was bombarded with 50 MeV diffused α-beam of diameter 8 mm. After passing through the target stack, the beam was allowed to fall on the 'Faraday Cup' so that the beam current and the total charge collected during the irradiation could be measured. The total incident flux on the target stack was 1.082 x $10^{11}$ α-particles/$cm^2$. s . The reactions $^{113}In(\alpha,n)^{116m}Sb$, $^{113}In(\alpha,2n)^{115}Sb$, $^{115}In(\alpha,n)^{118m}Sb$, $^{115}In(\alpha,2n)^{117}Sb$, $^{115}In(\alpha,3n)^{116m}Sb$, $^{115}In(\alpha,4n)^{115}Sb$, $^{115}In(\alpha,pn)^{117m}Sn$ and $^{115}In(\alpha,2p)^{117}In$ have been studied at ten different incident α-particle energies viz., 21.4 ± 1.4 MeV, 25.2 ± 1.2 MeV,

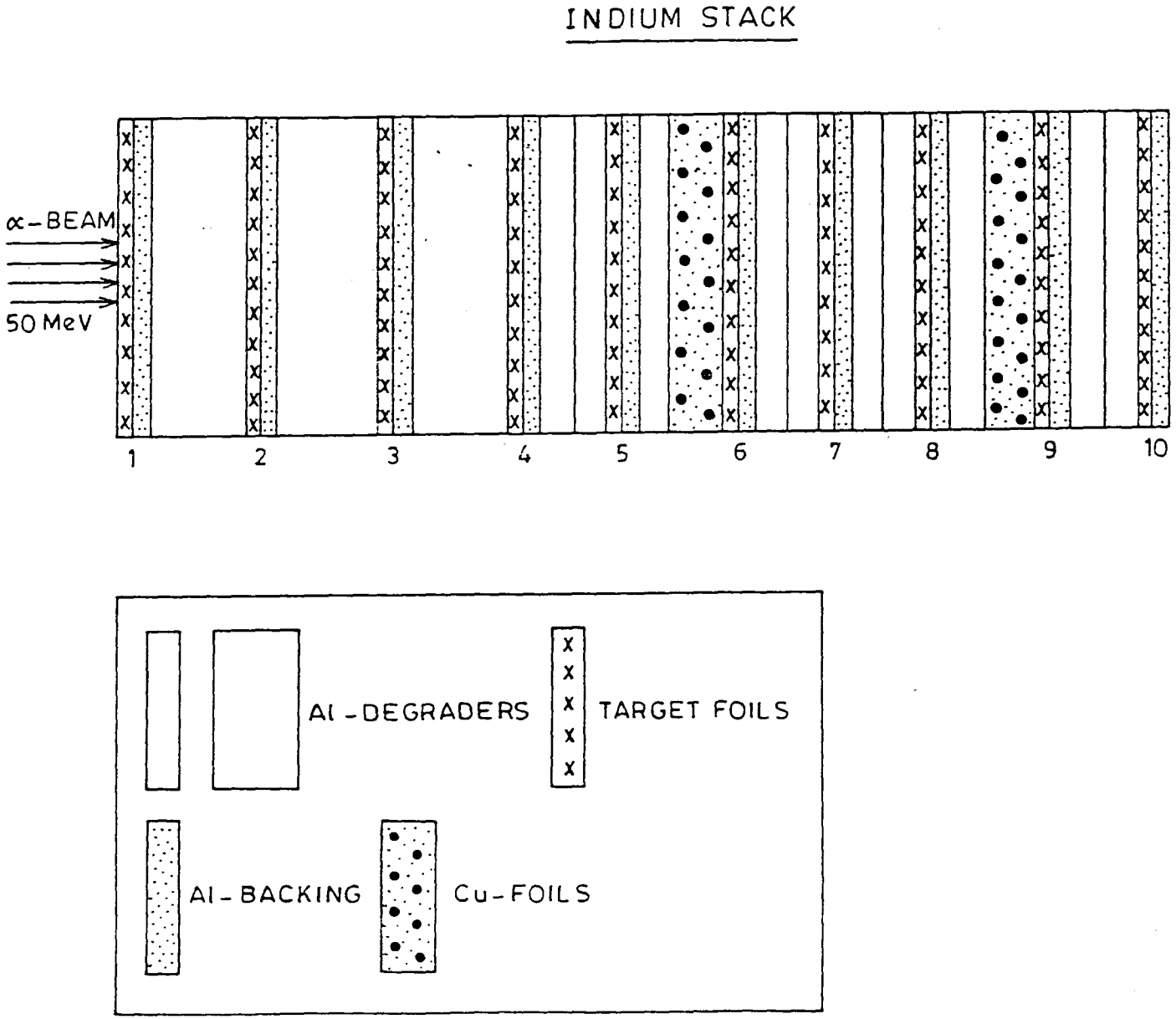


Fig. 4.5 Stack arrangement for indium target.

29.0 ± 1.0 MeV, 32.2 ± 0.8 MeV, 35.1 ± 0.8 MeV, 37.4 ± 0.7 MeV, 40.1 ± 0.7 MeV, 43.6 ± 0.7 MeV, 46.8 ± 0.6 MeV, 50.0 ± 0.5 MeV, The gamma ray spectrum of activated indium is shown in the fig. 4.6. The Q-value of the reactions are taken from the reference 17,18.

### 4.8.1.1 $^{113}In(\alpha,n)$ Reaction

This reaction can take place only when the alpha particles of minimum 8.25 MeV strikes the target or in other words we can say that its threshold energy is 8.25 MeV. The Q-value of this reaction is -7.97 MeV. In this reaction, the residual nucleus is $^{116}Sb$ which has two states; metastable state of half life $T_{1/2}$ = 1.005 hours, spin $8^-$ and ground state of half life $T_{1/2}$ = 15.8 minutes, Spin $3^+$. The metastable state of $^{116}Sb$ decays through electron capture mode as well as the $\beta^+$ emission. In case of metastable state, the 81% decay is through electron capture mode while the rest 19% decay is through $\beta^+$ emission. In ground state, 72% decay is through electron capture mode while 28% decay is through $\beta^+$ emission.

As the activity produced in the target foils was very high, so the stack of target foils was cooled down till the activity reached permissible dose rate and this cooling took a long time. So due to a long gap between start of counting of the gamma rays and stop of bombardment of target stack, there may not be any contribution of short lived ground state. Hence the

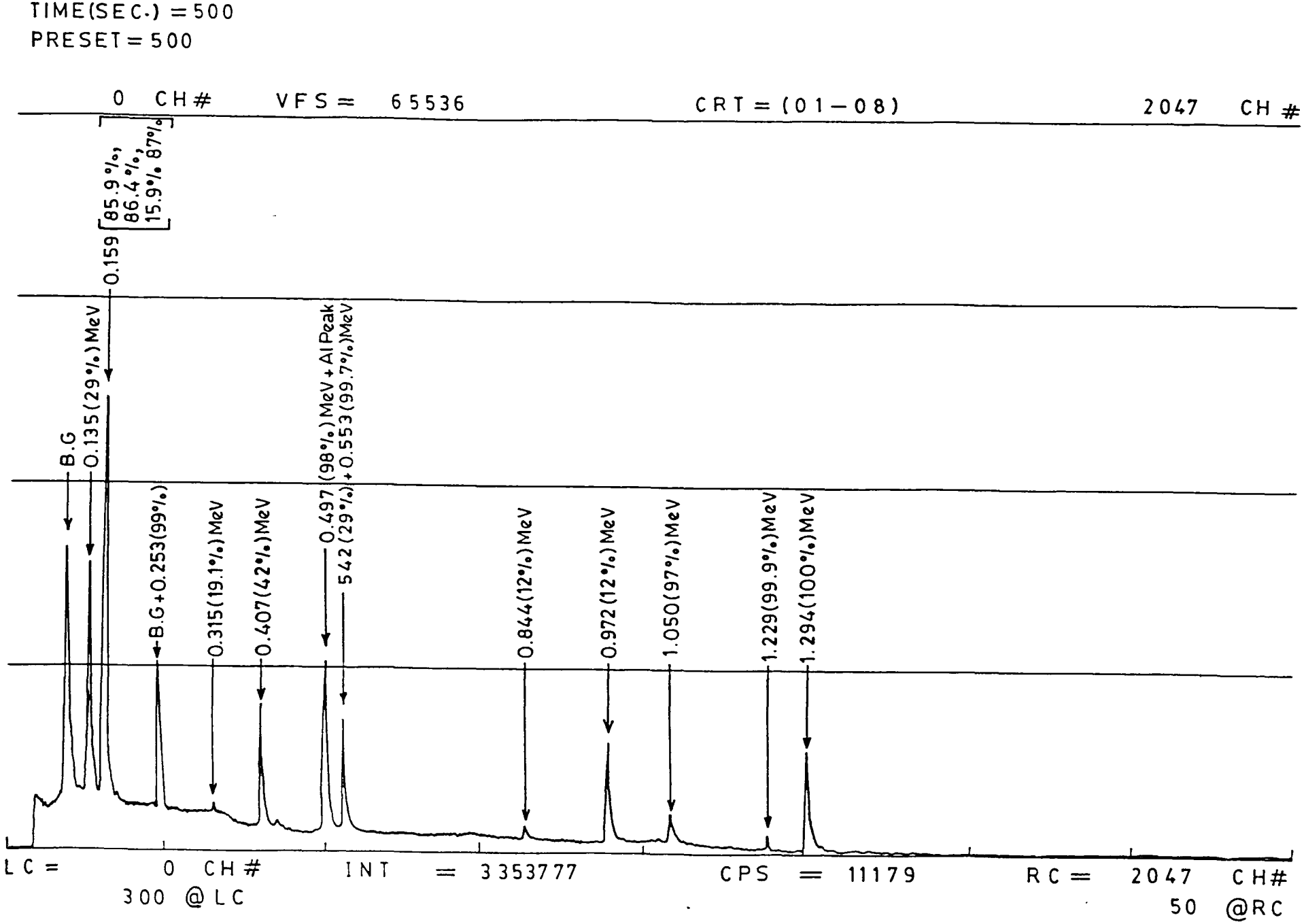


Fig. 4.6 A typical gamma ray spectrum of activated sample of indium.

activity due to metastable state only could be observed. In the calculation of cross-section of this reaction, gamma rays of energy 0.135 MeV, 0.407 MeV, 0.542 MeV, 0.972 MeV with the abundance 29.0%, 42.0%, 52.0%, 72.0% respectively were followed. The decay scheme of $^{116}Sb$ is given in the fig. 4.7. The details of parameters used in cross-section calculations are given in the table 4.4 and so obtained cross-sections are given in table 4.5.

Table 4.4

Experimental data for $^{113}In(\alpha,n)^{116m}Sb$ Reaction

Half life ($T_{1/2}$) = 1.005 h

Incident flux ($\phi$) = $1.082 \times 10^{11}$ $\alpha$-particles/$cm^2$.s

Number of interacting nuclei($N_o$) = $3.8459 \times 10^{17}$

| Particle Energy $E_\alpha$ (MeV) | Gamma Energy $E_\gamma$ (MeV) | Absolute $\gamma$-intensity $\Theta_\gamma$ (%) | Time lapse $t_2$ (sec) | Recording Time $t_3$ (sec) | Photo-peak counts A |
|---|---|---|---|---|---|
| 21.4±1.4 | 0.135 | 29.0 | 13560 | 300 | 624 |
| | 0.407 | 42.0 | | | 364 |
| | 0.542 | 52.0 | | | 397 |
| | 0.972 | 72.0 | | | 272 |
| 25.2±1.2 | 0.135 | 29.0 | 12720 | 300 | 375 |
| | 0.407 | 42.0 | | | 261 |
| | 0.542 | 52.0 | | | 213 |
| | 0.972 | 72.0 | | | 163 |

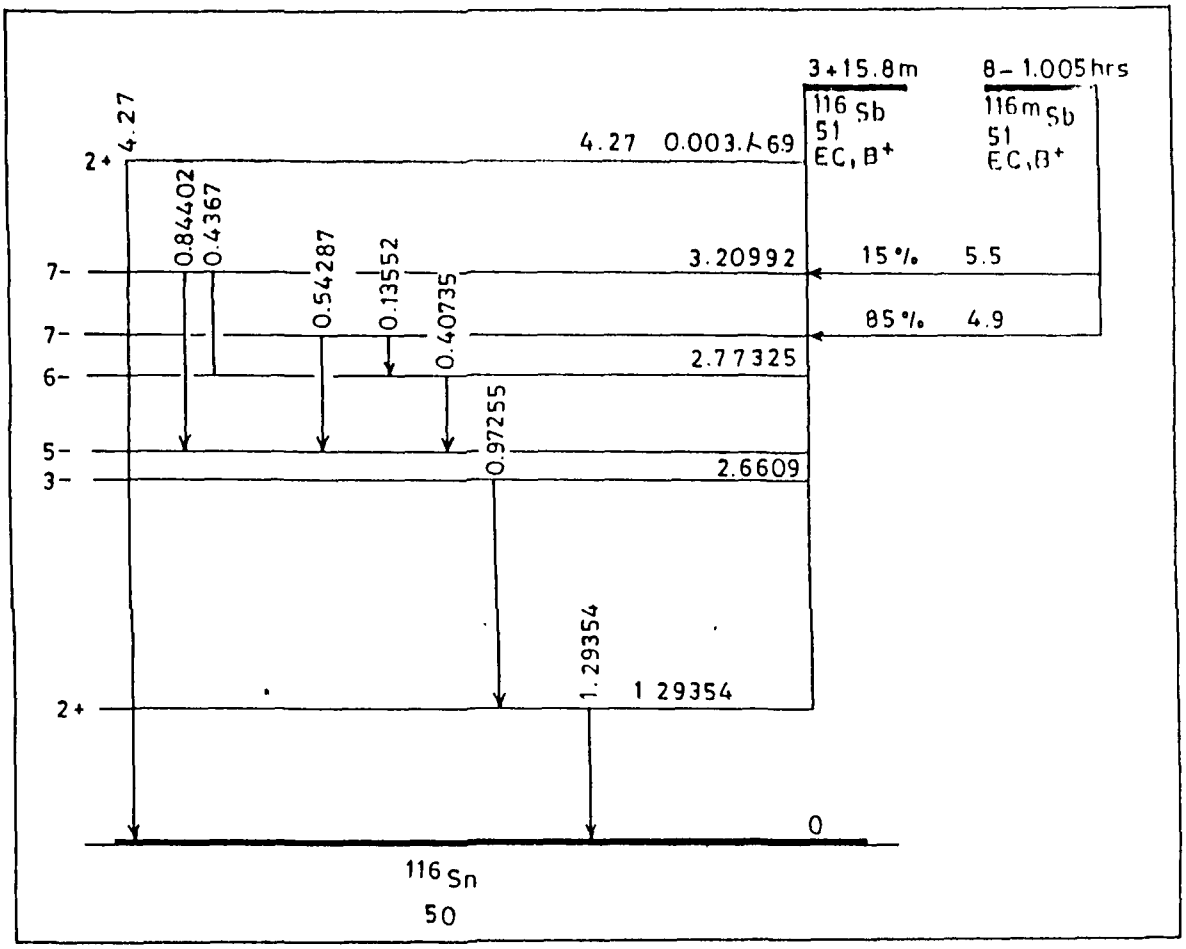


Fig. 4.7

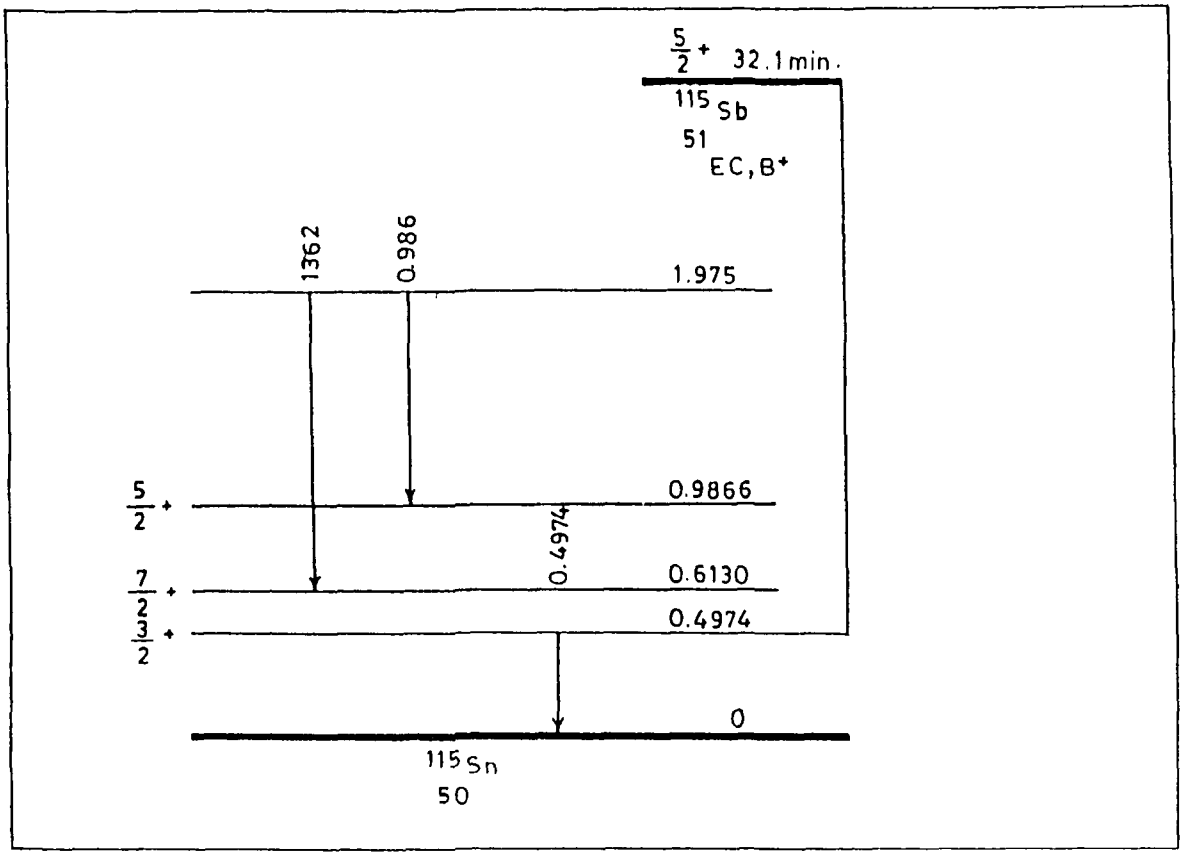


Fig. 4.8

Fig. 4.7 Partial decay scheme of $^{116}Sb$

Fig. 4.8 Partial decay scheme of $^{115}Sb$

Table 4.5

Cross-section for $^{113}In(\alpha,n)^{116m}Sb$ Reaction

| Incident α-particle Energy $E_\alpha$ (MeV) | Gamma Ray Energy $E_\gamma$ (MeV) | Cross-section σ (mb) | Weighted Average cross-section σ (mb) |
|---|---|---|---|
| 21.4±1.4 | 0.135 | 286.65±11.48 | 265.11±6.74 |
| | 0.407 | 248.23±13.01 | |
| | 0.542 | 285.22±14.31 | |
| | 0.972 | 231.86±14.06 | |
| 25.2±1.2 | 0.135 | 146.67±7.57 | 137.60±3.69 |
| | 0.407 | 151.54±9.38 | |
| | 0.542 | 130.29±8.93 | |
| | 0.972 | 118.30±9.26 | |

### 4.8.1.2 $^{113}In(\alpha,2n)$ Reaction

The Q-value of this reaction is -16.06 MeV and the threshold energy is 16.63 MeV. The residual nucleus of this reaction is $^{115}Sb$ which has only the ground state of half life 32.1 minutes and spin +5/2, no metastable state. The decay of this state is through electron capture mode as well as $\beta^+$ emission. In the decay of this state the electron capture is 67% and $\beta^+$ emission is 33%. The major decay through electron capture goes to first excited state of the residual nucleus $^{115}Sn$. The only gamma ray of 0.497 MeV with the abundance 98% has been followed

for the calculation of the cross-section of this reaction. No other good abundent gamma ray is available. The decay scheme of residual nucleus $^{115}Sb$ is shown in the fig. 4.8 and the parameters used to calculate the cross-sections are given in the table 4.6 while so obtained cross-sections are given in the table 4.7.

Table 4.6

Experimental data for $^{113}In(\alpha,2n)^{115}Sb$ Reaction

Half life ($T_{1/2}$) = 32.1 m

Incident flux ($\phi$) = $1.082 \times 10^{11}$ $\alpha$-particles/$cm^2$.s

Number of interacting nuclei ($N_o$) = $3.8459 \times 10^{17}$

| Particle Energy $E_\alpha$ (MeV) | Gamma Energy $E_\gamma$ (MeV) | Absolute $\gamma$-Intensity $\Theta_\gamma$ (%) | Time lapse $t_2$ (sec.) | Recording Time $t_3$ (sec.) | Photo-peak counts A |
|---|---|---|---|---|---|
| 21.4±1.4 | 0.497 | 98.0 | 13560 | 300 | 148 |
| 25.2±1.2 | 0.497 | 98.0 | 12720 | 300 | 349 |
| 29.0±1.0 | 0.497 | 98.0 | 11220 | 300 | 661 |
| 32.2±0.8 | 0.497 | 98.0 | 10440 | 300 | 484 |
| 35.1±0.8 | 0.497 | 98.0 | 9780 | 300 | 373 |
| 37.4±0.7 | 0.497 | 98.0 | 8880 | 300 | 241 |
| 40.1±0.7 | 0.497 | 98.0 | 6420 | 300 | 386 |
| 43.6±0.7 | 0.497 | 98.0 | 5640 | 300 | 397 |
| 46.8±0.6 | 0.497 | 98.0 | 3960 | 300 | 660 |
| 50.0±0.5 | 0.497 | 98.0 | 4800 | 300 | 429 |

Table 4.7

Cross-section for $^{113}In(\alpha,2n)^{115}Sb$ Reaction

| Incident α-particle Energy $E_\alpha$ (MeV) | Gamma Ray Energy $E_\gamma$ (MeV) | Cross-section σ (mb) | Weighted Average Cross-section σ (mb) |
|---|---|---|---|
| 21.4 ±1.4 | 0.497 | 391.80±32.20 | 391.80±32.20 |
| 25.2 ±1.2 | 0.497 | 682.92±36.55 | 682.92±36.55 |
| 29.0 ±1.0 | 0.497 | 753.97±29.33 | 753.97±29.33 |
| 32.2 ±0.8 | 0.497 | 416.98±18.95 | 416.98±18.95 |
| 35.1 ±0.8 | 0.497 | 253.42±13.12 | 253.42±13.12 |
| 37.4 ±0.7 | 0.497 | 118.44± 7.62 | 118.44± 7.62 |
| 40.1 ±0.7 | 0.497 | 78.29± 3.98 | 78.29± 3.98 |
| 43.6 ±0.7 | 0.497 | 60.81± 3.05 | 60.81± 3.05 |
| 46.8 ±0.6 | 0.497 | 55.24± 2.15 | 55.24± 2.15 |
| 50.0 ±0.5 | 0.497 | 48.57± 2.34 | 48.57± 2.34 |

### 4.8.1.3 $^{115}In(\alpha,n)$ Reaction

The Q-value of this reaction is -7.24 MeV. In this reaction the product nucleus is $^{118}Sb$ which has the ground state of half life ($T_{1/2}$) 3.6 minutes and the metastable state of half life ($T_{1/2}$) 5.0 h . Both the states of $^{118}Sb$ decay to the levels of $^{118}Sn$. The decay of metastable state is through electron capture mode and the $\beta^+$ emission, and the

percentage of these kinds of decays are 99.84% and 0.16% respectively. The decay of ground state is also through the electron capture mode and $\beta^+$ emission and the percentage of these decays are 22.5% and 75.0%. As the half life of ground state of product nucleus $^{118}Sb$ is very short so the contribution of this state to the developed activity could not be observed. The observed activity was due to the metastable state only. The gamma rays 0.253 MeV (99.0%), 1.229 MeV (99.9%) 1.050 MeV (97%) were followed to calculate the cross-sections of this reaction at various incident energies. The details of different parameters used in calculation of $\sigma$ are given in the table 4.8 and the cross-sections measured at different incident energies are given in the table 4.9. The decay scheme of the product nucleus is given in the fig. 4.9.

### 4.8.1.4 $^{115}In(\alpha,2n)$ Reaction

In this reaction, the product nucleus is $^{117}Sb$ which has the ground state of half life of 2.8 hours with spin $\frac{5}{2}^+$. There is no metastable state. This ground state of $^{117}Sb$ decays to first excited state of $^{117}Sn$ through electron capture mode and the $\beta^+$ emission then this excited state decays to the ground state. In the decay of $^{117}Sb$ the percentage of electron capture is 97.5% and the percentage of $\beta^+$ emission is 2.5%. In the calculation of cross-section, only one gamma ray of 0.159 MeV with abundance 85.9% was followed. There is no other gamma ray

## Table 4.8

### Experimental data for $^{115}In(\alpha,n)^{118m}Sb$ reaction

Half life ($T_{1/2}$) = 5.00 h

Incident flux ($\phi$) = $1.082 \times 10^{11}$ $\alpha$-particles/$cm^2$.s

Number of interacting nuclei ($N_o$) = $8.4105 \times 10^{18}$

| Particle Energy $E_\alpha$ (MeV) | Gamma Energy $E_\gamma$ (MeV) | Absolute $\gamma$-intensity $\Theta_\gamma$ (%) | Time lapse $t_2$ (sec.) | Recording Time $t_3$ (sec.) | Photo-peak counts A |
|---|---|---|---|---|---|
| 21.4±1.4 | 0.253 | 99.0 | 13560 | 300 | 56255 |
| | 1.050 | 97.0 | | | 16249 |
| | 1.229 | 99.9 | | | 14354 |
| 25.2±1.2 | 0.253 | 99.0 | 12720 | 300 | 28418 |
| | 1.050 | 97.0 | | | 8025 |
| | 1.229 | 99.9 | | | 6844 |
| 29.0±1.0 | 0.253 | 99.0 | 11220 | 300 | 12352 |
| | 1.050 | 97.0 | | | 3781 |
| | 1.229 | 99.9 | | | 3168 |
| 32.2±0.8 | 0.253 | 99.0 | 10440 | 300 | 7058 |
| | 1.050 | 97.0 | | | 1602 |
| | 1.229 | 99.9 | | | 1742 |
| 25.1±0.8 | 0.253 | 99.0 | 9780 | 300 | 3962 |
| | 1.050 | 97.0 | | | - |
| | 1.229 | 99.9 | | | - |

Table 4.9

Cross-section for $^{115}In(\alpha,n)^{118m}Sb$ reaction

| Incident α-particle Energy $E_\alpha$ (MeV) | Gamma ray Energy $E_\gamma$ (MeV) | Cross-section σ (mb) | Weighted Average Cross-section σ (mb) |
|---|---|---|---|
| 21.4±1.4 | 0.253 | 204.32±0.86 | 210.26±4.53 |
| | 1.050 | 237.66±1.98 | |
| | 1.229 | 213.13±1.67 | |
| 25.2±1.2 | 0.253 | 99.93±0.59 | 101.61±1.34 |
| | 1.050 | 109.71±1.33 | |
| | 1.229 | 101.91±1.14 | |
| 29.0±1.0 | 0.253 | 41.00±0.37 | 42.66±1.06 |
| | 1.050 | 47.93±0.85 | |
| | 1.229 | 45.32±0.74 | |
| 32.2±0.8 | 0.253 | 22.73±0.27 | 22.21±0.85 |
| | 1.050 | 25.56±0.61 | |
| | 1.229 | 18.64±0.47 | |
| 35.1±0.8 | 0.253 | 12.44±0.20 | 12.44±0.20 |

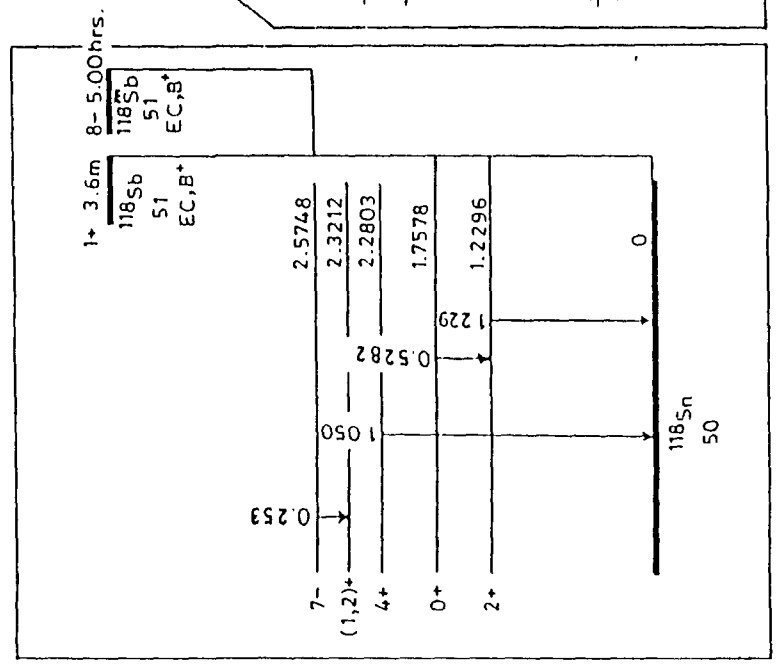


Fig. 4.9 Partial decay scheme of $^{118}Sb$.

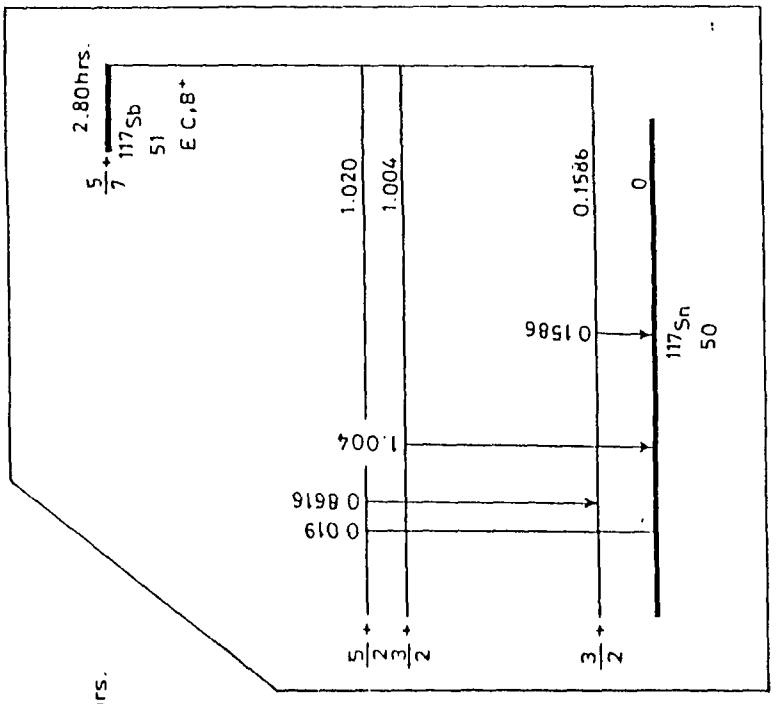


Fig. 4.10 Partial decay scheme of $^{117}Sb$.

of good abundance. The Q-value of this reaction is -14.62 MeV and the threshold is 15.13 MeV. The decay scheme of $^{117}Sb$ is given in the fig. 4.10. The spectroscopic and experimentally measured parameters used to calculate the cross-sections are represented in the table 4.10 and the measured cross-sections at different incident α-particle energies are given in the table 4.11.

### 4.8.1.5 $^{115}In(\alpha,3n)$ Reaction

The product nucleus, in this reaction, is $^{116}Sb$ which has two states i.e. one metastable state and otherone the ground state. The half life of the ground state is 15.8 minutes with spin $3^+$ and the half life of metastable state is 1.005 hour with spin $8^-$. These states decay independantly to the levels of $^{116}Sn$. As the product nucleus of this reaction is same as the product nucleus of $^{113}In(\alpha,n)$ reaction, so other details of this reaction already have been given in article 4.8.1.1. The Q-value and the threshold of $^{115}In(\alpha,3n)$ reaction are -24.31 MeV and 25.16 MeV respectively. Of course the threshold of $^{115}In(\alpha,3n)$ and $^{113}In(\alpha,n)$ reaction are different but even then there is some region in which the channel of both the reactions go on simultaneously. In the overlapping region the cross-sections can be separated by using the theoretical cross-sections but in the present case, it could not be done because the cross-section has been measured only for the metastable state while the theoretical

Table 4.10

Experimental data for $^{115}In(\alpha,2n)^{117}Sb$ reaction

Half life ($T_{1/2}$) = 2.80 h

Incident flux ($\phi$) = $1.082 \times 10^{11}$ $\alpha$-particles/$cm^2$.s

Number of interacting nuclei ($N_o$) = $8.4105 \times 10^{18}$

| Particle Energy $E_\alpha$ (MeV) | Gamma Energy $E_\gamma$ (MeV) | Absolute $\gamma$-intensity $\Theta_\gamma$ (%) | Time Lapse $t_2$ (sec.) | Recording Time $t_3$ (sec.) | Photo-peak Counts A |
|---|---|---|---|---|---|
| 21.4±1.4 | 0.159 | 85.9 | 13560 | 300 | 221150 |
| 25.2±1.2 | 0.159 | 85.9 | 12720 | 300 | 443310 |
| 29.0±1.0 | 0.159 | 85.9 | 11220 | 300 | 354541 |
| 32.2±0.8 | 0.159 | 85.9 | 10440 | 300 | 207835 |
| 35.1±0.8 | 0.159 | 85.9 | 9780 | 300 | 93400 |
| 37.4±0.7 | 0.159 | 85.9 | 8880 | 300 | 67106 |
| 40.1±0.7 | 0.159 | 85.9 | 6420 | 300 | 67167 |
| 43.6±0.7 | 0.159 | 85.9 | 5640 | 300 | 49611 |
| 46.8±0.6 | 0.159 | 85.9 | 3960 | 300 | 45076 |
| 50.0±0.5 | 0.159 | 85.9 | 4800 | 300 | 38160 |

Table 4.11

Cross-section for $^{115}In(\alpha,2n)^{117}Sb$ reaction

| Incident α-particle Energy $E_\alpha$ (MeV) | Gamma ray Energy $E_\gamma$ (MeV) | Cross-section σ (mb) | Weighted Average Cross-section σ (mb) |
|---|---|---|---|
| 21.4±1.4 | 0.159 | 836.92±20.32 | 836.92±20.32 |
| 25.2±1.2 | 0.159 | 1220.22±24.4 | 1220.22±24.46 |
| 29.0±1.0 | 0.159 | 880.99±19.01 | 880.99±19.01 |
| 32.2±0.8 | 0.159 | 489.48±12.75 | 489.48±12.75 |
| 35.1±0.8 | 0.159 | 210.20±10.52 | 210.20±10.52 |
| 37.4±0.7 | 0.159 | 141.97±9.70 | 141.97±9.70 |
| 40.1±0.7 | 0.159 | 119.98±7.57 | 119.98±7.57 |
| 43.6±0.7 | 0.159 | 83.99±6.23 | 83.99±6.23 |
| 46.8±0.6 | 0.159 | 67.94±5.32 | 67.94±5.32 |
| 50.0±0.5 | 0.159 | 60.93±4.37 | 60.93±4.37 |

cross-section is the sum of the cross-section of ground and metastable state both so the sum of cross-section of two reactions is represented. The details of the parameters used to calculate the cross-sections are given in the table 4.12 and measured cross-section are given in table 4.13. The decay scheme of the reaction product is given in the fig. 4.7.

### 4.8.1.6 $^{115}In(\alpha,4n)$ Reaction

The Q-value of this reaction is -32.40 MeV. $^{115}Sb$ is the product nucleus of this reaction which has only the ground state of half life 32.1 minutes with spin $\frac{5}{2}^+$. There is no metastable state. This product nucleus decays to the $^{115}Sn$ through the electron capture mode and $\beta^+$ emission. The percentage of electron capture mode and $\beta^+$ emission in this decay are 67% and 33%. The product nucleus $^{115}Sb$ of this reaction is also the product nucleus of $^{113}In(\alpha,2n)$ reaction. In spite of the difference of the Q-values these reactions have some common region. In this region the cross-sections are divided in the ratio of the theoretical cross-section of these reactions. The gamma ray of 0.497 MeV with the abundance 98% has been taken to calculate the cross-section. The detail of used parameters is given in the table 4.14 and the measured cross-sections are arranged in the table 4.15. The decay scheme of product nucleus $^{115}Sb$ of this reaction is given in the fig. 4.8.

Table 4.12

Experimental data for $^{115}In(\alpha,3n)^{116m}Sb+^{113}In(\alpha,n)^{116m}Sb$ reaction

Half life ($T_{1/2}$) = 1.005 h

Incident flux ($\phi$) = $1.082 \times 10^{11}$ $\alpha$-particles/$cm^2$.s

Number of interacting nuclei ($N_o$) = $8.4105 \times 10^{18}$

| Particle Energy $E_\alpha$ (MeV) | Gamma Energy $E_\gamma$ (MeV) | Absolute $\gamma$-Intensity $\theta_\gamma$ (%) | Time Lapse $t_2$ (sec.) | Recording Time $t_3$ (sec.) | Photo-peak Counts A |
|---|---|---|---|---|---|
| 29.0±1.0 | 0.135 | 29.0 | 11220 | 300 | 5074 |
| | 0.407 | 42.0 | | | 3191 |
| | 0.542 | 52.0 | | | 3212 |
| | 0.972 | 72.0 | | | 2748 |
| 32.2±0.8 | 0.135 | 29.0 | 10440 | 300 | 30531 |
| | 0.407 | 42.0 | | | 17760 |
| | 0.542 | 52.0 | | | 17166 |
| | 0.972 | 72.0 | | | 16142 |
| 35.1±0.8 | 0.135 | 29.0 | 9780 | 300 | 65736 |
| | 0.407 | 42.0 | | | 39292 |
| | 0.542 | 52.0 | | | 36141 |
| | 0.972 | 72.0 | | | 34722 |

Contd....

| | | | | | |
|---|---|---|---|---|---|
| 37.4±0.7 | 0.135 | 29.0 | 8880 | 300 | 94589 |
| | 0.407 | 42.0 | | | 61597 |
| | 0.542 | 52.0 | | | 57005 |
| | 0.972 | 72.0 | | | 44005 |
| 40.1±0.7 | 0.135 | 29.0 | 6420 | 300 | 118772 |
| | 0.407 | 42.0 | | | 64059 |
| | 0.542 | 52.0 | | | 62642 |
| | 0.972 | 72.0 | | | 68132 |
| 43.6±0.7 | 0.135 | 29.0 | 5640 | 300 | 107888 |
| | 0.407 | 42.0 | | | 66417 |
| | 0.542 | 52.0 | | | 48320 |
| | 0.972 | 72.0 | | | 50670 |
| 46.8±0.6 | 0.135 | 29.0 | 3960 | 300 | 101877 |
| | 0.407 | 42.0 | | | 59705 |
| | 0.542 | 52.0 | | | 60013 |
| | 0.972 | 72.0 | | | 53383 |
| 50.0±0.5 | 0.135 | 29.00 | 4800 | 300 | 78844 |
| | 0.407 | 42.0 | | | 44696 |
| | 0.542 | 52.0 | | | 40582 |
| | 0.972 | 72.0 | | | 38845 |

Table 4.13

Cross-section for $^{115}In(\alpha,3n)^{116m}Sb+^{113}In(\alpha,n)^{116m}Sb$

| Incident α-particle Energy $E_\alpha$ (MeV) | Gamma ray Energy $E_\gamma$ (MeV) | Cross-section σ (mb) | Weighted Average Cross-section σ (mb) |
|---|---|---|---|
| 29.0±1.0 | 0.135 | 68.08±0.96 | 66.87±0.56 |
| | 0.407 | 63.56±1.13 | |
| | 0.542 | 67.40±1.19 | |
| | 0.972 | 68.42±1.31 | |
| 32.2±0.8 | 0.135 | 352.82±2.02 | 329.12±6.27 |
| | 0.407 | 304.67±2.29 | |
| | 0.542 | 310.24±2.34 | |
| | 0.972 | 346.15±2.72 | |
| 35.1±0.8 | 0.135 | 669.44±2.61 | 625.69±11.70 |
| | 0.407 | 594.62±3.00 | |
| | 0.542 | 575.62±3.03 | |
| | 0.972 | 656.16±3.52 | |
| 37.4±0.7 | 0.135 | 810.64±2.64 | 770.80±15.04 |
| | 0.407 | 783.67±3.16 | |
| | 0.542 | 764.06±3.20 | |
| | 0.972 | 699.82±3.34 | |

Contd.....

| | | | |
|---|---|---|---|
| 40.1±0.7 | 0.135 | 635.29±1.84 | 580.35±19.63 |
| | 0.407 | 508.83±2.01 | |
| | 0.542 | 524.20±2.09 | |
| | 0.972 | 676.47±2.59 | |
| 43.6±0.7 | 0.135 | 497.08±1.51 | 445.03±15.05 |
| | 0.407 | 454.27±1.76 | |
| | 0.542 | 348.18±2.07 | |
| | 0.972 | 433.21±1.92 | |
| 46.8±0.8 | 0.135 | 340.27±1.07 | 321.01±5.12 |
| | 0.407 | 296.04±1.21 | |
| | 0.542 | 313.50±1.28 | |
| | 0.972 | 330.88±1.43 | |
| 50.0±0.5 | 0.135 | 309.23±1.10 | 281.27±8.04 |
| | 0.407 | 260.24±1.23 | |
| | 0.542 | 248.93±1.24 | |
| | 0.972 | 310.82±1.58 | |

Table 4.14

Experimental data for $^{115}In(\alpha,4n)^{115}Sb$ reaction

Half life ($T_{1/2}$) = 32.1 m

Incident flux ($\phi$) = $1.082 \times 10^{11}$ $\alpha$-particles/$cm^2$.s

Number of interacting nuclei ($N_o$) = $8.4105 \times 10^{18}$

| Particle Energy $E_\alpha$ (MeV) | Gamma Energy $E_\gamma$ (MeV) | Absolute $\gamma$-intensity $\theta_\gamma$ (%) | Time Lapse $t_2$ (sec.) | Recording Time $t_3$ (sec.) | Photo-peak Counts A |
|---|---|---|---|---|---|
| 35.1±0.8 | 0.497 | 98.0 | 9780 | 300 | 292 |
| 37.4±0.7 | 0.497 | 98.0 | 8880 | 300 | 785 |
| 40.1±0.7 | 0.497 | 98.0 | 6420 | 300 | 5254 |
| 43.6±0.7 | 0.497 | 98.0 | 5640 | 300 | 24139 |
| 46.8±0.6 | 0.497 | 98.0 | 3960 | 300 | 91901 |
| 50.0±0.5 | 0.497 | 98.0 | 4800 | 300 | 62506 |

Table 4.15

Cross-section for $^{115}In(\alpha,4n)^{115}Sb$ reaction

| Incident $\alpha$-particle Energy $E_\alpha$ (MeV) | Gamma ray Energy $E_\gamma$ (MeV) | Cross-section $\sigma$ (mb) | Weighted Average Cross-section $\sigma$ (mb) |
|---|---|---|---|
| 35.1±0.8 | 0.497 | 9.06±0.53 | 9.06±0.53 |
| 37.4±0.7 | 0.497 | 17.64±0.63 | 17.64±0.63 |
| 40.1±0.7 | 0.497 | 48.72±0.67 | 48.72±0.67 |

Contd.....

| | | | |
|---|---|---|---|
| 43.6±0.7 | 0.497 | 169.09±1.08 | 169.09±1.08 |
| 46.8±0.6 | 0.497 | 351.72±1.16 | 351.72±1.16 |
| 50.0±0.5 | 0.497 | 323.64±1.41 | 323.64±1.41 |

### 4.8.1.7 $^{115}In(\alpha,pn)$ Reaction

The product nucleus of this reaction is $^{117m}Sn$. This product nucleus has the metastable state of half life 13.61 days with spin $\frac{11^-}{2}$. This metastable state decays to an intermediate state having the spin $\frac{1^+}{2}$ and the half life of 28 ns. this intermediate state decays to the ground state through electron capture mode and $\beta^+$ emission. The emitted energy is 0.159 MeV. The Q-value of this reaction is -12.1 MeV and the threshold is 12.5 MeV. The decay scheme of $^{117}Sn$ is given in the fig. 4.11. The parameters used to calculate the cross-sections are given in the table 4.16 and the measured cross-sections are given in the table 4.17.

### 4.8.1.8 $^{115}In(\alpha,2p)$ Reaction

The Q-value of this reaction is -12.75 and the product nucleus is $^{117}In$ having the metastable state of half life 1.94 hours and the ground state of 43.8 minutes. The gamma rays followed to calculate the cross-section of metastable state are 0.159 MeV and 0.315 MeV with the abundance 15.9% and 19.0% respectively while in the calculation of that for ground state, the gamma rays followed are 0.159 MeV and 0.553 MeV with abundance

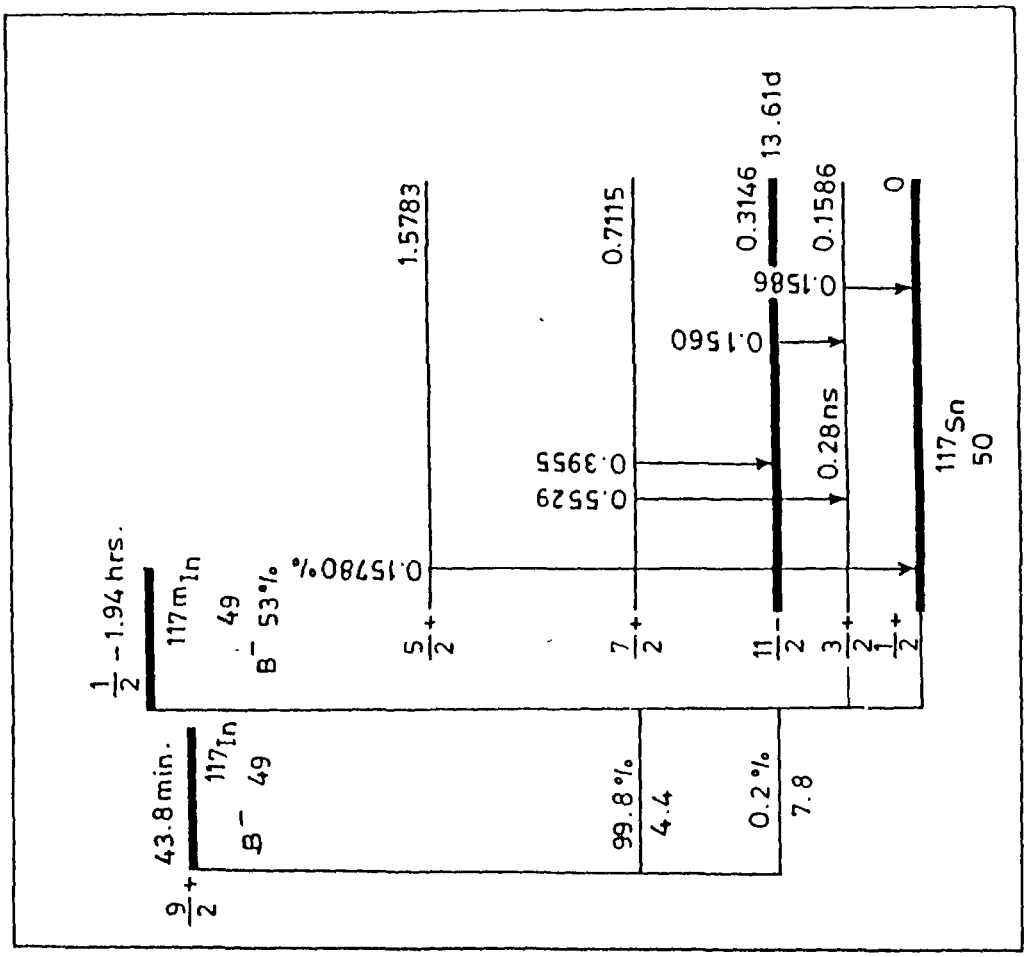


Fig. 4.12 Partial decay scheme of $^{117}In$.

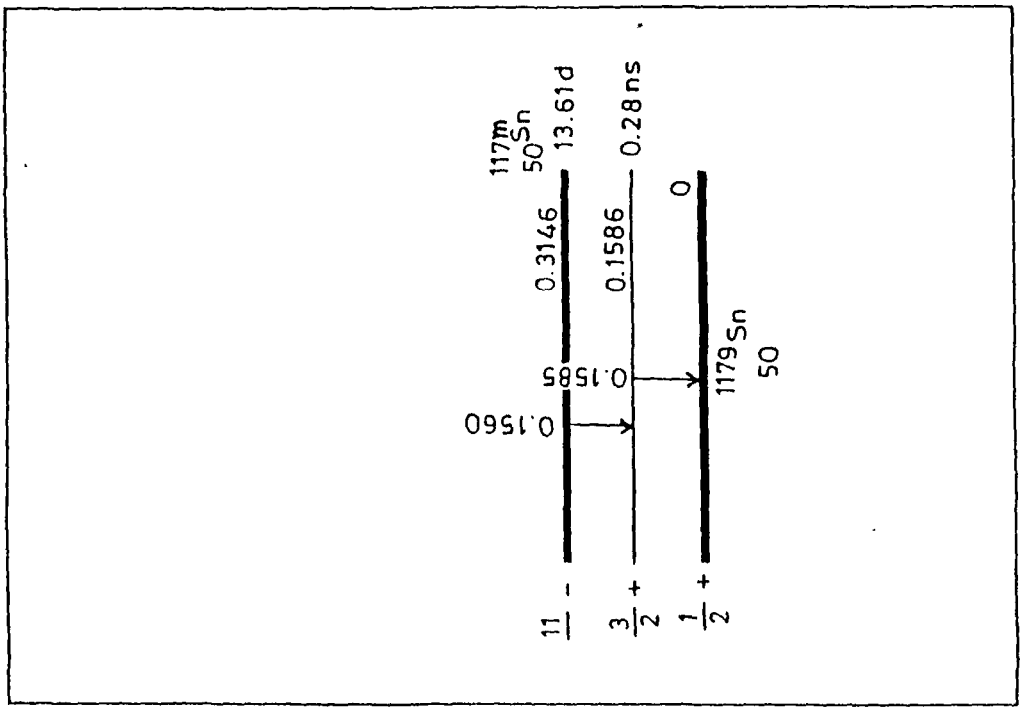


Fig. 4.11 Partial decay Scheme of $^{117m}Sn$.

Table 4.16

Experimental data for $^{115}In(\alpha,pn)^{117m}Sn$ reaction

Half life ($T_{1/2}$) = 13.61 d

Incident flux ($\phi$) = $1.082 \times 10^{11}$ $\alpha$-particles/$cm^2$.s

Number of interacting nuclei ($N_o$) = $8.4105 \times 10^{18}$

| Particle Energy $E_\alpha$ (MeV) | Gamma Energy $E_\gamma$ (MeV) | Absolute $\gamma$-Intensity $\Theta_\gamma$ (%) | Time Lapse $t_2$ (sec.) | Recording Time $t_3$ (sec.) | Photo-peak Counts A |
|---|---|---|---|---|---|
| 21.4±1.4 | 0.159 | 86.4 | 13560 | 300 | 154 |
| 25.2±1.2 | 0.159 | 86.4 | 12720 | 300 | 464 |
| 29.0±1.0 | 0.159 | 86.4 | 11220 | 300 | 1009 |
| 32.2±0.8 | 0.159 | 86.4 | 10440 | 300 | 1515 |
| 35.2±0.8 | 0.159 | 86.4 | 9780 | 300 | 1387 |
| 37.4±0.7 | 0.159 | 86.4 | 8880 | 300 | 971 |
| 40.1±0.7 | 0.159 | 86.4 | 6420 | 300 | 819 |
| 43.6±0.7 | 0.159 | 86.4 | 5640 | 300 | 666 |
| 46.8±0.6 | 0.159 | 86.4 | 3960 | 300 | 604 |
| 50.0±0.5 | 0.159 | 86.4 | 4800 | 300 | 567 |

Table 4.17

Cross-section for $^{115}In(\alpha,pn)^{117m}Sn$ reaction

| Incident α-particle Energy $E_\alpha$ (MeV) | Gamma ray Energy $E_\gamma$ (MeV) | Cross-section σ (mb) | Weighted Average Cross-section σ (mb) |
|---|---|---|---|
| 21.4±1.4 | 0.159 | 17.18±1.38 | 17.18±1.38 |
| 25.2±1.2 | 0.159 | 51.73±2.4 | 51.73±2.40 |
| 29.0±1.0 | 0.159 | 112.40±3.53 | 112.40±3.53 |
| 32.2±0.8 | 0.159 | 168.12±4.33 | 168.12±4.33 |
| 35.1±0.8 | 0.159 | 153.85±4.14 | 153.85±4.14 |
| 37.4±0.7 | 0.159 | 107.64±3.46 | 107.64±3.46 |
| 40.1±0.7 | 0.159 | 90.97±3.17 | 90.97±3.17 |
| 43.6±0.7 | 0.159 | 73.95±2.87 | 73.95±2.87 |
| 46.8±0.6 | 0.159 | 66.99±2.72 | 66.99±2.72 |
| 50.0±0.5 | 0.159 | 62.71±2.6 | 62.71±2.6 |

Table 4.18

Experimental data for $^{115}In(\alpha,2p)^{117g}In$ reaction

Half life ($T_{1/2}$) = 43.8 m

Incident flux ($\phi$) = $1.082 \times 10^{11}$ $\alpha$-particles/$cm^2$.s

Number of interacting nuclei($N_o$) = $8.4105 \times 10^{18}$

| Particle Energy $E_\gamma$ (MeV) | Gamma Energy $E_\gamma$ (MeV) | Absolute $\gamma$-Intensity $\Theta_\gamma$ (%) | Time Lapse $t_2$ (sec.) | Recording Time $t_3$ (sec.) | Photo-peak Counts A |
|---|---|---|---|---|---|
| 32.2±0.8 | 0.159 | 87.0 | 10440 | 300 | 199 |
| | 0.553 | 99.7 | | | 96 |
| 35.2±0.8 | 0.159 | 87.0 | 9780 | 300 | 415 |
| | 0.553 | 99.7 | | | 210 |
| 37.4±0.7 | 0.159 | 87.0 | 8880 | 300 | 1133 |
| | 0.553 | 99.7 | | | 439 |
| 40.1±0.7 | 0.159 | 87.0 | 6420 | 300 | 4329 |
| | 0.553 | 99.7 | | | 1792 |
| 43.6±0.7 | 0.159 | 87.0 | 5640 | 300 | 7926 |
| | 0.553 | 99.7 | | | 3474 |
| 46.8±0.6 | 0.159 | 87.0 | 3960 | 300 | 14219 |
| | 0.553 | 99.7 | | | 6355 |
| 50.0±0.5 | 0.159 | 87.0 | 4800 | 300 | 13043 |
| | 0.553 | 99.7 | | | 5319 |

Table 4.19

Cross-section for $^{115}In(\alpha,2p)^{117g}In$ reaction

| Incident α-particle Energy $E_\alpha$ (MeV) | Gamma ray Energy $E_\gamma$ (MeV) | Cross-section σ (mb) | Weighted Average Cross-section σ (mb) |
|---|---|---|---|
| 32.2±0.8 | 0.159 | 1.49±0.11 | 1.55±0.07 |
| | 0.553 | 1.69±0.17 | |
| 35.1±0.8 | 0.159 | 2.61±0.13 | 2.72±0.13 |
| | 0.553 | 3.01±0.21 | |
| 37.4±0.7 | 0.159 | 5.61±0.17 | 5.44±0.17 |
| | 0.553 | 5.09±0.24 | |
| 40.1±0.7 | 0.159 | 11.22±0.17 | 10.57±0.40 |
| | 0.553 | 10.89±0.26 | |
| 43.6±0.7 | 0.159 | 16.71±0.19 | 16.86±0.16 |
| | 0.553 | 17.19±0.29 | |
| 46.8±0.6 | 0.159 | 19.26±0.16 | 19.53±0.30 |
| | 0.553 | 20.20±0.25 | |
| 50.0±0.5 | 0.159 | 22.06±0.19 | 21.77±0.31 |
| | 0.553 | 21.10±0.29 | |

Table 4.20

Experimental data for $^{115}In(\alpha,2p)^{117m}In$ reaction

Half life ($T_{1/2}$) = 1.94 h

Incident flux ($\phi$) = $1.082 \times 10^{11}$ $\alpha$-particles/$cm^2$.s

Number of interacting nuclei ($N_o$) = $8.4105 \times 10^{18}$

| Particle Energy $E_\alpha$ (MeV) | Gamma Energy $E_\gamma$ (MeV) | Absolute $\gamma$-Intensity $\theta_\gamma$ (%) | Time Lapse $t_2$ (sec.) | Recording Time $t_3$ (sec.) | Photo-peak Counts A |
|---|---|---|---|---|---|
| 32.2±0.8 | 0.159 | 15.9 | 10440 | 300 | 125 |
| | 0.315 | 19.0 | | | 98 |
| 35.2±0.8 | 0.159 | 15.9 | 9780 | 300 | 283 |
| | 0.315 | 19.0 | | | 250 |
| 37.4±0.7 | 0.159 | 15.9 | 8880 | 300 | 446 |
| | 0.315 | 19.0 | | | 434 |
| 40.1±0.7 | 0.159 | 15.9 | 6420 | 300 | 710 |
| | 0.315 | 19.0 | | | 520 |
| 43.6±0.7 | 0.159 | 15.9 | 5640 | 300 | 971 |
| | 0.315 | 19.0 | | | 709 |
| 46.8±0.6 | 0.159 | 15.9 | 3960 | 300 | 1256 |
| | 0.315 | 19.0 | | | 1002 |
| 50.0±0.5 | 0.159 | 15.9 | 4800 | 300 | 1139 |
| | 0.315 | 19.0 | | | 905 |

Table 4.21

Cross-section for $^{115}In(\alpha,2p)^{117m}In$ reaction

| Incident α-particle Energy $E_\alpha$ (MeV) | Gamma ray Energy $E_\gamma$ (MeV) | Cross-section σ (mb) | Weighted Average Cross-section σ (mb) |
|---|---|---|---|
| 32.2±0.8 | 0.159 | 1.53±0.15 | 1.56±0.03 |
| | 0.315 | 1.60±0.17 | |
| 35.1±0.8 | 0.159 | 3.48±0.21 | 3.72±0.26 |
| | 0.315 | 4.08±0.26 | |
| 37.4±0.7 | 0.159 | 5.02±0.24 | 5.58±0.51 |
| | 0.315 | 6.50±0.31 | |
| 40.1±0.7 | 0.159 | 6.25±0.23 | 6.19±0.05 |
| | 0.315 | 6.10±0.27 | |
| 43.6±0.7 | 0.159 | 7.92±0.25 | 7.83±0.08 |
| | 0.315 | 7.70±0.29 | |
| 46.8±0.6 | 0.159 | 8.67±0.24 | 8.89±0.19 |
| | 0.315 | 9.21±0.29 | |
| 50.0±0.5 | 0.159 | 8.62±0.25 | 8.83±0.17 |
| | 0.315 | 9.12±0.30 | |

99.7% respectively. The spin of $^{117}In$ in metastable and ground state are $\frac{1}{2}^-$ and $\frac{9}{2}^+$ respectively. The decay scheme of $^{117}In$ is given in the fig. 4.12. The parameters used to calculate the cross-section for ground state are tabulated in the table 4.18 while the measured cross-sections are given in the table 4.19 and the parameters used to calculate the cross-section for metastable state are arranged in the table 4.20 and the measured cross-sections are given in the table 4.21 while the total cross-sections (ground state + metastable state) are tabulated in table 4.22.

Table 4.22

Total cross-section for $^{115}In(\alpha,2p)^{117(g+m)}In$ reaction

| Incident α-particle Energy $E_\alpha$ (MeV) | Total Cross-section σ (mb) |
|---|---|
| 32.2±0.8 | 3.11±0.08 |
| 35.1±0.8 | 6.44±0.29 |
| 37.4±0.7 | 11.02±0.53 |
| 40.1±0.7 | 16.76±0.40 |
| 43.6±0.7 | 24.69±0.18 |
| 46.8±0.6 | 28.42±0.36 |
| 50.0±0.5 | 30.60±0.35 |

### 4.8.2 Target Nucleus: $^{191,193}Ir$

The iridium target was made by iridium powder of purity better than 99.99% by the vaccum evaporation technique at Variable Energy Cyclotron Centre, Calcutta. This powder was deposited onto the aluminium sheet by using the aforesaid technique. After deposition of powder the measured thickness of iridium layer was 150 $\mu g/cm^2$. This target foil was cut into fifteen pieces and each of the piece was fixed on an aluminium frame having a circular hole of diameter 1.2 cm in its centre while the size of iridium foil was 1.5 x 1.5 cm. These foils of iridium, fixed on aluminium holders were arranged into the form of a stack. The aluminium degraders of different thickness were inserted in between the target foils. The stack arrangement is shown in the fig. 4.13. This stack was irradiated with the $\alpha$-beam of energy 55 MeV. The size of beam was 8 mm. The incident flux was $4.623 \times 10^{10}$ $\alpha$-particles/$cm^2$.s . The incident energy on the foils in the stack is 55.0±0.5, 52.9±0.6, 49.1±0.6, 45.9±0.6, 43.5±0.7, 40.5±0.7, 37.8±0.7, 34.9±0.8, 31.4±0.8, 29.2±0.8, 26.9±0.9, 24.4±0.9, 21.4±1.1, 18.4±1.2 and 16.8±1.3 Mev. In this case the reactions $^{191}Ir(\alpha,n)^{194}Au$, $^{191}Ir(\alpha,2n)^{193}Au$, $^{191}Ir(\alpha,3n)^{192}Au$, $^{191}Ir(\alpha,4n)^{191}Au$, $^{191}Ir(\alpha,5n)^{190}Au$, $^{193}Ir(\alpha,3n)^{194}Au$, $^{193}Ir(\alpha,4n)^{193}Au$, and $^{193}Ir(\alpha,5n)^{192}Au$ have been measured. The percentage of isotopes $^{191}Ir$ and $^{193}Ir$ in natural iridium is found 37.3% and 62.7% respectively. The gamma ray spectrum of activated iridium is shown in the fig. 4.14.

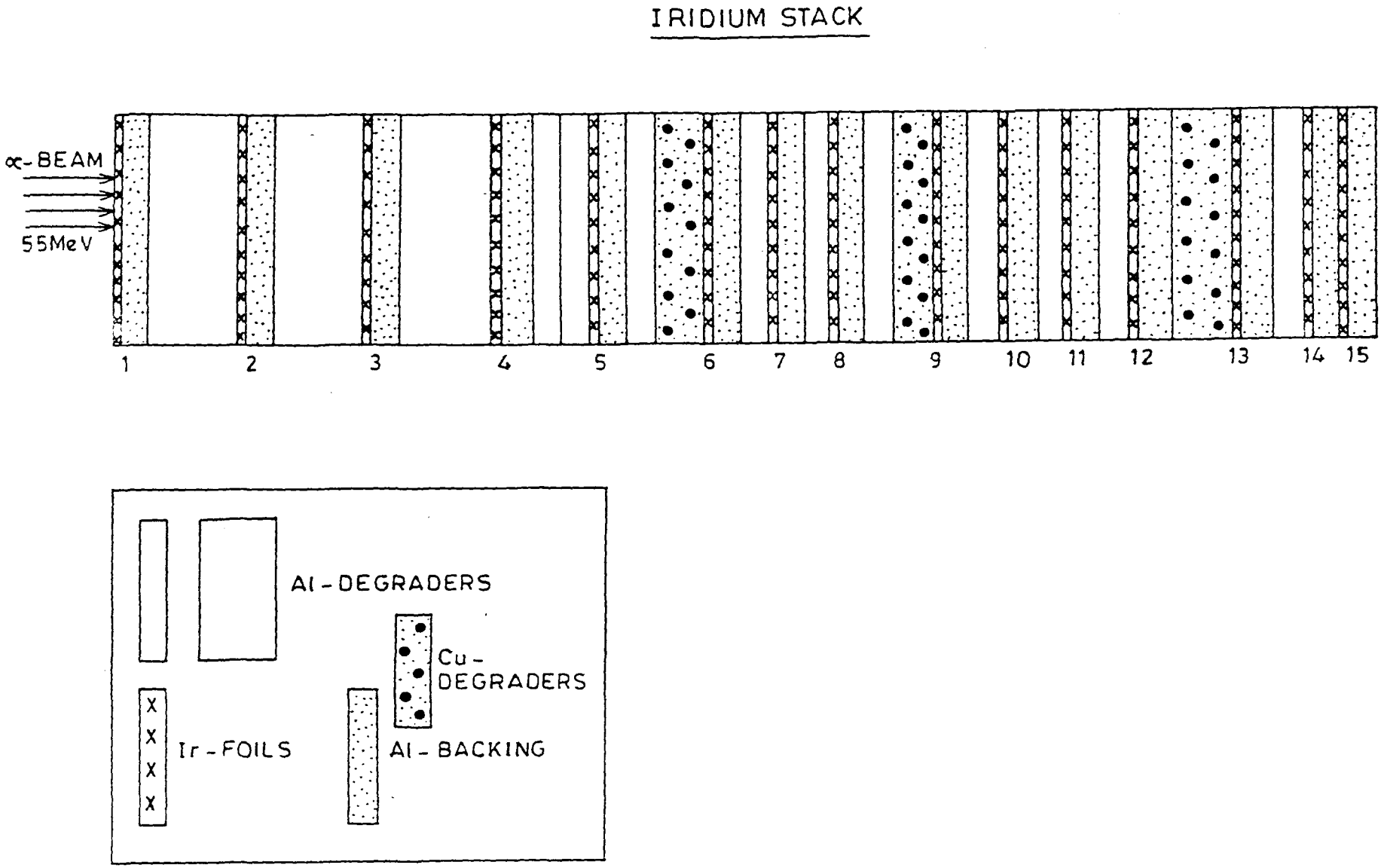


Fig. 4.13 Stack arrangement for the iridium target.

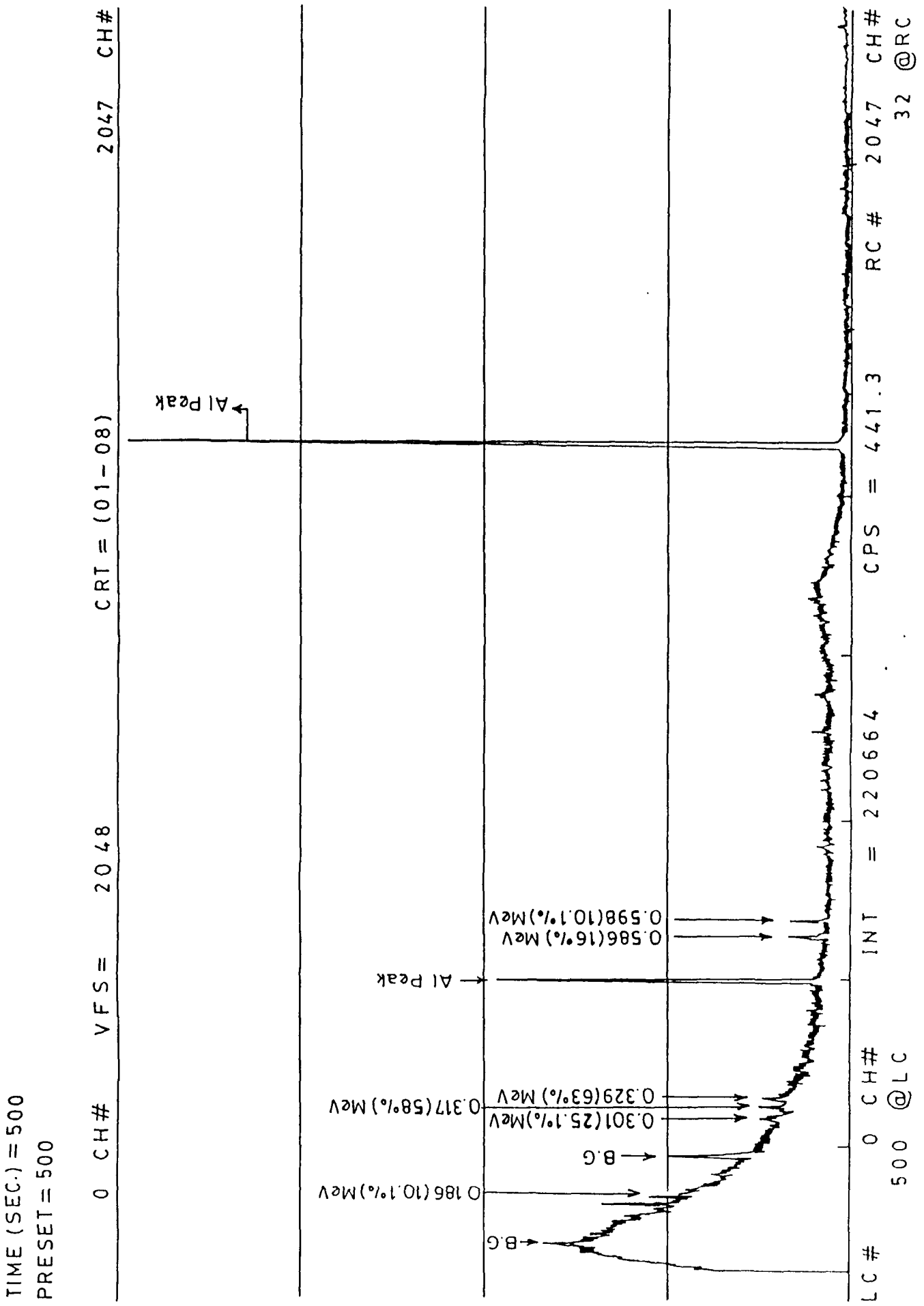


Fig.4.14A typical gamma ray spectrum of activated sample of iridium.

### 4.8.2.1 $^{191}Ir(\alpha,n)$ Reaction

The Q-value of this reaction is -10.09 MeV. The product nucleus $^{194}Au$ has two metastable states other than the ground state. The half life of first metastable state, second metastable state and the ground state is 420 ms with spin $10^-$, 600 ms with spin $5^+$ and 1.646 days with spin $1^-$ respectively. The first metastable state decays to the second metastable state and then the second metastable state decays to the ground state. This ground state of $^{194}Au$ decays to $^{194}Pt$ which gives the gamma rays of energies 0.294 MeV and 0.329 MeV. The absolute intensity of these gamma rays is 11.1% and 63% respectively. The gamma ray of energy 0.294MeV(11.1%) could not be seen in the spectrum due to very low abundance so the cross-sections of the reaction have been calculated by following the 0.329 MeV (63%) gamma ray only. In the decay of $^{194}Au$, some other gamma rays are also available but of negligible abundance. The decay scheme of $^{194}Au$ is shown in fig. 4.15.

The details of parameters used in calculation are given in table 4.23 and the cross-sections measured experimentally at different incident α-particle energies are given in table 4.24.

### 4.8.2.2 $^{191}Ir(\alpha,2n)$ Reaction

The Q-value of the reaction is -17.06 MeV. $^{193}Au$ is the product nucleus of this reaction and has a metastable state of half life 3.9 seconds with spin $\frac{11}{3}^-$ and the ground state of

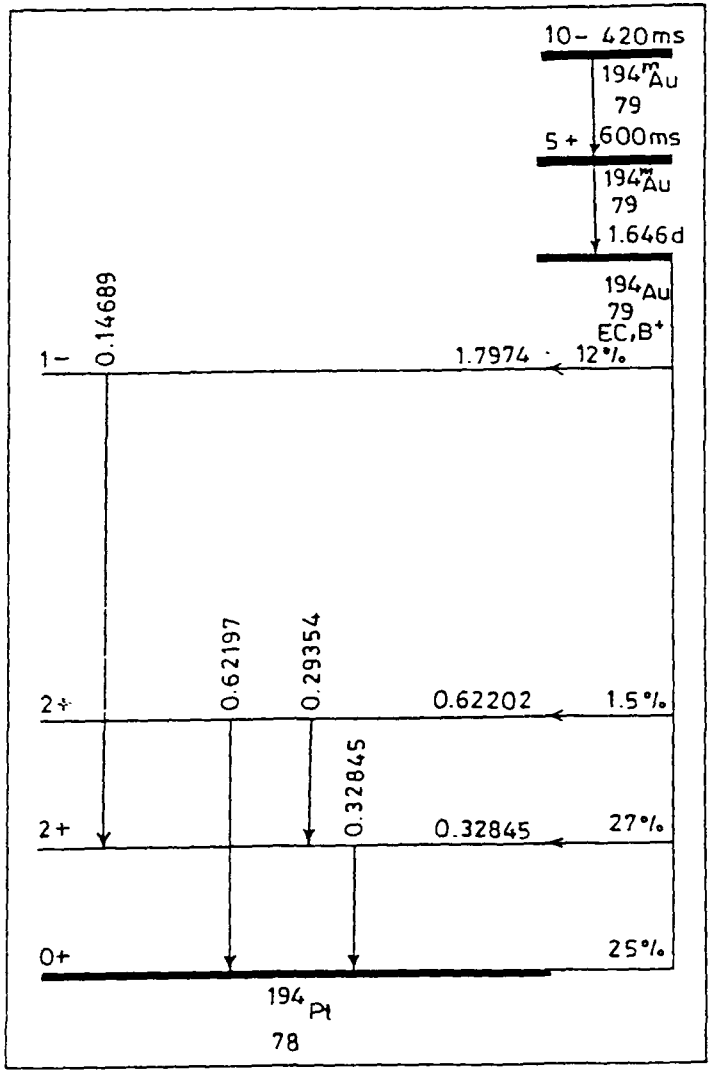


Fig. 4.15 Partial decay scheme of $^{194}Au$.

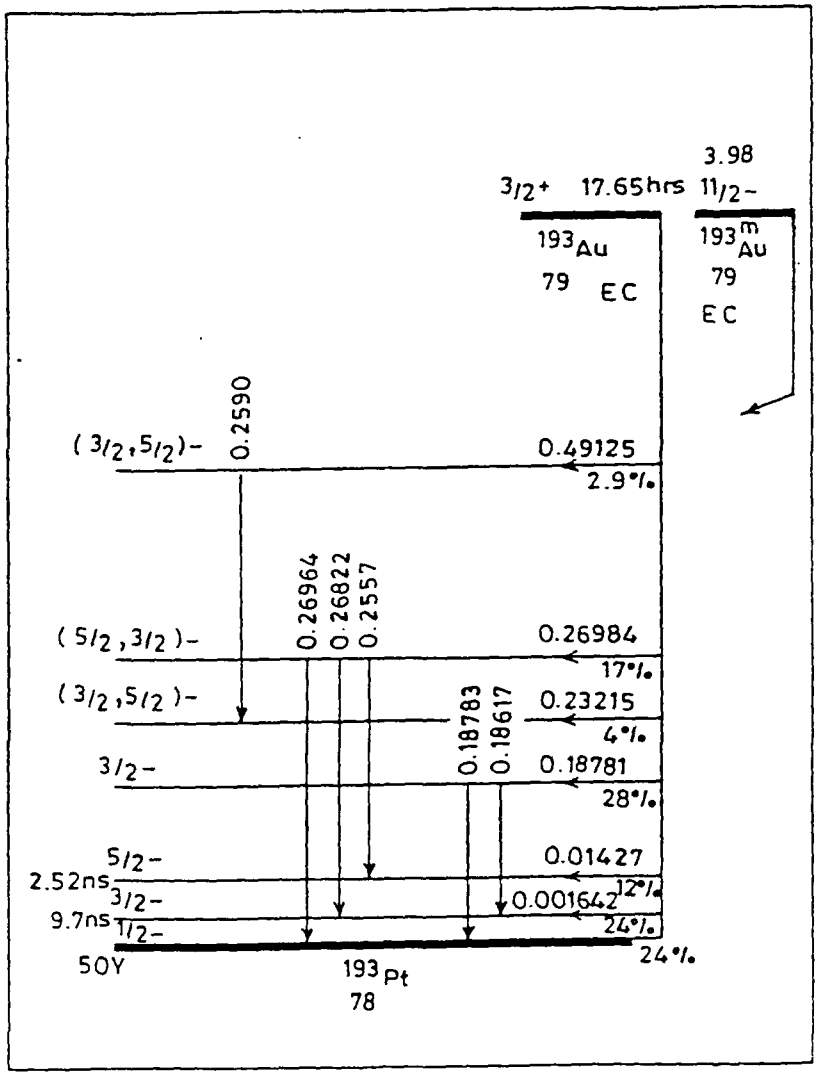


Fig. 4.16 Partial decay scheme of $^{193}Au$.

Table 4.23

Experimental data for $^{191}Ir(\alpha,n)^{194}Au$ reaction

Half life ($T_{1/2}$) = 1.646 d

Incident flux ($\phi$) = $4.623 \times 10^{10}$ $\alpha$-particle/$cm^2$.s

Number of interacting nuclei ($N_o$) = $8.864 \times 10^{16}$

| Particle Energy $E_\alpha$ (MeV) | Gamma Energy $E_\gamma$ (MeV) | Absolute $\gamma$-Intensity $\Theta_\gamma$ (%) | Time Lapse $t_2$ (sec.) | Recording Time $t_3$ (sec.) | Photo-peak Counts A |
|---|---|---|---|---|---|
| 16.8±1.3 | 0.329 | 63.0 | 15240 | 500 | 25 |
| 18.4±1.2 | 0.329 | 63.0 | 14400 | 500 | 29 |
| 21.4±1.1 | 0.329 | 63.0 | 12420 | 500 | 30 |
| 24.4±0.9 | 0.329 | 63.0 | 11640 | 500 | 14 |
| 26.9±0.9 | 0.329 | 63.0 | 10740 | 500 | 10 |
| 29.2±0.8 | 0.329 | 63.0 | 9600 | 500 | 11 |
| 31.4±0.8 | 0.329 | 63.0 | 8700 | 500 | 12 |
| 34.9±0.8 | 0.329 | 63.0 | 7440 | 500 | 10 |
| 37.8±0.7 | 0.329 | 63.0 | 6720 | 300 | 5 |

Table 4.24

Cross-section for $^{191}Ir(\alpha,n)^{194}Au$ reaction

| Incident α-particle Energy $E_\alpha$ (MeV) | Gamma ray Energy $E_\gamma$ (MeV) | Cross-section σ (mb) | Weighted Average Cross-section σ (mb) |
|---|---|---|---|
| 16.8±1.3 | 0.329 | 45.38±9.07 | 45.38±9.07 |
| 18.4±1.2 | 0.329 | 56.49±10.48 | 56.49±10.48 |
| 21.4±1.1 | 0.329 | 57.84±10.49 | 57.84±10.49 |
| 24.4±0.9 | 0.329 | 26.80±6.17 | 26.80±7.16 |
| 26.9±0.9 | 0.329 | 19.13±6.04 | 19.13±6.04 |
| 29.2±0.8 | 0.329 | 20.92±6.31 | 90.92±6.31 |
| 31.4±0.8 | 0.329 | 22.73±6.56 | 22.73±6.56 |
| 34.9±0.8 | 0.329 | 18.82±5.95 | 18.82±5.95 |
| 37.8±0.7 | 0.329 | 15.62±6.98 | 15.62±6.98 |

half life 17.65 h with the spin $\frac{3}{2}^+$. The metastable state decays 99.97% to the ground state and 0.03% to the metastable state of $^{193}Pt$ while the ground state of $^{193}Au$ decays totally to the metastable state of $^{193}Pt$ by emitting the gamma rays. In the calculation of reaction cross-section only one gamma ray of 0.186 MeV with abundance 10.1%was followed. Of course, some other gamma rays are also available in the decay of product nucleus understudy but with very low intensity so those gamma rayscould not be observed in our spectrum.

The decay scheme of product nucleus $^{193}Au$ is shown in the fig. 4.16. The parameters used in the calculations are arranged in the table 4.25 while the cross-sections calculated experimentally at different incident α-particle energies are given in the table 4.26.

### 4.8.2.3 $^{191}Ir(\alpha,3n)$ Reaction

The Q-value of this reaction is -25.71 MeV. In this reaction the product nucleus is $^{192}Au$ which has a metastable state of half life 167 ms with the spin $11^-$ and the ground state of half life 4.94 h with spin $1^-$. The metastable state decays totally to the ground state and this ground state decays to the levels of $^{192}Pt$. In the calculation of reaction cross-section the gamma ray of 0.317 MeV (58.0%) has been taken into the consideration.

Table 4.25

Experimental data for $^{191}Ir(\alpha,2n)^{193}Au$ reaction

Half life ($T_{1/2}$) = 17.65 h

Incident flux ($\phi$) = $4.623 \times 10^{10}$ $\alpha$-particles/$cm^2$.s

Number of interacting nuclei($N_o$) = $8.864 \times 10^{16}$

| Particle Energy $E_\alpha$ (MeV) | Gamma Energy $E_\gamma$ (MeV) | Absolute $\gamma$-Intensity $\Theta_\gamma$ (%) | Time Lapse $t_2$ (sec.) | Recording Time $t_3$ (sec.) | Photo-peak Counts A |
|---|---|---|---|---|---|
| 16.8±1.3 | 0.186 | 10.1 | 15240 | 500 | 22 |
| 18.4±1.2 | 0.186 | 10.1 | 14400 | 500 | 88 |
| 21.4±1.1 | 0.186 | 10.1 | 12420 | 500 | -- |
| 24.4±0.9 | 0.186 | 10.1 | 11640 | 500 | 249 |
| 26.9±0.9 | 0.186 | 10.1 | 10740 | 500 | 326 |
| 29.2±0.8 | 0.186 | 10.1 | 9600 | 500 | 309 |
| 31.4±0.8 | 0.186 | 10.1 | 8700 | 500 | -- |
| 34.9±0.8 | 0.186 | 10.1 | 7440 | 500 | 137 |
| 37.8±0.7 | 0.186 | 10.1 | 6720 | 300 | 43 |
| 40.5±0.7 | 0.186 | 10.1 | 6000 | 300 | 37 |
| 43.5±0.7 | 0.186 | 10.1 | 5340 | 300 | 31 |
| 45.9±0.6 | 0.186 | 10.1 | 4680 | 300 | 29 |
| 49.1±0.6 | 0.186 | 10.1 | 4020 | 300 | 24 |
| 52.9±0.6 | 0.186 | 10.1 | 3300 | 300 | 18 |
| 55.0±0.5 | 0.186 | 10.1 | 2280 | 300 | 16 |

Table 4.26

Cross-section for $^{191}Ir(\alpha,2n)^{193}Au$ reaction

| Incident α-particle Energy $E_\alpha$ (MeV) | Gamma ray Energy $E_\gamma$ (MeV) | Cross-section σ (mb) | Weighted Energy Cross-section σ (mb) |
|---|---|---|---|
| 16.8±1.3 | 0.186 | 49.96±10.65 | 49.96±10.65 |
| 18.4±1.2 | 0.186 | 198.03±21.11 | 198.03±21.11 |
| 21.4±1.1 | 0.186 | - | - |
| 24.4±0.9 | 0.186 | 543.78±34.46 | 543.78±34.46 |
| 26.9±0.9 | 0.186 | 704.97±39.04 | 704.97±39.04 |
| 29.2±0.8 | 0.186 | 659.95±37.54 | 659.95±37.54 |
| 31.4±0.8 | 0.186 | - | - |
| 34.9±0.8 | 0.186 | 285.76±24.41 | 285.76±24.41 |
| 37.8±0.7 | 0.186 | 148.15±22.59 | 148.15±22.59 |
| 40.5±0.7 | 0.186 | 126.49±20.79 | 126.49±20.79 |
| 43.5±0.7 | 0.186 | 109.16±19.60 | 109.16±19.60 |
| 45.9±0.6 | 0.186 | 97.72±18.15 | 97.72±18.15 |
| 49.1±0.6 | 0.186 | 80.29±16.39 | 80.29±16.39 |
| 52.9±0.6 | 0.186 | 59.74±14.08 | 59.74±14.08 |
| 55.0±0.5 | 0.186 | 52.51±13.12 | 52.51±13.12 |

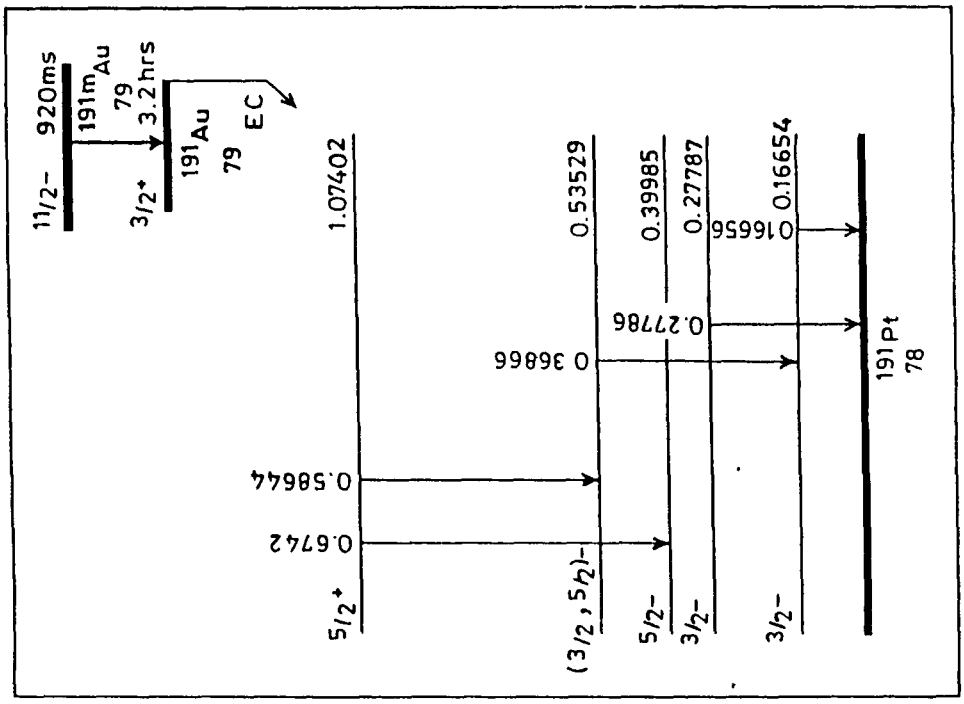


Fig. 4.18 Partial decay scheme of $^{191}_{79}Au$.

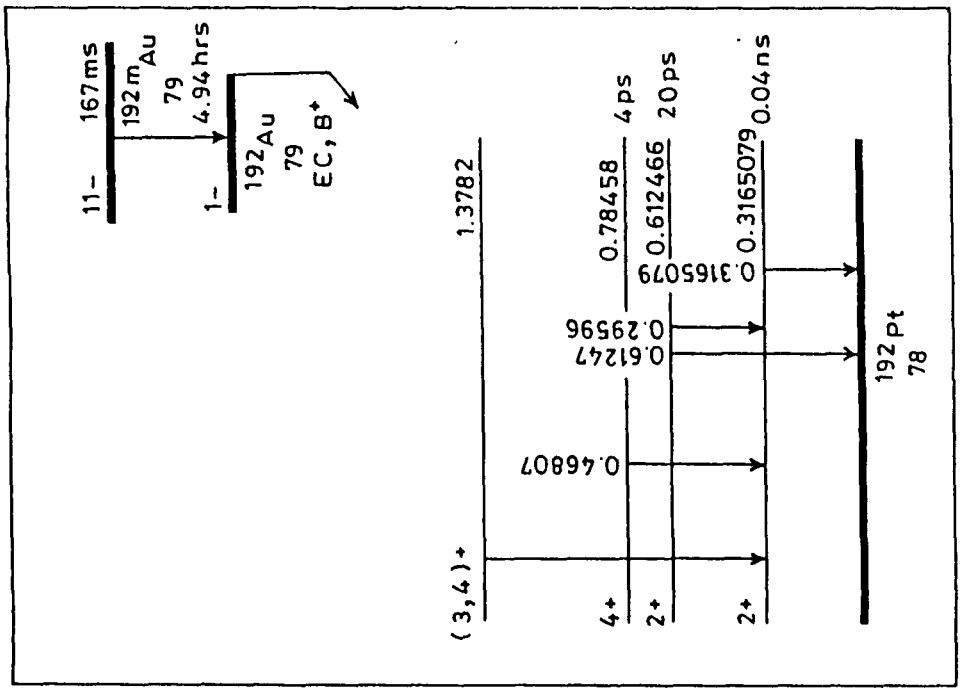


Fig. 4.17 Partial decay scheme of $^{192}_{79}Au$.

The decay scheme of the product nucleus understudy is shown in the fig. 4.17. The parameters used in the reaction cross-section calculation are given in the table 4.27 while the calculated cross-section with the incident α-particle energy is given in the table 4.28.

### 4.8.2.4 $^{191}Ir(\alpha,4n)$ Reaction

The product nucleus of this reaction is $^{191}Au$ which has the metastable state of half life 920 ms with $\frac{11^-}{2}$ spin and the ground state having the half life 3.18 h with the spin $\frac{3^+}{2}$. The metastable state decays to the ground state and the ground state decays to the levels of $^{191}Pt$ which emits few gamma rays. All the gamma ray energies except 0.586 MeV emitted in the decay of product nucleus understudy have very poor intensity (less than 1%), which could not be observed in our spectra hence in the claculation of reaction cross-section the photo-peak counts are calculated by following the 0.586 MeV (16%) gamma ray energy only. The Q-value of this reaction is -32.68 MeV.

The decay scheme of product nucleus $^{191}Au$ is shown in the fig. 4.18. The experimental parameters used in the calculation of reaction cross-section are given in the table 4.29 while the incident α-particle energies and the corresponding cross-sections are given in the table 4.30.

## Table 4.27

Experimental data for $^{191}Ir(\alpha,3n)^{192}Au$ reaction

Half life ($T_{1/2}$) = 4.94 h

Incident flux ($\phi$) = $4.623 \times 10^{10}$ $\alpha$-particles/$cm^2$.s

Number of interacting nuclei($N_o$) = $8.864 \times 10^{16}$

| Particle Energy $E_\alpha$ (MeV) | Gamma Energy $E_\gamma$ (MeV) | Absolute $\gamma$-Intensity $\theta_\gamma$ (%) | Time Lapse $t_2$ (sec.) | Recording Time $t_3$ (sec.) | Photo-peak Counts A |
|---|---|---|---|---|---|
| 26.9±0.9 | 0.317 | 58.0 | 10740 | 500 | 218 |
| 29.2±0.8 | 0.317 | 58.0 | 9600 | 500 | 947 |
| 31.4±0.8 | 0.317 | 58.0 | 8700 | 500 | 1577 |
| 34.9±0.8 | 0.317 | 58.0 | 7440 | 500 | 3781 |
| 37.8±0.7 | 0.317 | 58.0 | 6720 | 300 | 1949 |
| 40.5±0.7 | 0.317 | 58.0 | 6000 | 300 | 1710 |
| 43.5±0.7 | 0.317 | 58.0 | 5340 | 300 | 1117 |
| 45.9±0.6 | 0.317 | 58.0 | 4680 | 300 | 916 |
| 49.1±0.6 | 0.317 | 58.0 | 4020 | 300 | 579 |
| 52.9±0.6 | 0.317 | 58.0 | 3300 | 300 | 475 |
| 55.0±0.5 | 0.317 | 58.0 | 2280 | 300 | 409 |

Table 4.28

Cross-section for $^{191}Ir(\alpha,3n)^{192}Au$ reaction

| Incident α-particle Energy $E_\alpha$ (MeV) | Gamma ray Energy $E_\gamma$ (MeV) | Cross-section σ (mb) | Weighted Average Cross-section σ (mb) |
|---|---|---|---|
| 26.9±0.9 | 0.317 | 82.50±5.58 | 82.50±5.58 |
| 29.2±0.8 | 0.317 | 342.84±11.14 | 342.84±11.14 |
| 31.4±0.8 | 0.317 | 551.24±13.88 | 551.24±13.88 |
| 34.9±0.8 | 0.317 | 1262.35±20.46 | 1262.35±20.46 |
| 37.8±0.7 | 0.317 | 1047.25±23.72 | 1047.25±23.72 |
| 40.5±0.7 | 0.317 | 893.41±21.60 | 893.41±21.60 |
| 43.5±0.7 | 0.317 | 596.26±17.42 | 596.26±17.42 |
| 45.9±0.6 | 0.317 | 454.56±15.01 | 454.56±16.01 |
| 49.1±0.6 | 0.317 | 280.04±11.63 | 280.04±11.63 |
| 52.9±0.6 | 0.317 | 214.91±10.05 | 214.91±10.05 |
| 55.0±0.5 | 0.317 | 184.85±9.14 | 184.85±9.14 |

Table 4.29

Experimental data for $^{191}Ir(\alpha,4n)^{191}Au$ reaction

Half life ($T_{1/2}$) = 3.18 h

Incident flux ($\phi$) = $4.623 \times 10^{10}$ $\alpha$-particles/$cm^2$.s

Number of interacting nuclei ($N_o$) = $8.864 \times 10^{16}$

| Particle Energy $E_\alpha$ (MeV) | Gamma Energy $E_\gamma$ (MeV) | Absolute $\gamma$-Intensity $\Theta_\gamma$ (%) | Time Lapse $t_2$ (sec.) | Recording Time $t_3$ (sec.) | Photo peak Counts A |
|---|---|---|---|---|---|
| 40.5±0.7 | 0.586 | 16.0 | 6000 | 300 | 41 |
| 43.5±0.7 | 0.586 | 16.0 | 5340 | 300 | 134 |
| 45.9±0.6 | 0.586 | 16.0 | 4680 | 300 | 248 |
| 49.1±0.6 | 0.586 | 16.0 | 4020 | 300 | 325 |
| 52.9±0.6 | 0.586 | 16.0 | 3300 | 300 | 259 |
| 55.0±0.5 | 0.586 | 16.0 | 2280 | 300 | 151 |

Table 4.30

Cross-section for $^{191}Ir(\alpha,4n)^{191}Au$ reaction

| Incident $\alpha$-particle Energy $E_\alpha$ (MeV) | Gamma ray Energy $E_\gamma$ (MeV) | Cross-section $\sigma$ (mb) | Weighted Average Cross-section $\sigma$ (mb) |
|---|---|---|---|
| 40.5±0.7 | 0.586 | 115.06±17.96 | 115.06±17.96 |
| 43.5±0.7 | 0.586 | 361.35±31.21 | 361.35±31.21 |
| 45.9±0.6 | 0.586 | 642.58±40.80 | 642.58±40.80 |
| 49.1±0.6 | 0.586 | 809.11±44.88 | 809.11±44.88 |
| 52.9±0.6 | 0.586 | 617.30±38.36 | 617.30±38.36 |
| 55.0±0.5 | 0.586 | 338.34±27.53 | 338.34±27.53 |

### 4.8.2.5 $^{191}Ir(\alpha,5n)$ Reaction

The product nucleus $^{190}Au$ has no metastable state. The half life of ground state is 42.8 minutes and the spin is $1^-$. The decay of ground state of $^{190}Au$ to the levels of $^{190}Pt$ is through the electron capture and the $\beta^+$ emission. The percentage of decay through electron capture is 98% and that of through $\beta^+$ emission is 2% only. In the decay, the product nucleus understudy emits various gamma rays but most of them are of negligible intensity so these could not be observed in our experimental spectra. Only the gamma ray of 0.598 MeV and 0.301 MeV with intensity 10.1% and 25.1% respectively could be observed. So in the calculation of reaction cross-section the photopeak counts are calculated by following these gamma rays only. The Q-value of this reaction is -41.75 MeV.

The parameters used in the calculation of reaction cross-section are given in the table 4.31 and the cross-sections corresponding to the incidents $\alpha$-particle energies are given in the table 4.32. The decay scheme of product nucleus $^{190}Au$ is given in the fig. 4.19.

### 4.8.2.6 $^{193}Ir(\alpha,3n)$ Reaction

The Q-value of this reaction is -24.05 MeV respectively. The product nucleus of this reaction is $^{194}Au$ which is also the product nucleus of $^{191}Ir(\alpha,n)$ reaction. Hence every information

Table 4.31

Experimental data for $^{191}Ir(\alpha,5n)^{190}Au$ reaction

Half life ($T_{1/2}$) = 42.8 m.

Incident flux ($\phi$) = $4.623 \times 10^{10}$ $\alpha$-particles/$cm^2$.s

Number of interacting nuclei ($N_o$) = $8.864 \times 10^{16}$

| $\alpha$-particle Energy $E_\alpha$ (MeV) | Gamma Energy $E_\gamma$ (MeV) | Absolute $\gamma$-Intensity $\Theta_\gamma$ (%) | Time Lapse $t_2$ (sec.) | Recording Time $t_3$ (sec.) | Photo-peak Counts A |
|---|---|---|---|---|---|
| 49.1±0.6 | 0.301 | 25.1 | 4020 | 300 | 149 |
| | 0.598 | 10.1 | | | 22 |
| 52.9±0.6 | 0.301 | 25.1 | 3300 | 300 | 410 |
| | 0.598 | 10.1 | | | 95 |
| 55.0±0.5 | 0.301 | 25.1 | 2280 | 300 | 1600 |
| | 0.598 | 10.1 | | | 311 |

Table 4.32

Cross-section for $^{191}Ir(\alpha,5n)^{190}Au$ reaction

| Incident $\alpha$-particle Energy $E_\alpha$ (MeV) | Gamma ray Energy $E_\gamma$ (MeV) | Cross-section $\sigma$ (mb) | Weighted Average Cross-section $\sigma$ (mb) |
|---|---|---|---|
| 49.1±0.6 | 0.301 | 84.01±6.80 | 80.88±4.65 |
| | 0.598 | 67.07±14.30 | |
| 52.9±0.6 | 0.301 | 190.35±9.40 | 196.54±11.40 |
| | 0.598 | 238.51±24.47 | |
| 55.0±0.5 | 0.301 | 564.11±14.11 | 568.43±7.27 |
| | 0.598 | 592.94±33.62 | |

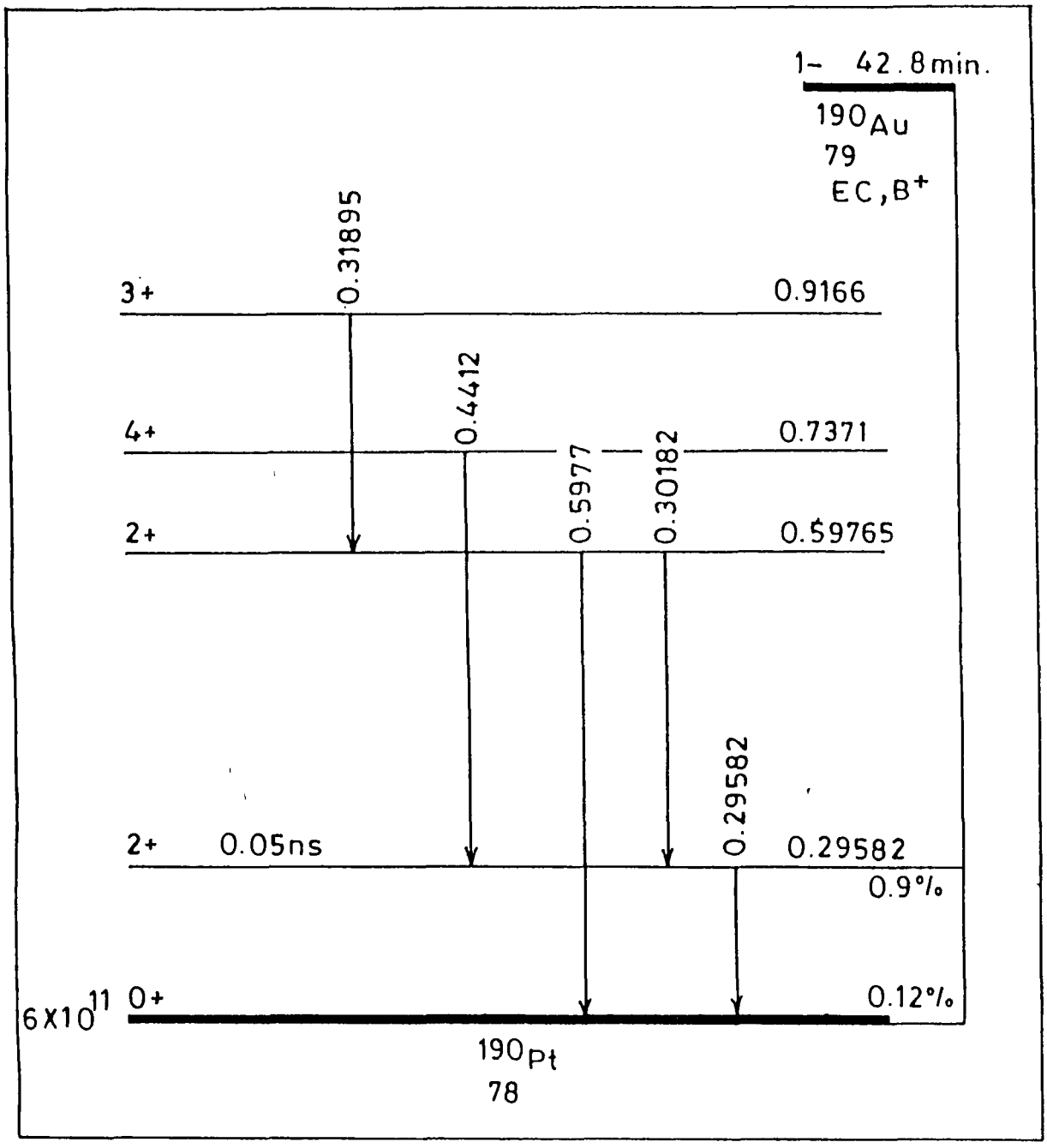


Fig. 4.19 Partial decay scheme of $^{190}Au$.

about the product nucleus is same as has been given in article 4.8.2.1. Beyond 24.40 MeV incident energy both the reactions $^{191}Ir(\alpha,n)$ and $^{193}Ir(\alpha,3n)$ go on simultaneously so the photo-peak counts of the gamma ray of 0.329 MeV (63%), are the total of the photo-peak counts of these two reactions. In order to calculate the cross-sections seperately the counts are separated using the theoretical cross-sections of these reactions.

The decay scheme of $^{194}Au$ is shown in fig. 4.15, and parameters used in the calculation of reaction cross-section are given in the table 4.33 and the experimentally measured cross-sections corresponding to the α-particle incident energies are given in the table 4.34.

### 4.8.2.7 $^{193}Ir(\alpha,4n)$ Reaction

The Q-value of this reaction is -28.50 MeV. The product nucleus of this reaction and $^{191}Ir(\alpha,2n)$ reaction is same i.e. $^{193}Au$, so half life, states, and decay etc. of $^{193}Au$ can be seen from article 4.8.2.2. After opening the channel of this reaction the counts under photo-peak are the sum of photo-peak counts of these two reactions separately. Hence to separate the activity of these two reactions, the help of theoretical cross-section has been taken.

The decay scheme of $^{193}Au$ is shown in the fig.4.16 and the parameters used in the calculation of reaction cross-sections are given in the table 4.35 while by the use of these parameters,

Table 4.33

Experimental data for $^{193}Ir(\alpha,3n)^{194}Au$ reaction

Half life ($T_{1/2}$) = 1.646 d

Incident flux ($\phi$) = $4.623 \times 10^{10}$ $\alpha$-particles/$cm^2$.s

Number of interacting nuclei($N_0$) = $1.475 \times 10^{17}$

| Particle Energy $E_\alpha$ (MeV) | Gamma Energy $E_\gamma$ (MeV) | Absolute $\gamma$-Intensity $\Theta_\gamma$ (%) | Time Lapse $t_2$ (sec.) | Recording Time $t_3$ (sec.) | Photo-peak Counts A |
|---|---|---|---|---|---|
| 24.4±0.9 | 0.329 | 63 | 11640 | 500 | 65 |
| 26.9±0.9 | 0.329 | 63 | 10740 | 500 | 189 |
| 29.2±0.8 | 0.329 | 63 | 9600 | 500 | 509 |
| 31.4±0.8 | 0.329 | 63 | 8700 | 500 | 1004 |
| 34.9±0.8 | 0.329 | 63 | 7440 | 500 | 1070 |
| 37.8±0.7 | 0.329 | 63 | 6720 | 300 | 565 |
| 40.5±0.7 | 0.329 | 63 | 6000 | 300 | 458 |
| 43.5±0.7 | 0.329 | 63 | 5340 | 300 | 335 |
| 45.9±0.6 | 0.329 | 63 | 4680 | 300 | 257 |
| 49.1±0.6 | 0.329 | 63 | 4020 | 300 | 149 |
| 52.9±0.6 | 0.329 | 63 | 3300 | 300 | 138 |
| 55.0±0.5 | 0.329 | 63 | 2280 | 300 | 135 |

Table 4.34

Cross-section for $^{193}Ir(\alpha,3n)^{194}Au$ reaction

| Incident α-particle Energy $E_\alpha$ (MeV) | Gamma ray Energy $E_\gamma$ (MeV) | Cross-section σ (mb) | Weighted Average Cross-section σ (mb) |
|---|---|---|---|
| 24.4±0.9 | 0.329 | 75.06±9.31 | 75.06±9.31 |
| 26.9±0.9 | 0.329 | 217.36±15.81 | 217.36±15.81 |
| 29.2±0.8 | 0.329 | 582.15±25.80 | 582.15±25.80 |
| 31.4±0.8 | 0.329 | 1143.25±36.08 | 1143.25±36.08 |
| 34.9±0.8 | 0.329 | 1210.93±37.05 | 1210.93±37.05 |
| 37.8±0.7 | 0.329 | 1062.06±62.67 | 1062.06±62.67 |
| 40.5±0.7 | 0.329 | 857.46±40.06 | 857.46±40.06 |
| 43.5±0.7 | 0.329 | 624.92±34.14 | 624.93±34.14 |
| 45.9±0.6 | 0.329 | 477.93±29.81 | 477.93±29.81 |
| 49.1±0.6 | 0.329 | 276.20±22.61 | 276.20±22.61 |
| 52.9±0.6 | 0.329 | 254.91±21.70 | 254.91±21.70 |
| 55.0±0.5 | 0.329 | 248.13±21.36 | 248.13±21.36 |

obtained cross-sections corresponding of incident α-particle energies are given in the table 4.36.

### 4.8.2.8 $^{193}Ir(\alpha,5n)$ Reaction

In this reaction the product nucleus is same as that in the reaction $^{191}Ir(\alpha,3n)$ i.e. $^{192}Au$. The properties of the product nucleus understudy have already been discussed in article 4.8.2.3. In common region of excitation function of $^{191}Ir(\alpha,3n)$ reaction and $^{193}Ir(\alpha,5n)$ reactions, cross-sections are separated by using the theoretical cross-section of these two reactions. The Q-value of this reaction is -39.68 MeV.

The decay scheme of product nucleus $^{192}Au$ is shown in the fig. 4.17. The parameters used to calculate the cross-sections are given in the table 4.37 while the obtained cross-section at different incident α-particle energies are given in the table 4.38.

## 4.8.3 Target Nucleus $^{121,123}Sb$

The natural antimony has two isotopes with the mass number 121 and 123. The abundance of $^{121}Sb$ and $^{123}Sb$ in natural Sb is 57.3% and 42.7% respectively. In the present experiment, the sample of this element was made by depositing the antimony powder on aluminium sheet of thickness 6.75 mg/cm$^2$, with the help of vaccum evaporation technique. This large target foil was cut into 12 pieces of size 1.5 cm x 1.5 cm. These pieces

Table 4.35

Experimental data for $^{193}Ir(\alpha,4n)^{193}Au$ reaction

Half life ($T_{1/2}$) = 17.65 h.

Incident flux ($\phi$) = $4.623 \times 10^{10}$ $\alpha$-particles/$cm^2$.s

Number of interacting nuclei ($N_o$) = $1.475 \times 10^{17}$

| Particle Energy $E_\alpha$ (MeV) | Gamma Energy $E_\gamma$ (MeV) | Absolute $\gamma$-Intensity $E_\gamma$ (MeV) | Time Lapse $t_2$ (sec.) | Recording Time $t_3$ (sec.) | Photo-peak Counts A |
|---|---|---|---|---|---|
| 34.9±0.8 | 0.186 | 10.1 | 7440 | 500 | 42 |
| 37.8±0.7 | 0.186 | 10.1 | 6720 | 300 | 261 |
| 40.5±0.7 | 0.186 | 10.1 | 6000 | 300 | 366 |
| 43.5±0.7 | 0.186 | 10.1 | 5340 | 300 | 493 |
| 45.9±0.6 | 0.186 | 10.1 | 4680 | 300 | 563 |
| 49.1±0.6 | 0.186 | 10.1 | 4090 | 300 | 453 |
| 52.9±0.6 | 0.186 | 10.1 | 3300 | 300 | 423 |
| 55.0±0.5 | 0.186 | 10.1 | 2280 | 300 | 305 |

Table 4.36

Cross-section for $^{193}Ir(\alpha,4n)^{193}Au$ reaction

| Incident α-particle Energy $E_\alpha$ (MeV) | Gamma ray Energy $E_\gamma$ (MeV) | Cross-section $\sigma$ (mb) | Weighted Average Cross-section $\bar{\sigma}$ (mb) |
|---|---|---|---|
| 34.9±0.8 | 0.186 | 52.66±8.13 | 52.66±8.13 |
| 37.8±0.7 | 0.186 | 540.61±33.46 | 540.61±33.46 |
| 40.5±0.7 | 0.186 | 752.18±39.32 | 752.18±39.32 |
| 43.5±0.7 | 0.186 | 1043.65±47.00 | 1043.65±47.00 |
| 45.9±0.6 | 0.186 | 1140.52±48.06 | 1140.52±48.06 |
| 49.1±0.6 | 0.186 | 911.09±42.80 | 911.09±42.80 |
| 52.9±0.6 | 0.186 | 844.04±41.04 | 844.04±41.04 |
| 55.0±0.5 | 0.186 | 601.81±34.46 | 601.81±34.46 |

Table 4.37

Experimental data for $^{193}Ir(\alpha,5n)^{192}Au$ reaction

Half life ($T_{1/2}$) = 4.94 h

Incident flux ($\phi$) = $4.623 \times 10^{10}$ $\alpha$-particles/$cm^2$ s

Number of interacting nuclei ($N_o$) = $1.4745 \times 10^{17}$

| Particle Energy $E_\alpha$ (MeV) | Gamma Energy $E_\gamma$ (MeV) | Absolute $\gamma$-Intensity $\theta_\gamma$ (%) | Time Lapse $t_2$ (sec.) | Recording Time $t_3$ (sec.) | Photo-peak Counts A |
|---|---|---|---|---|---|
| 45.9±0.6 | 0.317 | 58.0 | 4680 | 300 | 14 |
| 49.1±0.6 | 0.317 | 58.0 | 4020 | 300 | 367 |
| 52.9±0.6 | 0.317 | 58.0 | 3300 | 300 | 1365 |
| 55.0±0.5 | 0.317 | 58.0 | 2280 | 300 | 1823 |

Table 4.38

Cross-section for $^{193}Ir(\alpha,5n)^{192}Au$ reaction

| Incident $\alpha$-particle Energy $E_\alpha$ (MeV) | Gamma ray Energy $E_\gamma$ (MeV) | Cross-section $\sigma$ (mb) | Weighted Average Cross-section $\sigma$ (mb) |
|---|---|---|---|
| 45.9±0.6 | 0.317 | 4.17±1.11 | 4.17±1.11 |
| 49.1±0.6 | 0.317 | 106.70±5.56 | 106.70±5.56 |
| 52.9±0.6 | 0.317 | 385.89±10.44 | 385.89±10.44 |
| 55.0±0.5 | 0.317 | 495.30±11.60 | 495.30±11.60 |

were weighed accurately and it was found that thickness of antimony powder on aluminium sheet was 1 mg/cm$^2$. These pieces were fixed on aluminium frames (all of same size) with the circular hole in their centres. The diameter of this circular hole was measured 1.2 cm. These aluminium frames with the target foils were arranged into the form of a stack. In the stack, in between of the target foils, the aluminium degrader were also inserted so that we might hit the particle foil with the desired energy of incident α-beam. The incident energy on the target foils was 55.0±0.5 MeV, 52.1±0.6 MeV, 48.9±0.6 MeV, 45.7±0.7 MeV, 43.2±0.7 MeV, 40.1±0.8 MeV, 37.3±0.8 MeV, 34.3±0.8 MeV, 30.7±0.9 MeV, 27.2±1.0 MeV, 24.7±1.1 MeV, 21.9±1.2 MeV.

The reactions studied in the case of antimony are $^{121}Sb(\alpha,n)^{124}I$, $^{121}Sb(\alpha,2n)^{123}I$, $^{121}Sb(\alpha,4n)^{121}I$, $^{121}Sb(\alpha,p3n)^{121}Te$, $^{123}Sb(\alpha,n)^{126}I$ $^{123}Sb(\alpha,3n)^{124}I$ and $^{123}Sb(\alpha,4n)^{123}I$. The excitation functions for $^{121}Sb(\alpha,3n)^{122}I$ and $^{123}Sb(\alpha,2n)^{125}I$ could not be measured because in the former case the half life of product nucleus is short (3.6 minutes), so the developed activity decayed by the time the counting started and in later case the half life of the product nucleus is very large (60.1 days) so measurable activity could not be developed. The stack arrangement is shown in the fig. 4.20 while the gamma ray spectrum of activated sample is given in the fig. 4.21. The size of beam spot on the target was 8 mm and the measured flux was $1.482 \times 10^{11}$ α-particles/cm$^2$.s

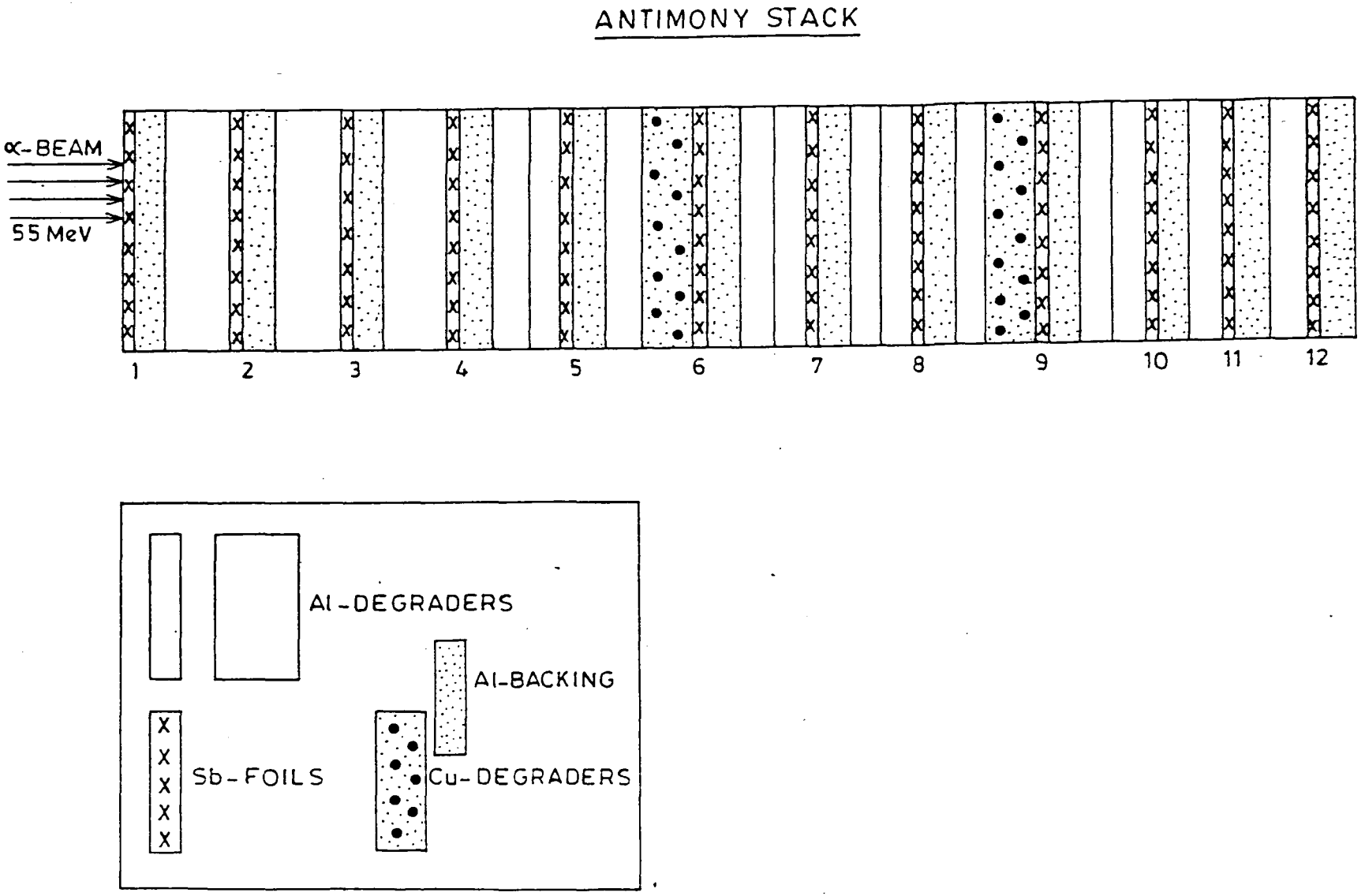


Fig. 4.20 Stack arrangement for antimony target.

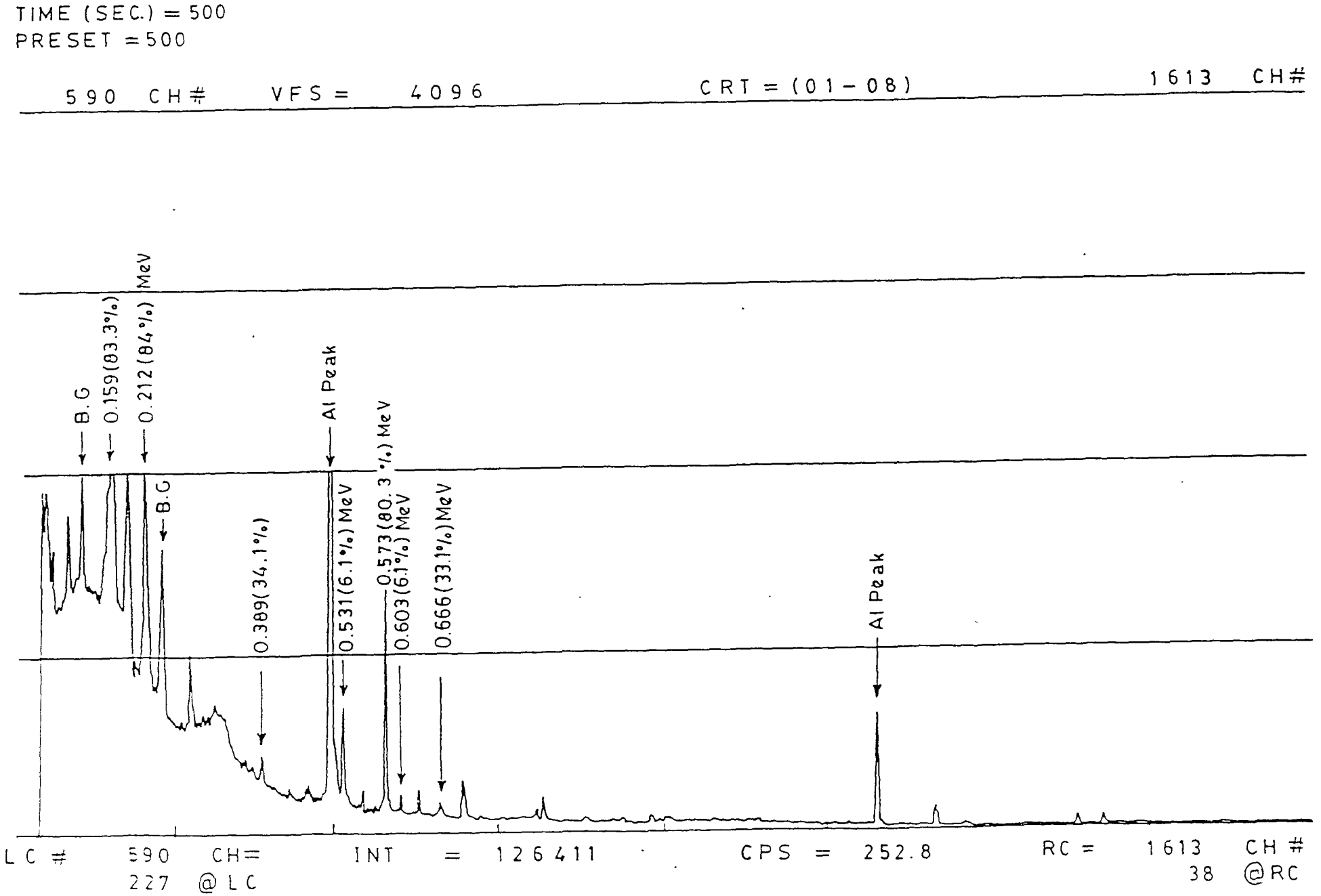


Fig.4.21 A typical gamma ray spectrum of activated sample of antimony.

### 4.8.3.1 $^{121}Sb(\alpha,n)$ Reaction

In this reaction the product nucleus is $^{124}I$ possessing the half life of 4.18 days. The spin of $^{124}I$ is $2^-$. This product nucleus decays to $^{124}Te$ which emits the few gamma rays. In the calculation of reaction cross-sections, only one gamma ray has been followed i.e. 0.603 MeV (61%). Some other gamma rays are also available but all those have either low abundance or low efficiency so could not be observed in our gamma ray spectrum. The Q-value of this reaction is -7.88 MeV. The decay scheme of $^{124}I$ product nucleus is shown in the fig. 4.22. Table 4.39 shows the value of parameter used to calculate the cross-section while the table 4.40 shows the measured cross-sections.

### 4.8.3.2 $^{121}Sb(\alpha,2n)$ Reaction

The product nucleus of this reaction is $^{123}I$ with $\frac{5}{2}^+$ spin. This $^{123}I$ has only the ground state, no isomeric state, having the half life of 13.2 hours. It decays to $^{123}Te$. In, whose, decay the emission of several gamma rays takes place but in the calculation of reaction cross-section, only gamma ray of 0.159 MeV (83.3%) has been taken into the consideration because all the other gamma rays are very weak hence could not be observed. The Q-value of this reaction is -15.35 MeV. The decay scheme of $^{123}I$ is shown in the fig. 4.23. The experimental data for

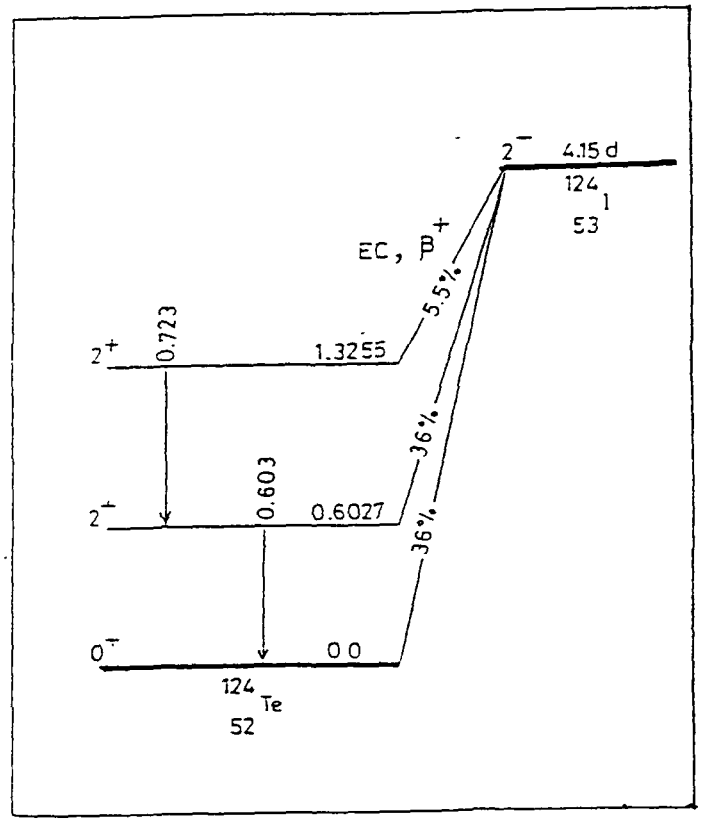


Fig. 4.22 Partial decay scheme of $^{124}I$.

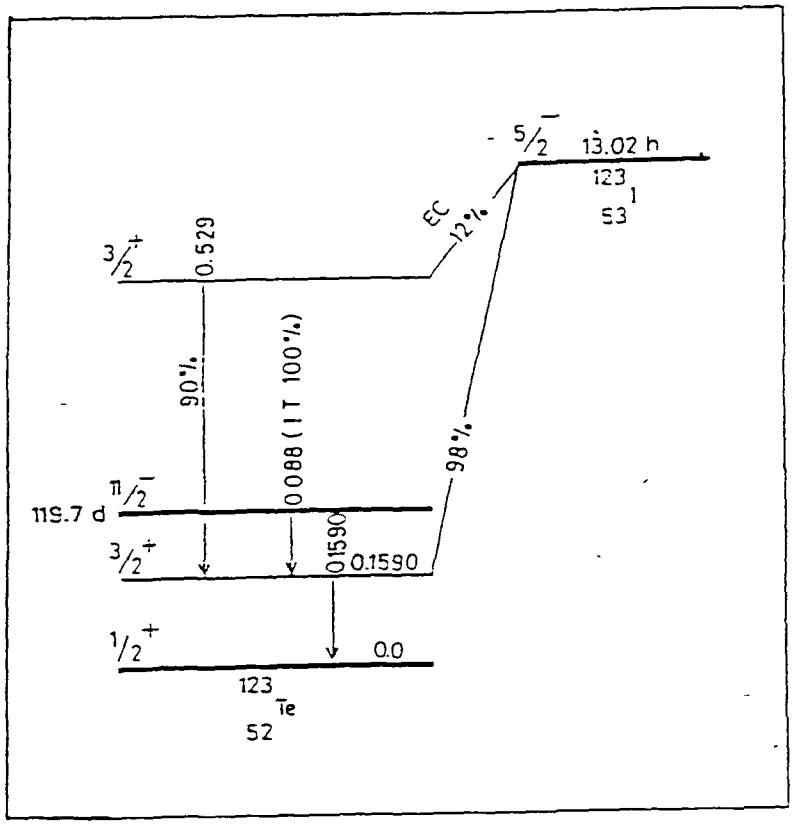


Fig. 4.23 Partial decay scheme of $^{123}I$.

Table 4.39

Experimental data for $^{121}Sb(\alpha,n)^{124}I$ reaction

Half life ($T_{1/2}$) = 4.18 d

Incident flux ($\phi$) = $1.4825 \times 10^{11}$ $\alpha$-particles/$cm^2$.s

Number of interacting nuclei($N_0$) = $1.4330 \times 10^{18}$

| $\alpha$-Particle Energy $E_\alpha$ (MeV) | Gamma Energy $E_\gamma$ (MeV) | Absolute $\gamma$-Intensity $\theta_\gamma$ (%) | Time Lapse $t_2$ (sec.) | Recording Time $t_3$ (sec.) | Photo-peak Counts A |
|---|---|---|---|---|---|
| 21.9±1.2 | 0.603 | 61.0 | 3060 | 500 | 560 |
| 24.7±1.1 | 0.603 | 61.0 | 5760 | 500 | 248 |
| 27.2±1.0 | 0.603 | 61.0 | 7020 | 500 | 156 |
| 30.7±0.9 | 0.603 | 61.0 | 7860 | 500 | 96 |
| 34.3±0.8 | 0.603 | 61.0 | 8940 | 500 | 106 |

Table 4.40

Cross-section for $^{121}Sb(\alpha,n)^{124}I$ reaction

| Incident $\alpha$-particle Energy $E_\alpha$ (MeV) | Gamma ray Energy $E_\gamma$ (MeV) | Cross-section $\sigma$ (mb) | Weighted Average Cross-section $\sigma$ (mb) |
|---|---|---|---|
| 21.9±1.2 | 0.603 | 101.07±3.53 | 101.07±3.53 |
| 24.7±1.1 | 0.603 | 44.99±2.34 | 44.99±2.34 |
| 27.2±1.0 | 0.603 | 28.37±1.99 | 28.37±1.99 |
| 30.7±0.9 | 0.603 | 17.48±1.78 | 17.48±1.78 |
| 34.3±0.8 | 0.603 | 19.35±1.88 | 19.35±1.88 |

this reaction are arranged in the table 4.41 while the cross-sections obtained versus incident α-particle energies are tabulated in the table 4.42.

### 4.8.3.3 $^{121}Sb(\alpha,4n)^{121}I$ Reaction

The Q-value of this reaction is -33.23 MeV and the product nucleus is $^{121}I$. $^{121}I$ is associated with $\frac{5}{2}^+$ spin and half life of 2.12 hrs. This $^{121}I$ decays to $^{121}Te$ which emits several gamma rays. All the gamma rays present in the decay of $^{121}Te$ except the gamma rays of 0.212 MeV and 0.531 MeV, are very weak. Hence, in the calculation of reaction cross-section, only the gamma of 0.212 MeV and 0.531 MeV energy have been taken into consideration. The intensity of these gamma rays is 84% , 6.1% respectively. The decay scheme of $^{121}I$ is shown in the fig. 4.24. The parameters used to calculate the cross-section is tabulated in the table 4.43 and the cross-section obtained is given in the table 4.44.

### 4.8.3.4 $^{123}Sb(\alpha,n)$ Reaction

The Q-value of this reaction is -6.95 MeV and the product nucleus is $^{126}I$. The half life of product nucleus is 13.02 days. It decays to $^{126}Te$ and $^{126}Xe$. In the decay of these, the gamma rays are of very low intensity except 0.389 MeV (34.1%) and 0.666 MeV (33.1%) gamma rays. Hence, in the calculation of reaction cross-section only aforesaid gamma rays are followed.

Table 4.41

Experimental data for $^{121}Sb(\alpha,2n)^{123}I$ reaction

Half life ($T_{1/2}$) = 13.20 h

Incident flux ($\phi$) = $1.8425 \times 10^{11}$ $\alpha$-particles/$cm^2$.s

Number of interacting nuclei ($N_o$) = $1.4330 \times 10^{18}$

| $\alpha$-Particle Energy $E_\alpha$ (MeV) | Gamma Energy $E_\gamma$ (MeV) | Absolute $\gamma$-Intensity $\Theta_\gamma$ (%) | Time Lapse $t_2$ (sec.) | Recording Time $t_3$ (sec.) | Photo-peak Counts A |
|---|---|---|---|---|---|
| 21.9±1.2 | 0.159 | 83.3 | 3060 | 500 | 203575 |
| 24.7±1.1 | 0.159 | 83.3 | 5760 | 500 | 249633 |
| 27.2±1.0 | 0.159 | 83.3 | 7020 | 500 | 254412 |
| 30.7±0.9 | 0.159 | 83.3 | 7860 | 500 | 171553 |
| 34.3±0.8 | 0.159 | 83.3 | 8940 | 500 | 160270 |
| 37.3±0.8 | 0.159 | 83.3 | 9900 | 500 | 71283 |
| 40.1±0.8 | 0.159 | 83.3 | 10800 | 500 | 40770 |
| 43.3±0.7 | 0.159 | 83.3 | 11700 | 500 | 31896 |
| 45.7±0.7 | 0.159 | 83.3 | 12600 | 500 | 26174 |
| 48.9±0.6 | 0.159 | 83.3 | 13500 | 500 | 24966 |
| 52.1±0.6 | 0.159 | 83.3 | 14460 | 500 | 21866 |
| 55.0±0.5 | 0.159 | 83.3 | 15540 | 500 | 18498 |

Table 4.42

Cross-section for $^{121}Sb(\alpha,2n)^{123}I$ reaction

| Incident α-particle Energy $E_\alpha$ (MeV) | Gamma ray Energy $E_\gamma$ (MeV) | Cross-section σ (mb) | Weighted Average Cross-section σ (mb) |
|---|---|---|---|
| 21.9±1.2 | 0.159 | 691.20±18.91 | 691.20±18.91 |
| 24.7±1.1 | 0.159 | 881.62±32.26 | 881.62±32.26 |
| 27.2±1.0 | 0.159 | 915.16±36.76 | 915.16± 36.76 |
| 30.7±0.9 | 0.159 | 624.71±20.52 | 624.71± 20.52 |
| 34.3±0.8 | 0.159 | 592.96±19.73 | 592.96±19.73 |
| 37.3±0.8 | 0.159 | 267.45±13.01 | 267.45±13.01 |
| 40.1±0.8 | 0.159 | 154.97±6.21 | 154.97±6.21 |
| 43.2±0.7 | 0.159 | 122.85±3.60 | 122.85±3.60 |
| 45.7±0.7 | 0.159 | 102.15±2.06 | 102.15±2.06 |
| 48.9±0.6 | 0.159 | 98.71±1.58 | 98.71±1.58 |
| 52.1±0.6 | 0.159 | 87.68±1.02 | 87.68±1.02 |
| 55.0±0.5 | 0.159 | 75.34±0.75 | 75.34±0.75 |

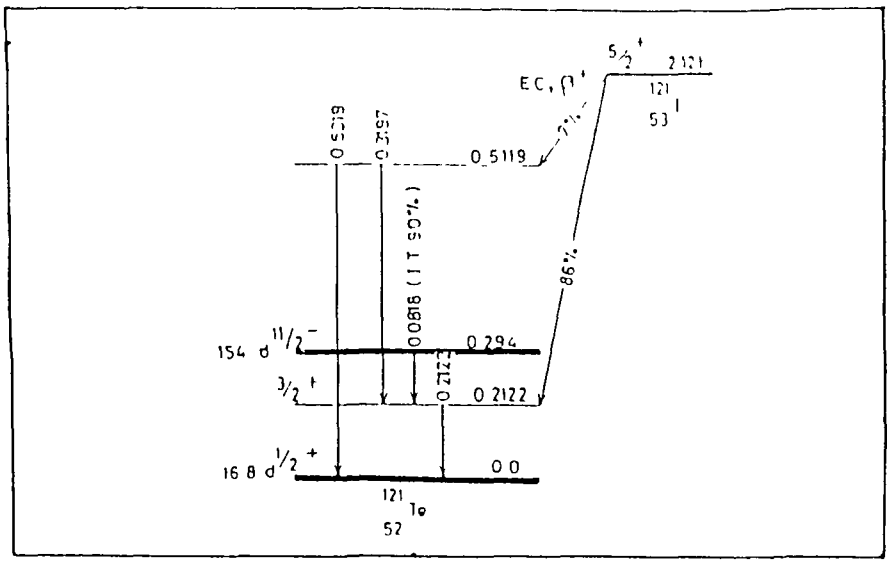


Fig. 4.24 partial decay scheme of $^{121}I$

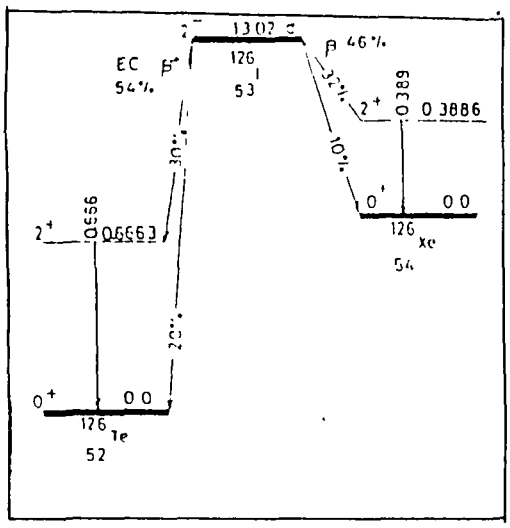


Fig.4.25 partial decay scheme of $^{126}I$

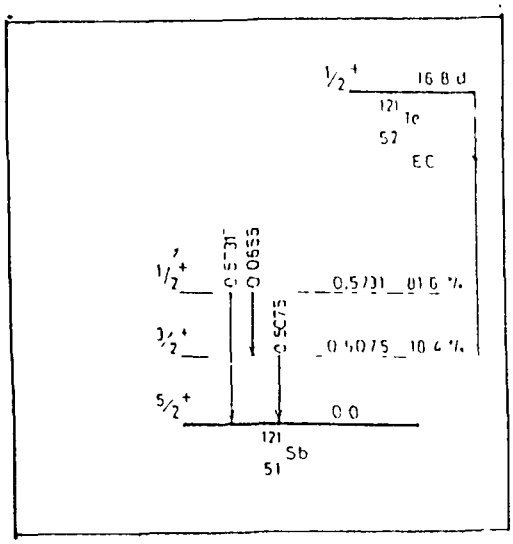


Fig.4.26 partial decay scheme of $^{121}Te$

Table 4.43

Experimental data for $^{121}Sb(\alpha,4n)^{121}I$ reaction

Half life ($T_{1/2}$) = 2.12 h

Incident flux ($\phi$) = $1.4825 \times 10^{11}$ $\alpha$-particles/$cm^2$.

Number of interacting nuclei ($N_o$) = $1.4330 \times 10^{18}$

| $\alpha$-particle Energy $E_\alpha$ (MeV) | Gamma Energy $E_\gamma$ (MeV) | Absolute $\gamma$-Intensity $\Theta_\gamma$ (%) | Time Lapse $t_2$ (sec) | Recording Time $t_3$ (sec.) | Photo-peak Counts A |
|---|---|---|---|---|---|
| 37.3±0.8 | 0.212 | 84.0 | 9900 | 500 | 4892 |
| | 0.531 | 6.1 | | | 172 |
| 40.1±0.8 | 0.212 | 84.0 | 10800 | 500 | 33283 |
| | 0.531 | 6.1 | | | 885 |
| 43.2±0.7 | 0.212 | 84.0 | 11700 | 500 | 97306 |
| | 0.531 | 6.1 | | | 2029 |
| 45.7±0.7 | 0.212 | 84.0 | 12600 | 500 | 156661 |
| | 0.531 | 6.1 | | | 3463 |
| 48.9±0.6 | 0.212 | 84.0 | 13500 | 500 | 221396 |
| | 0.531 | 6.1 | | | 5010 |
| 52.1±0.6 | 0.212 | 84.0 | 14460 | 500 | 215078 |
| | 0.531 | 6.1 | | | 4625 |
| 55.0±0.5 | 0.212 | 84.0 | 15540 | 500 | 152554 |
| | 0.531 | 6.1 | | | 3222 |

Table 4.44

Cross-section for $^{121}Sb(\alpha,4n)^{121}I$ reaction

| Incident α-particle Energy $E_\alpha$ (MeV) | Gamma ray Energy $E_\gamma$ (MeV) | Cross-section σ (mb) | Weighted Average Cross-section σ (mb) |
|---|---|---|---|
| 37.3±0.8 | 0.212 | 9.71±0.14 | 9.79±0.49 |
| | 0.531 | 15.74±1.20 | |
| 40.1±0.8 | 0.212 | 71.68±0.39 | 71.98±1.48 |
| | 0.531 | 87.89±2.96 | |
| 43.2±0.7 | 0.212 | 227.40±0.72 | 227.20±0.90 |
| | 0.531 | 218.66±4.86 | |
| 45.7±0.7 | 0.212 | 397.29±1.00 | 397.46±0.77 |
| | 0.531 | 404.97±6.88 | |
| 48.9±0.6 | 0.212 | 609.26±1.29 | 609.82±2.64 |
| | 0.531 | 635.78±8.98 | |
| 52.1±0.6 | 0.212 | 645.79±1.39 | 645.63±0.56 |
| | 0.531 | 640.37±9.41 | |
| 55.0±0.5 | 0.212 | 505.25±1.29 | 504.98±1.36 |
| | 0.531 | 492.08±8.67 | |

The decay scheme of $^{126}I$ is shown in the fig. 4.25. The parameters used to calculate the cross-section are arranged in the table 4.45 while the experimental cross-sections are tabulated in the table 4.46.

### 4.8.3.5 $^{123}Sb(\alpha,3n)$ Reaction

The product nucleus of this reaction is $^{124}I$ and, it decays to $^{124}Te$ which emits few gamma rays. In the calculation of reaction cross-section, the gamma ray of 0.603 MeV energy with the intensity 61% has been taken into the consideration. The half life of $^{124}I$ is 4.18 days. This product nucleus is same as the product nucleus of reaction $^{121}Sb(\alpha,n)$ reaction. So all the spectroscopic parameters for this reaction are same as in the $^{121}Sb(\alpha,n)$ reaction except the Q-value. The Q-value of this reaction is -23.64 MeV. Beyond the threshold of $^{123}Sb(\alpha,3n)$ reaction, both the $^{123}Sb(\alpha,3n)$ and $^{121}Sb(\alpha,n)$ reaction go on simultaneously. In this common region, the cross-sections are divided in the ratio of theoretical cross-section of these reactions.

The decay scheme of $^{124}Te$ is given in the fig. 4.22. The parameters used in the calculation of reaction cross-section are arranged in the table 4.47 while the measured cross-sections are given in the table 4.48.

Table 4.45

Experimental data for $^{123}Sb(\alpha,n)^{126}I$ reaction

Half life ($T_{1/2}$) = 13.02 d

Incident flux ($\phi$) = $1.4825 \times 10^{11}$ $\alpha$-particles/$cm^2$.s

Number of interacting nuclei ($N_o$) = $1.0505 \times 10^{18}$

| $\alpha$-Particle Energy $E_\alpha$ (MeV) | Gamma Energy $E_\gamma$ (MeV) | Absolute $\gamma$-Intensity $\Theta_\gamma$ (%) | Time Lapse $t_2$ (sec.) | Recording Time $t_3$ (sec.) | Photo-peak Countd A |
|---|---|---|---|---|---|
| 21.9±1.2 | 0.389 | 34.1 | 3060 | 500 | 73 |
| | 0.666 | 33.1 | | | 50 |
| 24.7±1.1 | 0.389 | 34.1 | 5760 | 500 | 41 |
| | 0.666 | 33.1 | | | 25 |
| 27.2±1.1 | 0.389 | 34.1 | 7020 | 500 | 29 |
| | 0.666 | 33.1 | | | 24 |

Table 4.46

Cross-section for $^{123}Sb(\alpha,n)^{126}I$ reaction

| Incident $\alpha$-particle Energy $E_\alpha$ (MeV) | Gamma ray Energy $E_\gamma$ (MeV) | Cross-section $\sigma$ (mb) | Weighted Average Cross-section $\sigma$ (mb) |
|---|---|---|---|
| 21.9±1.2 | 0.389 | 77.24±9.03 | 75.01±1.87 |
| | 0.666 | 71.93±10.17 | |
| 24.7±1.1 | 0.389 | 43.45±6.78 | 40.00±2.62 |
| | 0.666 | 36.02±7.20 | |
| 27.2±1.1 | 0.389 | 30.76±5.71 | 32.30±1.33 |
| | 0.666 | 34.61±7.06 | |

Table 4.47

Experimental data for $^{123}Sb(\alpha,3n)^{124}I$ reaction

Half life ($T_{1/2}$) = 4.18 d

Incident flux ($\phi$) = $1.4825 \times 10^{11}$ $\alpha$-particle/$cm^2$.s

Number of interacting nuclei ($N_o$) = $1.0505 \times 10^{18}$

| $\alpha$-particle Energy $E_\alpha$ (MeV) | Gamma Energy $E_\gamma$ (MeV) | Absolute $\gamma$-Intensity $\Theta_\gamma$ (%) | Time Lapse $t_2$ (sec.) | Recording Time $t_3$ (sec.) | Photo-peak Counts A |
|---|---|---|---|---|---|
| 27.2±1.0 | 0.603 | 61.0 | 7020 | 500 | 712 |
| 30.7±0.9 | 0.603 | 61.0 | 7860 | 500 | 2796 |
| 34.3±0.8 | 0.603 | 61.0 | 8940 | 500 | 5230 |
| 37.3±0.8 | 0.603 | 61.0 | 9900 | 500 | 6002 |
| 40.1±0.8 | 0.603 | 61.0 | 10800 | 500 | 4275 |
| 43.2±0.7 | 0.603 | 61.0 | 11700 | 500 | 2802 |
| 45.7±0.7 | 0.603 | 61.0 | 12600 | 500 | 1912 |
| 48.9±0.6 | 0.603 | 61.0 | 13500 | 500 | 1162 |
| 52.1±0.6 | 0.603 | 61.0 | 14460 | 500 | 716 |
| 55.0±0.5 | 0.603 | 61.0 | 15540 | 500 | 553 |

Table 4.48

Cross-section for $^{123}Sb(\alpha,3n)^{124}I$ reaction

| Incident α-particle Energy $E_\alpha$ (MeV) | Gamma ray Energy $E_\gamma$ (MeV) | Cross-section σ (mb) | Weighted Average Cross-section σ (mb) |
|---|---|---|---|
| 27.2±1.0 | 0.603 | 176.56±6.61 | 176.56±6.61 |
| 30.7±0.9 | 0.603 | 694.71±13.14 | 694.71±13.14 |
| 34.3±0.8 | 0.603 | 1302.05±18.00 | 1302.05±18.00 |
| 37.3±0.8 | 0.603 | 1497.18±19.33 | 1497.18±19.33 |
| 40.1±0.8 | 0.603 | 1068.31±16.34 | 1068.31±16.34 |
| 43.2±0.7 | 0.603 | 701.69±13.25 | 701.69±13.25 |
| 45.7±0.7 | 0.603 | 479.28±10.96 | 479.28±10.96 |
| 48.9±0.6 | 0.603 | 291.84±8.56 | 291.84±8.56 |
| 52.1±0.6 | 0.603 | 180.19±6.73 | 180.19±6.73 |
| 55.0±0.5 | 0.603 | 139.46±5.92 | 139.46±5.92 |

### 4.3.8.6 $^{123}Sb(\alpha,4n)$ Reaction

The Q-value of this reaction is -31.15 MeV and the product nucleus is $^{123}I$ which is also the product nucleus of $^{121}Sb(\alpha,2n)$ reaction. So all the properties of product nucleus in this case are same as explained in the article 4.3.8.4 for $^{121}Sb(\alpha,2n)$ reaction. In the tail protion of $^{121}Sb(\alpha,2n)$ reaction, the channel of $^{123}Sb(\alpha,4n)$ reaction also opens, so after opening of this channel, both the reactions go on. In this overlapping region, the experimental cross-section of these reactions have been divided by using the ratio of theoretical cross-section of these reactions.

The decay scheme of $^{123}I$ is given in the fig. 4.23 and the parameters used in the calculation of reaction cross-section are given in the table 4.49. The obtained cross-sections are tabulated in the table 4.50.

### 4.3.8.7 $^{121}Sb(\alpha,p3n)$ Reaction

In this reaction the product nucleus is $^{121}Te$ which has the ground state of half life of 16.78 d. In addition to this state $^{121}Te$ is associated with the metastable state of half life 154 d also. Later decays 83% to the former. In the present case the time of bombardment of the stack was very short in comparison of the half life of metastable state, so this state could not be excited. In the present calculation of cross-section, the gamma

Table 4.49

Experimental data for $^{123}Sb(\alpha,4n)^{123}I$ reaction

Half life ($T_{1/2}$) = 13.2 h

Incident flux ($\phi$) = $1.4825 \times 10^{11}$ $\alpha$-particles/$cm^2$.s

Number of interacting nuclei($N_o$) = $1.0505 \times 10^{18}$

| $\alpha$-particle Energy $E_\alpha$ (MeV) | Gamma Energy $E_\gamma$ (MeV) | Absolute $\gamma$-Intensity $\Theta_\gamma$ (MeV) | Time Lapse $t_2$ (sec.) | Recording Time $t_3$ (sec.) | Photo-peak Counts A |
|---|---|---|---|---|---|
| 37.3±0.8 | 0.159 | 83.3 | 9900 | 500 | 25497 |
| 40.1±0.8 | 0.159 | 83.3 | 10800 | 500 | 54500 |
| 43.2±0.7 | 0.159 | 83.3 | 11700 | 500 | 101005 |
| 45.7±0.7 | 0.159 | 83.3 | 12600 | 500 | 113447 |
| 48.9±0.6 | 0.159 | 83.3 | 13500 | 500 | 119759 |
| 52.1±0.6 | 0.159 | 83.3 | 14460 | 500 | 117504 |
| 55.0±0.5 | 0.159 | 83.3 | 15540 | 500 | 107669 |

Table 4.50

Cross-section for $^{123}Sb(\alpha,4n)^{123}I$ reaction

| Incident α-particle Energy $E_\alpha$ (MeV) | Gamma ray Energy $E_\gamma$ (MeV) | Cross-section σ (mb) | Weighted Average Cross-section σ (mb) |
|---|---|---|---|
| 37.3±0.8 | 0.159 | 130.48±0.82 | 130.48±0.82 |
| 40.1±0.8 | 0.159 | 282.58±1.21 | 282.58±1.21 |
| 43.2±0.7 | 0.159 | 530.63±1.67 | 530.63±1.67 |
| 45.7±0.7 | 0.159 | 603.87±1.79 | 603.87±1.79 |
| 48.9±0.6 | 0.159 | 645.89±1.87 | 645.89±1.87 |
| 52.1±0.6 | 0.159 | 642.66±1.88 | 642.66±1.88 |
| 55.0±0.5 | 0.159 | 598.22±1.82 | 598.22±1.82 |

ray of 0.573 MeV energy with the intensity 80.3% has been followed. The decay scheme of $^{121}$Te ($T_{1/2}$ = 16.78 d) is shown in the fig. 4.26. The parameters used to calculate the cross-section and so obtained cross-sections at different incident alpha particle energies are arranged in the table 4.51 and 4.52 respectively.

Table 4.51

Experimental data for $^{121}Sb(\alpha,p3n)^{121}Te$ reaction

Half life ($T_{1/2}$) = 16.78 d

Incident flux ($\phi$) = $1.4825 \times 10^{11}$ $\alpha$-particles/$cm^2$.s

Number of interacting nuclei($N_o$) = $1.4330 \times 10^{18}$

| $\alpha$-particle Energy $E_\alpha$ (MeV) | Gamma Energy $E_\gamma$ (MeV) | Absolute $\gamma$-Intensity $\theta_\gamma$ (%) | Time Lapse $t_2$ (sec.) | Recording Time $t_3$ (sec.) | Photo-peak Counts A |
|---|---|---|---|---|---|
| 37.3±0.8 | 0.573 | 80.3 | 9900 | 500 | 74 |
| 40.1±0.8 | 0.573 | 80.3 | 10800 | 500 | 370 |
| 43.2±0.7 | 0.573 | 80.3 | 11700 | 500 | 820 |
| 45.7±0.7 | 0.573 | 80.3 | 12600 | 500 | 1194 |
| 48.9±0.6 | 0.573 | 80.3 | 13500 | 500 | 1566 |
| 52.1±0.6 | 0.573 | 80.3 | 14460 | 500 | 2030 |
| 55.0±0.5 | 0.573 | 80.3 | 15540 | 500 | 1790 |

Table 4.52

Cross-section for $^{121}Sb(\alpha,p3n)^{121}Te$ reaction

| Incident α-particle Energy $E_\alpha$ (MeV) | Gamma ray Energy $E_\gamma$ (MeV) | Cross-section σ (mb) | Weighted Average Cross-section σ (mb) |
|---|---|---|---|
| 37.3±0.8 | 0.573 | 33.64±3.91 | 33.64±3.91 |
| 40.1±0.8 | 0.573 | 168.23±8.75 | 168.23±8.75 |
| 43.2±0.7 | 0.573 | 372.84±18.41 | 372.84±18.41 |
| 45.7±0.7 | 0.573 | 548.69±15.88 | 548.69±15.88 |
| 48.9±0.6 | 0.573 | 716.30±18.10 | 716.30±18.10 |
| 52.1±0.6 | 0.573 | 929.46±20.63 | 929.46±20.63 |
| 55.0±0.5 | 0.573 | 820.38±19.39 | 820.38±19.39 |

## REFERENCES

[1] S.M. Qaim: Radio Chemica Acta 25 (1978) 13, Inorg. Nucl. Chem. 36 (1974) 239.

[2] W.D. Hamilton: Electromagnetic Interaction in Nuclear Spectroscopy, (North Holland Publishing Company, U.K. 1975).

[3] G.F. Knoll: Radiation Detection and Measurements (John Wiley and Sons, New York, 1979).

[4] C.M. Lederer and V.S. Shirely: Table of Isotopes 7th Edition (John Wiley and Sons, New York, 1978).

[5] C.L. Branquinho, S.M.A. Hoffmann, G.W.A. Newton, V.J. Robinson, H.Y. Wang and I.S. Grant: J. Inorg. Nucl. Chem. 41 (1979) 617.

[6] W.W. Bowman and M. Blann: Nucl. Phys. 131 (1969) 513.

[7] J. Ernst. R. Ibowski, H. Klampfl, H. Machner, T. Mayer-Kuckuk and R. Schanz: Z. Phys. Atoms and Nuclei, A 308 (1982) 301.

[8] D.J. Frantsvog, A.R. Kunselman, R.L. Wilson, C.S. Zaidins and C. Detraz : Phys. Rev. C25 (1982) 770.

[9] J.B. Ball, A.W. Fairhall and I. Halpern: Phys. Rev. 114 (1959) 305.

[10] H. Morinaga: Phys. Rev. 101 (1956) 100.

[11] L.C. Northcliffe and R.F. Schilling: Nucl. Data Tables A7 (1970) 256.

[12] W.J. Rubinson: J. Chem. Phys. 17 (1949) 542.

[13] W.B. Lewis: Nucleonics No.10, 12 (1954) 30.

[14] E. Bleuler and G. Goldsmith: Experimental Nucleonics (Holt, Rinchart and Winston, New York, 1952) 86.

[15] E. Storm and H. Israel: Nucl. Data Tables 7 (1970) 565.

[16] S.F. Mughabghab, M. Divadeenam and N.E. Holden: Neutron cross-sections Vol. 1, Part-A Academic Press, Inc., N.Y. (1981) 89.

[17] N.B. Gova and A.H. Wapstra: Nucl. Data Tables A11 (1972) 127.

[18] Landolt-Bornstein: New Series I/SB, 'Excitation functions for nuclear reactions' (1973).

# CHAPTER-V

## RESULT AND DISCUSSION

After the development of isochronous cyclotron, the projectiles excited upto very high energies became available [1] and the experimental features of the nuclear reactions have been studied by several investigators and they pointed out that some reactions took place with intermediate time scale between two extremes. They manifest themselves in the high energy tails of the excitation function, non-Maxwellian hard components in the particle spectra and a gradually changing pattern of angular distribution from forward peaking to fore-and-off symmetry. So obtained experimental features could neither be explained by compound nucleus model nor by direct reaction model [2-4]. To explain these experimental facts of nuclear reactions, several new theories and models were proposed. [5-12]. To test the validity of these models more and more accurate measurements are necessary. A lot of work has been done on the study of excitation functions of α-particle induced reactions for various targets [13]. There are some cases for which no data is available. For many cases either the data is scanty or there are large discrepancies in the results. Hence there is need of more accurate experiments in many cases. Keeping this view, the excitation function for $^{113}In$, $^{115}In$, $^{191}Ir$, $^{193}Ir$, $^{121}Sb$ and $^{123}Sb$ have been measured..

## 5.1 Measured Results

In the present work the corss-sections have been measured for $^{113}In(\alpha,n)^{116}Sb$ + $^{115}In(\alpha,3n)^{116}Sb$, $^{113}In(\alpha,2n)^{115}Sb$, $^{115}In(\alpha,n)^{118}Sb$, $^{115}In(\alpha,2n)^{117}Sb$, $^{115}In(\alpha,4n)^{115}Sb$, $^{115}In(\alpha,pn)^{117}Sn$, $^{115}In(\alpha,2p)^{117}In$; $^{191}Ir(\alpha,n)^{194}Au$, $^{191}Ir(\alpha,2n)^{193}Au$, $^{191}Ir(\alpha,3n)^{192}Au$, $^{191}Ir(\alpha,4n)^{191}Au$, $^{191}Ir(\alpha,5n)^{190}Au$, $^{193}Ir(\alpha,3n)^{194}Au$ $^{193}Ir(\alpha,4n)^{193}Au$, $^{193}Ir(\alpha,5n)^{192}Au$; $^{121}Sb(\alpha,n)^{124}I$, $^{121}Sb(\alpha,p3n)^{121}Te$ $^{121}Sb(\alpha,2n)^{123}I$, $^{121}Sb(\alpha,4n)^{121}I$, $^{123}Sb(\alpha,n)^{126}I$, $^{123}Sb(\alpha,3n)^{124}I$, $^{123}Sb(\alpha,4n)^{123}I$ reactions. The cross sections of these reactions are displayed in the figs. from 5.1 - 5.22 . In these figures the literature values are also shown, if no literature value is shown, it means the results are reported for the first time with our best knowledge. In the figures horizontal and vertical bars are also mentioned. The horizontal bar shows the total estimated error spread in the incident energy while the vertical bar shows the cross-sectional error. The absence of vertical bar shows the cross-sectional error within the mark. The numerical values of experimentally measured cross-sections are tabulated in tables from 5.1 - 5.6. In case of Sb, some literature values are available in the low energy region and are shown in the figures. The target stacks of different elements were bombarded with different energy of α-particle beam. Stack of indium was bombarded with 50 MeV and this energy was degraded upto 21 MeV while the target stacks of iridium and antimony were bombarded with the α-particle beam of 55 MeV and this energy was degraded

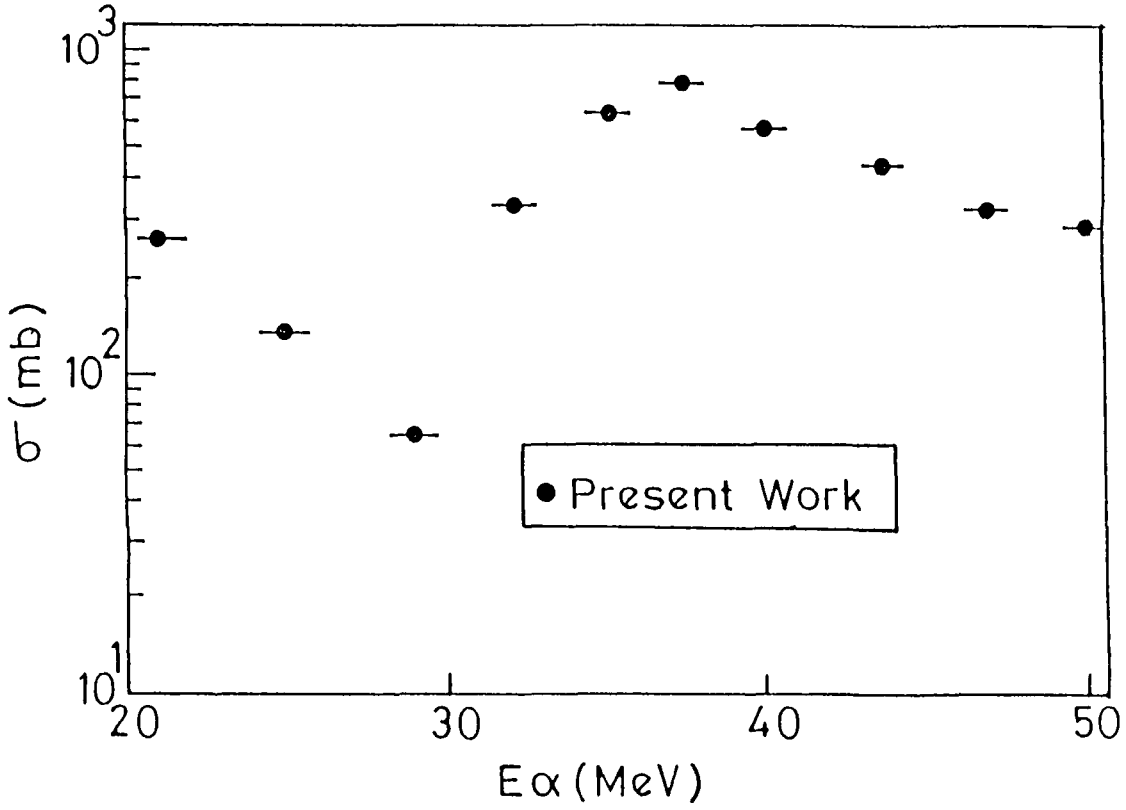


Fig. 5.1 Experimental excitation function for $^{113}In(\alpha,n)\ ^{116m}Sb$ + $^{115}In(\alpha,3n)\ ^{116m}Sb$. reaction

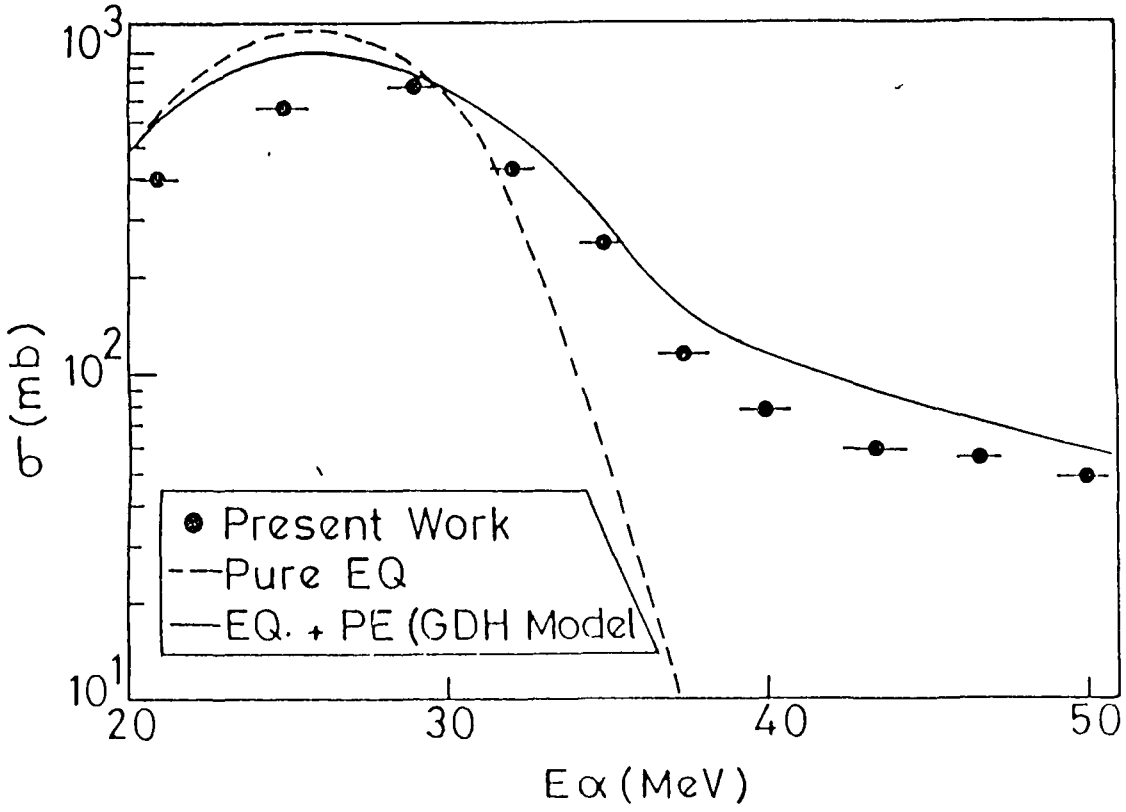


Fig.5.2 Theoretical and experimental excitation functions for $^{113}In\ (\alpha, 2n)\ ^{115}Sb$ reaction.

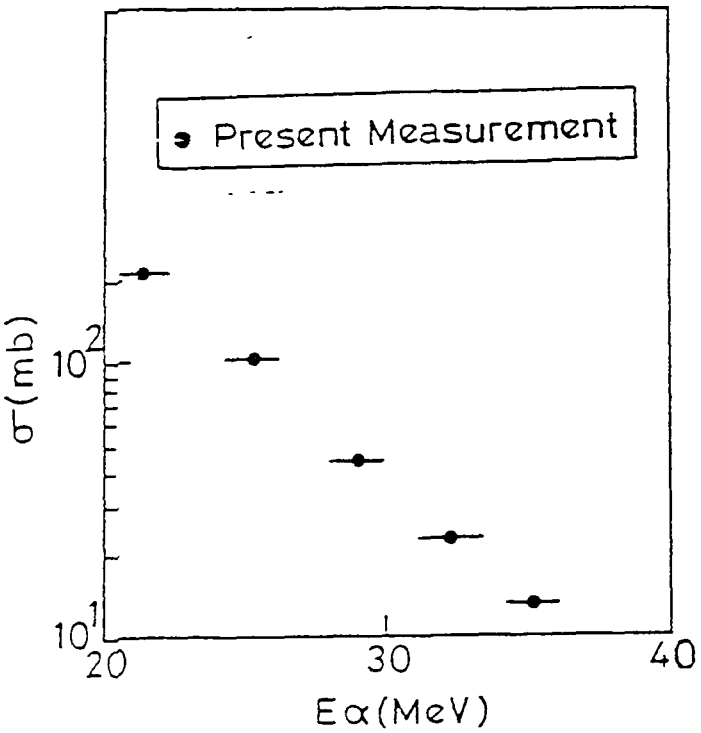


ig. 5.3 Experimental excitation function for $^{115}In(\alpha, n)^{118}Sb$ reaction.

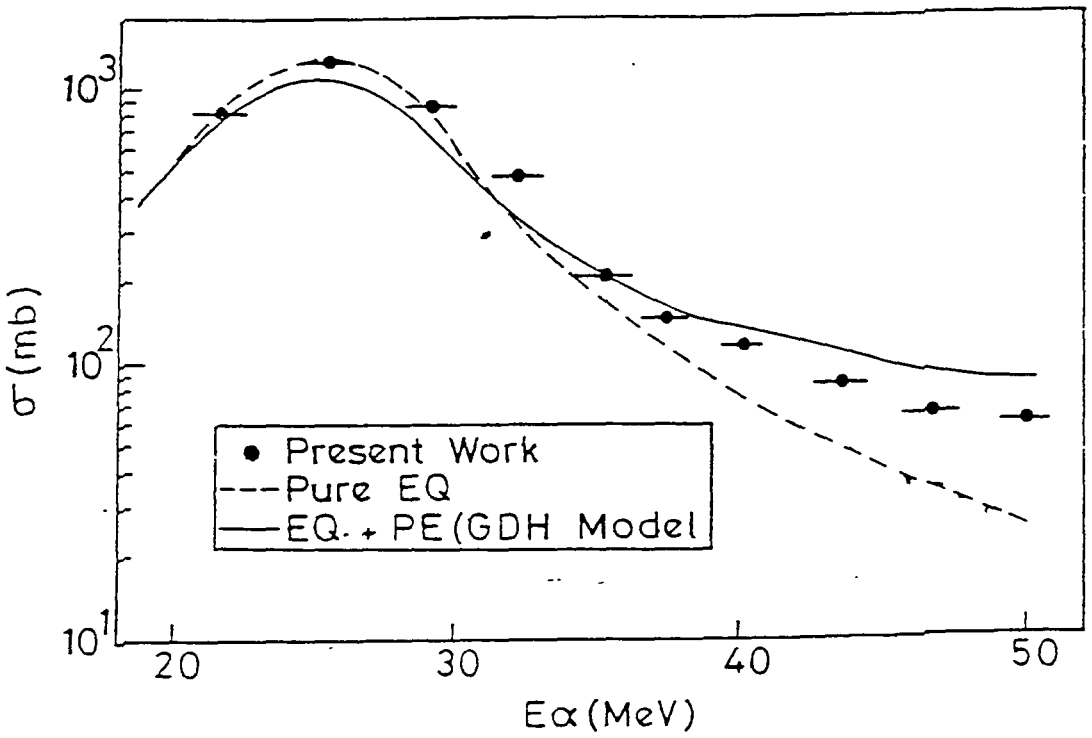


Fig. 5.4 Theoretical and experimental excitation functions for $^{115}In(\alpha, 2n)^{117}Sb$ reaction

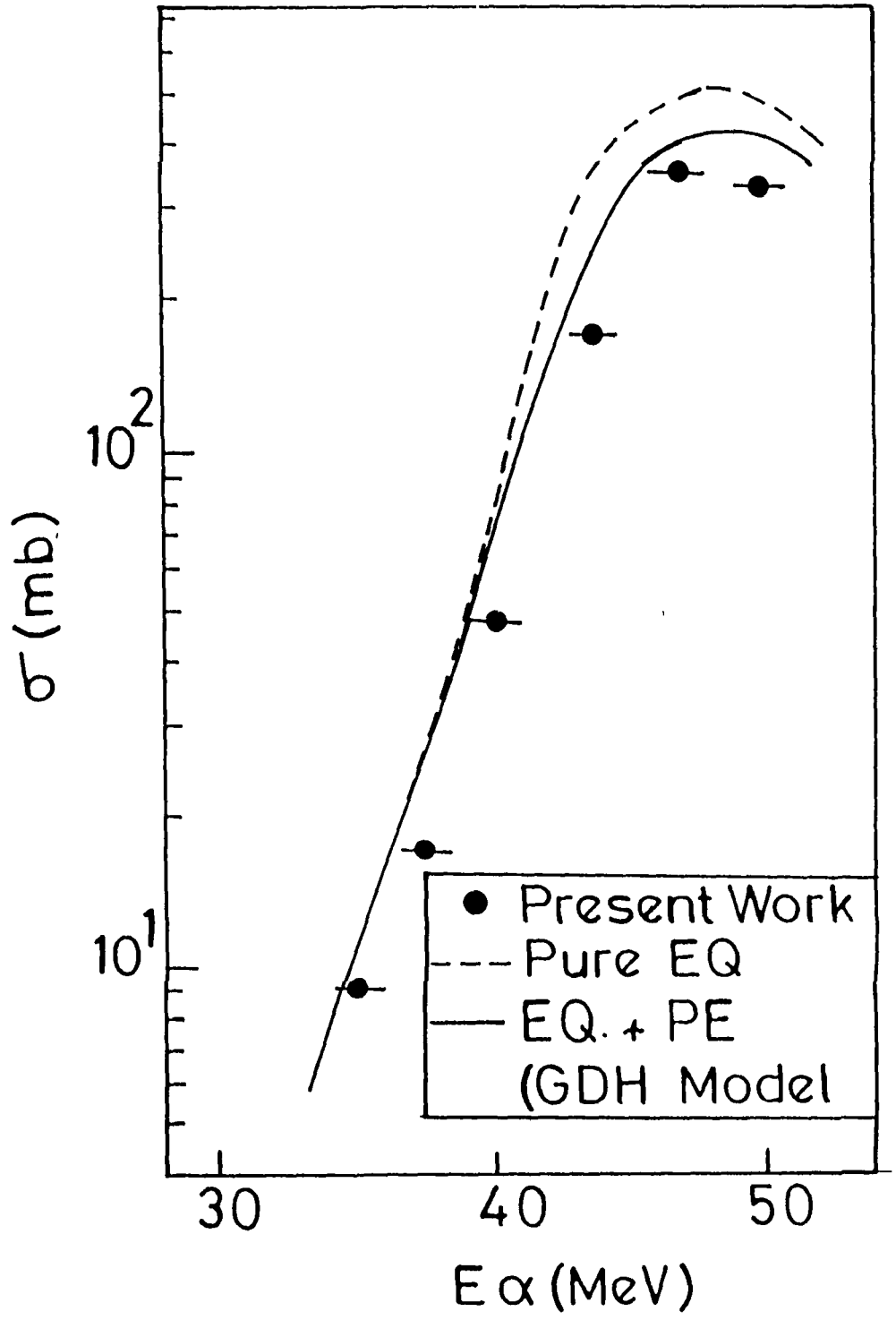


Fig.5.5 Theoretical and experimental excitation function for $^{115}In$ ($\alpha$, 4n) $^{115}Sb$ reaction

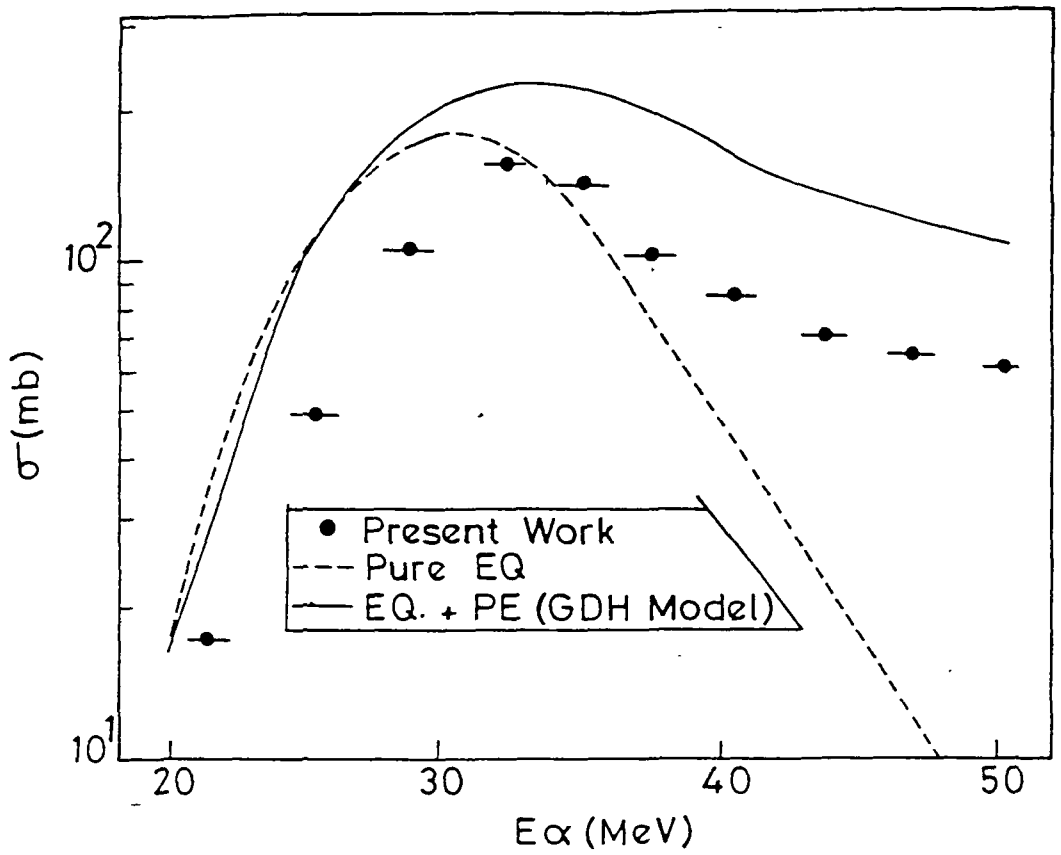


Fig. 5.6 Theoretical and experimental excitation function for $^{115}In$ ( $\alpha$ ,pn) $^{117m}Sn$ reaction

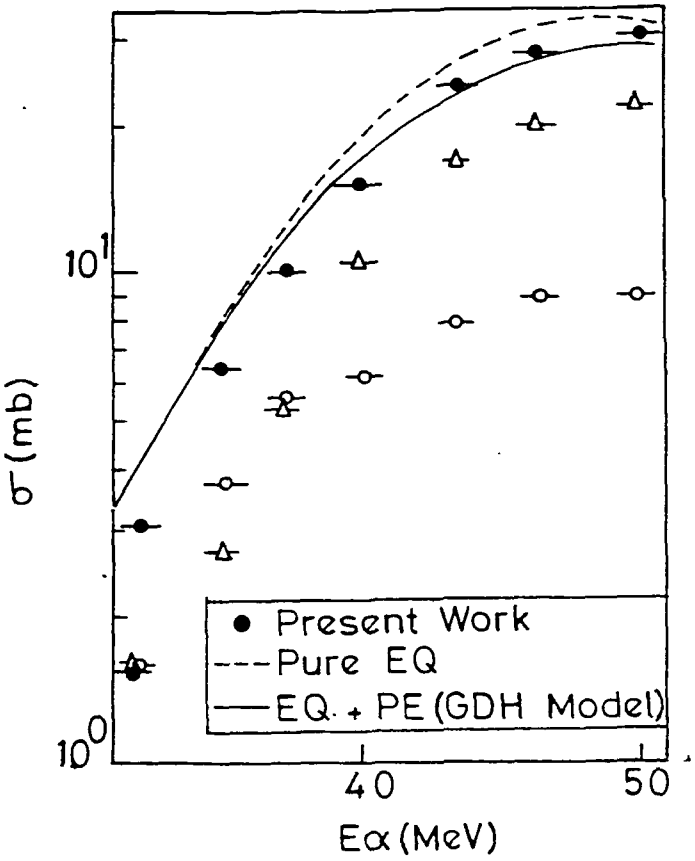


Fig. 5.7 Theoretical and experimental excitation function for $^{115}In$ ( $\alpha$ ,2p) $^{117}In$ reaction

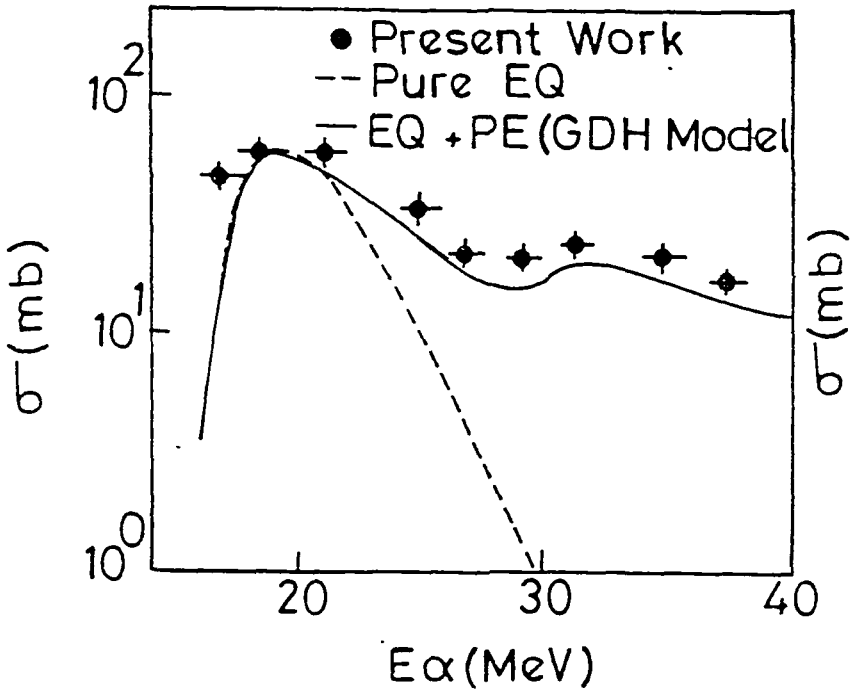


Fig.5.8 Theoretical and experiemental excitation function for $^{191}Ir\ (\alpha, n)^{194}Au$ reaction

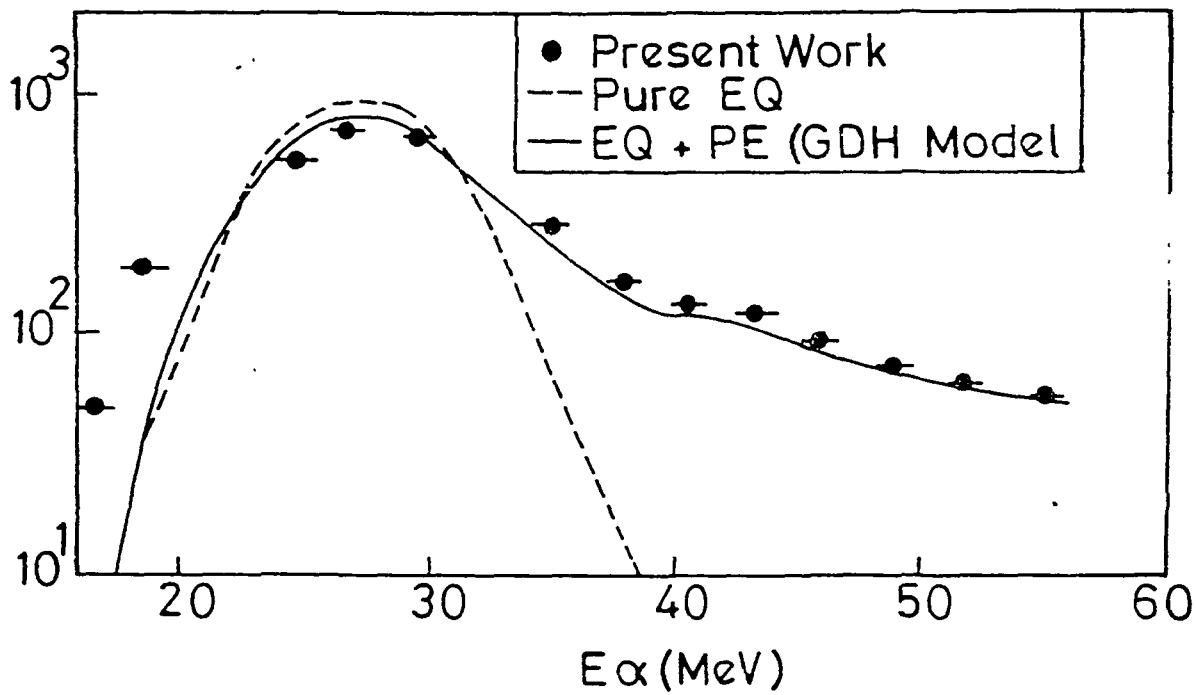


Fig.5.9 Theoretical and experimental excitation function for $^{191}Ir\ (\alpha, 2n)^{193}Au$ reaction

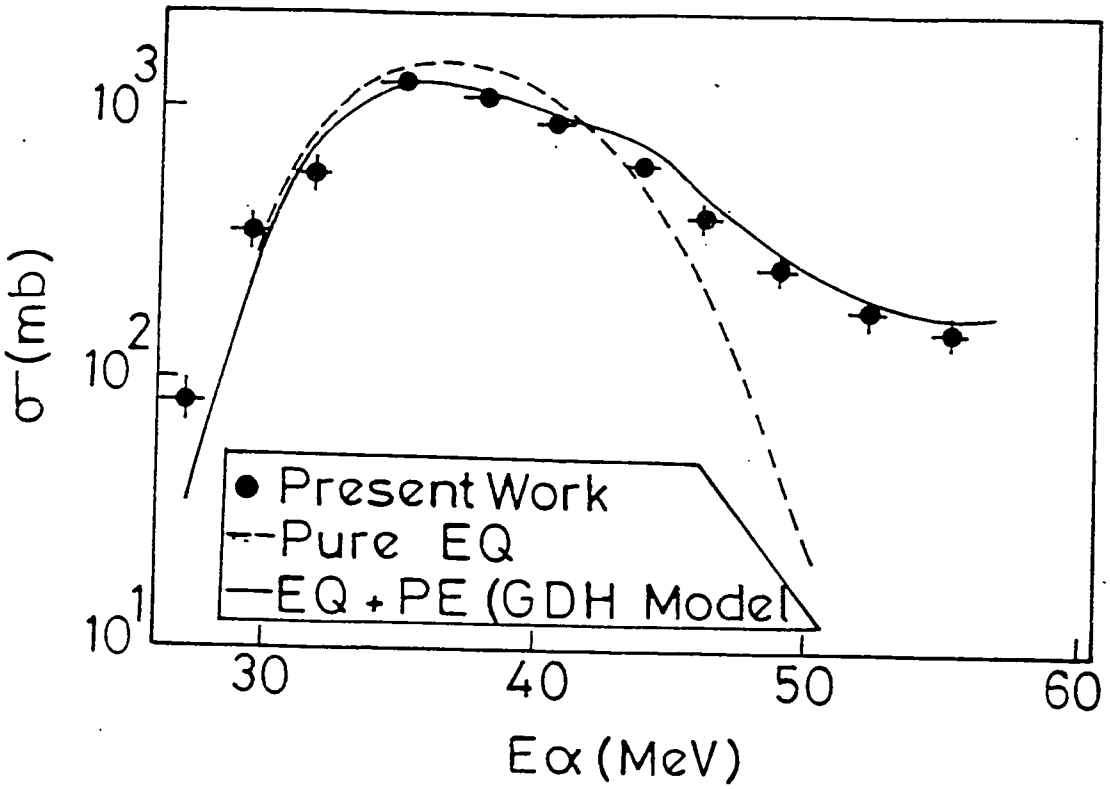


Fig. 5.10 Theoretical and experimental excitation function for $^{191}Ir(\alpha, 3n)^{192}Au$ reaction

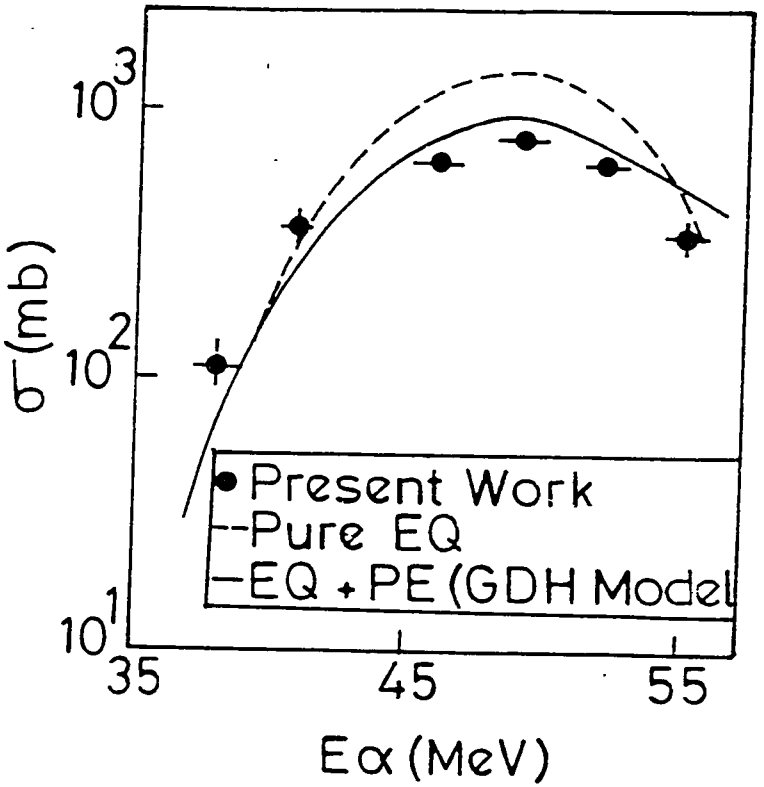


Fig.5.11 Theoretical and experimental excitation function for $^{191}Ir(\alpha, 4n)^{191}Au$ reaction

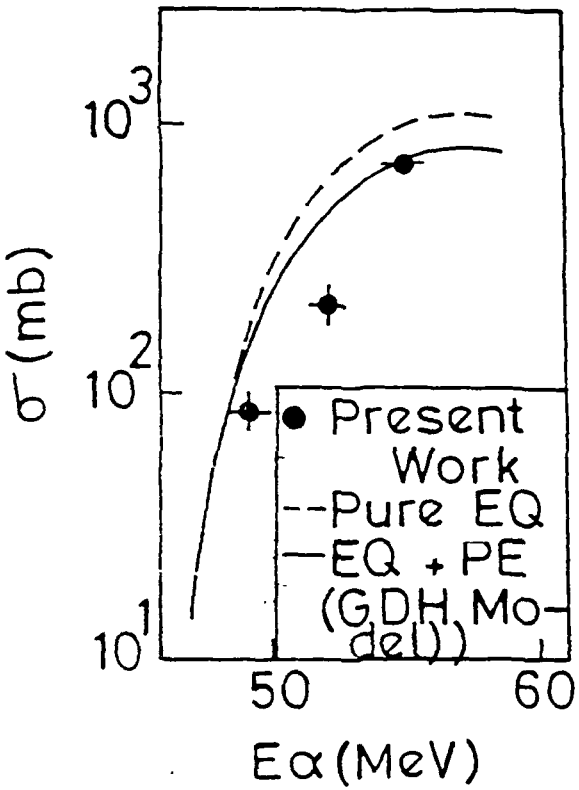


Fig.5.12 Theoretical and experimental excitation function for $^{191}Ir(\alpha,5n)^{190}Au$ reaction

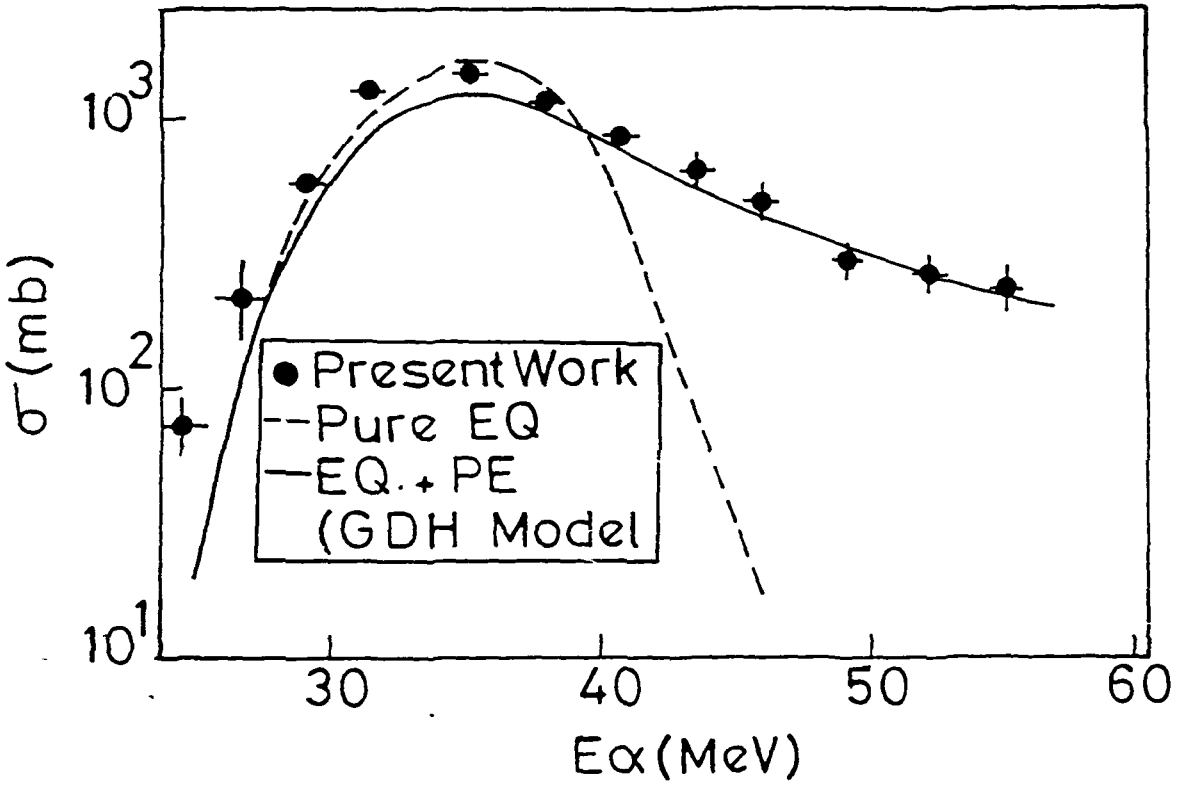


Fig.5.13 Theoretical and experimental excitation function for $^{193}Ir(\alpha,3n)^{194}Au$ reaction

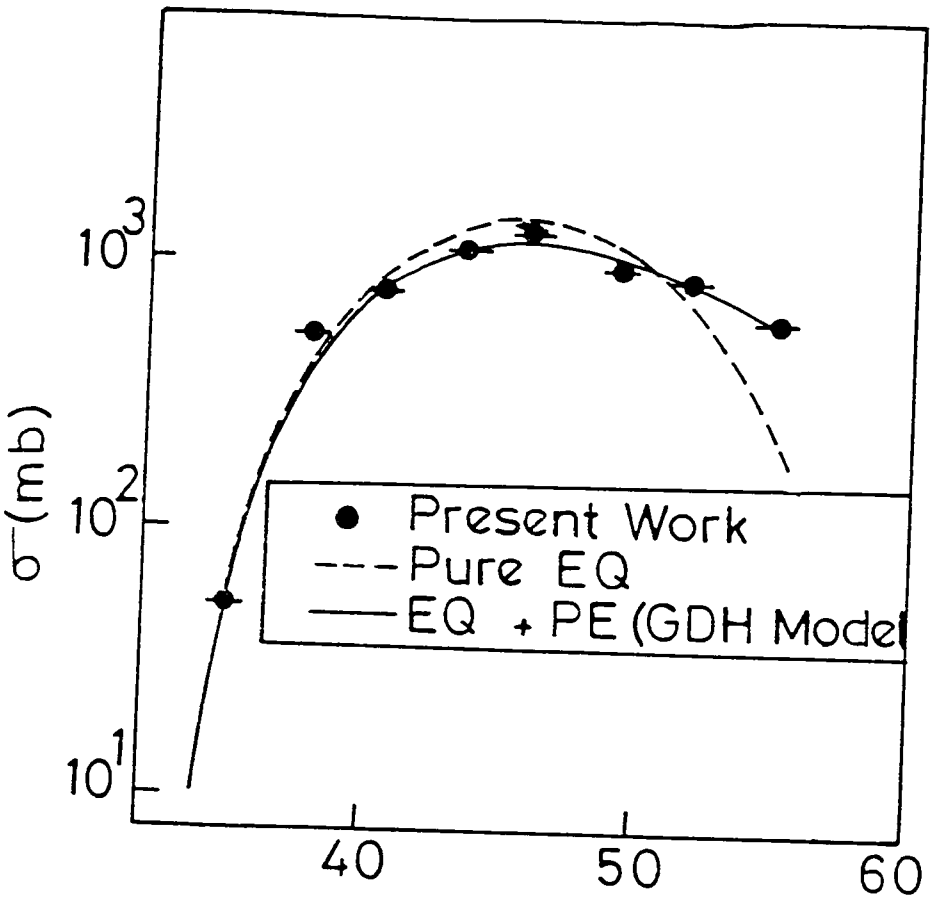


Fig.5.14 Theoretical and experimental excitation functionsfor $^{193}Ir(\alpha, 4n)^{193}Au$ reaction

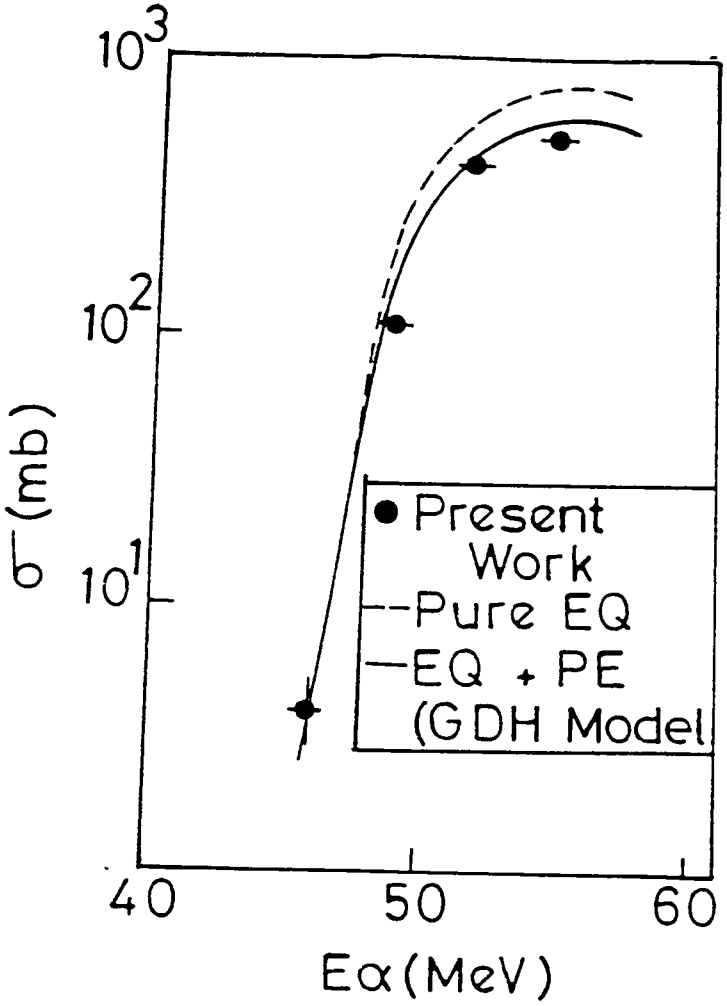


Fig.5.15 Theoretical and experimental excitation functionsfor $^{193}Ir(\alpha, 5n)^{192}Au$ reaction

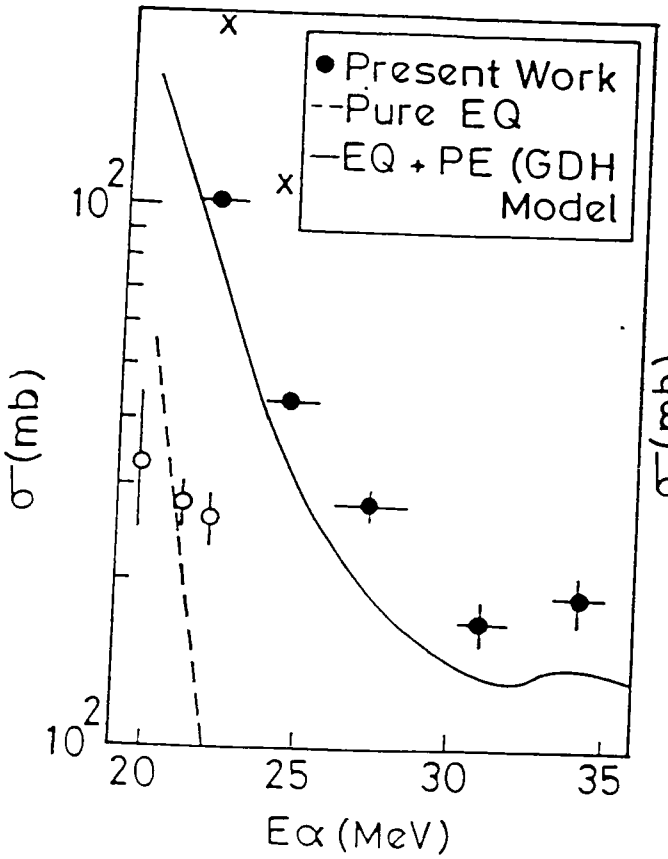


Fig.5.16

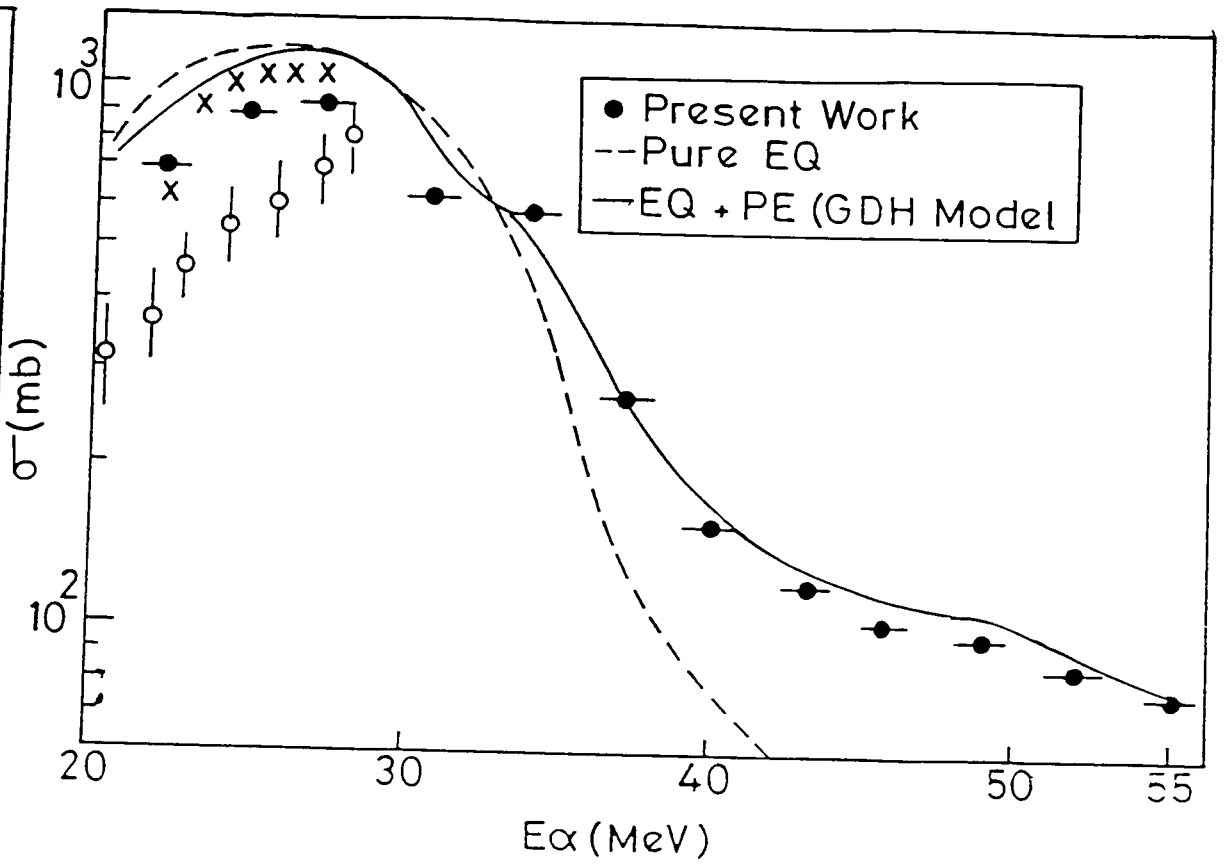


Fig. 5.17

Fig. 5.16 Theoretical and experimental excitation functions for $^{121}Sb$ $(\alpha,n)$ $^{124}I$ reaction

Fig. 5.17 Theorectical and experimental excitation functions for $^{121}Sb(\alpha,2n)$ $^{123}I$ reaction

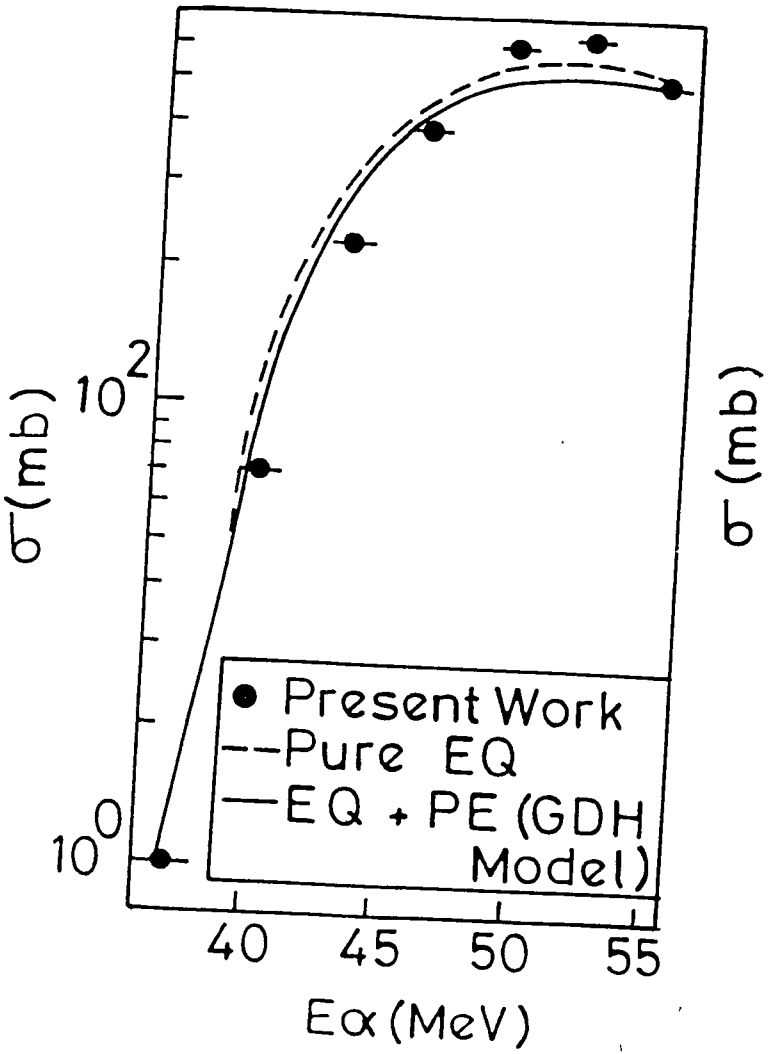


Fig.5.18 Theorectical and experimental excitation functions for $^{121}Sb(\alpha,4n)^{121}I$ reaction

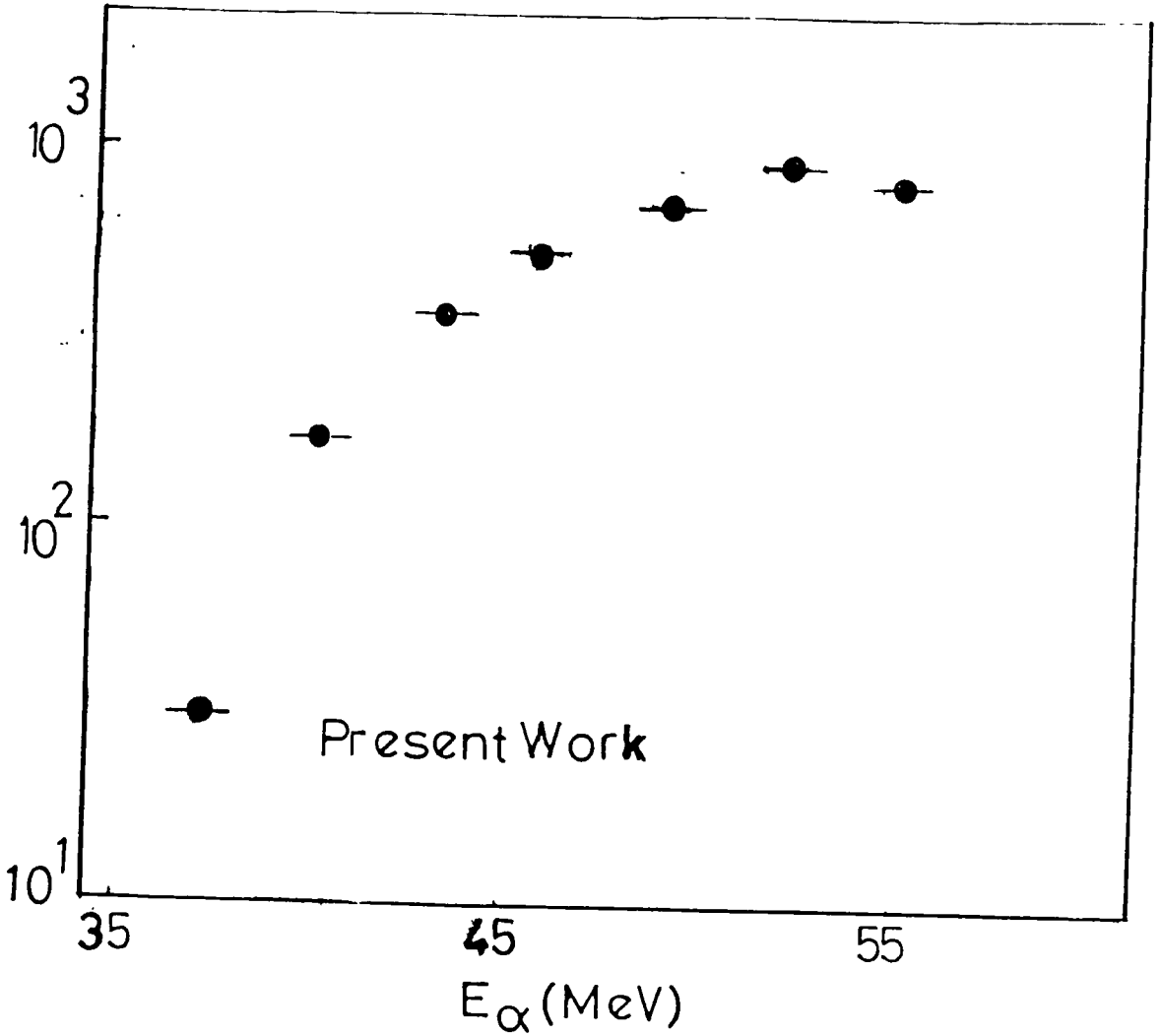


Fig.5.19 Experimental excitation function for $^{121}Sb(\alpha,p3n)^{121}Te$ reaction

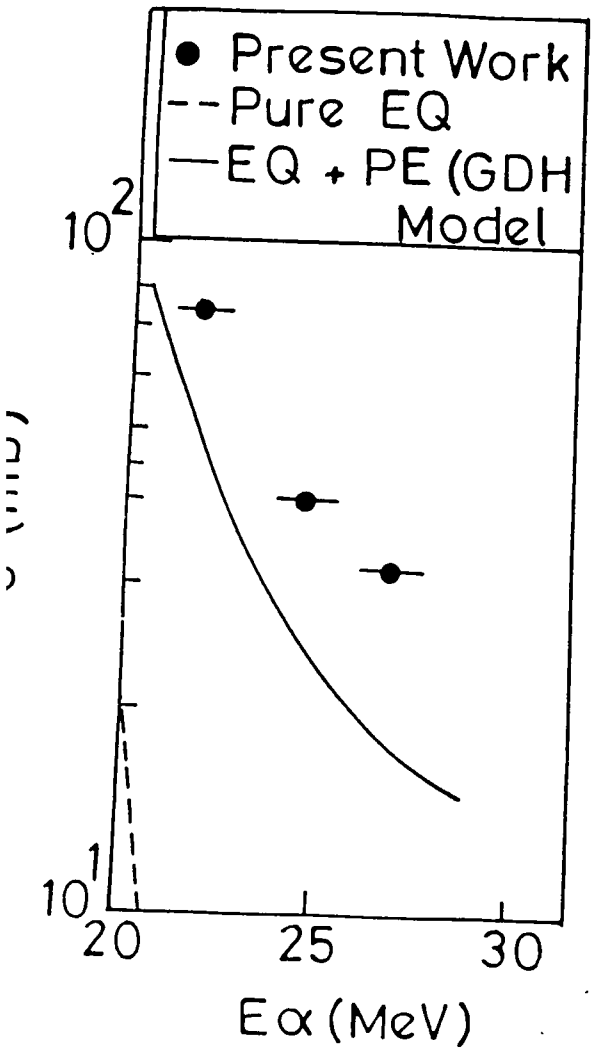


Fig.5.20 Theoretical and experimental excitation functions for $^{123}Sb$ ($\alpha$,n) $^{126}I$ reaction.

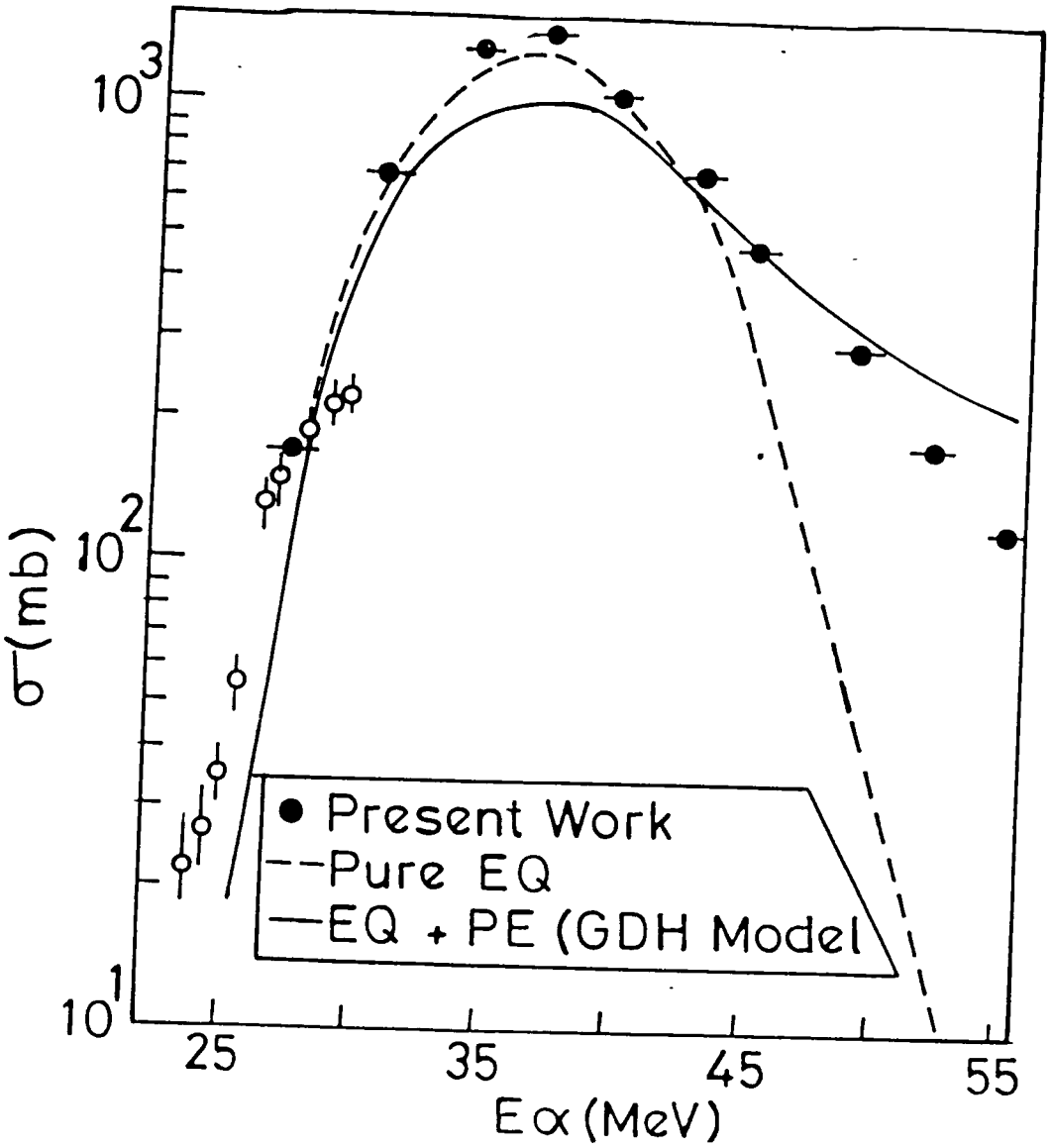


Fog. 5.21 Theoretical and experimental excitation functions for $^{123}Sb$ ($\alpha$,3n)$^{124}I$ reaction

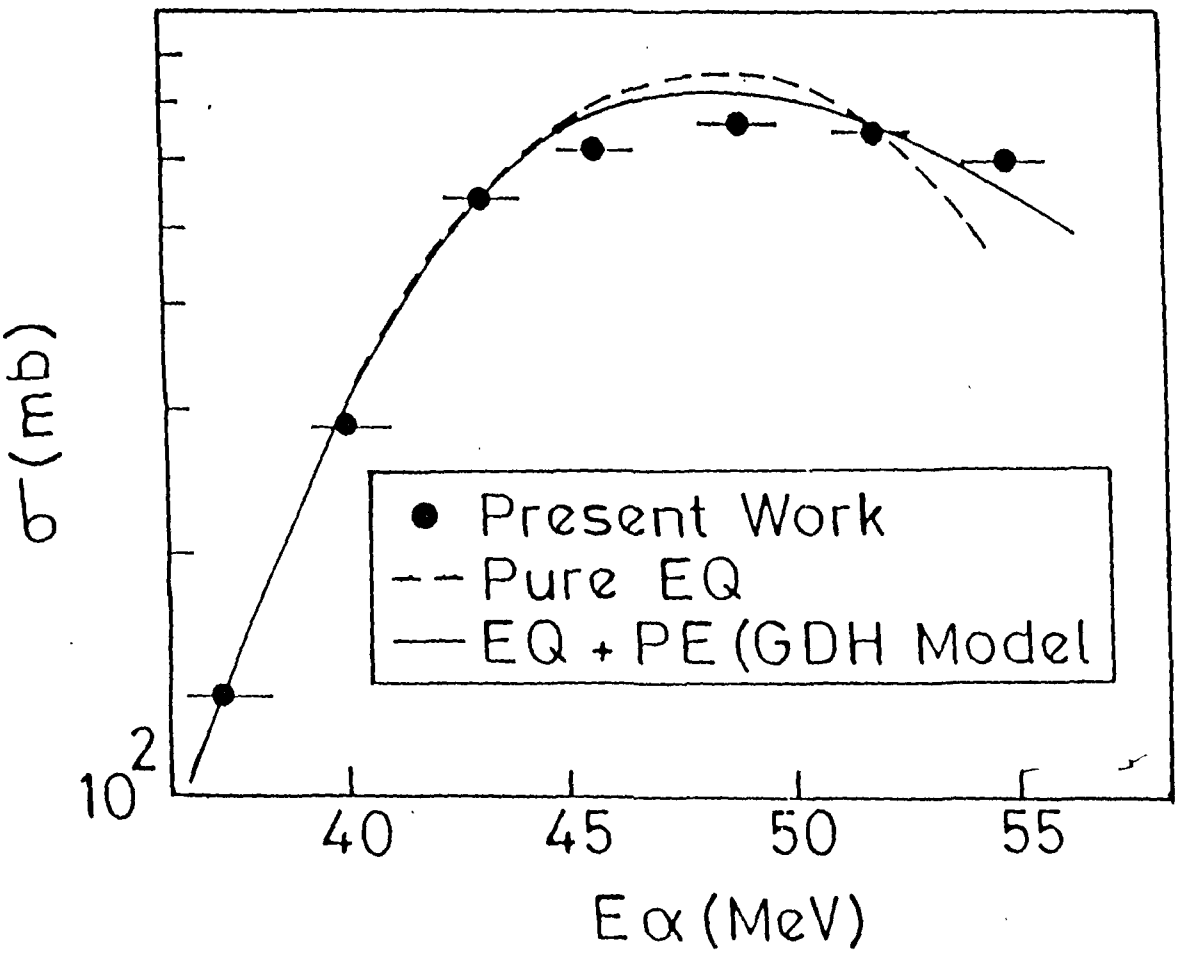


Fig.5.21 Theoretical and experimental excitation functions for $^{123}Sb$ ($\alpha$, 4n) $^{123}I$ reaction

## Table 5.1

Cross-section for the reactions in $^{113}In$.

| Projectile Energy $E_\alpha$ (MeV) | Reaction | $(\alpha,n)$ | $(\alpha,2n)$ |
|---|---|---|---|
| | Product Nucleus | $^{118m}Sb$ | $^{117}Sb$ |
| 21.4±1.4 | | 265.11±6.74 | 391.8C±32.20 |
| 25.2±1.2 | | 137.60±3.69 | 682.92±36.55 |
| 29.0±1.0 | | - | 753.97±29.33 |
| 32.2±0.8 | | - | 416.98±18.95 |
| 35.1±0.8 | | - | 253.42±13.12 |
| 37.4±0.7 | | - | 118.44±7.62 |
| 40.1±0.7 | | - | 78.29±3.98 |
| 43.6±0.7 | | - | 60.81±3.05 |
| 46.8±0.6 | | - | 55.24±2.15 |
| 50.0±0.5 | | - | 48.57±2.34 |

## Table 5.2

Cross-section for the reactions in $^{115}In$.

| Projectile Energies $E_\alpha$ (MeV) | Reaction | (α,n) | (α,2n) | (α,3n) | (α,4n) | (α,pn) | (α,2p) |
|---|---|---|---|---|---|---|---|
| | Product Nucleus | $^{118m}Sb$ | $^{117}Sb$ | $^{116}Sb$ | $^{115}Sb$ | $^{117m}Sn$ | $^{117}In$ |
| 21.4±1.4 | | 210.26±4.53 | 836.92±20.32 | - | - | 17.18±1.38 | - |
| 25.2±1.2 | | 101.61±1.34 | 1220.22±24.46 | - | - | 51.73±2.40 | - |
| 29.0±1.0 | | 42.66±1.06 | 880.99±19.01 | 66.87±0.56 | - | 112.40±3.53 | - |
| 32.2±0.8 | | 22.21±0.85 | 489.48±12.75 | 329.12±6.27 | - | 168.12±4.33 | 3.11±0.08 |
| 35.1±0.8 | | 12.44±0.20 | 210.20±10.52 | 625.69±11.70 | 9.06±0.53 | 153.85±4.14 | 6.44±0.29 |
| 37.4±0.7 | | - | 141.97±9.70 | 770.80±15.04 | 17.64±0.63 | 107.64±3.46 | 11.02±0.53 |
| 40.1±0.7 | | - | 119.98±7.57 | 580.35±19.63 | 48.72±0.67 | 90.97±3.17 | 16.76±0.40 |
| 43.6±0.7 | | - | 83.99±6.23 | 445.03±15.05 | 169.09±1.08 | 73.95±2.87 | 24.69±0.18 |
| 46.8±0.7 | | - | 67.94±5.32 | 321.01±5.12 | 351.72±1.16 | 66.99±2.72 | 28.42±0.36 |
| 50.0±0.5 | | - | 60.93±4.37 | 281.27±8.04 | 323.64±1.41 | 62.71±2.60 | 30.60±0.35 |

## Table 5.3

Cross-sections for the reactions in $^{191}Ir$.

| Projectile Energy $E_\alpha$ (MeV) | Reaction | $(\alpha,n)$ | $(\alpha,2n)$ | $(\alpha,3n)$ | $(\alpha,4n)$ | $(\alpha,5n)$ |
|---|---|---|---|---|---|---|
| | Product Nucleus | $^{194}Au$ | $^{193}Au$ | $^{192}Au$ | $^{191}Au$ | $^{190}Au$ |
| 16.8±1.3 | | 45.38±9.07 | 49.96±10.65 | - | - | - |
| 18.4±1.2 | | 56.49±10.48 | 198.03±21.11 | - | - | - |
| 21.4±1.1 | | 57.84±10.49 | - | - | - | - |
| 24.4±0.9 | | 26.80±7.16 | 543.78±34.46 | - | - | - |
| 26.9±0.9 | | 19.13±6.04 | 704.97±39.04 | 82.50±5.58 | - | - |
| 29.2±0.8 | | 20.92±6.31 | 659.95±37.54 | 342.84±11.14 | - | - |
| 31.4±0.8 | | 22.73±6.56 | - | 551.24±13.88 | - | - |
| 34.9±0.8 | | 18.82±5.95 | 185.64±19.57 | 1262.35±20.46 | - | - |
| 37.8±0.7 | | 15.62±6.98 | 148.15±22.59 | 1047.25±23.72 | - | - |
| 40.5±0.7 | | - | 126.49±20.79 | 893.41±21.60 | 115.06±17.96 | - |
| 43.5±0.7 | | - | 109.16±19.60 | 596.26±17.42 | 361.35±31.21 | - |
| 45.9±0.6 | | - | 97.72±18.15 | 454.56±15.01 | 642.58±40.80 | - |
| 49.1±0.6 | | - | 80.29±16.39 | 280.04±11.63 | 809.11±44.88 | 80.88±4.65 |
| 52.9±0.6 | | - | 59.74±14.08 | 214.91±10.05 | 617.30±38.36 | 196.54±11.40 |
| 55.0±0.5 | | - | 52.51±13.12 | 184.85±9.14 | 338.34±27.53 | 568.43±7.27 |

Table 5.4

Cross-sections for the reactions in $^{193}Ir$.

| Projectile Energy $E_\alpha$ (MeV) | Reaction | (α,3n) | (α,4n) | (α,5n) |
|---|---|---|---|---|
| | Product Nucleus | $^{194}Au$ | $^{193}Au$ | $^{192}Au$ |
| 16.8±1.3 | | - | - | - |
| 18.4±1.2 | | - | - | - |
| 21.4±1.1 | | - | - | - |
| 24.4±0.9 | | 75.06±9.31 | - | - |
| 26.9±0.9 | | 217.36+15.81 | - | - |
| 29.2±0.8 | | 582.15±25.80 | - | - |
| 31.4±0.8 | | 1143.25±36.08 | - | - |
| 34.9±0.8 | | 1210.93±37.05 | 117.87±12.15 | - |
| 37.8±0.7 | | 1062.06±62.67 | 540.61±33.46 | - |
| 40.5±0.7 | | 857.46±40.06 | 752.18±39.32 | - |
| 43.5±0.7 | | 624.98±34.14 | 1043.65±47.00 | - |
| 45.9±0.6 | | 477.93±29.81 | 1140.52±48.06 | 4.17±1.11 |
| 49.1±0.6 | | 276.20±22.61 | 911.09±42.80 | 106.70±5.56 |
| 52.9±0.6 | | 254.91±21.70 | 844.04±41.04 | 385.89±10.44 |
| 55.0±0.5 | | 248.13± 21.36 | 601.81±34.46 | 495.30±11.60 |

## Table 5.5

### Cross-section for the reactions in $^{121}Sb$

| Projectile Energy $E_\alpha$ (MeV) | Reaction | (α,n) | (α,2n) | (α,4n) | (α,p3n) |
|---|---|---|---|---|---|
| | Product Nucleus | $^{124}I$ | $^{123}I$ | $^{121}I$ | $^{121}Te$ |
| 21.9±1.2 | | 101.07±3.53 | 691.20±18.91 | - | - |
| 24.7±1.1 | | 44.99±2.34 | 881.62±32.26 | - | - |
| 27.2±1.0 | | 28.37±1.99 | 915.16±36.76 | - | - |
| 30.7±0.9 | | 17.48±1.78 | 624.71±20.52 | - | - |
| 34.3±0.8 | | 19.35±1.88 | 592.96±19.73 | - | - |
| 37.3±0.8 | | - | 267.45±13.01 | 9.79±0.49 | 33.64±3.91 |
| 40.1±0.8 | | - | 154.97±6.21 | 71.98±1.48 | 168.23±8.75 |
| 43.3±0.7 | | - | 122.85±3.60 | 227.20±0.90 | 372.84±18.41 |
| 45.7±0.7 | | - | 102.15±2.06 | 397.46±0.77 | 548.69±15.88 |
| 48.9±0.6 | | - | 98.71±1.58 | 609.82±2.64 | 716.30±18.10 |
| 52.1±0.6 | | - | 87.68±1.02 | 645.63±0.56 | 929.46±20.63 |
| 55.0±0.5 | | - | 75.34±0.75 | 504.98±1.36 | 820.38±19.39 |

## Table 5.6

Cross-section for the reactions in $^{123}Sb$.

| Projectile Energy $E_\alpha$ (MeV) | Reaction | (α,n) | (α,3n) | (α,4n) |
|---|---|---|---|---|
| | Product Nucleus | $^{126}I$ | $^{124}I$ | $^{123}I$ |
| 21.9±1.2 | | 75.01±1.87 | - | - |
| 24.7±1.1 | | 40.00±2.62 | - | - |
| 27.2±1.0 | | 32.30±1.33 | 176.56±6.61 | - |
| 30.7±0.9 | | - | 694.71±13.41 | - |
| 34.3±0.8 | | - | 1302.05±18.00 | - |
| 37.3±0.8 | | - | 1497.18±19.33 | 130.48±0.82 |
| 40.1±0.8 | | - | 1068.31±16.34 | 282.58±1.21 |
| 43.3±0.7 | | - | 701.69±13.25 | 530.63±1.67 |
| 45.7±0.7 | | - | 479.28±10.96 | 603.87±1.79 |
| 48.9±0.6 | | - | 291.84±8.56 | 645.89±1.87 |
| 52.1±0.6 | | - | 180.19±6.73 | 642.66±1.88 |
| 55.0±0.5 | | - | 139.46±5.92 | 598.22±1.82 |

upto 17 MeV and 22 MeV in these two stacks respectively.

## 5.2 Theoretical Predictions

The excitation function for the reactions (measured experimentally) were also calculated theoretically. These theoretical calculations were done using the hybrid model i.e. a combination of the pre-compound and compound nucleus model. This model calculates the spectra of emitted particles in the energy dissipation process for each step, whose induction takes place by the interaction between projectile and target nucleons. In this model, the calculation is done with an initial number of excitons (particles + holes), the Fermi level induced by the primary interaction and proceeds to state with an increasing exciton number. The emission probability for the particles for each of these states is calculated and in the last, integration spectra gives the cross-section for all possible reactions. This model has already been discussed in detail in Chapter II.

The theoretical calculations were done by using the computer code ALICE/LIVERMORE-82 [14]. In this code the input parameters are the option for mass formula, pairing correction , level density parameter, mean free path multiplier for the nucleon-nucleon scattering cross-section and the initial exciton number (particle + hole). In this code, there is a provision to calculate the excitation function by the consideration of equilibrium emission only and the equilibrium with pre-equilibrium both,

individually. For analysing the equlibrium part, the Weisskopf-Ewing model [15] was adopted while the pre-equilibrium part calculations were done according to the hybrid [9] as well as the geometry dependent hybrid (GDH) model [10] of Blann. The statistical part of this code can account for a large variety of reaction types [16,17], cluster such as deuteron and $\alpha$-particle can be considered besides the evaporation of neutrons and protons according to Weisskopf and Ewing. This is done with the conservation of angular momentum. The Q-values for the formation of compound nucleus and,neutron , proton, alpha and deuteron binding energies for all nuclides of interest in the evaporation chain are calculated with the help of Myers-Swiatecki/ Lysekil mass formula [18]. The pairing energy $\delta$ calculations are done by using the back shifted model. It's value is 0 for even-even nuclei,$-\delta$ for odd-even nuclei and $-2\,\delta$ for odd-odd nuclei with $\delta = 11/\sqrt{A}$, where A is the nucleon number of the element understudy. The inverse cross-sections were calculated with the help of optical model subroutine of ALICE/LIVERMORE-82 computer code, which uses the Becchetti and Greenlees [19] optical parameters. The Pauli corrected nucleon-nucleon scattering cross-sections were used to calculate the intranuclear transition rates. The mean free path was adjusted for intranuclear transitions.

The hight and shape of excitation function varies with the level density parameters [20]. The selection of value of

level density parameter is done according to the formula proposed by Lang and Le couteur [21] which tells that the value of level density parameter $a = A/K$ where A denotes nucleon number and K, a constant, for which values, spread over a wide region have been given in literature [22-24].

In the present case the value of mean free path multiplier was taken 2 and the value of level density parameters were 12,12, 10 for In, Ir, Sb respectively.

In the pre-equilibrium reactions the initial exciton configuration is a crucial quantity. It is described by the number of neutrons (n), protons (p) in excited states and the number of holes (h) after the first collision. For α-induced reactions the suggested value of it is 4 or 5. It is found by many investigators [20, 25-28] that the exciton number $n_o = 4$ gives the best fit to the experiment. In the present case the calculations were done by taking the value of $n_o = 4,5,6$ but it is found that $n_o = 4$ (2 neutron + 2 proton + 0 hole) gives the best fit to our experimental data.

## 5.3 Discussion Of The Results

In the figures from 5.1 - 5.22 our experimentally measured results are shown by the solid balls. Available literature values are shown by the rectangles while the theoretical excitation functions calculated with and without the inclusion of pre-equilibrium emission, are represented by the solid and dotted

curves respectively. The cross-section is plotted against the x-axis while the energy of α-particles incident on the particular foil is plotted against the y-axis. The cross-section has been measured in mili-barns denoted by mb while the energy of incident α-particle is measured in Mega electron volt represented as MeV. The maximum energy, on which the cross-section is measured is 50 MeV in case of indium; 55 MeV in case of iridium and antimoney.

In $^{113}In(\alpha,n)^{116}Sb$ reaction, the product nucleus is $^{116}Sb$ and has two states, ground state of half life 15.8 minutes and metastable state of half life 1.005 hrs. In the bombardment of stack, the produced activity was very high so just after the bombardment, the counting of the gamma rays could not be started and was done only when the level of activity came down with in the permissible limit from the Health Physics Control. This cooling time of samples was very large as compared to the half life of ground state of $^{116}Sb$. So the contribution of ground state to the cross-section could not be measured. Hence represented values of the cross-section are due the metastable state only. As the cross-section calculated theoretically is the sum of cross-sections of metastable and ground state both and also in the computer code ALICE/LIVERMORE-82, there is no provision to calculate the excitation function individually for each state of the product nucleus so the comparison between the theoretical and experimental values of excitation functions is not possible. Due to non-availability of the literature, the experimental

values of the excitation function could not be compared with the literature values. In the $^{115}In(\alpha,3n)^{116}Sb$ reaction also the product nucleus is $^{116}Sb$ so all the problems for this reaction are same as in the $^{113}In(\alpha,n)^{116}Sb$ reaction. Of course the Q-values of these two reactions are different but even then after opening the channel of $^{115}In(\alpha,3n)^{116}Sb$ reaction both the reactions go on simultaneously hence, a new problem of separation of cross-section of these reactions arises. The cross-section of the reactions can be separated with the help of the cross-sections calculated theoretically only but, in the present case, the cross-sections could be measured experimentally only for the metastable state while the theoretical cross-sections are the sum of the cross-sections of metastable and ground both, so the cross-sections of $^{113}In(\alpha,n)^{116m}Sb$ and $^{115}In(\alpha,3n)^{116m}Sb$ could not be separated. Hence the represented values are the sum of the cross-section of $^{113}In(\alpha,n)$ and $^{115}In(\alpha,3n)$. The sum of cross-section for these reactions have been measured at the energies $50 \pm 0.5$, $46.8 \pm 0.6$, $43.6 \pm 0.7$, $40.1 \pm 0.7$, $37.4 \pm 0.7$, $35.1 \pm 0.8$, $32.2 \pm 0.8$ and $29.0 \pm 1.0$ while the cross-sections at $25.2 \pm 1.2$, $21.4 \pm 1.4$ MeV energies are only for $^{113}Ir(\alpha,n)^{116m}Sb$ reaction. The measured excitation function is displayed in the fig. 5.1 and the numerical values of the cross-sections are arranged in the table 5.1.

In the $^{113}In(\alpha,2n)^{115}Sb$ reaction, $^{115}Sb$ is the product nucleus. This product nucleus has no metastable state. The half life of $^{115}Sb$ is 32.1 minutes $^{115}Sb$ is also the product

nucleus of $^{115}In(\alpha,4n)^{115}Sb$ reaction so beyond the threshold of $^{115}In(\alpha,4n)^{115}Sb$ reaction, the observed peak of the gamma rays understudy were the sum of two small peaks, one due to $^{113}In(\alpha,2n)^{115}Sb$ reaction while other one due to $^{115}In(\alpha,4n)^{115}Sb$ reaction. So in the tail region of $^{113}In(\alpha,2n)^{115}Sb$ reaction, the measured cross-sections **were** the sum of the cross-sections of these two reactions. The shares of these reactions from the total of the cross-section were divided with the help of the theoretical cross-sections. For the processing, first of all the cross-section, by the computer code, was calculated at the same α-particle energy at which the sum of the cross-section was measured experimentally then this sum of the corss-section was divided in the ratio of the individual cross-section of these reactions calculated by computer code. This individual cross-section of the one of the reaction was put in the cross-sectional formula to calculate the photo peak counts and so obtained photopeak counts were subtracted from the sum of the photopeak counts of the two reactions. Using these photopeak counts, the statistical error in the measured cross-section was calculated. At the energies $21.4 \pm 1.4$, $25.2 \pm 1.2$, $29.0 \pm 1.0$, $32.2 \pm 0.8$ MeV, the observed cross-section were purely due to $^{113}In(\alpha,2n)^{115}Sb$ reaction while beyond this, the observed cross-section was the sum of the cross-section of $^{113}In(\alpha,2n)^{115}Sb$ and $^{115}In(\alpha,4n)^{115}Sb$ reaction. So obtained results of the reactions $^{113}In(\alpha,2n)^{115}Sb$ and $^{115}In(\alpha,4n)^{115}Sb$ are represented in the fig. 5.2 and fig. 5.5 respectively.

In these figures, a comparison between the theoretically calculated (By GDH and Hybrid model) excitation function and the experimentally calculated excitation function is also shown. From the figures, it is clear that experimental results are not in very good agreement with the theoretical results, quantitatively but qualitatively, it is satisfactory. It is also seen in the figures that the experimental results are more closer to the geometry dependent hybrid (GDH) model calculations in comparison of the hybrid model calculations.

In the $^{115}In(\alpha,n)^{118}Sb$ reaction, the product nucleus is $^{118}Sb$. $^{118}Sb$ has a metastable state other than the ground state. The half life of metastable state and ground state is 5.0 hrs. and 3.6 minutes respectively. Due to very short half life of ground state and non-availability of any gamma ray with good intensity in its decay, the cross-section for this state could not be measured. The measured cross-section is only for the metastable state of $^{118}Sb$. Due to the non-availability of the provision to calculate the excitation function for each state of the product nucleus individually, the comparison between the theoretical and experimental excitation function could not be made. The measured values of the cross-section for this reaction are displayed in the fig. 5.3 The numerical values of the cross-section at different $\alpha$-particle energies are given in the

table5.2.

In the reaction $^{115}In(\alpha,2n)^{117}Sb$, $^{115}In(\alpha,pn)^{117m}Sn$ $^{115}In(\alpha,2p)^{117}In$, the product nuclei emit the gamma ray of same energy of0.159 MeV with the different branching ratios. So the peak obtained in the spectrum was the sum of the peaks due to $^{117}Sb$, $^{117m}Sn$, $^{117}In$. Hence the photopeak counts were the sum of the photopeak counts for these three reactions. So the problem of separation of the contribution of each of the state became very important. The half life of $^{117}Sb$, $^{117m}Sn$, $^{117m}In$, $^{117g}In$ is 2.80 hrs, 13.61 days, 1.94 hrs, 43.8 min. It is clear that the half life of these product nuclei is varying from minutes to days or in other words, it can be said that there is a large difference between the half life of the nuclei hence the problem of the separation of the photopeak counts was solved by using the technique of decay analysis. From the metastable state and the ground state, the $^{117}In$ emits the gamma ray of 0.315 (19.1%) MeV and 0.553 (99.7%) MeV also other than the gamma ray of0.159 MeV. So the cross-sections for $^{115}In(\alpha,2p)^{117}In$ reaction are also calculated by following the other gamma ray than the0.159 MeV gamma ray. The numerical values of the cross-sections are given in the table 5.2. The experimentally measured excitation function for $^{115}In(\alpha,2n)^{117}Sb$, $^{115}In(\alpha,pn)^{117m}Sn$, $^{115}In(\alpha,2p)^{117}In$ are displayed in the fig. 5.4 5.6, 5.7 respectively. In these figures, the experimental excitation function is also compared with the excitation function calculated theoretically by taking into the consideration of

compound nucleus formation only by using Weisskopf-Ewing model and that calculated by taking into the consideration of equilibrium and pre-equilibrium decay both using GDH model of Blann. In the reaction $^{115}In(\alpha,pn)^{117m}Sn$, the cross-sections are calculated only for the metastable state , hence in the fig. 5.6 the experimental excitation function is looking lower than the theoretical excitation functions because the solid curve and the dotted curve are representing the total excitation function (metastable state + ground state). The fig. 5.7 represents the excitation function curve for $^{115}In(\alpha,2p)^{117}In$ reaction. In this figure, the small circles show the cross-sections for the metastable state and the triangles show the cross-sections for ground state of $^{117}In$ while the total cross-section is represented by the solid balls.

The $(\alpha,xn)$ reactions in $^{191}Ir$ with $x = 1-5$ and in $^{193}Ir$, $x = 3-5$ have been measured. In $^{191}Ir(\alpha,n)^{194}Au$ and $^{193}Ir(\alpha,3n)^{194}Au$ the product nucleus is $^{194}Au$ with two metastable states of half lives 420 ms and 600 ms respectively and the ground state of half life 1.65 days. Due to very short half life of the metastable states, the contribution of these to the excitation function could not be measured distinguishably but these states decay to the ground state so the total excitation function could be measured. After opening the channel of $^{193}Ir(\alpha,3n)^{194}Au$ reaction, the measured cross-section was the sum of the cross-sections of two reactions. So the cross-section

of each reaction was divided by using the ratio of theoretical cross-section of the aforesaid reactions. The numerical values of the cross-sections of $^{191}Ir(\alpha,n)^{194}Au$ and $^{193}Ir(\alpha,3n)^{194}Au$ reaction are arranged in the table 5.3 and 5.4 and are displayed in the fig. 5.8 and fig.5.13 respectively.

In $^{191}Ir(\alpha,2n)^{193}Au$ and $^{193}Ir(\alpha,4n)^{193}Au$ the product nucleus is $^{193}Au$ which has one metastable state as well as the ground state.The half life of metastable state and ground state is 3.9 sec. and 17.6 hrs. respectively. The half life of metastable state is very short but it decays 99.97% to the ground state so the total excitation function could be measured. Beyond the threshold of $^{193}Ir(\alpha,4n)^{193}Au$ reaction, in the overlapping region, the cross-sections were divided with the help of the ratio of the theoretical cross-sections. The value of the cross-sections of $^{191}Ir(\alpha,2n)^{193}Au$ and $^{193}Ir(\alpha,4n)^{193}Au$ reactions are given in the table 5.3 and 5.4 and are displayed in the fig. 5.9 and 5.14 respectively.

In the reaction $^{191}Ir(\alpha,3n)^{192}Au$ and $^{193}Ir(\alpha,5n)^{192}Au$ the product nucleus is $^{192}Au$. $^{192}Au$ has the metastable state of half life 167 ms while the ground state of half life 4.9 hrs. 167 ms is a very short period so the contribution of this state to the excitation function could not be measured distinguishably but it decays to the ground state so the total excitation function was measured. In the overlapping region of these reactions, the cross-sections were divided by using the ratio of theoretical

cross-sections. The value of the cross-sections of $^{191}Ir(\alpha,3n)^{192}Au$ and $^{193}Ir(\alpha,5n)^{192}Au$ reaction at various incident α-particle energies are given in the table 5.3 and 5.4. Pictorially the excitation functions are shown in the fig. 5.10 and fig. 5.15 respectively.

In the reaction $^{191}Ir(\alpha,4n)^{191}Au$ the product nucleus is $^{191}Au$ possessing the metastable state of half life 920 ms and ground state of half life 3.2 hrs. The metastable state decays to the ground state so total excitation function was measured. In $^{191}Ir(\alpha,5n)^{190}Au$ the product nucleus $^{190}Au$ has only the ground state of half life 42.8 minute. The measured cross-sections of the reactions are tabulated in the table 5.3 and are displayed in the fig. 5.11 and fig. 5.12 respectively.

In the figures, it is seen that the experimentally measured excitation function is approaching the theoretical predictions done by taking into the consideration of equilibrium and pre-equilibrium emission both.

In $^{121}Sb(\alpha,n)^{124}I$ reaction, the product nucleus is $^{124}I$. The half life of $^{124}I$ is 4.18 days. It has no metastable state other than the ground state. $^{124}I$ is the product nucleus of $^{123}Sb(\alpha,3n)^{124}I$ reaction also, so after opening the channel of this reaction, the measured cross-section is the sum of cross-sections of these two reactions. In the overlapping region the cross-sections are divided in the ratio of the theoretically calculated cross-sections. At the α-particle beam energies

29.93 ± 1.2 and 24.68 ± 1.1 Mev, the developed activity was due to the $^{121}Sb(\alpha,n)$ reaction only. The numerical values of the cross-sections of $^{121}Sb(\alpha,n)^{124}I$ and $^{123}Sb(\alpha,3n)^{124}I$ reaction at different energies are given in the table 5.5 and 5.6 respectively while the results are shown in the fig. 5.16 and fig. 5.21 respectively. In these figures the experimentally measured results are also compared with the theoretical predictions and literature (A. Calboreanu et al. and I.A. Waston et al.). The results of Calboreanu et al. are reproduced by the sign of cross and those of I.A. Waston et al. are reproduced by rings. In $^{121}Sb(\alpha,n)^{124}I$ reaction, the results of A. Calboreanu et al. are upto the 24.0 MeV and are very high than the theoretical predictions while the results of I.A. Waston et al. are upto 22.0 MeV only and are very low to the theoretical predictions. In the present measurement the excitation function curve has been extended upto the 34.26 MeV and is lying in between of two literature values and also satisfactorily matching with the theoretical excitation function (calculated by GDH model) curve.

In $^{121}Sb(\alpha,2n)^{123}I$ and $^{123}Sb(\alpha,4n)^{123}I$ reaction, the product nucleus is same i.e. $^{123}I$ which has the ground state of half life 13.2 hrs. with no metastable state. Below the threshold of $^{123}Sb(\alpha,4n)^{123}I$ reaction the cross-section is due to the $^{121}Sb(\alpha,2n)^{123}I$ reaction only. The activity measured at the energies 21.93 ± 1.2, 24.68 ± 1.1, 27.24 ± 1.0, 30.7 ± 0.9,

34.3 ± 0.8 MeV was due to the $^{121}Sb(\alpha,2n)^{123}I$ reaction only while beyond this the measured activity was the composite activity of two reactions. In the overlapping region, the cross-sections were divided with the help of the theoretical cross-sections calculated at the same energy. The value of the cross-sections of $^{121}Sb(\alpha,2n)^{123}I$ and $^{123}Sb(\alpha,4n)^{123}I$ reactions are arranged in the table 5.5 and 5.6 and are displayed in the fig. 5.17 and 5.22 respectively. In the $^{121}Sb(\alpha,2n)^{123}I$ reaction the literature values [29,30] are also available. The values calculated in ref. 29 and 30 are upto peak of excitation function only, the tail portion has not been measured while in the present measurements, the excitation function curve has been calculated upto 55 MeV energy. The results of I.A. Waston et al. [30] are very low and showing the shift of peak also. In the tail portion of the excitation function curve present measurements are in very good matching with the GDH model calculations. In the $^{123}Sb(\alpha,4n)$ reaction the measured results are in good agreement with the theoretical calculations (GDH model) qualitatively as well as the quantitatively. No literature value is available. In the $^{123}Sb(\alpha,n)^{126}I$ reaction, the cross-section could be measured at 21.93 ± 1.2, 24.68 ± 1.1, 27.24 ± 1.0 MeV only. In this reaction measured results are higher than the GDH model calculations. In $^{121}Sb(\alpha,4n)^{121}I$ reaction, the reported results are in satisfactorily agreement with the theoretical predictions(done by GDH model). In $^{121}Sb(\alpha,p3n)^{121}Te$ the measured results are only for ground state, so can not be compared with the theory. The value of the measured results for $^{121}Sb(\alpha,p3n)^{121}Te$,

$^{121}Sb(\alpha,4n)^{121}I$ are given in table 5.5, while the results for $^{123}Sb(\alpha,n)^{126}I$ reaction are given in table 5.6. These experimental excitation function and theoretical excitation function (calculated with and without inclusion of PE) are displayed in the fig. 5.19, fig. 5.18 and fig. 5.20 respectively.

## 5.4 Conclusions

The study of excitation function of α-induced reactions in $^{113}In$, $^{115}In$, $^{121}Sb$, $^{123}Sb$, $^{191}Ir$ and $^{193}Ir$ has been done. These excitation functions are displayed in the figs. 5.1 - 5.22. In these figures, it is very clear that the measured results are in agreement, qualitatively, with the theoretical results but the quantitative agreement is not very good. From the figs. 5.1 - 5.22, it can be concluded that the experimental results are more agreed to the results calculated theoretically by taking the consideration of equilibrium as well as the pre-equilibrium decay (GDH model calculations), shown by solid curve in the figures, in comparison of those which are calculated by taking the consideration of pure equilibrium reaction mechanism (Weisskopf-Ewing model calculations), shown by broken curve in the figures. The discrepancy between the results obtained from Weisskopf-Ewing model calculations and those measured experimentally, increases with increasing $E_\alpha$ in the sloping down portion of the excitation function. According to the Weisskopf-Ewing model calculations, the excitation function comes down very

fast beyond peak while according to the GDH model calculations, it comes down very slowly and hence, has a long tail. Thus the high energy tails of the excitation function can not be accounted for by pure equilibrium reaction mechanism, it can be explained, only, by the proper admixture of equilibrium and pre-equilibrium process which is justified by the comparison of our experimentally measured results, solid curve, and broken curve in the figs. 5.1-5.22. It is also concluded that the initial exciton number configuration $n_o = 4$ (2n + 2p + Oh) gives the best fit to our experimental data and supports the many earlier investigators [20, 25-28].

The comparison of theory and experiment shows that the pre-equilibrium process is present in the α-induced reactions and gives a significant contribution. The pre-equilibrium fraction is a measure of the relative weight of the pre-equilibrium contribution needed for the reproduction of experimental data. The total pre-equilibrium fraction (for all possible reaction) is more meaningful and is calculated for $^{113}In$, $^{115}In$, $^{121}Sb$, $^{123}Sb$, $^{191}Ir$ and $^{193}Ir$ using ALICE/LIVERMORE-82 computer code [14]. It is plotted against the α-particle beam energy and shown in the fig. 5.23. From the fig. 5.23, it is inferred that threshold of pre-equilibrium process increases with the decrease of mass number and increases very fast with the increase of incident α-particle energy. On increasing the multiplicity of out going particles at higher energies, the rate of increament of the pre-equilibrium fraction decreases.

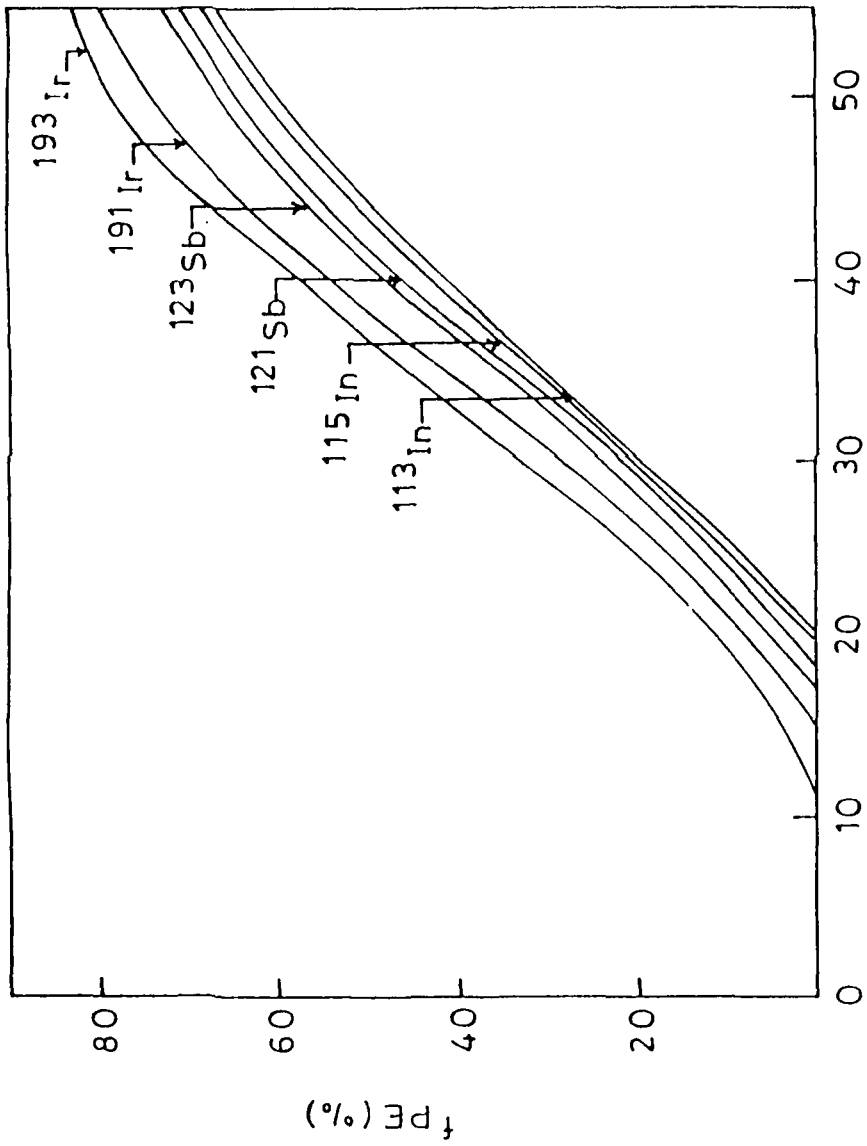


Fig. 5.23 $f_{PE}$(%) for $^{191,193}$Ir, $^{121,123}$Sb and $^{113,115}$In.

## REFERENCES


[1] Emilio Segre, J. Robb Groves, H. Picere Mayes: Ann. Rev. Nucl. Sci. 25 (1975) 124.

[2] V.A. Sidorov: Nucl. Phys. 35 (1965) 253.

[3] C. Holbrow, H. Barschall: Nucl. Phys. 42 (1963) 264.

[4] R. Wood, R. Brochers, H. Barschall: Nucl. Phys. 71 (1965) 529.

[5] J.J. Griffin: Phys. Rev. Lett. 17 (1956) 478.

[6] G.D. Harp and J.M. Miller: Phys. Rev. C3 (1971) 1847.

[7] M. Blann: Ann. Rev. Nucl. Sci. 25 (1975) 123.

[8] E. Gadioli, E. Gadioli-Erba and P.G. Sona: Nucl. Phys. A217 (1973) 589.

[9] M. Blann: Phys. Rev. Lett. 27 (1971) 337; 27 (1971) 700(E); 27 (1971) 1550(E).

[10] M. Blann: Phys. Rev. Lett. 28 (1972) 757.

[11] G.D. Harp, J.M. Miller and J.B. Berne: Phys. Rev. 165 (1968) 1166.

[12] C.K. Cline and M. Blann: Nucl. Phys. A172 (1971) 225.

[13] EXFOR Library, Nuclear Data Section, I.A.E.A. Vienna (1991).

[14] M. Blann and J. Bisplinghoff: ALICE/LIVERMORE-82 LLNL Report UCID 19614 (1982).

[15] V.F. Weisskopf and D.H. Ewing: Phys. Rev. 57 (1940) 472.

[16] R. Michel and G. Brinkmann: Nucl. Phys. A 338, (1980) 167.

[17] R. Michel, F. Peiffer and R. Stuck. Nucl. Phys. A 441 (1985) 617.

[18] W.D. Myers and W.J. Swiatecki: Ark. Fys. 36 (1967) 343.

[19] F.D. Becchetti and G.W. Greentess: Phys. 182 (1969) 1190.

[20] P. Misaelides and H. Munzel: J. Inorg. Nucl. Chem. 42 (1980) 937.

[21] J.M. Lang and K.J. Le Counter: Proc. Phys. Soc. 67A (1954) 586.

[22] D.G. Sarntiles: Nucl. Phys. A93 (1967) 576.

[23] C. Hurwitz, S.J. Speneer, R.A. Esterlund, B.D. Pate and J.B. Reynolds: Nucl. Phys. 54 (1964)65.

[24] S. Fukushima, S. Hayashi, S. Kume, H. Okumura , K. Oztazai, K. Sakamoto and Y. Yoshizawa: Nucl. Phys. 41 (1963) 275.

[25] M. Blann and T.T. Komoto: Phys. Rev. C29 (1984) 1678.

[26] G.W.A. Newton, V.J. Robinson and E.M. Show: J. Inorg. Nucl. Chem. 43 (1991) 2221.

[27] M.K. Bhardwaj, I.A. Rizvi and A.K. Chaubey: Phys. Rev. Vol. 45 No. 5 (1992) 2338

[28] I.A. Rizvi, M. Afzal Ansari, R.P. Gautam, R.K.Y. Singh and A.K. Chaubey: J. Phys. Soc. Japan 56 (1987) 3135.

[29] A. Calboreanu, C. Pencea amd O. Salagean: Nucl. Phys. A383 (1982) 251.

[30] I.A. Waston, S.L. Waters and D.J. Silvester, I. Inorg. Nucl. Chem. 35 (1973) 3047.

# LIST OF PUBLICATION

Paper In International Journals :

1. Pre-equilibrium emission of multiparticles in alpha induced reactions with 55Mn nucleus.
   I.A. RIZVI, M.K. BHARDWAJ, M. AFZAL ANSARI and A.K. CHAUBEY
   Can. J. Phys. 67, 1091(1989)

2. Pre-equilibrium decay process in alpha induced reactions of Silver isotopes.
   A.K. CHAUBEY, M.K. BHARDWAJ , R.P. GAUTAM, R.K.Y.SINGH, M.AFZAL ANSARI, I.A. RIZVI and H. SINGH.
   Appl. Radiot. Isot. Vol.41 No. 4 pp 401-405.1990.

3. Non-equilibrium reaction mechanism in alpha-particle induced excitation function for 290 Bi upto 60 MeV.
   I.A. RIZVI, M.K. BHARDWAJ, M. AFZAL ANSARI AND A.K. CHAUBEY
   App. Radiat. Isot. Vol.41 No.2 pp 215-219-1990.

4. Non-equilibrium effect in alpha induced reactions on gallium isotopes.
   I.A. RIZVI, M.K. BHARDWAJ M.AFZAL ANSARI AND A.K. CHAUBEY.
   Can. J. Phys. 67, 870(1989).

5. Alpha-induced reactions in iridium: Phys. Rev. C Vol. 45 No.5 (1992)2338. M.K.Bhardwaj, I.A.Rizvi and A.K. Chaubey.

6. Excitation function studies for the alpha-induced reactions in indium : IJMPE (Accepted for the publication).
   M.K. Bhardwaj, I.A. Rizvi and A.K. Chaubey.

Papers Reported at ICTP, Italy

Study of alpha induced reactions in natural iridium.
A.K. Chaubey, M.K. Bhardwaj, I.A. Rizvi and H. Singh.

2. Excitation function measurements for the alpha induced reactions in indium.

A.K. CHAUBEY, M.K. BHARDWAJ , I.A. RIZVI and H.SINGH. IC/89/149.

3. Multiparticle Emission in the Pre-equilibrium Decay of Light and Heavy Nuclei in $\alpha$ -Induced Reaction upto 60 MeV.

M.AFZAL ANSARI, I.A. RIZVI, M.K. BHARDWAJ AND A.K. CHAUBEY

Int. Cent. Theoret. Phys (Italy ) Internal Report IC/89/57.

Papers in International Conferences

1. Study of ($\alpha$,xn )reaction in Iridium at 50 to 30 MeV Energies

M.K. Bharadwaj, M.Afzal Ansari, I.A. Rizvi and A.K. Chaubey.

Int. Conf. Nucl. React. Mechanism, Calcutta (India)p.51,1989.

2. Non-equilibrium Reaction Mechanism in a-particle Induced Excitation Function for Bi-209 upto 60 MeV.

I.A. Rizvi, M.Afzal Ansari, M.K. Bhardwaj and A.K. Chaubey

Papers in National Symposia

1. Excitation Functions for Alpha- Induced Reactions on Gallium Isotopes.

I.A. Rizvi, M.Afzal Ansari, Manoj Kumar, R.P. Gautam and A.K.Chaubey

Proc. Nucl. Phys. Symposium, 30B, D29 , 256, 1987.

2. Study of ($\alpha$, xn) Reactions in Silver from 37-60 MeV Energies.

M.K. Bharadwaj, M.A. Ansari, I.A. Rizvi, H.V. Singh and A.K. Chaubey

Proc. Nucl. Phys. Symposium, 31B, p69, 1988.

3. Alpha Induced Reactions in Indium.

M.K. Bhardwaj, I.A. Rizvi H. Singh and A.K.Chaubey.

Proc.Nucl. Phys. Symposium 32B, 036, 1989.

4. Setting and Testing of a Compton Supressed Gamma Ray Spectroscopy System.

H. Singh, M.K. Bhardwaj, I.A. Rizvi and A.K. Chaubey.

Proc. Nucl. Phys. Symposium, 32B ,p.57, 1989.

5. Study of Excitation Function for Alpha Induced Reactions in Natural Iridium From 17-55 MeV.

M.K. Bhardwaj, H. Singh, I.A. Rizvi and A.K. Chaubey .

Proc. Nucl. Phys. Symposium, 33B, p.121,1990.

THE PHYSICAL REVIEW

AND

027

PHYSICAL REVIEW LETTERS

EDITORIAL OFFICES · 1 RESEARCH ROAD

BOX 1000 · RIDGE, NEW YORK 11961

Telephone (516) 924 5533

Telex Number: 971599 Cable Address: PHYSREVRIDGENY

FAX: (516) 924-5294

29 January 1992

Dr. A.K. Chaubey
Nuclear Physics Lab.
Department of Physics
Aligarh Muslin University
Aligarh-202002, INDIA

Re: CL4539
Alpha-induced reactions in iridium

By: M.K. Bhardwaj, I.A. Rizvi, and A.K. Chaubey

Dear Dr. Chaubey:

We are pleased to inform you that the above manuscript has been accepted for publication as a regular article in Physical Review C.

Please note the publication charge information below and return the attached form indicating 'acceptance' or 'nonacceptance' as soon as possible.

Sincerely yours,

Gerard t. Dreiss
Associate Editor
Physical Review C

The current publication charge is $50 per printed page plus $50 per article in support of publication of the abstract in Physical Review Abstracts. The estimated charge for your manuscript is $350 which includes the $50 abstract charge; the final charge based on the actual number of printed pages may differ. PLEASE NOTE: Free reprints are not provided. Reprint orders involving multiple institutions must be signed by an authorized agent from each institution.

PHYSICAL REVIEW C VOLUME 45, NUMBER 4 APRIL 1992

# Alpha-induced reactions in iridium

M. K. Bhardwaj, I. A. Rizvi, and A. K. Chaubey
*Department of Physics, Aligarh Muslim University, Aligarh 202002, India*
(Received 25 November 1991)

The excitation function of $(\alpha,xn)$ reactions on $^{191}$Ir (abundance 37.3%) and on $^{193}$Ir (abundance 62.7%) has been measured for the 17–55 MeV alpha-particle bombarding energy range. The stacked foil activation technique and $\gamma$-ray spectroscopy were used to determine the cross sections. The experimental data were compared with calculated values obtained by means of a geometry-dependent hybrid model. The initial exciton number $n_0=4$ with $n=2$, $p=2$, and $h=0$ gives the best agreements with the presently measured results. To calculate the excitation function theoretically a computer code was used. This set of excitation functions provides a data basis for probing the validity of combined equilibrium and pre-equilibrium reaction models in a considerable energy range.

PACS number(s): 25.55.−e

## I. INTRODUCTION

During the last decade a lot of study has been done in understanding of nonequilibrium reaction mechanisms. The high-energy tail observed in the excitation function of the light particle reactions contains important information about the reaction mechanisms. Several models [1–8] have been proposed to interpret this experimentally observed feature of the excitation functions. The hybrid and geometry-dependent hybrid models [5,6] are found to give the best verification for the above-mentioned fact in a broad range of experimental data. More elaborate quantum-mechanical theories [9–15] which are not applied to routinely measurable preequilibrium cross sections have tended to support the foundation on which the classical models are built [16]. Presently the measurements are performed to compare the excitation function of the reactions in the isotopes of the natural iridium with Blann's geometry-dependent hybrid (GDH) model via the code ALICE, which contains both the compound and preequilibrium (PE) processes. We have measured the excitation function of the reactions $^{191}$Ir$(\alpha,n)$, $^{191}$Ir$(\alpha,2n)$, $^{191}$Ir$(\alpha,3n)$, $^{191}$Ir$(\alpha,4n)$, $^{191}$Ir$(\alpha,5n)$, $^{193}$Ir$(\alpha,3n)$, $^{193}$Ir$(\alpha,4n)$, and $^{193}$Ir$(\alpha,5n)$ and reported them to the best of our knowledge.

## II. EXPERIMENTAL PROCEDURE

### A. Sample preparation

Samples of the element under study were made from spectroscopic iridium having purity better than 99.99% by the vacuum evaporation technique in the target division of the variable Energy Cyclotron Centre, Calcutta, India. The target foils were squares of side, 1.5 cm, and of the thickness, 150 $\mu$g/cm$^2$. The foils were fixed on aluminium sheets having a circular hole with a diameter of 1.2 cm in its center. The aluminium degraders of the different thickness were also inserted in the target stack so that the alpha beam of 55 MeV energy might be degraded considerably.

### B. Irradiation and counting

The target stack was irradiated with a 55 MeV energy alpha-particle beam at the Variable Energy Cyclotron Centre (VECC), Calcutta, India for 3900 sec, keeping in view the thickness of the sample, the melting point of the element, and the half-lives of the yields. A typical experimental setup for the stack irradiation is shown in Fig. 1. After cooling, the target foils were brought, one by one to the counting room and the residual activity was recorded with the help of a 100 cm$^3$ ORTEC Ge(Li) detector coupled with a precalibrated 4096 multichannel analyzer and associated electronics. The efficiency and energy calibrations were performed using a standard $^{152}$Eu point source of known strength keeping it at target position.

### C. Flux measurements

During the irradiation of the stack, the counting of the incoming $\alpha$ particles was done from an integrated beam charge. Here the beam was totally stopped in the electrically insulted irradiation heads serving as a kind of Faraday cup [17–21] where secondary electrons were prevented from escaping. Using this charge, the flux was calcu-

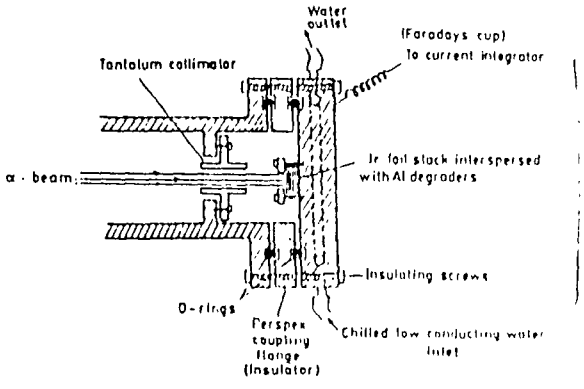


FIG. 1. Experimental setup for stack foil irradiation with an $\alpha$-particle beam.

lated. Copper foil was used as a flux monitor [18] for checking the flux and good agreement was found with $< 10\%$ discrepancy.

### D. Energy spread

The important factors contributing to the energy spread of the $\alpha$ particles incident on a particular target foil are the spread in the initial beam energy, foil thickness, stopping power values, and path length. In the present measurements, the uncertainty in the initial beam energy was $\pm 0.5$ MeV.

The stopping power values are adopted from the tables of Northcliffe and Schilling [22], which are accurate within 5%.

Multiple scattering at small angles increases the path length of the stopping materials [23]. However, in the case of $\alpha$ particles, the path length correction is very small [17] ($\leq 0.5\%$) and, hence, neglected.

### E. Cross-section determination

The activation cross section was computed using the following expression [19–21,24]:

$$\sigma(E)=\frac{A\lambda \exp(\lambda t_2)}{N\Phi(G\epsilon)\theta K[1-\exp(-\lambda t_1)][1-\exp(-\lambda t_3)]},$$

where $A$ is the count under the photopeak of characteristic $\gamma$ rays, $\lambda$ is the decay constant of product nucleus, $N$ is the number of nuclei of the isotope under investigation, $\Phi$ is the incident $\alpha$-particle flux, $(G\epsilon)$ is the geometry-dependent efficiency of the Ge(Li) detector, $\theta$ is the absolute intensity of the characteristic $\gamma$ rays, $K$ is the self-absorption correction factor for the $\gamma$ rays in the sample, $t_1$ is the irradiation time, $t_2$ is the time lapsed between stopping the beam and start of counting, and $t_3$ is the counting time.

The cross section of a particular reaction was calculated for various identified $\gamma$ rays arising from the same product nucleus. For this purpose only those $\gamma$ rays were considered that had good statistics. The reported value is the weighted average [25] of the various cross-section values so obtained. All the decay parameters of the nuclei studied here were taken from the Table of Isotopes by Lederer and Shirley [26].

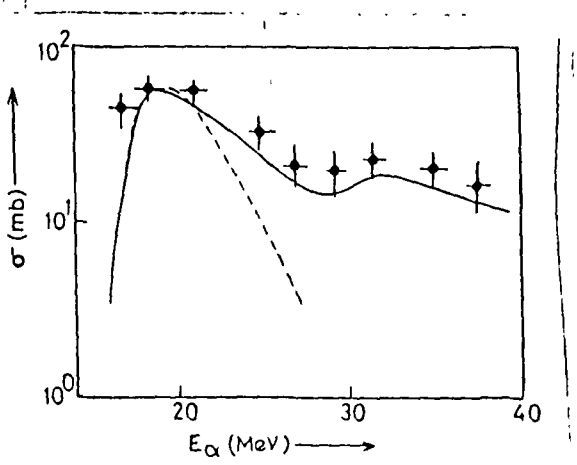


FIG. 2. Experimental and theoretical excitation functions for the reaction $^{191}$Ir($\alpha$,$n$)$^{194}$Au. ●, present work; (– – –), pure EQ; and (——), EQ with the PE [$n_0=4(2n+2p+0h)$] GDH model.

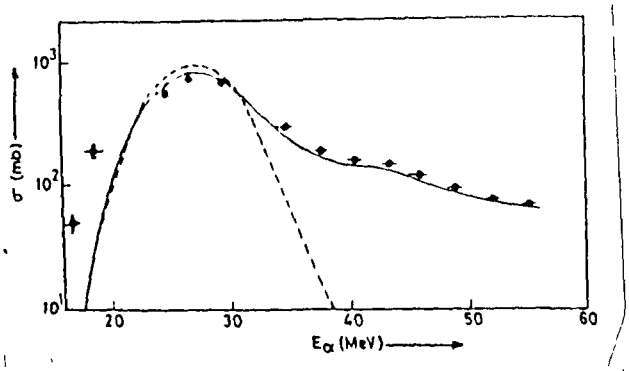


FIG. 3. Experimental and theoretical excitation functions for the reaction $^{191}$Ir($\alpha$,$2n$)$^{193}$Au. ●, present work; (– – –), pure EQ; and (——), EQ with the PE [$n_0=4(2n+2p+0h)$] GDH model.

## III. RESULTS AND DISCUSSION

### A. Theoretical predictions

The theoretical excitation function calculations were done using the compound nucleus model with and without the inclusion of the PE emission of particles. For analyzing the equilibrium (EQ) part, the compound nucleus model of Weisskopf and Ewing [27] was adopted. The contribution from the PE process has been included only at the first step of evaporation. The GDH model was used for analyzing the PE part [6]. For performing these calculations, the computer code ALICE/LIVERMORE-82 [28] was used. Since the program system and the theories involved have been discussed by several authors already,

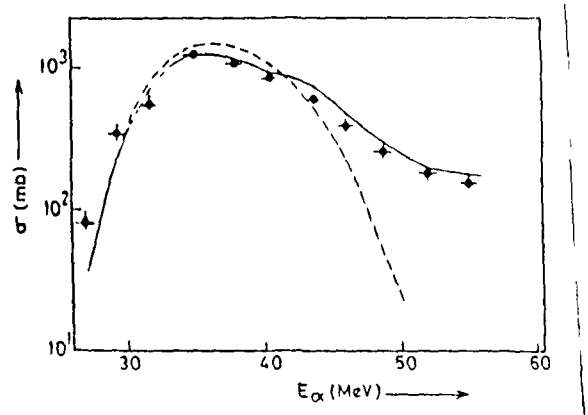


FIG. 4. Experimental and theoretical excitation functions for the reaction $^{191}$Ir($\alpha$,$3n$)$^{192}$Au. ●, present work; (– – –), pure EQ; and (——), EQ with the PE [$n_0=4(2n+2p+0h)$] GDH model.

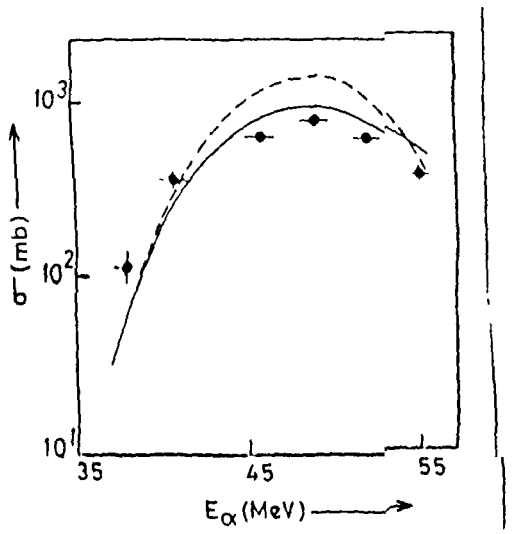


FIG. 5. Experimental and theoretical excitation functions for the reaction $^{191}$Ir(α,4n)$^{191}$Au. ●, present work; (– – –), pure EQ; and (——), EQ with the PE [$n_0=4(2n+2p+0h)$] GDH model.

we restrict ourselves here by referring only to a review of Blann [3] on PE decay. The statistical model part of ALICE/LIVERMORE-82 can account for a large variety of reaction types [29,30], clusters such as deuterons and α particles can be considered in addition to the evaporation of neutrons and protons according to Weisskopf and Ewing. Using a level density assuming $\rho(J)\propto(2J+1)$, i.e., no constraint on angular momenta. For the level density parameter, the value of $A/8$ was taken since it is not possible in the code to use an individual level density parameter for a particular residual nucleus [30]. In the PE calculations, the initial exciton number $n_0=4$ with configuration $(2n+2p+0h)$ was taken, which is the best choice for α-induced reactions [31–34].

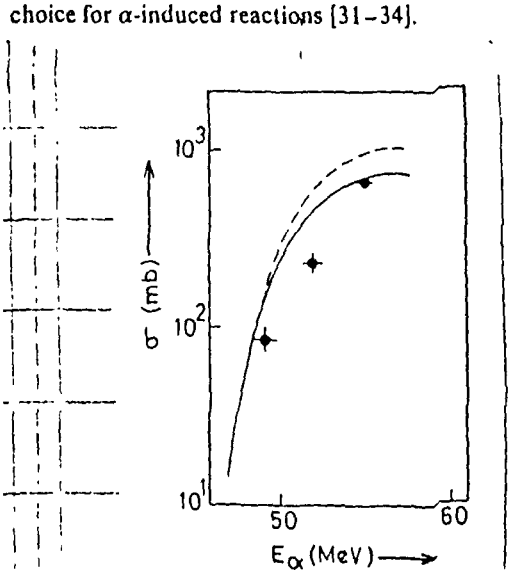


FIG. 6. Experimental and theoretical excitation functions for the reaction $^{191}$Ir(α,5n)$^{190}$Au. ●, present work; (– – –), pure EQ; and (——), EQ with the PE [$n_0=4(2n+2p+0h)$] GDH model.

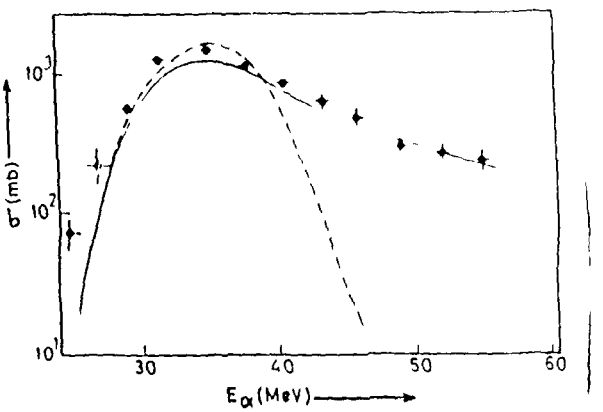


FIG. 7. Experimental and theoretical excitation functions for the reaction $^{191}$Ir(α,3n)$^{194}$Au. ●, present work; (– – –), pure EQ; and (——), EQ with the PE [$n_0=4(2n+2p+0h)$] GDH model.

### B. Experimental results

The measured excitation functions for the reactions $^{191}$Ir(α,n), $^{191}$Ir(α,2n), $^{191}$Ir(α,3n), $^{191}$Ir(α,4n), $^{191}$Ir(α,5n), $^{193}$Ir(α,3n), $^{193}$Ir(α,4n), and $^{193}$Ir(α,5n) are shown in Figs. 2–9. Our experimentally measured results are shown by the solid circles. The total estimated energy spread is shown by the horizontal bar and the cross-sectional error is shown by the vertical bar. Where no vertical bar is shown, the error is within the data points.

In the reactions $^{191}$Ir(α,n) and $^{191}$Ir(α,3n); $^{191}$Ir(α,2n) and $^{191}$Ir(α,4n), $^{191}$Ir(α,3n) and $^{191}$Ir(α,5n), the product nuclei is the same, so all the decay parameters are the same but differ in $Q$ value. As a result, the observed activity in the irradiated sample is the composite activity

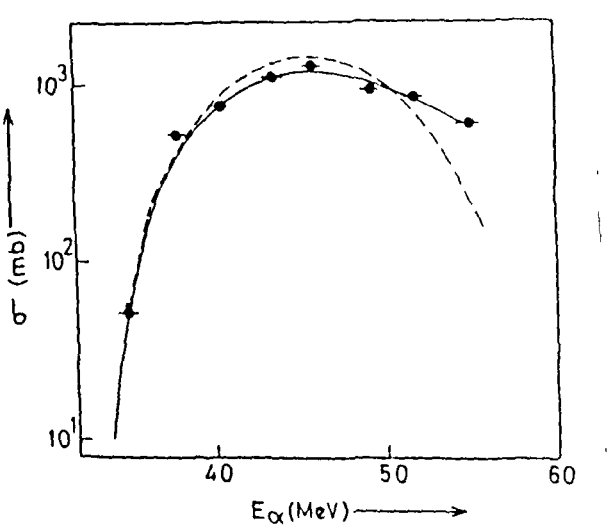


FIG. 8. Experimental and theoretical excitation functions for the reaction $^{191}$Ir(α,4n)$^{191}$Au. ●, present work; (– – –), pure EQ; and (——), EQ with the PE [$n_0=4(2n+2p+0h)$] GDH model.

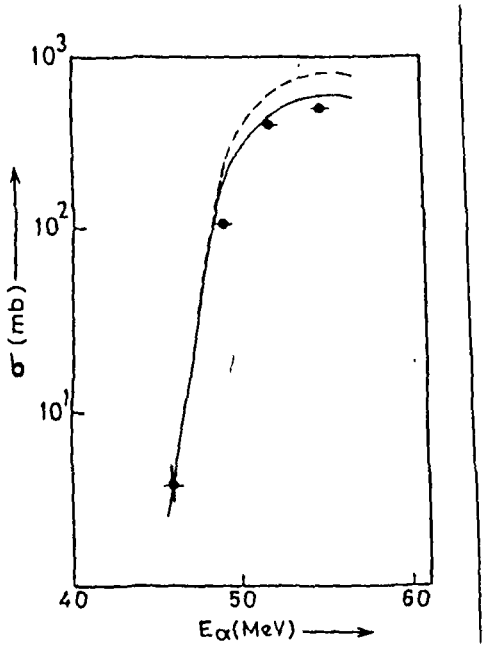


FIG. 9. Experimental and theoretical excitation functions for the reaction $^{193}$Ir$(\alpha,5n)^{192}$Au. ●, present work; (— — —), pure EQ; and (——), EQ with the PE [$n_0=4(2n+2p+0h)$] GDH model.

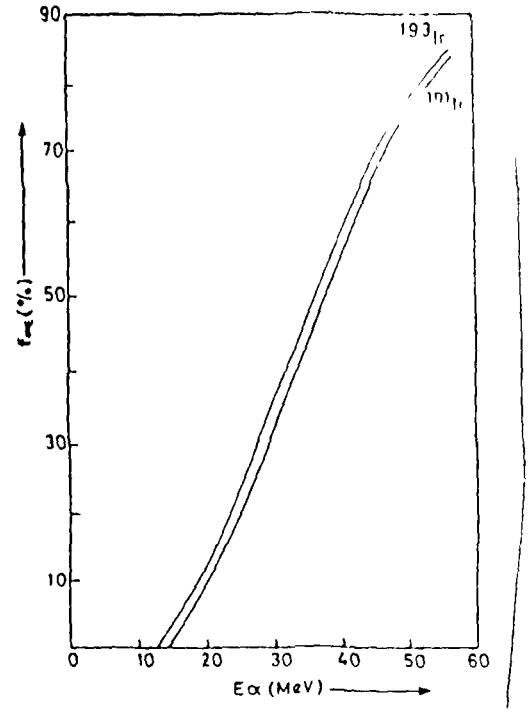


FIG. 10 Preequilibrium fraction $f_{PE}$ of the total reaction cross section as a function of the α-particle energy

due to the reactions in the same set mentioned above. For example, below the threshold of $^{193}$Ir$(\alpha,5n)$, the observed activity is due to the $^{191}$Ir$(\alpha,3n)$ reaction only, but beyond it, the observed activity will be the total of the activities produced due to these two reactions. In this overlapping region the cross sections are divided in the ratio of the theoretical cross sections of these two reactions.

In the reactions $^{191}$Ir$(\alpha,n)$ and $^{193}$Ir$(\alpha,3n)$, $^{191}$Ir$(\alpha,2n)$ and $^{193}$Ir$(\alpha,4n)$, $^{191}$Ir$(\alpha,3n)$ and $^{193}$Ir$(\alpha,5n)$, the product nuclei have one or more isomeric states other than the ground state. In all these cases the half-lives of the isomeric states are very short (sec/msec), so the contribution of these to the excitation function could not be measured distinguishably due to a long cooling time because the high activity was there. But, these isomeric states decay to the ground state, so the total excitation functions were measured.

Since all the measurements are reported for the first time to the best of our knowledge, that is why no literature value is shown in the figures but the presently measured results match very well with the theoretical results.

## IV. CONCLUSION

The excitation functions of eight α-induced reactions have been measured for $^{191}$Ir and $^{193}$Ir. The experimental data and the results of geometry-dependent hybrid model calculations are in surprising agreement without any parameter adjustment for individual product. In the tail portion of the excitation functions, the experimental data and the results from the Weisskopf-Ewing model calculations are not in agreement, this is due to the PE process, which has not been considered in this model. For α-induced reactions, the choice of a four-exciton state $(2n+2p+0h)$ for the initial configuration of the compound system gives satisfactory results and supports the finding of many earlier investigators [30–33]. The preequilibrium fraction ($f_{PE}$) for $^{191}$Ir and $^{193}$Ir has also been calculated and shown in Fig. 10. It is concluded that the preequilibrium fraction increases very fast with the increase of incident α-particle energy. The threshold for preequilibrium emission is higher for the lower mass number. It is also concluded that the value of $f_{PE}$ is higher for the system of higher mass number at a given α-particle energy.

## ACKNOWLEDGMENTS

The authors are grateful to the Department of Physics, Aligarh Muslim University, Aligarh, for providing the facilities to carry out this work and to Dr. S. N. Chintalapudi and VECC personnel for their kind cooperation during the experiment. Two of the authors (M.K.B.) and (I.A.R.) are thankful to the University Grants Commission and Council of Scientific and Industrial Research, New Delhi, for financial support.

[1] J. J. Griffin, Phys. Rev. Lett 17, 478 (1966).
[2] G. D. Harp and J. M. Miller, Phys. Rev. C 3, 1847 (1971).
[3] M. Blann, Annu. Rev Nucl. Sci. 25, 123 (1975).
[4] E. Gadioli, E. Gadioli-Erba, and P. G. Sona, Nucl. Phys. A 217, 589 (1973).
[5] M. Blann, Phys. Rev Lett. 27, 337 (1971); 27, 700(E) (1971); 27, 1550(E) (1971).
[6] M Blann, Phys. Rev Lett 28, 757 (1972).
[7] G. D. Harp, J. M. Miller, and J. B. Berne, Phys. Rev. 165, 1166 (1968).
[8] C K Cline and M Blann, Nucl Phys A 172, 225 (1971).
[9] D. Agassi, H. A. Weidenmuller, and G. Mantzouranis, Phys. Rev. 22, 145 (1975).
[10] T. Tamura, T. Udagawa, D. H. Feng, and K. K. Kan, Phys Lett. 68B, 109 (1977).
[11] T. Tamura and T. Udagawa, Phys. Lett 78B, 189 (1978)
[12] P. E. Hodgson, ICTP Report SMR/284-5, 1988.
[13] H. Feshbach, A. Kerman, and S. Koonin, Ann. Phys 125, 429 (1980).
[14] L. Avaldi, R. Bonetti, and L. Colli-Milazzo, Phys. Lett 94B, 463 (1980)
[15] G. M Field, R. Bonetti, and P. E Hodgson, J. Phys. G 12, 93 (1986).
[16] M. Ismail and A. S. Diyatia, Pramana-J. Phys. 30, 193 (1988).
[17] J. Ernst, R. Ibowski, H. Klampfl, H. Machner, T. Mayer-Kuckuk, and R Schanz, Z. Phys. A 308, 301 (1982).
[18] N. L. Singh, S. Agrawal, L Chaturvedi, and J. Rama Rao, Nucl. Istrum Methods B 24/25, 480 (1987).
[19] I. A. Rizvi, M. K. Bhardwaj, M. Afzal Ansari, and A K. Chaubey, Appl. Radiat. Isot. 41, 215 (1990).
[20] I. A Rizvi, M K Bhardwaj, M Afzal Ansari, and A K Chaubey, Can J Phys 67, 1091 (1989)
[21] I. A. Rizvi, M. K Bhardwaj, M Afzal Ansari, and A K Chaubey, Can J. Phys 67, 870 (1989)
[22] L C Northcliffe and R. F Schilling, Nucl Data Tables A 7, 256 (1970)
[23] U Fano, Annu Rev Nucl Sci 13, 1 (1963)
[24] M Afzal Ansari, R. K Y. Singh, M L Sehgal, V K Mittal, D K Avasthi, and I M Govil, Ann Nucl Energy 11, 173 (1984).
[25] S F Mughabghab, M Divadeenam, and M E Holden, *Neutron Cross Sections* (Academic, New York, 1981), Vol 1, Part A, p 89.
[26] C M Lederer and V S Shirley, *Table of Isotopes* 7th ed (Wiley, New York, 1978)
[27] V F Weisskopf and D H Ewing, Phys. Rev. 57, 472 (1940)
[28] M Blann and J Bisplinghoff, ALICE/LIVERMORE 82, Lawrence Livermore National Laboratory Report UCID 19614, 1982.
[29] R Michel and G Brinkmann, Nucl Phys A 338, 167 (1980)
[30] R Michel, F Peiffer, and R Stuck, Nucl Phys A 441, 617 (1985)
[31] I A. Rizvi, M Afzal Ansari, R P Gautum, R K Y Singh, and A. K. Chaubey, J. Phys Soc Jpn 56, 3135 (1987)
[32] P Misaelides and M Munzel, J Inorg Nucl Chem 42, 937 (1980)
[33] G W. A Newton, V. J. Robinson, and E M Shaw, J Inorg Nucl Chem 43, 2227 (1981).
[34] M Blann and T. T Komoto, Phys Rev C 29, 1678 (1984)

World Scientific Publishing Co Pte Ltd

**Postal & Correspondence:**
Farrer Road
P O Box 128
Singapore 9128

**Office:**
1022 Hougang Avenue 1 #05-3520
Tai Seng Industrial Estate
Singapore 1953

Tel (65) 382 5663
Tlx RS 28561 WSPC
Fax (65) 382 5919 Cable COSPUB

14 April 1992

Dr A K Chaubey
Department of Physics
Aligarh Muslim University
Aligarh - 202002
INDIA

Dear Dr Chaubey

**RE: TRANSFER OF PAPER FROM IJMPA TO IJMPE - REPORTS ON NUCLEAR PHYSICS**

I am pleased to inform you that your paper entitled

EXCITATION FUNCTION STUDIES FOR THE ALPHA INDUCED REACTIONS IN INDIUM

has been accepted, with minor revision necessary, for publication in IJMPA.

I enclose herewith the referees' reports. Kindly advise if the paper will be amended as recommended and if so, when I may expect the paper to be resubmitted.

As recommended by our Editors, we seek your permission, as well as those of your co-authors, to transfer the paper from IJMPA to IJMPE. Let me tell your more about IJMPE.

IJMPE, the first issue of which will be launched in May 1992, will be launched from IJMPA. In 1987, IJMPA expanded its coverage to include nuclear physics. As a result of overwhelming response from authors and subscribers, the area of nuclear physics in the journal loses emphasis in IJMPA. After consulting our Editors as well as our Advisors in nuclear physics, we have launched a new and separate journal designed solely for papers in nuclear physics.

We hope to publish your paper in IJMPE particularly because the target audience for this journal are nuclear physicists. We aim to make IJMPE a journal of outstanding standard, publishing top class research and review articles.

We look forward to a favourable reply soon.

Thank you and best wishes.

Yours sincerely

Raha A Hassan (Ms)
Editor
IJMPE

RAH/mf

# EXCITATION FUNCTION STUDIES FOR THE ALPHA INDUCED REACTIONS IN INDIUM

M.K. BHARDWAJ, I.A. RIZVI and A.K. CHAUBEY
Department of Physics, Aligarh Muslim University
Aligarh-202002 INDIA.

Excitation function of the reactions (α,n), (α,2n), (α,3n), (α,4n), (α,pn), (α,2p) for $^{115}$In and (α,n), (α,2n) for $^{113}$In have been measured upto 50 MeV bombarding energy using stacked foil activation technique. A stack of the target foils was irradiated at the Variable Energy Cyclotron Centre, Calcutta. The α-particle flux was monitored by charge collection method using Faraday Cup, kept just behind the targets. Cross sections were measured at ten α-particle energies. The experimental data were compared with the thecretical predictions using ALICE/LIVERMORE-82 Code based on the geometry dependent hybrid model of Blann. The best consequence was obtained for exciton number $n_o = 4$ with the configuration (2n+2p+0h).

---

PACS No : 25.55 $^{3}$He - $^{4}$He Induced Reactions and Scattering

## 1. Introduction

After the development of Variable Energy Cyclotron, projectiles accelerated upto very high energies became available[1] and experimental features of the nuclear reactions have been studied by several investigators. They manifesttrather anomalous features in the high energy tails of the excitation function. So obtained new experimental features could neither be explained by compound nucleus model nor by direct reaction model[2-4]. To explain the experimental fact many semi-classical models have been proposed[5-12] The hybrid and geometry dependent hybrid models[(9,10)] proposed by Blann have been found to be relatively simple and of closed form for the successful reproduction of experimental data[13]. Apart from these semi-classical models of the nuclear reactions for the successful reproduction of the excitation function data, efforts are in progress to give a full quantum mechanical picture[14-20] in the frame work of multistep theories proposed by Feshbach et al.[18] and others[17,19,20].

In order to have a more accurate knowledge about the pre-equilibrium emission mechanism, more and more experimental data are necessary. Keeping this motivation in the mind the excitation functions for $^{113}In$ and $^{115}In$ with alphas were measured. Theoretica predictions based on the geometry dependent hybrid model were carrie out for comparison with the observed data.

## 2. Experimental Procedure

Samples of the element under study were made from spectrographically pure indium having purity better than 99.99% . In the preparation of the target sample the indium metal of thickness 3.34 mg/cm$^2$ (natural abundance $^{113}$In = 4.3% , $^{115}$In = 95.7%) was deposited onto the aluminium backing of thickness 6.75 mg/cm$^2$ by vacuum evaporation technique at target division of Variable Energy Cyclotron Centre (VECC), Calcutta (India). The indium foil was cut into the pieces of size 1.5 cm x 1.5 cm and each of them was glued to an aluminium frame having a circular hole of diameter 1.2 cm in the centre. These pieces were arranged into the form of a stack. Aluminium and copper foils were also used in between the indium foils to get desired incident energy on each foil. The stack was irradiated by 50 MeV diffused α beam for one and half hour in a chamber specially constructed for irradiation. The diameter of the beam spot on the target was limited to 8.0 mm by using a collimator in front of the target stack. The current during the irradiation was around 100 nA. The α-particle flux was monitored by the total charge collection method, using a Faraday Cup kept just behind the target stack[21-26]. The typical experimental set up for the stack irradiation is shown in fig. 1. The α beam was obtained from the cyclotron at Variable Energy Cyclotron Centre (VECC), Calcutta (India). After the irradiation the target samples were brought into the counting room of VECC and gamma rays emitted from residual nuclei were measured by 100 cc ORTEC Ge (Li) detector and the gamma ray

spectra were taken with the help of pre-calibrated 4096 channel analyzer and associated electronics. Efficiency and energy calibration were done using a standard $^{152}Eu$ γ-point source of known strength by keeping it at the source position. The energy of the particle after they had traversed the thickness of each foil was computed from the stopping power table of Northcliffe and Schilling[27].

The expression to calculate the cross section has been described in reference 28. Half-lives, gamma rays, absolute γ-intensity corresponding to the product nuclei are taken from the table of isotopes by Lederer and Shirley[29]. In the calculation of incident α-particle energy both the inherent beam spread of ± 0.5 MeV and energy spread in the foils were taken into account. The α-particle energies incident on the foils were 50 ± 0.5, 46.8 ± 0.6, 43.6 ± 0.7, 40.1 ± 0.7, 37.4 ± 0.7, 35.1 ± 0.8, 32.2 ± 0.8, 29.0 ± 1.0, 25.2 ± 1.2, and 21.4 ± 1.4 MeV.

## 3. Result and Discussion

Experimental results are shown in fig.2 in the form of excitation function. The total energy spread associated with each incident α-particle energy is shown by the horizontal bar, while the total estimated error in the excitation function is represented by the vertical bar. At some points the vertical bars are not shown, it means, the estimated error in the cross section is within the mark. The estimated error is only the statistical error. The reported value is the weighted average[30] of the various cross sections

calculated for the various gamma rays at the same incident α-particle energy. The errors has been calculated according to the ref. 30.

Experimentally measured excitation functions are also compared with those calculated theoretically. The theoretical calculations are on the basis of compound and pre-equilibrium (PE) reaction mechanisms using the GDH model proposed by Blann[10] and they are represented by the solid line, whereas those obtained by taking into consideration the compound nucleus formation only, by the compound model of Weisskopf-Ewing[31], are represented by broken line. A computer code ALICE/LIVERMORE-82[32] was used for these calculations[33,34]. The values of level density parameter and mean free path multiplier 12.0 and 3.0 respectively were choosen for throughout the calculations.

The reactions $^{113}In(\alpha,2n)\ ^{115}Sb$ and $^{115}In(\alpha,4n)\ ^{115}Sb$ have different Q value but even then in the tail region of $^{113}In(\alpha,2n)\ ^{115}Sb$ reaction the other reaction channel should compete with it. In this region each cross section would not be determined distinguishably, and so the observed cross section was divided in parts according to the ratio of the theoretical cross sections at the given α-particle energy.

In the $^{113}In(\alpha,n)\ ^{116}Sb$ and $^{115}In(\alpha,3n)\ ^{116}Sb$ reactions the product nucleus $^{116}Sb$ has two states, ground state of half-life 16 minutes and metastable state of half-life 60.4 minutes. As the half life of ground state is very short, hence, in the counting of the activity for this reaction, no contribution from the ground state was observed so the observed cross section is due to the metastable state only.

The situation about the metastable ($t\frac{1}{2}$ = 5.0 hrs) and ground ($t\frac{1}{2}$ = 3.5 minutes) state of the product nucleus in the reaction $^{115}In\ (\alpha,n)\ ^{118}Sb$ was the same as in the above case. The comparison of the measured results of $^{113}In\ (\alpha,n)\ ^{116}Sb$, $^{115}In\ (\alpha,n)\ ^{118}Sb$, $^{115}In\ (\alpha,3n)\ ^{116}Sb$ reactions with the theory was not possible because the excitation function of these reactions were measured for the metastable state only.

In the reaction $^{115}In\ (\alpha,2n)\ ^{117}Sb$, $^{115}In\ (\alpha,pn)\ ^{117m}Sn$ and $^{115}In\ (\alpha,2p)\ ^{117}In$ the product nuclei emit the gamma ray of same energy, 158.56 MeV with different emission probabilities. Therefore, the obtained photopeak area was the sum of the photopeak areas due to these three reaction products. The contribution of each product nucleus was separated out with the help of decay analysis.

The figures 2-5 represent the experimentally measured results for the reaction $^{113}In\ (\alpha,n)$, $^{113}In\ (\alpha,2n)$, $^{115}In\ (\alpha,n)$, $^{115}In\ (\alpha,2n)$, $^{115}In\ (\alpha,3n)$, $^{115}In\ (\alpha,4n)$, $^{115}In\ (\alpha,2p)$, $^{115}In\ (\alpha,pn)$ respectively and also the comparison between theory and experiment wherever possible.

## 4. Conclusion

The eight excitation functions have been measured for α-induced reactions with $^{113}In$ and $^{115}In$. From the figs. 2-5, it is very clear that the experimentally measured result are not in very good agreement with the theoretical results calculated by the geometry dependent hybrid model, but qualitatively it is satisfactory. High energy tails

in the α-induced excitation function cannot be accounted for by the pure equilibrium reaction mechanism as is clearly shown by comparing the experimental results with the broken lines. It can be explained by proper admixture of equilibrium and pre-equilibrium processes. This statement can be justified by the comparison of experimentally measured result and the solid line. It was concluded that the initia exciton configuration $n_o$ = 4 (2n+2p+0h) gave the best fit to our experimental data. This supports the finding of many earlier investigators[21,35-39]. The pre-equilibrium fraction ($f_{PE}$) for the total reaction cross section has also been calculated and is shown in fig. 6. It is concluded that the pre-equilibrium fraction increases very fast with the increase of incident α-particle energy. The threshold for pre-equilibrium emission is higher for the lower mass number. It is also concluded that the value of $f_{PE}$ is higher for the system of higher mass number at a given α-particle energy.

## Acknowledgement

Authors wish to express the sincere thanks to Prof.B.N.Khanna, Chairman, Department of Physics, Aligarh Muslim University, Aligarh for his interest in this work. We are also thankful to Dr. S.N. Chintalapudi and VECC personnel for their co-operation during the experiment at Cyclotron Centre, Calcutta. One of the authors (MKB) would like to thank the University Grants Commission for assistance in the form of a fellowship under D.S.A. Programme.

## References


1. Emilio Segre, J. Robb Groves and H. Pieere Mayes, Ann. Rev. Nucl. Sci. 25, (1975) 124.

2. V.A. Sidorov, Nucl. Phys. 35, (1965) 253.

3. C. Holbrow and H. Barschall, Nucl. Phys. 42, (1963) 264.

4. R. Wood, R. Brochers and H. Barschall, Nucl. Phys. 71, (1965) 529.

5. J.J. Griffin, Phys. Rev. Lett. 17, (1966) 478.

6. G.D. Harp and J.M. Miller, Phys. Rev. C 3, (1971) 1847.

7. M. Blann, Ann. Rev. Nucl. Sci. 25, (1975) 123.

8. E. Gadioli, E. Gadioli - ERBA, and P.G. Sona, Nucl. Phys. A217, (1973) 589.

9. M. Blann. Phys, Rev. Lett. 27, 337 (1971); 27, (1971); 700(E) 27, (1971) 1550 (E).

10. M. Blann, Phys. Rev. Lett. 28, (1972) 757.

11. G.D. Harp, J.M. Miller and J.B. Berne, Phys. Rev. 165, (1968) 1166.

12. C.K. Cline and M. Blann, Nucl. Phys. A172, (1971) 225.

13. M. Afzal Ansari, I.A. Rizvi, M.K. Bhardwaj and A.K. Chaubey, IC/88/57, Internal Report (1988).

14. D. Agassi, H.A. Weidenmuller and G. Mantzouranis, Phys. Rev. 22, (1975) 145.

15. T. Tamura, T. Udagawa, D.H. Feng and K.K. Kan., Phys. Lett. B68, (1977) 109.

16. T. Tamura and T. Udagawa, Phys. Lett. B78, (1978) 189.

17. P.E. Hodgson, Workshop on Applied Nuclear Theory and Nuclear Model Calculations for Nuclear Technology Applications, Report ICTP, SMR/284-5 (1988).

18. H. Feshbach, A. Kerman and S. Koonin, Ann. Phys. 125, (1980) 429.

19. L. Avaladi, R. Bonetti and L. Colli-Milazzo, Phys. Lett. 94B, (1980) 463.

20. G.M. Field, R. Bonetti and P.E. Hodgson, J. Phys. G12, (1986) 93.

21. M. Ismail and A.S. Divatia. Pramana. J. Phys. 30, (1988) 193.

22. J. Ernst. R. Iowski, H. Klampfl, H. Machner, T. Mayer-Kuckuk and Schanz, Z. Phys. A: Atoms and Nuclei 308, (1982) 301.

23. N.L. Singh, S. Agrawal, L. Chaturvedi and J. Rama Rao, Nucl. Istrum. Meth.B24/25, (1987) 480.

24. I.A. Rizvi, M.K. Bhardwaj, M. Afzal Ansari and A.K. Chaubey, Appl. Radiat. Isot. 41, (1990) 215.

25. I.A. Rizvi, M.K. Bhardwaj, M. Afzal Ansari and A.K. Chaubey, Can. J. Phys. Vol. 67 (1989) (1091)

26. I.A. Rizvi, M.K. Bhardwaj, M. Afzal Ansari and A.K. Chaubey, Can. J. Phys. 67, (1989) 870.

27. L.C. Northcliffe and R.F. Schilling, Nucl. Data Tables A 7, (1970) 256.

28. M. Afzal Ansari, R.K.Y. Singh, M.L. Sehgal, V.K. Mittal, D.K. Avasthi and I.M. Govil, Ann. Nucl. Energy. 11, (1984) 173.

29. C.M. Lederer and V.S. Shirley, Table of Isotopes. 7th Ed. Wiley and Sons Inc., New York. 1978.

30. S.F. Mughabghab, M. Divadeenam and N.E. Holden, Neutron cross-sections Vol. 1. Academic Press, New York 1981 Part A. p. 89.

31. V.F. Weisskopf and D.H. Ewing, Phys. Rev. 57, (1940) 472.

32. M. Blann and J. Bisplinghoff, ALICE/LIVERMORE-82 LLNL Report UCID-19614 (1982).

33. R. Michel and G. Brinkmann, Nucl. Phys. A338, (1980) 167.

34. R. Michel. F. Peiffer and R. Stuck, Nucl. Phys. A441 (1985) 617.

35. I.A. Rizvi, M. Afzal Ansari, R.P. Gautam, R.K.Y. Singh and A.K. Chaubey, J. Phys. Soc. Jpn. 56, (1987) 3135.

36. P. Misaelides and H. Munzel, J. Inorg. Chem. 42 (1980) 937.

37. G.W.A. Newton, V.J. Robinson and E.M. Shaw, J. Inorg. Nucl. Chem. 43, (1981) 2227.

38. M. Blann and T.T. Komoto, Phys. Rev. C29, (1984) 1678.

## Figure Captions

Fig. 1. Experimental set-up for stack foil irradiation with α-particle beam.

Fig. 2. Excitation function for the reactions $^{113}In(\alpha,n)\ ^{116}Sb^{m}$ + $^{115}In(\alpha,3n)\ ^{116}Sb^{m}$ , $^{113}In(\alpha,2n)\ ^{115}Sb$.

● : $^{113}In(\alpha,n)\ ^{116}Sb^{m}$ + $^{115}In(\alpha,3n)\ ^{116}Sb^{m}$ Reaction

o : $^{113}In(\alpha,2n)\ ^{115}Sb$ Reaction

——: PE with EQ (GDH model)

---: Pure EQ

Fig. 3. Excitation function for the reactions $^{115}In(\alpha,n)\ ^{118}Sb^{m}$, $^{115}In(\alpha,2n)\ ^{117}Sb$, $^{115}In(\alpha,4n)\ ^{115}Sb$.

▽ : $^{115}In(\alpha,n)\ ^{118}Sb^{m}$ Reaction.

● : $^{115}In(\alpha,2n)\ ^{117}Sb$

o : $^{115}In(\alpha,4n)\ ^{115}Sb$ Reaction.

——: PE with EQ (GDH model)

---: Pure EQ.

Fig. 4. Excitation function for the reaction $^{115}In(\alpha,2p)\ ^{117}In$.

● : Present work (ground state + metastable state)

o : Present work (metastable state only)

▽ : Present work (ground state only)

Fig. 5. Excitation function for the reaction $^{115}In(\alpha,pn)\ ^{117}Sn^{m}$.

: Present work (metastable state only)

Fig. 6. Pre-equilibrium fraction (fPE) of the total reaction cross section as a function of α-particle energy.

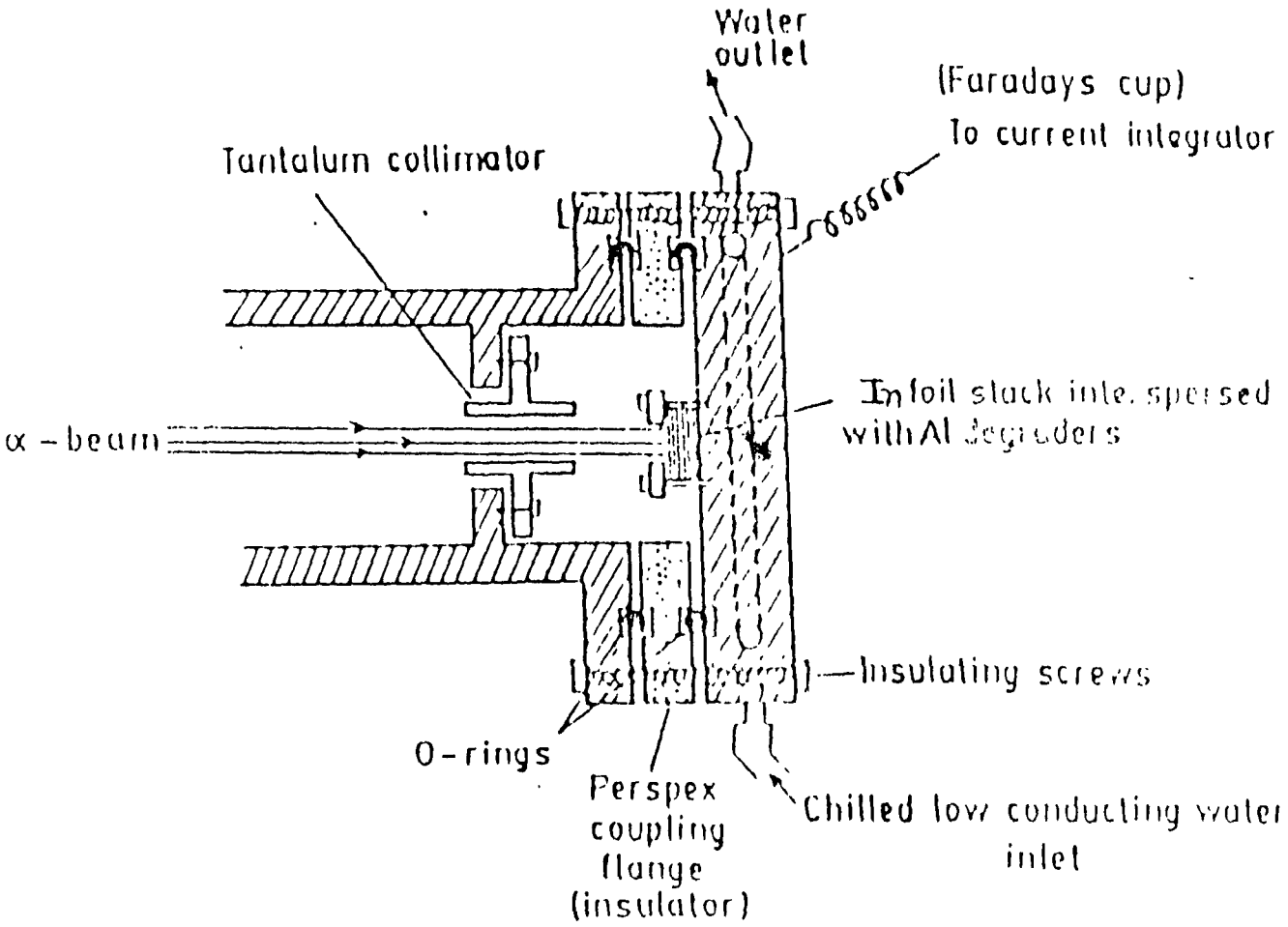
Water outlet
(Faradays cup)
To current integrator
Tantalum collimator
α - beam
In foil stack inte. spersed with Al degraders
Insulating screws
O-rings
Perspex coupling flange (insulator)
Chilled low conducting water inlet

Fig.1

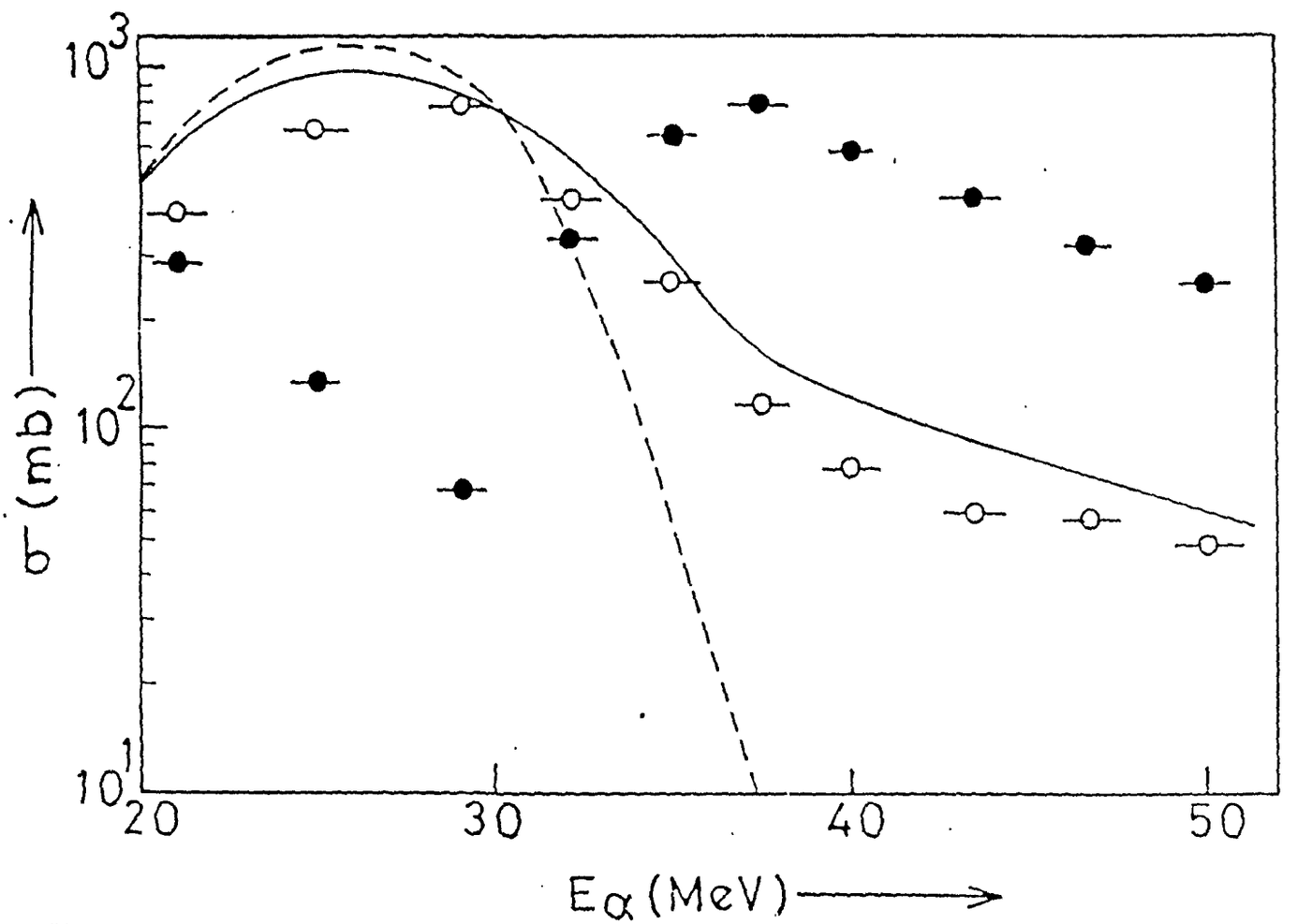


Fig. 2

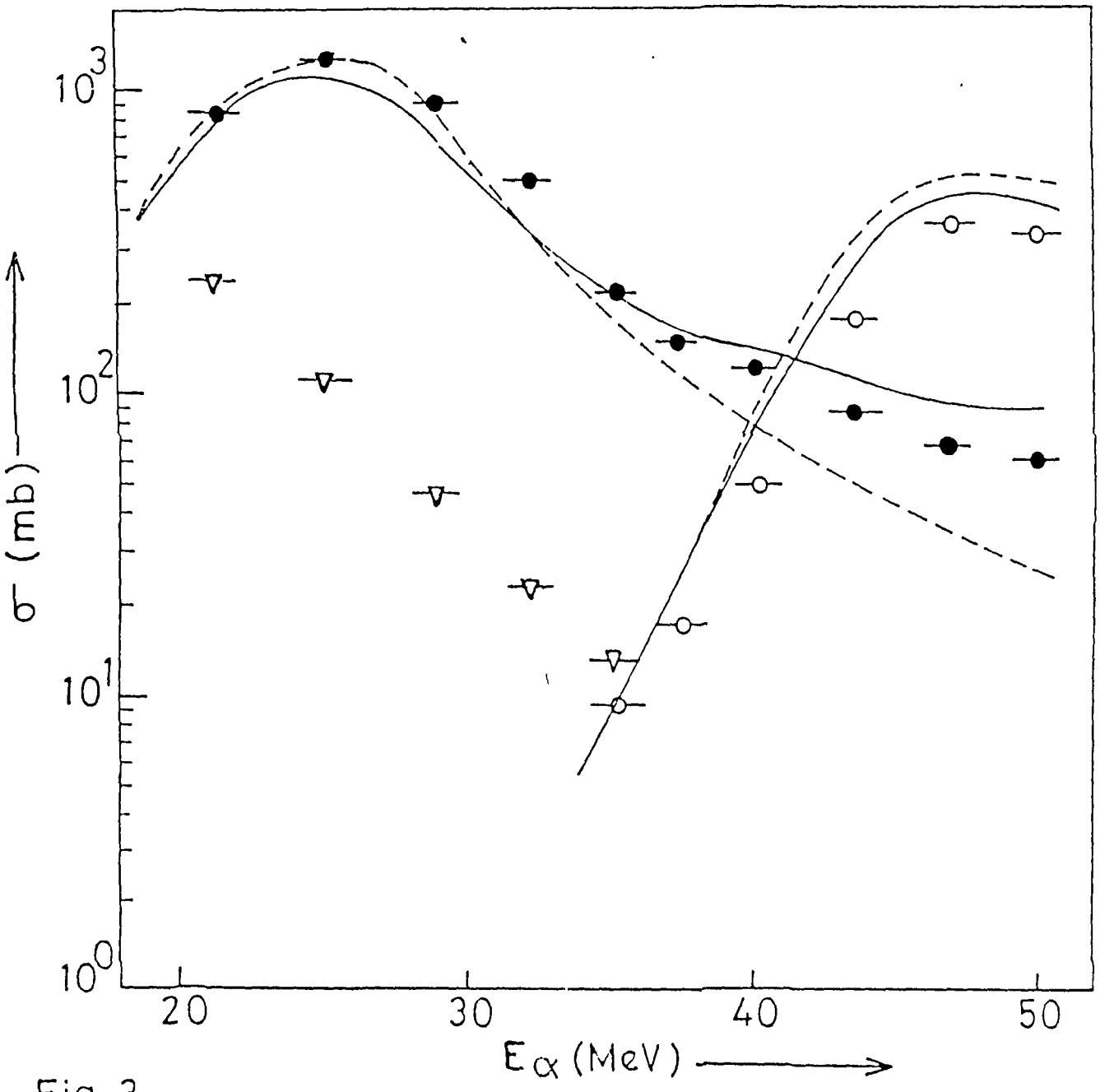


Fig. 3

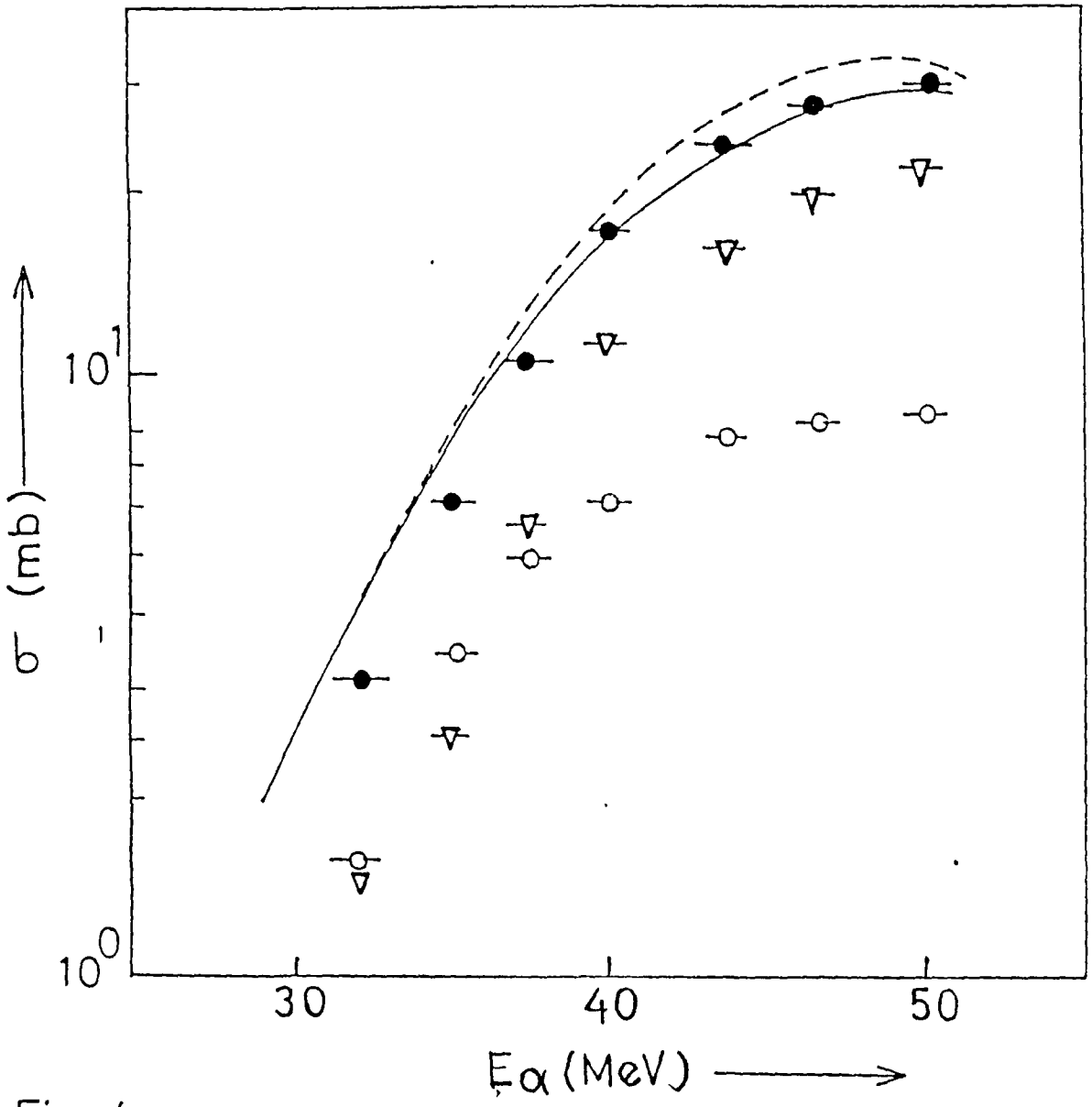


Fig. 4

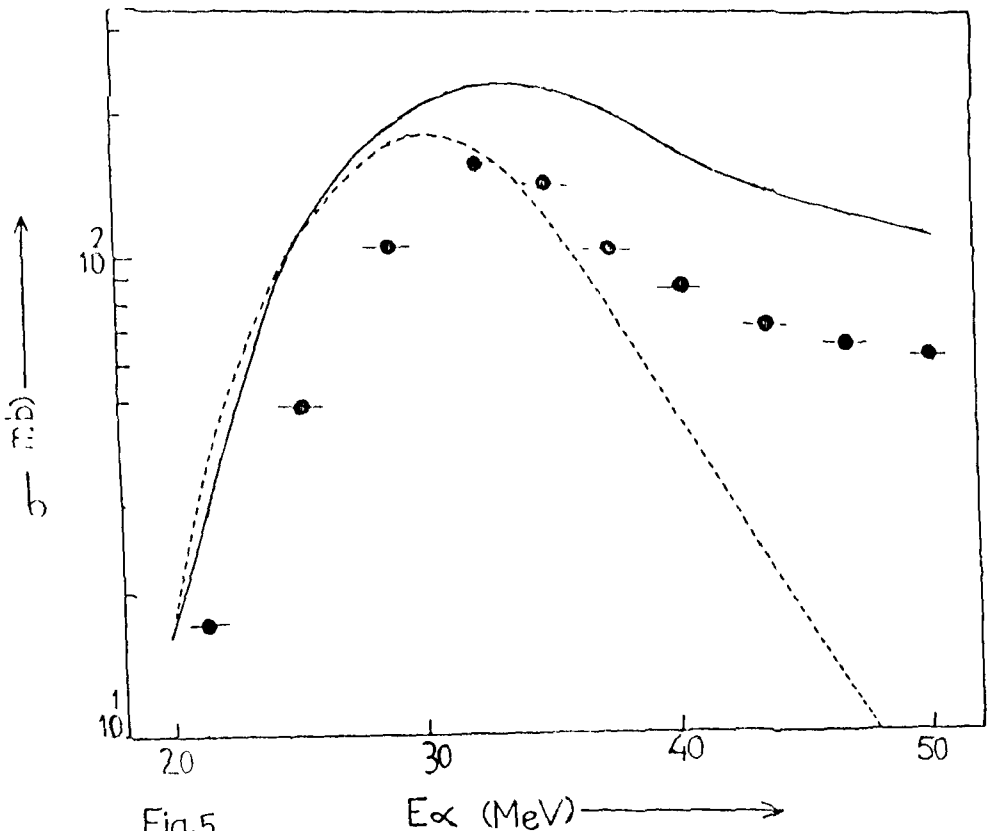


Fig.5